

**GEOTECHNICAL CHARACTERIZATION OF ORGANIC SOILS FOR  
ENGINEERING DESIGN OF BURIED ENERGY PIPELINES**

by

Thushara Dilrukshi Jayasinghe

B.Sc.Eng.(Hons), University of Moratuwa, 2017

A THESIS SUBMITTED IN PARTIAL FULFILLMENT OF  
THE REQUIREMENTS FOR THE DEGREE OF

DOCTOR OF PHILOSOPHY

in

THE FACULTY OF GRADUATE AND POSTDOCTORAL STUDIES  
(Civil Engineering)

THE UNIVERSITY OF BRITISH COLUMBIA

(Vancouver)

April 2024

© Thushara Dilrukshi Jayasinghe, 2024

The following individuals certify that they have read, and recommend to the Faculty of Graduate and Postdoctoral Studies for acceptance, the dissertation entitled:

Geotechnical characterization of organic soils for engineering design of buried energy pipelines

---

submitted by Thushara Dilrukshi Jayasinghe in partial fulfillment of the requirements for

the degree of Doctor of Philosophy

---

in Civil Engineering

---

**Examining Committee:**

Dr. Dharma Wijewickreme, Professor, Department of Civil Engineering, UBC - V  
Supervisor

Dr. John Howie, Associate Professor Emeritus, Department of Civil Engineering, UBC - V  
Supervisory Committee Member

Dr. Sumi Siddiqua, Professor, School of Engineering, UBC - O  
Supervisory Committee Member

Dr. Reza Vaziri, Professor, Department of Civil Engineering, UBC - V  
University Examiner

Dr. Zheng Liu, Professor, School of Engineering, UBC - O  
University Examiner

Dr. Ian D. Moore, Professor, Department of Civil Engineering, Queen's University, Canada  
External Examiner

## **Abstract**

Organic soils (i.e., muskeg, peat deposits) cover 5 to 8% of the land surface of the earth, and in Canada, many energy pipelines cross these soils over large distances. Thermal changes due to operational and environmental reasons pose a significant threat to the structural integrity and safety of pipeline systems in these soils. Engineering design of pipelines in muskeg terrains involves many challenges, mainly due to the lack of understanding of the mechanical behavior of organic soils. Such knowledge gaps have caused an absence of well-adapted soil-pipe interaction (SPI) assessment methodologies for pipeline design in organic soils, unlike the methods readily available for pipes buried in mineral sandy and clayey soils (e.g., PRCI 2009). For these reasons, pipeline designs in organic soils are often conducted with significant conservatism.

A research study is undertaken to characterize organic soils primarily using geotechnical field investigation tools and obtain representative strength and stiffness parameters for SPI analysis. It was found that the ball penetrometer test (BPT) is effective as a field testing tool for investigating organic soil along pipeline corridors. A reasonable stress-strain (constitutive) model to represent organic soils in numerical modeling was selected by validating with respect to data from field pressuremeter testing, and in turn, that model was employed to simulate SPI problems. High-quality experimental datasets on axial and lateral loading SPI mechanisms in pipes buried in organic soil were developed based on results obtained through full-scale physical modeling. The lateral SPI of pipes buried in organic soils was modeled numerically, and the developed SPI model was verified using full-scale physical testing results to justify its suitability for engineering evaluations. Using the validated numerical framework, a series of pipeline configurations were simulated to reach a comprehensive understanding of lateral SPI in organic soils. Considering the

comparisons of load-displacement response from numerical analysis and/or full-scale experimental results with those arising from equations proposed in current pipeline guidelines, recommendations are made for modifying the total stress approaches specified in PRCI guidelines (2009) for soft clayey soils to assess axial and lateral soil restraints on pipes buried in organic soils.

## **Lay Summary**

Pipelines are one of the safest ways of transporting fluids over large distances. It is of relevance to note that a key part of global oil and gas transportation infrastructure is formed by buried pipeline systems. Any significant disruption to the performance of these systems often translates into undesirable impacts on the living conditions of citizens, environment, and regional economies. This research study was undertaken to characterize the mechanical properties of organic soils (muskeg) in order to advance the knowledge of the behavior of such soils and improve the pipeline design approaches in organic soils. The research outcomes directly contribute to safe and sustainable energy pipelines and cost-effective pipeline engineering designs, effectively transporting commodities to markets. The methodologies developed from this project can be applied to similar soils anywhere in the world contributing to multi-faceted pipeline engineering problems with particular relation to pipeline integrity and safety.

## **Preface**

This dissertation compiles the details of a research program undertaken by the author, Thushara Dilrukshi Jayasinghe, under the supervision of Dr. Dharma Wijewickreme at the Department of Civil Engineering, University of British Columbia from 2018 – 2023. Throughout the entirety of this research study, Dr. Dharma Wijewickreme, as the primary supervisor, provided invaluable guidance and direction across every phase, spanning from conceptual development, experimental investigation, numerical analysis, data interpretation, and manuscript composition. Furthermore, all technical writings and research publications stemming from this study were completed under his direct supervision and input.

This study comprised of design and fabrication of laboratory test devices for soil-pipe interaction testing and performing full-scale pipe testing using these devices. The concept design of the horizontal soil-pipe interaction test chamber was developed by the author with suggestions from Dr. Dharma Wijewickreme. The structural design was carried out by the author with suggestions from laboratory engineer, Mr. Mehrtash Motamedi. The fabrication of the test chamber and installation of the actuator system was carried out by the UBC Civil Engineering machine shop staff; Mr. Doug Hudniuk, Mr. Arthur Mak, Mr. Shota Inoda and Mr. Jun Sang Song. The design and development of the data acquisition system was carried out by Mr. John Wong from the UBC civil machine shop. Discussions with Mr. Scott Jackson and Mr. Simon Lee with regard to the development of the data acquisition system is acknowledged. The test chamber used for axial pipe displacement tests was modified with a reinforced structure by the author with guidance from Dr. Ruslan Amarasinghe and support from Mr. Bill Leung.

The soil specimen preparation procedure for both full-scale soil-pipe interaction test chambers was developed by the author. All the full-scale SPI experiments were conducted by the author with support from undergraduate students Mr. Johnson Li and Mr. Zander Pierson. Laboratory element tests were performed by the author. Interpretation of the test data and discussions were performed by the author with guidance from Dr. Dharma Wijewickreme.

Field geotechnical investigations presented in this thesis were carried out by ConeTec Investigations Ltd. under the supervision of the Ms. Jennifer Liu and guidance from Dr. Dharma Wijewickreme. In-place penetration tests during full-scale SPI tests were also performed by ConeTec Investigations Ltd. under the supervision of the author and guidance from Dr. Dharma Wijewickreme. The data generated from the field tests and in-place penetration tests provided by ConeTec Investigations Ltd. were analyzed and applied by the author with supervision from Dr. Dharma Wijewickreme for the mechanical characterization of organic soils.

The numerical analysis of pressuremeter and lateral SPI was performed by the author with insight and guidance from Dr. Sadana Gamage and Dr. Dharma Wijewickreme, and additional revisions were provided by Dr. Prajakta Jadhav and Dr. Devdeep Basu.

Review of the thesis was carried out by Dr. Dharma Wijewickreme and the supervisory committee.

# Table of Contents

<b>Abstract.....</b>	<b>iii</b>
<b>Lay Summary.....</b>	<b>v</b>
<b>Preface.....</b>	<b>vi</b>
<b>Table of Contents .....</b>	<b>viii</b>
<b>List of Tables .....</b>	<b>xv</b>
<b>List of Figures.....</b>	<b>xvii</b>
<b>List of Symbols .....</b>	<b>xxxii</b>
<b>List of Abbreviations .....</b>	<b>xxxv</b>
<b>Acknowledgements .....</b>	<b>xxxvii</b>
<b>Dedication .....</b>	<b>xxxix</b>
<b>Chapter 1: Introduction .....</b>	<b>1</b>
1.1    Research Background .....	1
1.2    Problem Statement .....	2
1.3    Scope and Research Objectives .....	4
1.4    Specific Research Tasks .....	8
1.5    Thesis Outline .....	9
<b>Chapter 2: Literature Review and Research Scope Development .....</b>	<b>12</b>
2.1    Soil Restraints on Buried Pipelines Subjected to Relative Ground Movement.....	13
2.1.1    Axial soil restraints on buried pipes.....	15
2.1.2    Horizontal soil restraints on buried pipes .....	20

2.1.3	Commentary – Soil restraints on buried pipelines subjected to relative ground movement.....	28
2.2	Current Practice for the Design of Buried Pipes in Organic Soils.....	29
2.3	Mechanical Behavior of Organic Soils.....	31
2.3.1	Considerations for selecting a constitutive relationship for SPI modeling.....	31
2.3.2	Shear strength characteristics.....	33
2.3.3	Shear stiffness characteristics .....	38
2.4	Summary.....	39
<b>Chapter 3: Material Characterization of Organic Soils for SPI Analysis.....</b>		<b>42</b>
3.1	Field Geotechnical Investigation Program.....	43
3.1.1	Site locations and overall test program.....	43
3.1.2	Seismic cone penetration tests .....	49
3.1.3	Full flow ball penetrometer tests.....	49
3.1.4	Electronic vane shear tests .....	51
3.1.5	Pressuremeter tests.....	52
3.2	Geotechnical Laboratory Element Tests.....	53
3.2.1	Direct simple shear tests .....	54
3.2.2	Interface direct shear tests.....	55
3.2.2.1	Direct shear test program .....	56
3.3	Interpretation of Field and Laboratory Test Results.....	59
3.3.1	Undrained shear strength properties .....	60
3.3.2	Shear stiffness properties .....	64
3.3.3	Shear strength and stiffness correlations.....	66

3.3.4	Interface shear properties .....	68
3.4	Summary .....	70
<b>Chapter 4: Soil-Pipe Interaction Physical Modeling Aspects.....</b>		<b>72</b>
4.1	Axial SPI Test chamber .....	74
4.1.1	Loading mechanism .....	76
4.1.2	Instrumentation and data acquisition .....	79
4.1.2.1	Load measurements .....	79
4.1.2.2	Pipe displacements.....	80
4.1.3	Interface shear zone thickness and test-chamber boundary constraints.....	80
4.1.4	Testing program .....	82
4.1.5	Preparation of axial SPI test chamber and test procedure.....	82
4.2	Horizontal SPI test chamber .....	87
4.2.1	Loading mechanism and actuator connections .....	89
4.2.2	Instrumentation and data acquisition .....	92
4.2.2.1	Load measurements .....	93
4.2.2.2	Pipe displacements.....	93
4.2.3	Effect of test chamber boundary constraints (sidewall friction).....	94
4.2.4	Testing program .....	96
4.2.5	Preparation of horizontal SPI test chamber and test procedure .....	96
4.3	Summary .....	99
<b>Chapter 5: Axial and Horizontal Loading Response of Pipes Buried in Organic Soil... 100</b>		
5.1	Axial Loading Response of Pipes Buried in Organic Soil.....	101
5.1.1	Summary of test parameters.....	101

5.1.2	Axial load-displacement response .....	102
5.1.3	Discussion of test results.....	105
5.2	Horizontal Loading Response of Pipes Buried in Organic Soil .....	110
5.2.1	Summary of test parameters.....	111
5.2.2	Characterization of organic soil in chamber-specimens using test-specific penetration testing.....	112
5.2.3	Horizontal load-displacement response .....	115
5.2.4	Visual observations during horizontal pipe displacement tests .....	122
5.3	Summary .....	124
<b>Chapter 6: Constitutive Model for Organic Soil: Selection and Validation of a Model through Numerical Modeling of Pressuremeter .....</b>		<b>126</b>
6.1	Role of Pressuremeter as a Controlled Test Reflecting Mechanical Response of Soil .....	128
6.2	Selection of Constitutive Relationship to Represent Mechanical Response of Organic Soils.....	129
6.3	Finite Difference Modeling of PMT .....	130
6.3.1	Development of mesh configurations .....	131
6.3.2	Soil parameters for numerical modeling of PMT .....	133
6.4	Comparison of Test Results from Field PMT Tests and Numerical Analyses .....	135
6.5	Summary .....	142
<b>Chapter 7: Numerical Modeling of Lateral Soil-Pipe Interaction .....</b>		<b>143</b>
7.1	Numerical Modeling of SPI During Full-Scale Horizontal Pipe Displacement .....	144
7.1.1	Development of mesh configurations .....	144

7.1.2	Soil parameters for numerical analysis .....	147
7.1.3	Modeling of soil-pipe interface.....	148
7.1.4	Numerical analysis steps - application of gravity and pipe displacement .....	149
7.1.5	Comparison of numerical and experimental load-displacement behavior.....	151
7.2	Assessment of the Findings in Relation to Design Practice Guidelines .....	157
7.2.1	Predictions of lateral soil restraint versus displacement curves using numerical analysis.....	158
7.2.1.1	Development of mesh configurations .....	159
7.2.1.2	Soil parameters for numerical analysis .....	160
7.2.1.3	Modeling of soil-pipe interface and stress state prior to pipe displacement .....	162
7.2.2	Development of equivalent bi-linear soil springs from numerically computed p-y curves.....	164
7.2.3	Numerical predictions of load-displacement behavior .....	165
7.3	Summary .....	169
<b>Chapter 8: Summary, Conclusions and Recommendations .....</b>		<b>171</b>
8.1	Overview.....	171
8.2	Summary of the Key Findings and Contributions .....	173
8.2.1	Characterization of organic soil using field and laboratory test program.....	173
8.2.2	Apparatus for lateral and axial SPI physical modeling.....	174
8.2.3	Selection of a Constitutive Model for Numerical Analysis .....	176
8.2.4	Axial soil restraint on buried pipelines .....	177
8.2.5	Lateral soil restraint on buried pipelines.....	178

8.2.5.1	Comparison of bi-linear lateral soil springs from numerical analysis versus PRCI guidelines .....	179
8.2.6	Recommended procedure of developing p-y curves based on the research findings .....	180
8.3	Limitations and Errors Associated with the Present Study.....	182
8.4	Recommendations for Future Work.....	184
<b>Bibliography</b> .....		<b>186</b>
<b>Appendices</b> .....		<b>202</b>
<b>Appendix A Field and Laboratory Test Results</b> .....		<b>202</b>
A.1	Seismic Cone Penetration Test Results .....	203
A.2	Ball Penetration Test Results.....	207
A.3	Electronic Vane Shear Test Results.....	209
A.4	Pressuremeter Test Results.....	211
A.5	Laboratory Index Properties of the Tested Organic Soil .....	215
A.6	Direct Simple Shear Test Results .....	216
A.7	Direct Shear Test Program and Test Results .....	218
<b>Appendix B Effect of Horizontal SPI Test Chamber Size</b> .....		<b>222</b>
B.1	Assessment of Effect of the Horizontal SPI Test Chamber Size Using Numerical Analysis.....	223
<b>Appendix C Full-Scale Physical Modeling Test Results and Photographs</b> .....		<b>228</b>
C.1	Axial Load versus Displacement Response Measured from Full-Scale Tests .....	229
C.2	Test Specific In-place Penetration Tests.....	232
C.3	Photographs Illustrating In-Place Penetration Tests.....	245

<b>Appendix D P-y Curve Comparisons.....</b>	<b>249</b>
D.1 Comparison of P-y Curves Generated Based on the Numerical Predictions and PRCI Guidelines (2009) .....	249
D.2 Comparison of P-y Curves Generated Based on the Numerical Models of the Horizontal Full-Scale Tests and PRCI Guidelines (2009) .....	263
D.3 Additional Analysis to Examine the Sensitivity of $P_u$ - Comparison of p-y Curves Generated Based on the Numerical Models of the Horizontal Full-Scale Tests and PRCI Guidelines (2009) .....	268

## List of Tables

Table 1.1 Research needs to be addressed .....	4
Table 3.1 Summary of test equipment dimensions and test depths of the field investigation program .....	44
Table 5.1 Summary of test parameters: axial soil-pipe interaction tests performed in organic soil .....	101
Table 5.2 Test parameter summary of horizontal soil-pipe interaction tests .....	111
Table 6.1 Summary of input soil parameters used for each of the PMT simulations in FLAC 2D .....	134
Table 7.1 Summary of mesh configurations used in the FLAC 2D modeling of full-scale horizontal pipe displacement.....	146
Table 7.2 Soil strength and stiffness parameters used in the numerical simulations of full-scale horizontal pipe displacement. ....	147
Table 7.3 Summary of peak lateral soil restraint ( $P_u$ ) from full-scale test results and FLAC modeling of full-scale tests .....	157
Table 7.4 Summary of mesh configurations used in the FLAC 2D predictions of lateral soil restraint .....	159
Table 7.5 Soil strength and stiffness parameters used in FLAC 2D predictions of lateral soil restraint .....	162
Table A.1 Index properties of organic soil tested in laboratory test program from Site 01 in Surrey, British Columbia, Canada, and Site 02 in Wabasca, Alberta, Canada .....	215
Table A.2 Direct Shear test program .....	218

Table A.3 Summary of laboratory direct shear test results.....	221
Table C.1 Summary of test equipment dimensions and test depths of in-place BPT, eVST and CPT tests .....	233
Table D.1 Summary of soil spring parameters from PRCI guidelines and FLAC modeling of lateral soil restraint.....	262
Table D.2 Summary of soil spring parameters from PRCI guidelines and FLAC modeling of full-scale horizontal pipe displacement tests .....	267

## List of Figures

Figure 1.1 Modes of relative movements considered for development of SPI p-y curves .....	3
Figure 2.1 Spring analog for analyzing soil-pipe interaction (PRCI 2009) .....	15
Figure 2.2 Recommended bounds for adhesion factor (PRCI 2009) .....	17
Figure 3.1 Location of test site 01: Surrey, British Columbia, Canada from Google maps, by Google <a href="https://www.google.ca/maps/place/Bolivar+Park/">https://www.google.ca/maps/place/Bolivar+Park/</a> .....	45
Figure 3.2 Location of test site 02: Wabasca, Alberta, Canada from Google maps, by Google ( <a href="https://www.google.ca/maps/@55.4055596,-112.701179,6.71z">https://www.google.ca/maps/@55.4055596,-112.701179,6.71z</a> ) .....	46
Figure 3.3 Field geotechnical investigations at Site 01 in Surrey, British Columbia, Canada: (a) Test hole location layout (Plan view); (b) Depth locations of eVST and PMT testing at Test Group 1-01 and Test Group 1-02. Note: Test hole identification numbers are given beside the hole location markings .....	47
Figure 3.4 Field geotechnical investigations at Site 02 in Wabasca, Alberta, Canada: (a) Test hole location layout (Plan view); (b) Depth locations of eVST and PMT testing at Test Group 2-01 and Test Group 2-02. Note: Test hole identification numbers are given beside the hole location markings .....	48
Figure 3.5 a) Illustration of vane attached to the vane roads b) Dimensions of the vane used for testing (ConeTec 2017) .....	52
Figure 3.6 DSS test specimen preparation a) extracting the samples into a stainless-steel ring of 70 mm diameter; b) 70 mm diameter sample placed inside the DSS membrane. ....	55
Figure 3.7 Schematic diagram of the Direct Shear Apparatus (DSA) used to study interface properties between organic soil and pipe surfaces (Note: not to true scale) .....	57

Figure 3.8 (a) Green epoxy coating (GE) and (b) sand blasted mild steel (MS) solid surfaces tested in the DSA.....	58
Figure 3.9 Reconstituted organic soil specimen in the shear box prior to placement of the top loading platen.....	59
Figure 3.10 Variation of undrained shear strength, $s_u$ with depth based on SCPT, BPT, eVST, PMT field tests and laboratory DSS tests at Site 01: (a) Test Group 01 (b) Test Group 02 [ConeTec 2017) and reported in Elmouchi (2021)] .....	62
Figure 3.11 Variation of undrained shear strength, $s_u$ with depth based on SCPT, BPT, eVST and PMT field tests at Site 02: (a) Test Group 01 (b) Test Group 02 (ConeTec 2017) .....	63
Figure 3.12 Variation of small stress shear stiffness, $G_0$ and $G_{ur}$ from first unload-reload from PMT test results with depth at Site 01 in Surrey, British Columbia, Canada: (a) Test Group 01 (b) Test Group 02. ....	65
Figure 3.13 Variation of small stress shear stiffness, $G_0$ and $G_{ur}$ from first unload-reload from PMT test results with depth at Site 02 in Wabasca, Alberta, Canada: (a) Test Group 01 (b) Test Group 02.....	66
Figure 3.14 $G_0$ from $v_s$ measurements versus $s_u$ from eVST based on test data from two Test Sites 01 and 02.....	67
Figure 3.15 Shear stress vs normal stress strength envelopes; a) organic soil - GE and organic soil – MS interfaces, and organic soil alone from Site 01 in Surrey, British Columbia, Canada.....	69
Figure 4.1 Perspective view of the axial soil-pipe interaction test apparatus .....	74
Figure 4.2 Photographs taken (a) before and (b) after installation of the aluminum structure to reinforce the axial SPI test chamber .....	76
Figure 4.3 Loading system and connections of the axial SPI test apparatus: a) Components of the loading system and b) Stepper motor and linear actuator rod connections .....	77

Figure 4.4 Connection of load cell and pipe .....	78
Figure 4.5 Force and displacement measurement sensors attached to the test pipe: a) Load cell; and b) String potentiometer .....	80
Figure 4.6 Photographs showing different steps of the soil bed preparation prior to a test: a) Soil bed preparation before placing the pipe; b) Test pipe lowered on to the soil bed; c) Preparing the sides along the soil-pipe interface; and d) Soil cover preparation .....	84
Figure 4.7 Schematic diagram illustrating a cross section of the test chamber tested for higher overburden stress levels (Note: not true scale) .....	85
Figure 4.8 a) Placement of geotextile on prepared organic soil cover; and b) Preparation of FR sand bed in layers.....	86
Figure 4.9 Final set up of the SPI test chamber prior to axial displacement test.....	87
Figure 4.10 Photographs of horizontal SPI chamber construction stages: a) Construction of the metal frame using box steel bars; b) Construction of the PVC and plexiglass walls and metal platform for equipment mounting; c) Final view of the soil chamber including the actuator system and motor controller system; and d) Installation of the actuator system consisting of an AC motor and linear actuator rod .....	89
Figure 4.11 Loading system of the horizontal SPI test chamber .....	91
Figure 4.12 (a) Load cell and Linear actuator rod connections outside the horizontal SPI test chamber; and (b) Pulling cable and pipe connections inside the horizontal SPI test chamber.....	92
Figure 4.13 String potentiometer placement outside the horizontal SPI test chamber .....	94
Figure 4.14 Photographs showing the process of test soil bed preparation prior to pipe placement: (a) Mixing of organic soil to achieve a relatively uniform soil mix; (b) Soil mixer paddle; (c) Placing the soil in loose lifts of 6-8 inches prior to leveling; and (d) Pipe placement on the prepared soil bed (dense) before placing the soil cover.....	97

Figure 4.15 Photographs showing the process of test soil bed preparation after pipe placement: (a) Connecting the pipe and pulling cables; (b) Placing the soil cover in loose lifts of 6-8 inches; (c) Plan view of the SPI test chamber prior to a horizontal pipe displacement test; and (d) Side view of the SPI test chamber prior to a horizontal pipe displacement test..... 98

Figure 5.1 Response of normalized axial soil restraint versus displacement during axial loading tests conducted in organic soil ..... 104

Figure 5.2 Comparison of normalized axial soil restraint versus displacement response of repeated and original tests of the axial pipe displacement test series..... 105

Figure 5.3 Response of normalized axial soil restraint versus displacement during test A1-4-2.5-260 and the corresponding curve determined based on PRCI (2009) guidelines. .... 107

Figure 5.4 Response of normalized axial soil restraint versus displacement during tests A2-4-4.0-240 and A6-4-4.0-240-2 and the corresponding curve determined based on PRCI (2009) guidelines. .... 107

Figure 5.5 Response of normalized axial soil restraint versus displacement during tests A3-4-6.0-230 and A7-4-6.0-200-2 and the corresponding curve determined based on PRCI (2009) guidelines ..... 108

Figure 5.6 Response of normalized axial soil restraint versus displacement during test A4-4-8.5-280 and the corresponding curve determined based on PRCI (2009) guidelines ..... 108

Figure 5.7 Response of normalized axial soil restraint versus displacement during tests A5-4-10.5-260 and A8-4-10.5-240-2 and the corresponding curve determined based on PRCI (2009) guidelines. .... 109

Figure 5.8 Comparison of the normalized peak axial soil restraint from PRCI guidelines (2009) and full-scale experiments presented in Figures 5.3 through 5.7. .... 110

Figure 5.9 Correlation between  $s_u$  inferred from BPT data versus moisture content of the test organic soil..... 115

Figure 5.10 Load-displacement response measured from Test H1-6-1.9-1.5-360 and the corresponding bi-linear curve determined based on PRCI (2009).....	117
Figure 5.11 Load-displacement response measured from Test H2-6-3.5-2.0-340 and the corresponding bi-linear curve determined based on PRCI (2009).....	118
Figure 5.12 Load-displacement response measured from Test H6-8-1.6-9.8-200 and the corresponding bi-linear curve determined based on PRCI (2009).....	118
Figure 5.13 Load-displacement response measured from Tests H5-8-1.6-9.8-210 and H6-8-1.6-9.8-200 and the corresponding bi-linear curve determined based on PRCI (2009).....	119
Figure 5.14 Load-displacement response measured from Test H7-6-1.9-9.8-220 and the corresponding bi-linear curve determined based on PRCI (2009).....	119
Figure 5.15 Load-displacement response measured from Test H3-6-2.9-5.9-270 and the corresponding bi-linear curve determined based on PRCI (2009).....	120
Figure 5.16 Load-displacement response measured from Test H4-8-1.9-7.3-250 and the corresponding bi-linear curve determined based on PRCI (2009).....	120
Figure 5.17 Comparison of the peak soil restraint ( $P_u$ ) determined from PRCI guidelines (2009) and measured during full-scale experiments extracted from Figures 5.10 through 5.16.....	121
Figure 5.18 a) – f) Backfill soil deformation during Test H6-8-1.6-9.8-200 from 0 to 300 mm of pipe displacement. Note: Arrows show the direction of pipe displacement and the lines are sketched based on the visual observations through the plexiglass during testing. The information is presented to provide an understanding of the approximate failure mechanisms developed during lateral soil restraint testing .....	123
Figure 5.19 Top soil surface deformation at the end of Test H6-8-1.6-9.8-200.....	124

Figure 6.1 Schematic of the two-dimensional FLAC axi-symmetric model with a uniform mesh of size 70 x 49 elements covering a 3.5 m (wide) x 2.5 m (high) area to represent the soil domain tested in pressuremeter tests..... 132

Figure 6.2 Horizontal displacement contours after application of uniform displacement rate along the length of PMT boundary: Model PMT 1-01 350..... 134

Figure 6.3 The lateral pressure versus radial displacement comparison of field PMT and FLAC analyses at Site 01: Test Group 01 at 3.50 m depth below the ground surface ..... 135

Figure 6.4 The lateral pressure versus radial displacement comparison of field PMT and FLAC analyses at Site 01: Test Group 01 at 4.80 m depth below the ground surface ..... 136

Figure 6.5 The lateral pressure versus radial displacement comparison of field PMT and FLAC analyses at Site 01: Test Group 01 at 6.50 m depth below the ground surface ..... 136

Figure 6.6 The lateral pressure versus radial displacement comparison of field PMT and FLAC analyses at Site 01: Test Group 02 at 3.50 m depth below the ground surface ..... 137

Figure 6.7 The lateral pressure versus radial displacement comparison of field PMT and FLAC analyses at Site 01: Test Group 02 at 5.05 m depth below the ground surface ..... 137

Figure 6.8 The lateral pressure versus radial displacement comparison of field PMT and FLAC analyses at Site 01: Test Group 02 at 6.50 m depth below the ground surface ..... 138

Figure 6.9 The lateral pressure versus radial displacement comparison of field PMT and FLAC analyses at Site 02: Test Group 01 at 1.35 m depth below the ground surface ..... 138

Figure 6.10 The lateral pressure versus radial displacement comparison of field PMT and FLAC analyses at Site 02: Test Group 01 at 4.50 m depth below the ground surface ..... 139

Figure 6.11 The lateral pressure versus radial displacement comparison of field PMT and FLAC analyses at Site 02: Test Group 02 at 1.50 m depth below the ground surface ..... 139

Figure 6.12 The lateral pressure versus radial displacement comparison of field PMT and FLAC analyses at Site 02: Test Group 02 at 3.20 m depth below the ground surface .....	140
Figure 6.13 The lateral pressure versus radial displacement comparison of field PMT and FLAC analyses at Site 02: Test Group 02 at 4.25 m depth below the ground surface .....	140
Figure 7.1 Example schematic of dimensions and extent of the (30 x 80) mesh considered for the 2D FLAC model for lateral pipe displacement analysis of NPS6 pipe and H/D ratio of 1.6 (Model: F H6-8-1.6-9.8-200).....	146
Figure 7.2 Total stress contours prior to pipe displacement; a) vertical and b) horizontal for NPS 6 pipe and H/D ratio of 1.6 (Model: F H6-8-1.6-9.8-200).....	150
Figure 7.3 Comparison of lateral load-displacement behavior from FLAC analyses and full-scale test results; Test configuration: H1-6-1.9-1.5-360.....	153
Figure 7.4 Comparison of lateral load-displacement behavior from FLAC analyses and full-scale test results; Test configuration: H2-6-3.5-2.0-340.....	153
Figure 7.5 Comparison of lateral load-displacement behavior from FLAC analyses and full-scale test results; Test configuration: H6-8-1.6-9.8-200.....	154
Figure 7.6 Comparison of lateral load-displacement behavior from FLAC analyses and full-scale test results; Test configuration: H3-6-2.9-5.9-270.....	154
Figure 7.7 Comparison of lateral load-displacement behavior from FLAC analyses and full-scale test results; Test configuration: H4-8-1.9-7.3-250.....	155
Figure 7.8 Comparison of lateral load-displacement behavior from FLAC analyses and full-scale test results; Test configuration: H5-8-1.6-9.8-210.....	155
Figure 7.9 Comparison of lateral load-displacement behavior from FLAC analyses and full-scale test results; Test configuration: H7-6-1.9-9.8-220.....	156

Figure 7.10 Comparison of the peak soil restraint ( $P_u$ ) from full-scale experiments and FLAC analyses cases presented in Figures 7.3 through 7.9.....	156
Figure 7.11 Example schematic of dimensions and extent of the (64 x 120) mesh considered for the two-dimensional FLAC model for lateral pipe displacement analysis of NPS12 pipe and H/D ratio of 2 (Model ID: 2_D12_LD_MC).....	160
Figure 7.12 $s_u$ versus $G_0/s_u$ plots based on test data from two test sites and $s_u$ - $G_0/s_u$ combinations as soil input parameters for FLAC simulations of lateral pipe displacement. ....	161
Figure 7.13 Total stress contours prior to pipe displacement; a) vertical and b) horizontal for NPS 12 pipe and H/D ratio of 2 (Model: 2_D12_LD_MC).....	163
Figure 7.14 Schematic showing steps required to obtain bi-linear approximation of lateral soil restraint versus pipe displacement curves from FLAC analyses (Example used herein for the Set A Case 1: $s_u = 25$ kPa and $G_0/s_u = 30$ ; H/D = 2 and NPS36).....	165
Figure 7.15 Comparison between the peak soil restraint ( $P_u$ ) determined based on PRCI guidelines (2009) and numerical parametric analyses. ....	167
Figure 7.16 Graphical representation of correlations between $\Delta_p/D$ and pipe diameter (D) from numerical analyses .....	169
Figure A.1 The variation of tip resistance ( $q_t$ ), sleeve resistance ( $f_s$ ), pore pressure ( $u_2$ ), and shear wave velocity ( $v_s$ ) with depth below the ground surface at Site 01 in Surrey, British Columbia, Canada: Test Group 01 (UBC 2017) .....	203
Figure A.2 The variation of tip resistance ( $q_t$ ), sleeve resistance ( $f_s$ ), pore pressure ( $u_2$ ), and shear wave velocity ( $v_s$ ) with depth below the ground surface at Site 01 in Surrey, British Columbia, Canada: Test Group 02 (UBC 2017) .....	204
Figure A.3 The variation of tip resistance ( $q_t$ ), sleeve resistance ( $f_s$ ), pore pressure ( $u_2$ ), and shear wave velocity ( $v_s$ ) with depth below the ground surface at Site 02 in Wabasca, Alberta, Canada: Test Group 01 (UBC 2017).....	205

Figure A.4 The variation of tip resistance ( $q_t$ ), sleeve resistance ( $f_s$ ), pore pressure ( $u_2$ ), and shear wave velocity ( $v_s$ ) with depth below the ground surface at Site 02 in Wabasca, Alberta, Canada: Test Group 02 (UBC 2017).....	206
Figure A.5 The variation of ball tip resistance ( $q_b$ ) with depth below the ground surface at Site 01 in Surrey, British Columbia, Canada: a) Test Group 01; b) Test Group 02 (UBC 2017) .....	207
Figure A.6 The variation of ball tip resistance ( $q_b$ ) with depth below the ground surface at Site 02 in Wabasca, Alberta, Canada: a) Test Group 01; b) Test Group 02 (UBC 2017) .....	208
Figure A.7 The variation of peak and remolded shear stress with the vane rotation based on eVSTs conducted at Site 01 in Surrey, British Columbia, Canada: (a) Test Group 01; (b) Test Group 02 (UBC 2017).....	209
Figure A.8 The variation of peak and remolded shear stress with the vane rotation based on eVSTs conducted at Site 02 in Wabasca, Alberta, Canada: (a) Test Group 01; (b) Test Group 02 (UBC 2017) .....	210
Figure A.9 Lateral pressure vs radial displacement curves generated from pressuremeter tests conducted at Site 01 in Surrey, British Columbia, Canada: (a) Test Group 01 at 3.50 m; (b) Test Group 01 at 4.80 m; (c) Test Group 01 at 6.50 m depths below the ground surface (UBC 2017) .....	211
Figure A.10 Lateral pressure vs radial displacement curves generated from pressuremeter tests conducted at Site 01 in Surrey, British Columbia, Canada: (a) Test Group 02 at 3.50 m; (b) Test Group 02 at 5.05 m; (c) Test Group 02 at 6.50 m depths below the ground surface (UBC 2017) .....	212
Figure A.11 Lateral pressure vs radial displacement curves generated from pressuremeter tests conducted at Site 02 in Wabasca, Alberta, Canada: (a) Test Group 01 at 1.35 m; (b) Test Group 01 at 4.52 m depths below the ground surface (UBC 2017).....	213

Figure A.12 Lateral pressure vs radial displacement curves generated from pressuremeter tests conducted at Site 02 in Wabasca, Alberta, Canada: a) Test Group 02 at 1.50 m; (b) Test Group 02 at 3.21 m; (c) Test Group 02 at 4.25 m depths below the ground surface (UBC 2017) ..... 214

Figure A.13 DSS Monotonic shear test results at vertical effective stress 20 kPa ..... 216

Figure A.14 DSS Monotonic shear test results at vertical effective stress 30 kPa ..... 217

Figure A.15 Shear stress vs shear displacement at 10, 20, 50 and 100 kPa from interface direct shear tests on; a) Organic soil from Site 01 in Surrey, British Columbia, Canada – GE coating solid test surface and b) Organic soil from Site 01 in Surrey, British Columbia, Canada – MS solid test surface ..... 219

Figure A.16 Shear stress vs shear displacement at 10, 20 and 50 kPa of direct shear tests on organic soil at Site 01 in Surrey, British Columbia, Canada ..... 220

Figure B.1 Comparison of load-displacement behavior using test chambers with different dimensions based on numerical simulations for NPS 8 pipe, H/D 1.9; Test No H4-8-1.9-7.3-250 ..... 224

Figure B.2 Comparison of load-displacement behavior using test chambers with different dimensions based on numerical simulations for NPS 6 pipe, H/D 3.5; Test No H2-6-3.5-2.0-340 ..... 225

Figure B.3 Horizontal total stress contours after 100 mm of horizontal pipe displacement: (a) Numerical model of full-scale Test No H4-8-1.9-7.3-250 and (b) Numerical model simulating a horizontal SPI test chamber of 4 m in length and 1.5 m in height..... 226

Figure B.4 Horizontal total stress contours after 100 mm of horizontal pipe displacement: (a) Numerical model of full-scale Test No H2-6-3.5-2.0-340 and (b) Numerical model simulating a horizontal SPI test chamber of 4 m in length and 1.5 m in height..... 227

Figure C.1 Response of axial pullout load versus displacement during test A1-4-2.5-260..... 229

Figure C.2 Response of axial pullout load versus displacement during tests A2-4-4.0-240 and A6-4-4.0-240-2.....	229
Figure C.3 Response of axial pullout load versus displacement during tests A3-4-6.0-230 and A7-4-6.0-200-2.....	230
Figure C.4 Response of axial pullout load versus displacement during test A4-4-8.5-280.....	230
Figure C.5 Response of axial pullout load versus displacement during tests A5-4-10.5-260 and A8-4-10.5-240-2.....	231
Figure C.6 Variation of $s_u$ with depth during BPT: H1-6-1.9-1.5-360 – Test Locations 1 and 2 .....	234
Figure C.7 Variation of shear stress with vane rotation during eVST at peak and remolded stages: H1-6-1.9-1.5-360 – Test Location 1 .....	235
Figure C.8 Variation of shear stress with vane rotation during eVST at peak and remolded stages: H1-6-1.9-1.5-360 – Test Location 2 .....	235
Figure C.9 The variation of tip resistance ( $q_t$ ), sleeve resistance ( $f_s$ ), friction ration ( $R_f$ ) and pore pressure ( $u$ ) with depth below the ground surface during CPT: H1-6-1.9-1.5-360 – Test Location 1.....	236
Figure C.10 The variation of tip resistance ( $q_t$ ), sleeve resistance ( $f_s$ ), friction ration ( $R_f$ ) and pore pressure ( $u$ ) with depth below the ground surface during CPT: H1-6-1.9-1.5-360 – Test Location 2.....	237
Figure C.11 Variation of $s_u$ with depth during BPT: H2-6-3.5-2.0-340 – Test Locations 1 and 2 .....	238
Figure C.12 Variation of shear stress with vane rotation during eVST at peak and remolded stages: H2-6-3.5-2.0-340 – Test Location 1 .....	239

Figure C.13 Variation of shear stress with vane rotation during eVST at peak and remolded stages: H2-6-3.5-2.0-340 – Test Location 2 .....	239
Figure C.14 The variation of tip resistance ( $q_t$ ), sleeve resistance ( $f_s$ ), friction ratiion ( $R_f$ ) and pore pressure ( $u$ ) with depth below the ground surface during CPT: H2-6-3.5-2.0-340 – Test Location 1.....	240
Figure C.15 The variation of tip resistance ( $q_t$ ), sleeve resistance ( $f_s$ ), friction ratiion ( $R_f$ ) and pore pressure ( $u$ ) with depth below the ground surface during CPT: H2-6-3.5-2.0-340 – Test Location 2.....	241
Figure C.16 Variation of shear stress with vane rotation during eVST at peak and remolded stages: H6-8-1.6-9.8-200 – Test Location 1 .....	242
Figure C.17 Variation of shear stress with vane rotation during eVST at peak and remolded stages: H6-8-1.6-9.8-200 – Test Location 2 .....	242
Figure C.18 The variation of tip resistance ( $q_t$ ), sleeve resistance ( $f_s$ ), friction ratiion ( $R_f$ ), and pore pressure ( $u$ ) and undrained shear strength ( $s_u$ ) with depth below the ground surface during CPT: H6-8-1.6-9.8-200 – Test Location 1 .....	243
Figure C.19 The variation of tip resistance ( $q_t$ ), sleeve resistance ( $f_s$ ), friction ratiion ( $R_f$ ), and pore pressure ( $u$ ) and undrained shear strength ( $s_u$ ) with depth below the ground surface during CPT: H6-8-1.6-9.8-200 – Test Location 2 .....	244
Figure C.20 (a), (b) Square frame moving on linear railings (moving in x, y directions) which is built at UBC to mount the torque head connected to the vane and (c) Torque head mounted on the mobile frame prior to testing.....	245
Figure C.21 (a) Double tapered 60 x 120 mm ( $45^\circ$ , $45^\circ$ ) vane head used for the vane shear tests; (b) and (c) vane mounted on the frame prior to penetrating into the organic soil bed .....	246
Figure C.22 (a), (b) 150 cm <sup>2</sup> ball penetrometer prior to performing the test and (c) ball tip extraction after completion of a test.....	247

Figure C.23 (a) 15 cm<sup>2</sup> (4.37 cm diameter) cone tip used for the cone penetration tests; (b) cone penetrometer mounted on the platform prior to performing the test; (c) cone penetrating into the organic soil bed..... 248

Figure D.1 Horizontal force per unit length versus pipe displacement ( $\Delta_p/D$ ) from FLAC analyses and PRCI guidelines (2009). Analysis Case: Set A Case 1 ( $s_u = 25$  kPa,  $G_0/s_u = 30$ ,  $H/D = 2$ ): (a) NPS 12 pipe; (b) NPS 24 pipe ..... 250

Figure D.2 Horizontal force per unit length versus pipe displacement ( $\Delta_p/D$ ) from FLAC analyses and PRCI guidelines (2009). Analysis Case: Set A Case 1 ( $s_u = 25$  kPa,  $G_0/s_u = 30$ ,  $H/D = 2$ ): (a) NPS 36 pipe; (b) NPS 48 pipe. .... 251

Figure D.3 Horizontal force per unit length versus pipe displacement ( $\Delta_p/D$ ) from FLAC analyses and PRCI guidelines (2009). Analysis Case: Set A Case 2 ( $s_u = 25$  kPa,  $G_0/s_u = 60$ ,  $H/D = 2$ ): (a) NPS 12 pipe; (b) NPS 24 pipe. .... 252

Figure D.4 Horizontal force per unit length versus pipe displacement ( $\Delta_p/D$ ) from FLAC analyses and PRCI guidelines (2009). Analysis Case: Set A Case 2 ( $s_u = 25$  kPa,  $G_0/s_u = 60$ ,  $H/D = 2$ ): (a) NPS 36 pipe; (b) NPS 48 pipe. .... 253

Figure D.5 Horizontal force per unit length versus pipe displacement ( $\Delta_p/D$ ) from FLAC analyses and PRCI guidelines (2009). Analysis Case: Set A Case 3 ( $s_u = 25$  kPa,  $G_0/s_u = 90$ ,  $H/D = 2$ ): (a) NPS 12 pipe; (b) NPS 24 pipe. .... 254

Figure D.6 Horizontal force per unit length versus pipe displacement ( $\Delta_p/D$ ) from FLAC analyses and PRCI guidelines (2009). Analysis Case: Set A Case 3 ( $s_u = 25$  kPa,  $G_0/s_u = 90$ ,  $H/D = 2$ ): (a) NPS 36 pipe; (b) NPS 48 pipe. .... 255

Figure D.7 Horizontal force per unit length versus pipe displacement ( $\Delta_p/D$ ) from FLAC analyses and PRCI guidelines (2009). Analysis Case: Set B Case 1 ( $s_u = 40$  kPa,  $G_0/s_u = 30$ ,  $H/D = 2$ ): (a) NPS 12 pipe; (b) NPS 24 pipe ..... 256

Figure D.8 Horizontal force per unit length versus pipe displacement ( $\Delta_p/D$ ) from FLAC analyses and PRCI guidelines (2009). Analysis Case: Set B Case 1 ( $s_u = 40$ kPa, $G_0/s_u = 30$ , $H/D = 2$ ): (a) NPS 36 pipe; (b) NPS 48 pipe .....	257
Figure D.9 Horizontal force per unit length versus pipe displacement ( $\Delta_p/D$ ) from FLAC analyses and PRCI guidelines (2009). Analysis Case: Set B Case 2 ( $s_u = 40$ kPa, $G_0/s_u = 60$ , $H/D = 2$ ): (a) NPS 12 pipe; (b) NPS 24 pipe .....	258
Figure D.10 Horizontal force per unit length versus pipe displacement ( $\Delta_p/D$ ) from FLAC analyses and PRCI guidelines (2009). Analysis Case: Set B Case 2 ( $s_u = 40$ kPa, $G_0/s_u = 60$ , $H/D = 2$ ): (a) NPS 36 pipe; (b) NPS 48 pipe .....	259
Figure D.11 Horizontal force per unit length versus pipe displacement ( $\Delta_p/D$ ) from FLAC analyses and PRCI guidelines (2009). Analysis Case: Set B Case 3 ( $s_u = 40$ kPa, $G_0/s_u = 90$ , $H/D = 2$ ): (a) NPS 12 pipe; (b) NPS 24 pipe .....	260
Figure D.12 Horizontal force per unit length versus pipe displacement ( $\Delta_p/D$ ) from FLAC analyses and PRCI guidelines (2009). Analysis Case: Set B Case 3 ( $s_u = 40$ kPa, $G_0/s_u = 90$ , $H/D = 2$ ): (a) NPS 36 pipe; (b) NPS 48 pipe .....	261
Figure D.13 Comparison of bi-linear p-y curves generated using PRCI (2009) and FLAC analyses results; Test configuration: H1-6-1.9-1.5-360 .....	264
Figure D.14 Comparison of bi-linear p-y curves generated using PRCI (2009) and FLAC analyses results; Test configuration: H2-6-3.5-2.0-340 .....	264
Figure D.15 Comparison of bi-linear p-y curves generated using PRCI (2009) and FLAC analyses results; Test configuration: H6-8-1.6-9.8-200 .....	265
Figure D.16 Comparison of bi-linear p-y curves generated using PRCI (2009) and FLAC analyses results; Test configuration: H3-6-2.9-5.9-270 .....	265
Figure D.17 Comparison of bi-linear p-y curves generated using PRCI (2009) and FLAC analyses results; Test configuration: H4-8-1.9-7.3-250 .....	266

Figure D.18 Comparison of bi-linear p-y curves generated using PRCI (2009) and FLAC analyses results; Test configuration: H7-6-1.9-9.8-220 ..... 266

Figure D.19 Comparison of lateral load-displacement behavior from FLAC analyses and full-scale test results – sensitivity analysis; Test configuration: H3-6-2.9-5.9-270 ..... 268

Figure D.20 Comparison of lateral load-displacement behavior from FLAC analyses and full-scale test results – sensitivity analysis; Test configuration: H4-8-1.9-7.3-250 ..... 269

Figure D.21 Comparison of lateral load-displacement behavior from FLAC analyses and full-scale test results – sensitivity analysis; Test configuration: H5-8-1.6-9.8-210 ..... 269

Figure D.22 Comparison of lateral load-displacement behavior from FLAC analyses and full-scale test results – sensitivity analysis; Test configuration: H6-8-1.6-9.8-200 ..... 270

## List of Symbols

B	Bulk modulus
c	Shear strength intercept of soil failure envelope
d <sub>50</sub>	Median particle size
D	Outer diameter of pipe
F <sub>A</sub>	Axial soil restraint
F' <sub>A</sub>	Dimensionless axial soil restraint
G	shear modulus
G <sub>0</sub>	Small strain shear modulus
G <sub>ur</sub>	Shear modulus determined based on unload-reload cycles of PMT
H	Burial depth to pipe centerline
K <sub>0</sub>	Coefficient of lateral earth pressure at rest
N <sub>ball</sub>	Undrained shear strength factor for su based on net ball tip resistance
N <sub>ch</sub>	Horizontal bearing capacity factor for clay
N <sub>h</sub>	Horizontal bearing capacity factor
N <sub>kt</sub>	Undrained shear strength factor for su based on net cone tip resistance
N <sub>qh</sub>	Horizontal bearing capacity factor for sand
N <sub>yu</sub>	Dimensionless factor depending on the embedment of the pipe
P	Horizontal soil restraint
$\bar{p}$	Normalized horizontal soil restraint
P <sub>u</sub>	Peak horizontal soil restraint

$q_c$	Measured cone tip resistance
$q_{net}$	Net tip resistance
$S_t$	Soil sensitivity defined as the ratio of the undrained shear strength of undisturbed soil to the undrained shear strength of remolded soil at the same water content
$s_u$	Undrained shear strength
$T_u$	Peak axial soil restraint
$v_s$	Shear velocity
$y$	Pipe displacement
$\alpha$	Adhesion factor used in soil-pipe interaction analysis using the total stress based approach
$\gamma$	Average bulk unit weight of soil
$\gamma'$	Average effective unit weight of the soil
$\Delta$	Pipe displacement
$\delta$	Soil-pipe interface friction angle
$\Delta_p$	Pipe displacement at peak horizontal soil restraint
$\Delta_t$	Pipe displacement at peak axial soil restraint
$\nu$	Poisson's ratio
$\sigma_0$	Initial vertical stress
$\sigma_n$	Average total normal stress acting on the soil-solid interface
$(\sigma'_n)_{av}$	Average effective normal stress on the pipe
$\sigma'_v$	Effective overburden stress
$\sigma'_{vo}$	Initial effective overburden stress

$\phi'$

Effective friction angle of soil

## List of Abbreviations

BPT	Ball Penetration Test
CPT	Cone Penetration Tests
DEM	Discrete Element Modeling
DS	Direct Shear
DSA	Direct Shear Apparatus
DSS	Direct Simple Shear
eVST	Electronic Vane Shear Test
FD	Finite Difference
FDM	Finite Difference Modeling
FEM	Finite Element Modeling
FLAC	Fast Lagrangian Analysis of Continua
FR	Fraser River
GE	Green Epoxy
LC	Load Cell
LVDT	Linear Variable Differential Transformer
MS	Mild Steel
NPS	Nominal Pipe Size
PMT	Pressuremeter Test
PVC	Poly-vinyl chloride
SCPT	Seismic Cone Penetration Test

SPI            Soil-Pipe Interaction  
UBC            University of British Columbia

## **Acknowledgements**

My heartfelt gratitude goes to Dr. Dharma Wijewickreme, my research supervisor, whose steadfast support, invaluable guidance, and extensive knowledge not only made this work possible but also shaped me as a professional. His words of encouragement and unwavering patience provided a constant source of motivation, especially during the challenging phases of my research. I am genuinely thankful for his friendly and supportive mentorship.

I would like to express my gratitude to the members of the supervisory committee, Dr. John Howie and Dr. Sumi Siddiqua, for their valuable comments and suggestions. I highly appreciate their extensive expertise, encouragement, and support throughout my research work and the process of preparing this dissertation. The valuable insights and kind support provided by Dr. Sadana Gamage, Dr. Prajakta Jadhav, and Dr. Devdeep Basu are thankfully appreciated.

The success of this research program owes much to the generous financial support extended by the Natural Sciences and Engineering Research Council of Canada (NSERC) and esteemed industry partners of the Pipeline Integrity Institute (PII) at The University of British Columbia. Also, I want to convey my appreciation to Dr. Bill Liu from TC Energy and Ilmar Weemee from ConeTec Investigations Ltd. for their invaluable technical support and kind assistance throughout the duration of this research. Further, the in-kind technical support extended by ConeTec Investigations Ltd, Richmond, during the geotechnical site investigations at the test research sites, and full-scale testing conducted at UBC is greatly appreciated.

Technical assistance received from UBC Civil Engineering Workshop personnel including Messers Doug Hudniuk, Scott Jackson, Mehrtash Motamedi, Arthur Mak, Bill Leung, Simon Lee, Harald Schrempp, John Wong, Shota Inoda, and Jun Sang Song is immensely valued and

appreciated. Thanks are also due to Zander Pierson and Johnson Li for their immense support during full-scale SPI testing.

I extend my sincere gratitude to my friends and colleagues at Rust Hut Geotech Lab, Achala soya, Ana Valverde, Ruslan Amarasinghe, Simon Wong, Priyesh Verma, Caroline Zulkoski, Michelle Wesolowski, Vinoth Ganapathiraman, Sara Ataii, Vincent McClelland, Sanjei Chithravel, Ilaibi Omunguye, Zarnain Fayaz, Yassein Keshty for their warm support, engaging discussions, and enjoyable moments both within the lab and beyond. Friends I met and/or reunited at UBC and Vancouver, Swapna Premasiri, Thamali Kariyawasam, Poornima Gayangi and Shashikala Rathnayake are remembered fondly. Prabuddi Kalpana, Damithri Melegoda, Manu Nirasha and Chathurika Wijekoon hold a special place despite the distance that kept us apart.

I extend my deepest gratitude to my parents for their love, support, and unwavering faith in me, and I am grateful for the love and comfort my little sisters Gayathri and Ruwanthi have always provided.

I would like to thank my husband Asela for his love, patience, and sacrifices. My work at UBC would not be possible without him and I cannot thank him enough for being my rock and guiding light.

පිටුම

අම්මාටත් තාත්තාටත් ආදරෙන්

# **Chapter 1: Introduction**

## **1.1 Research Background**

Pipelines offer one of the safest ways of transporting fluids over large distances, and buried pipeline systems form a key part of Canadian oil and gas transportation infrastructure. Geotechnical hazards arising from soil movements due to landslides, earthquakes, slope movements, adjacent earthworks, ground subsidence, etc., along pipeline corridors have the potential to impact and cause unacceptable strains in buried pipelines. Any significant disruption to the performance of these systems often translates into undesirable impacts on the health and safety and living conditions of citizens, the environment, and regional economies.

Over 1.5M km<sup>2</sup> of the Canadian landscape is covered with muskeg which is soft in stiffness and weak in strength. The term “muskeg” is commonly used in North America, referring to organic soils concerning vegetation cover, sub-surface soil, and topographical characteristics. This term originated from Chippewa First Nation word “maskeg” which directly translates to “grassy bog” and has evolved in its use (Radforth 1969). Due to the abundance of muskeg in Canada, many of the energy pipelines cross areas covered with these soils. Thermal changes arising due to operational and environmental reasons has been recognized as a threat to the structural integrity and safety of buried oil and gas pipeline systems in organic soils such as muskeg. In particular, thermally induced large deformations tend to cause buckling and potential integrity concerns of pipelines because of the low restraint between the pipe and the surrounding soil at locations of pipe direction change, i.e., at bends, elbows, etc. As indicated in Pipeline Research Council International - PRCI - guidelines (PRCI 2009) for constructing pipelines in areas subject to

geotechnical hazards, subsidence occurring due to drainage and the associated potential for upheaval buckling of buried pipelines in organic soils is another valid concern. The engineering design of pipelines in these terrains involves many challenges, some arising mainly due to the lack of understanding of the mechanical behavior of organic soils. These concerns are of great relevance to the pipeline sector due to the direct and significant benefits arising from the reduced risk of pipeline damage and enhanced safety. In particular, the pipeline owners and operators and engineers are interested in new systematic approaches to solve design problems related to buried pipelines in organic soil terrain (Marshall and Ruban 1983, Oswell 2002).

These broad considerations formed the backdrop and impetus for the research work undertaken in this thesis. The problem statement in this regard, and proposed tasks are described below.

## **1.2 Problem Statement**

The need for advancing the understanding of mechanical behavior of organic soils and the associated response of pipelines buried in such soils under anticipated operating and environmental conditions is significant. Several key knowledge gaps have constrained the development of soil-pipe interaction (SPI) assessment methodologies for the engineering design of buried pipelines in organic soils. For example, there are well-established engineering approaches available from pipeline design guidelines such as PRCI (2009) and ALA (2001) to determine the soil force versus relative pipe displacement relationships (usually expressed as p-y curves or “soil springs”) when relative ground movements occur in pipelines buried in coarse-grained or fine-grained mineral soils. These guidelines categorize the soil springs as axial, lateral, vertical uplift, and vertical

bearing, depending on the direction of soil displacement relative to the pipeline (see Figure 1.1) and provide p-y curves in the respective directions for soil-pipe interaction (SPI) analysis.

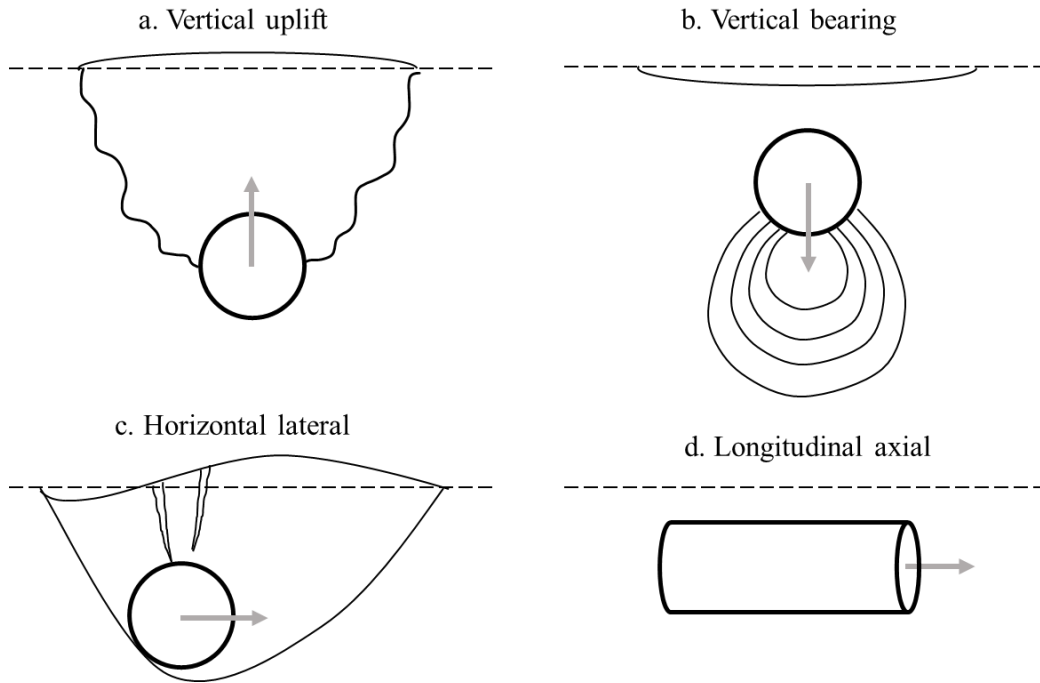


**Figure 1.1 Modes of relative movements considered for development of SPI p-y curves**

Presently, these guidelines are directly used in industry practice for developing soil springs for design of pipeline buried in soft and weak organic soils in spite of the fact that the applicability of these approaches to such soils have not been assessed or validated in a systematic way. As a result, pipeline designs in organic soils are often conducted with significant conservatism.

Difficulties in obtaining reliable information on the shear stiffness and strength parameters of organic soils, further heightened by their in situ spatial variability and difficulties in field geotechnical investigations, are main contributors to the present engineering issues faced by the profession. There is a need to address these considerations during the engineering analysis of SPI

problems; for example, specific attention need to be paid in using effective versus total stress approaches in formulating the related boundary value problems. In addition to the stress-strain response of organic soils alone, it is also essential to obtain insights on pipe soil interaction mechanisms during relative ground deformations to address this complex real life problem. Often, this requires conducting physical modeling to obtain the needed data for numerical modeling of SPI and associated interpretations; again, there has not been any systematic experimentation and associated analysis undertaken on this front.

### 1.3 Scope and Research Objectives

The main objective of this research is to advance the knowledge on the methodologies to assess the soil-pipe interaction (SPI) response of buried pipelines in organic soils subjected to relative ground movements. This objective, with the background presented above, led to the identification of a number of research needs to be addressed during the present doctoral research as summarized in Table 1.1 and briefly described below.

**Table 1.1 Research needs to be addressed**

Research needs	Approach to address identified research need
(a) Characterization of organic soils:	<ul style="list-style-type: none"> <li>• Identify relatively simple and cost-effective methods for in situ characterization</li> <li>• important to use tools that would capture the “bulk” behavior of soft and weak organic soils.</li> <li>• conduct specialized tests that would invoke well-defined boundary value problem - for numerical analysis to assess</li> </ul>

	and validate suitable stress-strain models to represent organic soils
(b) Understanding SPI mechanisms in organic soils:	<ul style="list-style-type: none"> <li>• Develop full-scale physical testing equipment to obtain high quality experimental data on axial and lateral loading SPI mechanisms in pipes buried in organic soil.</li> <li>• Conduct axial pullout and lateral soil restraint tests using the test devices.</li> <li>• Use experimental data from physical modeling for validating numerical modeling frameworks</li> </ul>
(c) Selection of a suitable constitutive model for organic soils:	<ul style="list-style-type: none"> <li>• Numerical modeling of a field test situation comprising a well-defined boundary value problem [e.g., pressuremeter tests as per (a) above].</li> <li>• Use numerical modeling to select and validate a reasonable stress-strain (constitutive) model to represent organic soils in the modeling, and then use that model to simulate SPI problems.</li> </ul>
(d) Numerical modeling of lateral SPI:	<ul style="list-style-type: none"> <li>• Analyze the tested physical model configurations numerically and then compare the outcomes with experimental results</li> <li>• Use this basis to validate and develop representative numerical frameworks to investigate the lateral SPI problem in detail.</li> </ul>
(e) Applicability of current practice guidelines to assess lateral SPI of pipes buried in organic soils:	<ul style="list-style-type: none"> <li>• Use the numerical framework as per (d) above to simulate the lateral SPI problem under different organic soil strength and stiffness levels and pipe configurations.</li> <li>• Compare the lateral soil restraint p-y curves from numerical analysis with those from current practice guidelines. Using this approach, assess the suitability of current guidelines to assess the lateral SPI of pipes buried in organic soils.</li> </ul>

(a) Characterization of organic soils:

In general, there is a need to undertake relatively simple and cost-effective methods to characterize the soils for design and assessment of pipelines that extend through long distances. A significant volume of soil in the vicinity of the pipe would get mobilized when pipelines are subjected to relative lateral movements [see Figure 1.1 (a), 1.1 (b), and 1.1 (c)]; therefore, it would be important to identify soil characterization tools that would capture the “bulk” behavior of soil, especially in the presence of spatially variable, soft, and weak, organic soils.

From a research point of view, it would be useful to also conduct specialized in situ testing that mobilizes a bulk mass of soil while invoking a well-defined boundary value problem – e.g., pressuremeter test that simulates a well-defined cavity expansion problem. The idea herein is that such an in situ test could be meaningfully modeled numerically, and in turn, this would allow to assess and validate suitable stress-strain models for use in the numerical models that would be investigated as a part of this research.

(b) Understanding the SPI mechanisms in organic soils:

Understanding the complex SPI mechanisms in organic soils is critical in addressing the overall research objective. Observations and data from physical modeling under controlled conditions play a critical role in developing this understanding. This gives rise to the need to develop two full-scale physical testing equipment to obtain high quality experimental data on axial and lateral loading SPI mechanisms in pipes buried in organic soil; a series of axial pullout and lateral soil restraint tests were then conducted in these two newly developed testing devices, respectively.

Experimental data from these physical model tests provides the basis for validating (as well as providing some of the input needed) for numerical modeling specifically related to lateral loading of pipelines in organic soils.

(c) Selection of a suitable constitutive model for organic soils:

It was recognized prudent to select a reasonable and relatively simple material stress-strain (constitutive) model that is commensurate with the high spatial variability and non-homogeneity of organic soils along pipeline corridors extending over long-distances. With this factor in mind, it was considered that numerical modeling of a field test comprising a well-defined boundary value problem would be suitable to address this need. This was accomplished by numerically simulating field cases of pre-bored pressuremeter tests (PMTs) conducted at two geotechnical test sites [see Section (a) above]. The outcomes provided a basis to select a reasonable stress-strain (constitutive) model to represent organic soils in the modeling, and the selected constitutive model was used to simulate SPI problems.

(d) Numerical modeling of lateral SPI:

It was identified that the physical model lateral pipe loading configurations tested [as per (b) above] should be numerically analyzed and the outcomes compared with those from experiments to validate and develop representative numerical model representing the underlying SPI mechanics problem under lateral loading. The developed model could then be used as a framework for

investigation of the lateral SPI problem in detail. The research was accomplished using the commercially available finite difference software FLAC (Itasca 2016).

(e) Applicability of current practice guidelines to assess lateral SPI of pipes buried in organic soils:

The numerical framework developed as per (d) above was used to simulate the lateral SPI problem under different organic soil strength and stiffness levels as well as pipe diameter and depths of burial configurations. The lateral soil restraint p-y curves arising from the developed SPI model was then used to compare with those derived from current practice guidelines. Using this approach, the suitability of the recommended guidelines PRCI (2009) to assess the lateral SPI of pipes buried in organic soils was studied.

#### **1.4 Specific Research Tasks**

Based on the above, the following specific research tasks were undertaken to address the main objectives of this thesis:

- i. Effective characterization of organic soil to obtain strength and stiffness parameters for the SPI analysis and development of empirical (or semi-empirical) correlations between strength and stiffness properties of organic soil based on the field test data for SPI analysis.
- ii. Selection of a meaningful stress-strain (constitutive) model to simulate the soil-pipe interaction for pipes buried in organic soils while keeping to a practical and cost-effective engineering process.
- iii. Validation of the developed soil-pipe interaction model to justify its suitability for engineering evaluations using full-scale physical testing results.

- iv. Numerical predictions of lateral soil restraint using the validated numerical framework for further understanding of SPI in organic soil.

## **1.5 Thesis Outline**

This thesis is presented in eight chapters and four appendices in the thesis that are outlined as below:

Chapter 1 introduces the research background, identifies overall objective, and presents the problem statement, along with identified research tasks, and details on the organization of the thesis.

Chapter 2 reviews the current state of knowledge on pipelines subjected to ground deformations with a specific focus on horizontal and axial soil-pipe interaction and the design guidelines and current approaches used to determine soil restraints on buried pipes. Further it addresses the mechanical behavior of organic soil for SPI analysis with a main focus on the stress-strain characteristics and summarizes the knowledge gaps and basis for the identified scope and objectives of the current study.

Details of the field geotechnical investigations with an array of field sampling conducted at two organic soil research sites and associated laboratory testing are presented in Chapter 3. The approaches used to characterize the soil based on the performed field tests and interpreted shear strength and stiffness properties are also presented.

Chapter 4 presents the newly developed axial and lateral full-scale testing chambers and details of the design works, test setups, loading mechanisms, and data acquisitions systems. Experimental

aspects related to the tests conducted in the new testing chambers are also presented with details on soil specimen (test bed) preparation procedures for the respective physical modeling tests.

Discussions of full-scale axial and horizontal pipe displacement test results and soil restraint versus pipe displacement responses are presented in Chapter 5.

Chapter 6 discusses the numerical analysis undertaken using FLAC finite-difference software to select and validate the constitutive model - based on the strength and stiffness characterization of bulk organic soil mass from field geotechnical characterization tools. In this regard, details of the numerical analysis performed to validate the selected constitutive model by simulating the data from field PMT tests is presented along with the results.

Chapter 7 presents details and results of the FLAC numerical model developed to simulate lateral soil-pipe interaction and comparison of the numerically generated p-y curves, the full-scale test results and curves developed using PRCI guidelines (2009).

Chapter 8 summarizes the work undertaken and highlights the important findings and conclusions arising from the research, along with recommendations on developing p-y curves based on the research findings. Limitations of the study and recommendations for future work and improvements are also presented.

Appendix A presents the field and laboratory test results plots and test results summaries from seismic cone penetration tests, ball penetration tests, electronic vane shear tests, pressuremeter tests, direct simple shear tests and direct shear tests.

Details of FLAC 2D numerical modeling utilized to assess the impact of boundary conditions and size of the horizontal test chamber during the design and fabrication stage of the test chamber is presented in appendix B.

Appendix C compiles measured load-displacement behavior from axial pipe pullout tests and test-chamber-specific in place penetration test results and photographs during physical model tests. Comparisons between the bi-linear horizontal p-y (soil spring) curves developed using the numerical predictions and PRCI guidelines (2009) are presented in Appendix D.

## **Chapter 2: Literature Review and Research Scope Development**

The first section of this chapter covers current knowledge on buried pipelines subjected to ground deformations with a specific focus on relative axial and horizontal soil movements. In particular, past experimental and numerical studies carried out to study the soil restraints on buried pipelines subjected to different modes of ground displacement are presented. The current engineering design practice related to soil-pipe interaction (SPI) analysis is then reviewed with respect to design guidelines and current approaches used to determine soil restraints on buried pipes. While keeping in mind that the past focus has been mainly on pipelines buried in mineral soils (e.g., sands and clays), this chapter then focuses on the available information on the performance and design of buried pipelines in organic soils. The final section concentrates on the stress-strain characteristics of organic soil since it is an important input for the SPI analysis of pipelines buried in organic soil – which is the ultimate objective of the current study. The chapter concludes by highlighting the knowledge gaps and building the case to conduct the needed research to advance the understanding of the performance of buried pipelines in organic soils subjected to ground movements.

## 2.1 Soil Restraints on Buried Pipelines Subjected to Relative Ground Movement

Buried pipelines traverse in a wide variety of soil terrains extending over large geographical regions. As discussed in Chapter 1, pipelines located in areas subject to ground displacements may experience potentially high soil loads, in turn, leading to unacceptable strains in pipe sections. Permanent ground displacements could arise due to different natural hazards such as earthquakes, slope instability, landslides, and creeping ground as well as construction activities. In particular, earthquake-induced geotechnical hazards include: surface fault movements, lateral spreading of liquefied ground, ground settlements due to liquefaction, bearing capacity failures, etc. Apart from the ground displacements due to geo-hazards, pipe movements due to thermally induced large deformations, and poor ability of the soil embedment to support and restrict pipe movement are other aspects to be considered in the design of pipelines.

A given buried pipeline can be subject to 3-dimensional relative soil movements with respect to the pipeline alignment as illustrated in Figure 1.1: a) vertical-uplift; b) vertical-bearing; c) horizontal-lateral; d) longitudinal-axial. The soil restraints on the pipelines developed due to one or a combination of these movements are accounted for in the assessment of soil-pipe interaction (SPI). The soil restraints can lead to bending, shear, tension, or compression in pipe sections which in turn can lead to pipeline strain demands exceeding the structural strain capacity of the pipe. The outcomes of numerous analytical, experimental, and numerical investigations on this subject have led to the establishment of pipeline design guidelines, and these guidelines mainly provide recommendations to assess the levels of soil restraints (i.e., force-displacement curves, or soil-spring curves, or P-y curves) as input to analyzing the SPI problems.

American Society of Civil Engineers (ASCE 1984) was one of the earliest to establish design guidelines for buried pipelines, followed by the American Lifelines Alliance (ALA 2001) in North America. Pipeline Research Council International (PRCI 2009) provides the most recent design guidelines considering SPI. It suggests load-displacement curves in axial, lateral, and vertical directions for soil-pipe interaction analysis. In current practice, soil-pipe interaction problems are widely modeled and analyzed as pipe elements attached to soil spring elements. Herein, the pipe is represented by structural beam elements while the soil response is idealized by discrete, nonlinear soil springs representing soil loads acting on the pipeline along three orthogonal axes as shown in Figure 2.1. Similar to common assumption for the analytical representation of pile foundations and similar buried structures, the pipeline design techniques assume that the equivalent springs perform independent of each other.

There exists much uncertainty in determining soil springs depending on the assumptions behind the design guidelines and the complexity of the engineering problem. However, horizontal, and axial soil restraints represent the most studied cases of soil-pipe interaction problems, and understanding of load-displacement behavior is critical in defining these soil springs for design purposes.

A wide range of research undertaken to study the development of soils restraints on buried pipelines subject to ground displacement relative while accounting for the effects of soil type, pipe material and coating, burial mode, burial depth, trench geometry, etc. was reported in past literature. It is of relevance to note that the focus of much of these studies has been the SPI of pipelines buried in mineral soils, and not for those in very soft and weak organic soils.

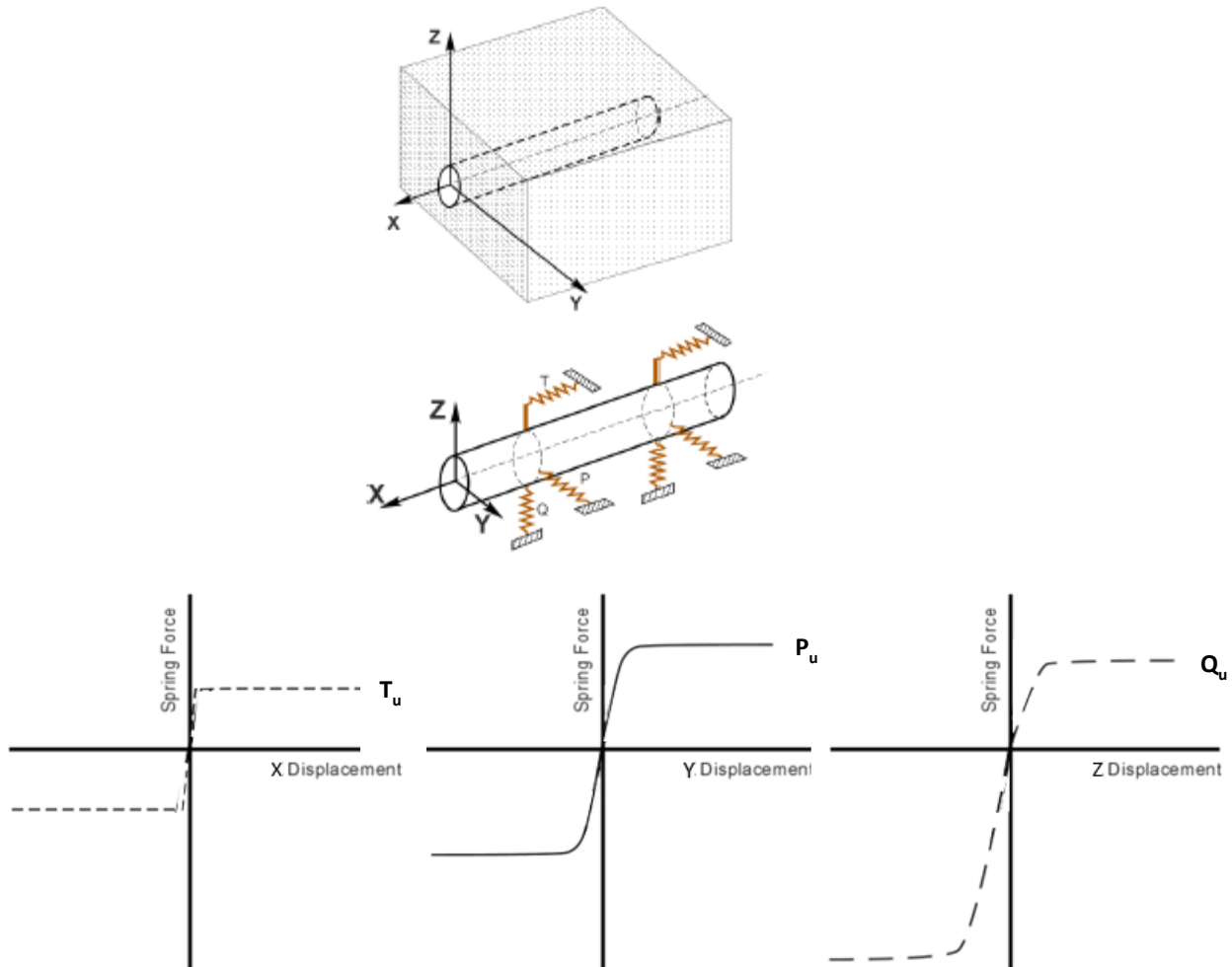


Figure 2.1 Spring analog for analyzing soil-pipe interaction (PRCI 2009)

### 2.1.1 Axial soil restraints on buried pipes

In SPI analysis, axial soil springs are represented by bi-linear force-displacement relationships, and the approach is similar to that used in the design of pile foundations (API 2011). The peak axial soil restraint caused by axial movement of the pipe relative to the surrounding soil is estimated based on the well-established: (i) effective stress based  $\beta$ -method (is related to the effective interface friction angle); or (ii) total stress based  $\alpha$ -method [where the soil-pipe interface

shear strength is related to the undrained shear strength ( $s_u$ ) of the soil through an empirical adhesion factor ( $\alpha$ ]. Depending on the rate of relative soil-pipe displacement, the axial soil-pipe interaction response in real-life can be undrained, drained, or partially drained, particularly in fine grained soils.

Design guidelines such as ALA (2001) and PRCI (2004, 2009) recommend using the Equation 2.1 below for estimating axial soil restraint while using Figure 2.2 to select appropriate  $\alpha$ . Further, recommendations for displacement ( $\Delta_t$ ) at  $T_u$  are given as 3 mm for dense sand, 5 mm for loose sand, 8 mm for stiff clay, and 10 mm for soft clay based on previous studies conducted by researchers.

$$T_u = \pi D \alpha s_u \quad 2.1$$

According to Equation 2.1,  $T_u$  is the maximum axial soil load caused by the axial movement of the pipe relative to the surrounding soil,  $s_u$  is the undrained shear strength of the soil,  $D$  is the outside diameter of the pipe, and  $\alpha$  is the adhesion factor defined by an upper and lower bound defined as follows (Equations 2.2 and 2.3) based on the initial vertical stress.

$$\alpha = 0.7 \left( \frac{0.12\sigma_0}{s_u} \right)^{0.8} \leq 1 \text{ (lower bound)} \quad 2.2$$

$$\alpha = 0.5 \left( \frac{0.55\sigma_0}{s_u} \right)^{0.8} \leq 1 \text{ (upper bound)} \quad 2.3$$

The above  $\alpha$ -method is used to determine axial soil restraints in fine-grained soils when the rate of displacement of the pipe provides little or no time for excess pore-water drainage. This method is

extensively followed in cases of offshore pipelines (Randolph and Gourvenec 2011). Finch (1999) suggests that for very soft clays with low shear strength, values of  $\alpha$  should be 1.0 for peak resistance and about  $1/S_t$  where  $S_t$  is the sensitivity of the soil for residual strength.

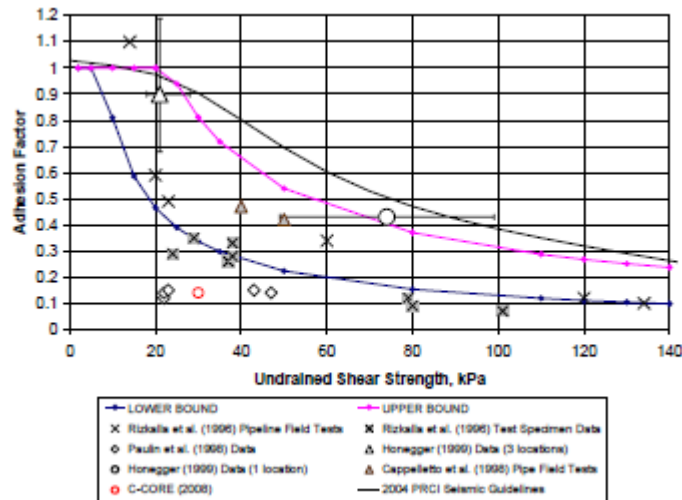


Figure 2.2 Recommended bounds for adhesion factor (PRCI 2009)

The  $\beta$ -method which was originally developed for the estimation of skin friction of piles (Burland 1973) has been adopted in the guidelines for the estimation of axial soil restraints based on when an effective stress approach is considered for analysis. According to ASCE (1984), ALA (2001), and PRCI (2009), the peak axial soil restraint ( $T_u$ ) is determined using Equation 2.4.

$$T_u = \pi D(\sigma'_n)_{av} \tan(\delta) \quad 2.4$$

Where,  $\delta$  is the soil-pipe interface friction angle,  $\gamma'$  is the average effective unit weight of the soil,  $K_0$  is the coefficient of lateral earth pressure at rest, and  $(\sigma'_n)_{av}$  is the average effective normal stress on the pipe, given by Equation 2.5.

$$(\sigma'_n)_{av} = \left(\frac{1+K_0}{2}\right)\gamma'H \quad 2.5$$

The basis for the above guidelines arise from the efforts of many researchers focusing on full-scale testing of axial displacement of buried pipes in mineral soils like sands and clays including different backfill materials. Some of the key contributions from the literature are presented below. Paulin et al. (1998) conducted the earliest full-scale tests to study the axial soil restraints using a 324 mm diameter steel pipes buried in loose and dense sands and soft and stiff clays. Experimental results from the axial dense sand tests were comparable to the load suggested in the literature (Eq 2.4, ASCE 1984) while in the loose sand tests, the suggested method over predicts the axial loading. However, axial soil restraint predictions in clay, based on ASCE (1984) yielded values 5 fold higher than the experimental results. But the experimental relative force-displacement curves agreed with other field studies found in the literature.

Cappelletto et al. (1998) performed a series of field full-scale axial pullout tests in clay, silty clay and sand with 200-mm and 600-mm pipes with different coating materials. They compared the experimental results with ASCE (1984) recommended  $\alpha$  and  $\beta$  methods and claimed that use of cohesion ( $s_u$ ) to predict the axial soil loads on pipe overestimate the load when the pipes are subjected to slow rates of longitudinal ground deformations. Authors concluded that the use of an effective stress model provides reasonable estimate of soil loads than the total stress model as a small area around the pipe is sheared during axial displacement.

Studies carried out by Wijewickreme et al. (2009) based on series of full-scale axial pipe displacement tests demonstrated that axial soil restraint values for loose dry sand are comparable to those determined using the equations from commonly used guidelines. However, for pipes buried in dense sand, the results indicated values two times or more higher than those predicted by the ASCE (1984) guidelines; this was attributed to the increase in normal stress on the pipe due to the shear-induced dilation at the soil-pipe interface getting constrained by the surrounding soil mass. As such, they concluded that an earth pressure coefficient higher than  $K_0$  may be more appropriate for use in the case of pipelines in dense sands. Further these research findings have confirmed that displacement rates less than 50 mm/s applied in a direction perpendicular to the pipe and along the pipe axis, have no noticeable effect on the axial forces developed on pipes buried in sand (Karimian 2006).

White et al. (2011) presented findings of a series of axial soil-pipe model tests performed in a soft fine-grained clayey soil collected from a deepwater location offshore West Africa which had an initial  $s_u$  slightly over 1 kPa. A plastic pipe was pulled in different displacement rates to study the effects of displacement rate on the axial restraint at low embedment conditions, and it was observed that the axial restraint is influenced by the rate of displacement. This study highlights the complexity of axial SPI problem and illustrates the influence of pore pressure and consolidation effects, and drainage conditions during the movements of pipes buried in clay. They claimed that the undrained behavior is not well captured in the conventional design calculations as the slow draining clay used in these tests caused very low equivalent axial friction factors.

Daiyan et al. (2011) found that the axial and lateral soil-pipe interaction coupling can be significant based on findings from centrifuge model testing and numerical simulations. Further, they concluded that the weight of the pipe can affect the axial soil restraint in some soils, which are not

explicitly accounted for in current guidelines. Hsu et al. (2006) tested pipe specimens with outside diameters ranging from 152 mm to 305 mm to study the oblique soil restraint of buried pipes in dense sand. They reported that the normalized peak axial soil restraint from experimental results is close to the theoretical predictions using  $\beta$  method (Equation 2.6). However, the axial pipe displacement at failure during testing was around 0.2D which is much larger than the usual range of about 3 mm expected for dense sand (PRCI 2009).

Wang and Yang (2016) studied the axial friction response of subsea pipelines coated in polyethylene in soft clays using full-scale test setup. 17.23 cm and 22.31 cm diameter pipes and 1.7 m in length were tested in soft clay beds (undrained shear strengths ranging from 7.5 – 17.5 kPa). The tests were conducted at different loading rates to study the effect of loading rate on the peak axial load, and it is concluded that the increase of ultimate axial friction coefficient is within 15% when the loading rate increases from 5 mm/h to 30 mm/h.

Previous research findings by Karimian (2006) on the effect of displacement on soil restraints in sand have confirmed that displacement rates less than 50 mm/s applied in a direction perpendicular to the pipe and along the pipe axis, have no noticeable effect on the forces developed.

### **2.1.2 Horizontal soil restraints on buried pipes**

The peak lateral soil restraint on a buried pipe and the displacement at which the soil restraint occurs can be determined according to PRCI (2009), based on Equation 2.6 and Equation 2.7, respectively.

$$P_u = N_{ch}cD + N_{qh}\bar{\gamma}HD \quad 2.1$$

$$\Delta_p = 0.04 \left( H + \frac{D}{2} \right) \leq 0.10D \text{ to } 0.15D \quad 2.2$$

where,  $P_u$  is the maximum lateral soil load caused by pipe movement relative to the surrounding soil,  $\Delta_p$  is the relative displacement between pipe and soil in the lateral direction necessary to develop  $P_u$ ,  $c$  is the shear strength intercept of soil failure envelope [usually taken as undrained strength ( $s_u$ ) in total stress approach],  $D$  is the outside diameter of the pipe,  $\bar{\gamma}$  is the effective unit weight of soil,  $H$  is the burial depth to pipe centerline (called springline),  $N_{ch}$  is the horizontal bearing capacity factor for clay ( $N_{ch} = 0$  when  $c = 0$ ) and  $N_{qh}(H,D)$  is horizontal bearing capacity factor for sand ( $N_{qh} = 0$  when fine-grained soils are characterized using  $s_u$ ).

Similar to the studies on axial loading in the previous section, the above guidelines were supported by research findings arising from full-scale testing and numerical modeling representing the performance of buried pipes primarily in sands and clays. Some of the highlights from these past works are presented below.

The earliest attempts on predicting the behavior of lateral soil restraint on buried pipelines in sand was made by Hansen (1961). Hansen's model (1961) proposes a horizontal bearing capacity factor ( $N_{qh}$ ) which is used to predict the soil restraint and has been the initial basis for the guidelines for the design of buried pipes such as ASCE (1984) and PRCI (2009). But this model led to the overprediction of lateral soil forces due to the upward movement tendency of buried pipes when subjected to lateral displacements (Trautmann and O'Rourke 1985). Ovesen (1964) developed an analytical model to determine the passive loads on anchors based on a series of experiments on plate anchors subjected to lateral ground displacements in loose and dense sand simulating a plane strain condition. Due to the free upward movements of the anchor, these predictions showed a reduction in soil loads compared to Hansen (1961). Neely et al. (1973) and Das and Seeley (1975)

investigated the effects of geometry on lateral soil restraints, focusing on examining the magnitude of lateral soil force on piles and anchor plates. In addition to the magnitude of soil restraint, the displacement at which the maximum soil restraint occurs is essential in developing bi-linear soil springs. Neely et al. (1973) observed that the displacement at failure varied with the overburden ratio, for the tests conducted with plane strain conditions, providing insight about displacement at which the peak soil restraint occurs.

Large-scale testing facilities allow for physical modeling of soil-structure interaction at full-scale so that conditions in the field can be simulated reliably under laboratory control, with detailed characterization and response measurements of soil and structure. Most of the full-scale physical modeling performed has been focused on pipelines buried in mineral soils, such as sands and clays. The first well-documented series of such full-scale tests studying lateral loads on pipes buried in both loose and dense sand was conducted by Audibert and Nyman (1977). Using a small-scale test chamber (0.38 m x 0.46 m x 0.71 m) and small diameter pipes (25 to 111 mm in diameter), they related the magnitude of soil restraint to the resultant lateral pipe displacement and concluded that soil restraint was a function soil friction angle, burial depth, and soil density. The tests conclusively demonstrated that the relationship between lateral soil restraint and pipe displacement is nonlinear and the soil restraint reaches a peak value after reaching a given pipe displacement. This study demonstrated that the force-displacement relationship approximates a rectangular hyperbolic curve, and it can be represented by a set of non-dimensional parameters relating a normalized force ( $\bar{P} = P/P_u$ ) with normalized displacement ( $\bar{y} = y/y_u$ ).

Trautmann (1983) and Trautmann and O'Rourke (1985) conducted a series of full-scale pipe displacement tests using the Large – scale Lifelines Testing Facility at the Cornell University, New York, especially focusing on lateral forces resulting from relative movement between pipes and

the sand under plane strain conditions. Pipe specimens having diameters of 102 mm and 324 mm were tested at burial depth ratios ranging from 1.5 to 11 with densities of the soil surrounding ranging from 15 to 18 kN/m<sup>3</sup> in a test chamber of size 1.2 m x 2.3 m x 1.2 m. The work led to the introduction of a non-dimensional force  $N_h$  to define the horizontal soil restraint and pipe displacement was presented as a non-dimensional ratio ( $Y'$ ) as defined in Equation 2.8 where,  $Y$  is the pipe displacement and  $D$  is the pipe diameter.

$$Y' = Y/D \quad 2.3$$

The results of these tests from Cornell University indicated that the maximum soil restraint ( $P_u$ ) was in good agreement with analytical models by Ovesen (1964) and Rowe and Davis (1983) for medium and dense sands. The  $P_u$  was found to be much lower than that predicted by Hansen (1961) mainly due to the differences in the level of vertical restraint during horizontal pipe movement where the  $N_h$  values were based on permitting the pipe to move vertically as the pipe was pulled horizontally.

Hsu (1993) conducted large scale lateral displacement tests of pipes buried in dry sand to study the effects of soil density, burial depth, pipe diameter, and relative ground movement velocity on the horizontal soil restraint and developed a force-displacement relationship of pipe-soil interaction represented by a hyperbolic equation depending on the pipe velocity. Karimian (2006) and Karimian et al. (2006a) conducted a series of full-scale tests on large diameter steel pipes buried in sand at ASPIRE<sup>TM</sup> full-scale testing facility at the University of British Columbia, Vancouver, BC, Canada to investigate axial and lateral soil restraints. The experiments were performed using varying pipe diameters, backfill material and backfill densities, and the studies have concluded that the shape of load-displacement response during lateral loading is in good

agreement with the analytical relation adopted by Trautmann and O'Rourke (1985). Using a modified version of the same ASPIRE™ full-scale testing facility, (Monroy-Concha 2013) studied the mobilization of soil restraints on buried pipelines with full-scale SPI tests simulating lateral, combined axial and lateral, and vertical oblique soil restraints in buried pipelines. This study characterized soil restraint on buried pipelines essential for the design of pipeline systems crossing seismic faults, contributing to reducing the risk of pipeline damage due to geotechnical earthquake hazards. Moreover, using the UBC facilities, Katebi et al. (2021) studied the lateral force-displacement behavior of pipes buried in dense sandy slopes using a series of full-scale tests and numerical simulations using finite-element modeling. This study showed that the soil restraint is affected by the grade of the slope in addition to the burial depth ratio, emphasizing the importance of accounting for the slope grade in soil-pipe interaction analysis and quantifies how the horizontal bearing capacity ( $N_{qh}$ ) factor is varied as a function of the burial depth ratios and slope grades which can be used in determining soil springs to evaluate the lateral pipeline response in slopes. Researchers have also complemented experimental studies using numerical modeling of relative lateral soil displacements on buried pipes in support of developing lateral p-y curves. Since the soil restraints are influenced by many factors, such as the properties of soil and pipe, backfill conditions, pipe orientation with respect to soil movement, boundary conditions, rate of pipe movement, numerical modeling efforts have led to create the opportunity to simulate these different soil-pipe interaction factors which can be limited during analytical and laboratory experimental studies.

Popescu et al. (2002) calibrated a continuum finite element model for SPI involving large relative displacements and validated the said model based on a full-scale pipe displacement test database by Paulin et al. (1998) and used the model to investigate different complex SPI aspects that require

expensive physical experimental setups. They modeled a series of full-scale soil-pipe interaction tests of lateral loading in loose and dense sand and soft and stiff clay beds (Paulin et al. 1998) with finite element code ABAQUS Standard. With the use of Modified Cam-Clay and Mohr-Coulomb constitutive models were used to represent clay and sand respectively. The numerical model predictions showed good agreement with the experimental results capturing the peak load and the mobilization loads in both clays and sands. However, assessment of this data is difficult as the soil restraints were presented in terms of percentage of the maximum load and absolute value of the results were not reported.

Yimsiri et al. (2004) applied the experimental results of lateral pipe displacement tests in sand up to H/D of 11.5 by Trautmann and O'Rourke (1985) to validate a finite element (FE) numerical model investigating soil-pipe interaction under deep embedment conditions. Using two different constitutive models: Mohr-Coulomb and Nor-Sand, they calibrated the FE model to estimate the peak forces exerted on the pipeline for different friction angles for deeper embedment ratios of as large as 100.

Guo and Stolle (2005) studied the effects of burial depth, burial depth ratio, soil properties and model scale on lateral soil restraints of pipes buried in sand through finite element analysis. ABAQUS software was used to simulate SPI using a strain hardening Mohr-Coulomb with constant dilation angle and constant friction angle and compare the numerical analysis results with published experimental findings. This study concluded that the effect of soil dilatancy increases the horizontal bearing capacity factor ( $N_h$ ), and an equation was proposed to take this effect into account which matches the experimental data in literature. Further, conclusions mention that the scaling effect depends on pipe diameter and not on overburden ratio.

Karimian et al. (2006b) conducted a comprehensive study on buried pipelines subjected to transverse ground movement focusing on both full-scale testing and numerical modeling using a finite-difference based approach. The soil response was simulated using Mohr-Coulomb and hyperbolic elastic constitutive models, and the soil parameters were based on element testing of Fraser River sand. They validated the model to use for the prediction of soil loads on pipes during lateral soil displacements for a variety of material properties and geometric configurations. The study concluded that the hyperbolic nonlinear model, in which stress dependency of material stiffness and peak friction angle are included, reasonably capture the load-displacement behavior observed in full-scale tests. Further, the effect of soil dilatancy is concluded to be negligible for shallow buried pipes (overburden ratio lower than 5).

Roy et al. (2016) emphasized the influence of the constitutive model used to represent the soil towards successful representation of SPI in numerical modeling for a reliable design. They investigated lateral soil-pipeline interaction using a modified Mohr-Coulomb model which captured important features of stress strain behavior of dense sand, such as the nonlinear pre and post-peak variation of the internal friction angle and dilation angle with plastic shear strain, loading conditions, density, and mean effective stress. This study concluded that the presented modified Mohr-Coulomb model captures the lateral force-displacement better than Mohr-Coulomb model even though the Mohr-Coulomb model is capable of matching the peak lateral soil restraint.

Dilrukshi and Wijewickreme (2020) conducted comprehensive studies on buried pipelines subjected to lateral ground movements using two-dimensional discrete-element modeling (DEM) approaches studying the effect of trench backfill particle size on the lateral soil restraints.

Analytical studies and full-scale tests investigating clay-pipe interaction with a focus on lateral pipe displacement is limited compared to those on pipes buried in sand. Many studies of SPI in

clay are related to off-shore shallow embedment pipelines. Cathie et al. (2005) reported an extensive literature survey with more emphasis on upheaval than lateral pipe response. This study claimed that work of Merifield et al. (2001) on plate anchors in undrained clay can be used to determine the ultimate lateral resistance of buried pipelines bases on the Equation 2.9.

$$P_y = N_{yu} D s_u + \gamma' D (H + D) \quad 2.4$$

Where  $N_{yu}$  is a dimensionless factor depending on the embedment of the pipe and to a lesser extent on its surface roughness. Considering conservatively the results of the lower bound plasticity analysis quoted by Merifield et al. (2001), the dimensionless factor  $N_{yu}$  can be written as Equation 2.10.

$$N_{yu} = 2.46 \ln \left( \frac{2(H+D)}{D} \right) + 0.89 \quad 2.5$$

But  $N_{yu}$  has a limiting number written as in Equation 2.11 which reflects the transition from shallow to deep embedment behavior.

$$N_{yu} + \frac{\gamma'(H+D/2)}{s_u} \leq 10.47 \quad 2.6$$

Paulin et al. (1998) discuss the establishment of a full-scale pipeline-soil interaction testing facility at Memorial University, St. John's Newfoundland, Canada where 24 large scale pipe tests have been conducted. Lateral pipe displacement tests were conducted on both sand and clays with loose and dense soil beds. The clay used in the experiments was Kaolinite with a liquid limit of 56% and plastic limit of 31% reconstituted from powder form at 33% and 37% water content to achieve soft and stiff soil bed conditions respectively. A number of cone penetration, laboratory vane, and hand vane tests were carried out during soil bed preparation to characterize the clay. These strength

measurements indicated approximate undrained strengths of 25 to 35 kPa in the soft soil beds and 65 to 70 kPa in the stiff soil beds before the pipe testing. The pipe displacement test results showed that post peak lateral loads in stiff clay were 100% higher than soft clay suggesting the effect of the difference in soil strength on the soil-pipe interaction. Further ASCE (1984) guidelines were found to yield peak lateral loads 100% greater than the experimental results in soft clay and 150% higher than stiff clay.

Oliveira et al. (2010) studied lateral clay pipe interaction using physical model testing. In this work, a series of centrifuge tests were performed for a model pipeline at shallow burial depths of soft clay. Experimental results were then used to develop a simple analytical model to compute the normalized horizontal load, derived exclusively from geometrical relations and geotechnical parameters. Resulting horizontal forces from the analytical model were well in agreement with those from ALA (2001) equations and numerical analysis.

### **2.1.3 Commentary – Soil restraints on buried pipelines subjected to relative ground movement**

As may be notable from the above review, most of the focus in past studies on soil-pipe interaction has been on pipes buried in sand and clayey soils. SPI of buried pipes in sand has been well studied and established whereas this aspect in clay is mostly investigated with respect to offshore pipelines which are commonly partially embedded. The role of full-scale laboratory physical model testing to understand the complex SPI problem, provide valuable data for validation of numerical models, and in turn, develop guidelines is well demonstrated.

In contrast to the above, in spite of the existence of a many hundreds of kilometers of energy pipelines located in extensive organic soil terrains, there is only limited research work conducted on the development of soil restraints on pipelines buried in organic soils. Understanding the mechanical (stress-strain) behavior of organic soils as a geomaterial also forms a key component in advancing our knowledge in this regard. Difficulty of accessing organic terrain and handling organic soils for laboratory and field experimental work presents a number of challenges on this front.

With this recognition, the following information is presented in the next three sections to form the background, identify the current knowledge gaps, and develop the research scope for this thesis: a) current practice approaches for the design of pipelines in organic soils (Section 2.2); b) current understanding of the mechanical behavior of organic soils (Section 2.3); and c) Summary and scope of thesis.

## **2.2 Current Practice for the Design of Buried Pipes in Organic Soils**

The current practice has been developed with the main focus in solving engineering problems involving stability and compressibility of organic soil masses. So far, there are no well-documented studies that have been undertaken to support and develop input parameters for SPI analysis for buried pipelines in organic soils except for examples of some of the related work as identified below.

PRCI (2009) identifies ground subsidence due to drainage of saturated organic soils and landslides in organic-rich deposits as geohazards in pipeline design. It observes that, as per the National Research Council (1991), about 9,000 km<sup>2</sup> of land the United States has subsided due to the

drainage problems of organic soils. The aim has been to identify the threats to pipeline integrity in terms a qualitative assessment of geohazards. Thermal changes arising as a result of operational and environmental reasons are recognized as a threat to the structural integrity and safety of buried oil and gas pipeline systems in organic soils such as muskeg. In particular, thermally induced large deformations in the pipe tend to cause buckling and potential integrity concerns because of the low restraint between the pipe and the surrounding soil at locations of pipe direction change, i.e., at bends, elbows, etc. However, none of the pipeline design guidelines (ASCE 1984, ALA 2001 and PRCI 2009) provide specific recommendations to determine load-displacement curves for pipes buried in organic soils.

Blakeman (1974) outlined geotechnical considerations with respect to a proposed iron ore slurry pipeline route extending through muskeg terrains in the province of Quebec. One of the major concerns discussed is the effect of frozen muskeg backfill on the pipe after the placement of the pipe. The approaches to weighting of pipelines (or anchoring with clamps) to counteract the peat and water buoyancy effects, especially during construction, were noted. Furthermore, Robertson and Curle (1995) have investigated alternatives to traditional concrete weights to control the buoyancy of large diameter pipes across wet muskeg-type terrains and have developed screw anchors as a means of cost-effective buoyancy control.

Marshall and Ruban (1983) examined the geotechnical problems that the pipeline industry faces in design, construction, and operation in the Province of Alberta, Canada. One main constraint identified is the presence of extensive muskeg and swampy areas which was classified under the category of physical constraints. It was suggested that, if possible, such areas should be avoided during preliminary route selection. If unavoidable, it was noted that the next challenge is implementation of construction in such areas - for example, pipelines that cross extensive areas of

muskeg (in northern Alberta) need to be constructed in the winter where a frozen crust of soil would allow construction vehicle mobility and reasonable stable trench excavations. Bedair (2013) also has documented engineering challenges during a large-scale Oil sand project in Alberta, Canada. It was identified that areas of muskeg, silt, and clay with various degrees of softness are challenging as the soft and weak soil is incapable of supporting the sustained loading making it unsuitable for construction. Further, the presence of water near the ground surface was identified as a factor contributing to construction delays. Moreover, the uncertainty in the soil design parameters and the wide variation of the soil composition have been recognized as causes of foundation failures. These construction and load-bearing concerns of foundations were identified to be applicable to pipeline design as well.

## **2.3 Mechanical Behavior of Organic Soils**

From a geotechnical engineering perspective, organic soils are often referred to as “problematic” soils, owing to their inferior engineering properties compared to other inorganic soils. Moreover, characterization of mechanical behavior of organic soil presents challenges due to the highly inhomogeneous and spatially variable nature of soft and weak organic soils. The following subsections will provide information on selection of a constitutive model as well as commentary with respect to shear strength and shear stiffness characteristics of organic soils, with particular reference to SPI analysis.

### **2.3.1 Considerations for selecting a constitutive relationship for SPI modeling**

Considering the high spatial variability and non-homogeneity of organic soils, it is of relevance to select a constitutive relationship that is effective and relatively less complex. From the typically available approaches, the stress strain modeling can be performed either using an effective stress formulation or total stress based formulation.

For the representation of soil constraints developed during numerical modeling of relative lateral soil movements against pipelines, many studies have been carried out studying soil-pipe interaction in soft sensitive clays and offshore soils based on a total stress approach (undrained) to represent the shear behavior of the soil (Chatterjee et al. 2012, Chen et al. 2016). Furthermore, Merifield et al. (2008) report ultimate resistance of shallowly embedded pipelines under combined vertical and lateral loading conditions using finite element (FE) analysis undertaken assuming total stress conditions with undrained behavior for the surrounding soil; the resulting ultimate load from this work was shown to compare well with plasticity based solutions, with the computed soil displacements matching those observed from experimental work. Tan (2008) also reports finite element analysis work to understand the soil–structure interaction mechanism of a sheet pile wall embedded in peat during roadway construction. This, again, had been achieved using an undrained soft soil creep model, and the results have satisfactorily matched with the field measurements at different construction stages. Further, Boylan and Long (2014) report the strength of peat for stability assessments using laboratory undrained simple shear tests and compare with different field testing methods such as widely used vane shear tests. Hence, it is evident that recognizing challenges both in practical applications and research settings, the total stress approach employing undrained shear strength parameters has proven effective in addressing issues related to organic soils.

Based on this evidence, along with the other considerations below, it was considered justifiable to choose a total stress based model for the lateral soil-pipe interaction of pipes buried in organic soils. It is also important to note that the use of an effective stress model as an alternative would not be feasible since the excess pore water pressure generation during shear in a highly variable inhomogeneous organic soil deposit would not be meaningfully captured – on the other hand, a total stress approach would not require such pore water pressure for the analysis. Furthermore, it is of relevance to note that PRCI (2009) also uses a total stress approach for developing p-y curves in soft fine-grained soils such as clays.

### **2.3.2 Shear strength characteristics**

Being mainly composed of partially decomposed plant matter, peat is known to have high compressibility and low strength properties (Lea and Brawner 1963, Hobbs 1986, Mesri and Ajlouni 2007, O’Kelly 2017). Therefore, the shear behavior of peats has been studied over many decades as a way of contributing to the engineering solution of stability and compressibility problems. In general, the shear behavior of peats has been identified to be extremely varied even within a given deposit. Shear strength parameters have been found to depend on the orientation of the shearing plane relative to the inherent anisotropic fabric generated by the alignment of the fibers (Yamaguchi et al. 1985, O’Kelly 2017). In essence the strength and stiffness of peat can be expressed as a function of the presence of organic fiber layers, fiber orientation, fiber properties (based on source plant species), and degree of humification. With distinct and variable properties compared to inorganic soils such as clays and sands, quantification of different peat structures in

terms of their physical, chemical, and strength properties has always been a difficult task (MacFarlane 1969, Yamaguchi et al. 1985).

Shear strength of peat is typically reported using undrained shear strength ( $s_u$ ) when for total stress analysis, or in terms of a cohesion ( $c'$ ) intercept and effective angle of friction ( $\phi'$ ) when design calculations are made assuming effective stress approach. In general, in situ or laboratory testing is used to obtain the above shear strength parameters. Yamaguchi et al. (1985) observed that, in contrast to inorganic soils, undrained shear behavior of peats under triaxial compression or extension loading conditions is independent of the magnitude of initial confining pressure or by the loading path during shear. However, in spite of the low magnitude of shear strength, peat exhibited an exceptionally high value of normalized undrained shear strength ( $s_u/\sigma'_{v0}$ ), where  $\sigma'_{v0}$  is the initial confining stress – i.e.,  $s_u/\sigma'_{v0}$  values for peat were found to be over 0.6, whereas, for soft clay and silt deposits, it is typically 0.32 or less (Mesri and Ajlouni 2007). Boylan and Long (2009) and Haan and Grognet (2014) developed DSS test apparatus to test peats, allowing the soil to test under low normal stresses which are prevailing under field conditions. Boylan and Long (2014) also conducted a study of DSS tests on peats over hundred samples collected from sixteen sites and concluded that  $s_u$  of peat is strongly influenced by the stress history as well as water content and fiber content.

When effective shear parameters are considered,  $c'$  and  $\phi'$  can be determined by laboratory triaxial tests, direct shear tests, and ring shear tests using both relatively undisturbed and reconstituted samples. Many researchers including Landva and La Rochelle (1983), Hebib and Farrell (2000), Hebib (2001), Long (2005), Mesri and Ajlouni (2007), O'Kelly and Zhang (2013) have conducted triaxial testing of fibrous peats that has resulted in values of  $\phi'$  ranging from  $40^\circ$  to  $60^\circ$ . Typically,

peat exhibits higher effective angles of friction due to the interlocking and the sliding resistance of the fibers, reinforcing the peat structure (MacFarlane, 1969). Direct shear and ring shear testing have generally yielded  $\phi'$  values lower than triaxial testing, ranging from  $20^\circ$  to  $40^\circ$  (Hebib and Farrell 2000, Hebib 2001). This wide range of friction angle values have been attributed to the dependence of strength parameters on the orientation of the shearing plane relative to its predominantly horizontally orientated fabric (O'Kelly 2017). Yamaguchi et al. (1985) conducted triaxial tests using relatively undisturbed samples extracted and cut in both vertical and horizontal direction (parallel to fibers); the study has shown that  $\phi'$  is greater in the specimens cut in the vertical direction. It has been suggested that this is due to the tensile resistance of the fibers, and in turn, confirming the highly anisotropic nature of the peat structure.

Obtaining relatively undisturbed representative samples, specimen preparation and handling of laboratory testing poses challenges due to the soft and fibrous nature of organic soils. Therefore, field investigations using in-situ tests such as vane shear tests (VST), cone penetration tests (CPT), full-flow penetrometer tests, and pressuremeter tests (PMT) have shown to serve as promising alternative methods in the characterization of mechanical behavior of peats. For example, VSTs have been conducted to determine  $s_u$  of peats over many decades on various types of peats, and it has found that at depths less than 2 m, in situ shear strength is generally 5-20 kN/m<sup>2</sup> (MacFarlane, 1969). Due to the relative simplicity of the test, vane shear tests are well used by the industry in obtaining undrained shear strength parameters of peats (Landva 1980, Liu 2019, Wijewickreme 2019).

Cone penetration testing (CPT) with pore pressure measurements has been widely done in peaty soils; especially for material identification purposes and to a lesser extent of obtaining strength parameters (Boylan et al. 2011). Unlike laboratory tests and vane shear tests, CPTs give continuous

profiles of measurement. But the results of CPTs in peat are complicated, resulting in scattered variations due to the interaction of the cone with fibers (Boylan and Long 2006). Further, Lunne et al. (1997) stated that cone penetration in peats likely to occur under partially drained conditions resulting in higher values of resistance than that of undrained conditions. Viergever (1985) found that cones with larger projected areas (50 and 10 cm<sup>2</sup>) tend to give more accurate measurements of resistance, increasing the sensitivity of measurements, and reducing the partial drainage. Based on this, full-flow penetrometers (T-bar and ball penetrometers) which have larger projected areas have been noted to provide improved accuracy in soft soils such as peats. As peats are soft, shearing displaces a large amount of soil volume. When using full-flow penetrometers, soil flows around these probes effectively simulating the shear behavior of bulk peat mass. It has been noted that this results in minimal adjustments to the measured resistances to obtain the net resistance, thus, giving higher confidence in results compared to CPT (Boylan et al. 2011). The bulk behavior of organic soil is of great importance in mechanical behavior characterization as it is identified as a varying anisotropic material. Therefore, use of larger probes can arguably capture the bulk shear stress-strain behavior of peat, and in turn, generate soil stiffness and strength parameters that are relevant in SPI analysis as pipelines would also mobilize larger soil masses when subjected to relative ground movements.

Pressuremeter is a tool that has the capability to mobilize a relatively bulk soil volume during testing. Benoît and Howie (2014) identified pressuremeter as a tool applicable in difficult ground conditions given a suitable test hole can be prepared. Hughes et al. 1977 presented a method to determine the angle of friction and angle of dilation using a self-boring pressuremeter incorporating the effects of volume change in sand occurred due to shearing during testing. Further, values of lateral effective pressure and shear modulus are also studied and the values of shear

modulus were found to be reasonable. Pressuremeter generates lateral deformation in the soil and mobilizes a significant volume of the soil, causing a radial strain field – commencing with larger strains induced at the pressuremeter-soil contact and those reducing with increasing radial distance away from the centerline of the pressuremeter. In essence, a pressuremeter would specifically invoke a lateral deformation cavity expansion mechanism that can be interpreted using fundamental soil mechanics principles (Baguelin et al. 1978; Houlsby and Withers 1988). As PMT provides a direct measurement of the in-situ stress-deformation characteristics when the test-hole cavity expands, it has served as a well-suited method of assessing both stiffness and strength parameters of soil through numerical model validations. For example, PMT data have been used in determining the relation between the soil reaction ( $P$ ) and the pile deflection ( $y$ ), again usually called  $p$ - $y$  curves, for laterally loaded cylindrical piles at specific depths below the ground surface (Robertson et al. 1984; Dyson and Randolph 2001; Bouafia 2007; Farid et al. 2013). Another example is where Palmer (1972) studied PMTs conducted in clay using undrained plain-strain cylindrical cavity expansion and confirmed that the assumption of undrained deformation in PMT is justified in determining a complete stress-strain relation of clay. Even though PMT is widely used in inorganic soils, there is a very limited number of studies of PMTs in peats. Campanella et al. (1990) have performed pressuremeter tests in soft cohesive soils at three different sites in Lower Mainland area of British Columbia to evaluate the full displacement pressuremeter tests where one site consisted of organic soil layers. Further, Edil (2001) reports that there are a few examples of the application of pressuremeter and dilatometer tests in peat soils, although there are no available guidelines in the interpretation of such tests.

### 2.3.3 Shear stiffness characteristics

In concurrence with the strength properties, shear stiffness of peat is typically low and highly variable. Since shear stiffness of soil is an important parameter to characterize the stress-strain behavior, it becomes significant in the design of any engineered structure including soil-pipe interaction problems. A limited number of studies are available on stiffness properties of peat using both field and laboratory testing. Hallam (1978) have reported Young's modulus values in the range of 0.4 to 2.0 MPa for peats and Dhowian and Edil (1980) have stated values of initial modulus ranging from 2.0 to 7.0 MPa depending on the applied consolidation stress. This is in accord with the expected high variability of organic soil deposits.

Kishida et al. (2006) have studied the small strain stiffness ( $G_0$ ) of peat found in the Sacramento-San Joaquin Delta, California, USA, based on a combination of laboratory one-dimensional consolidation tests carried out with bender elements to measure the shear wave velocity ( $V_s$ ). They have developed regression equations for estimation of  $G_0$  or  $v_s$  in terms of stress history and organic content, and they have also concluded that information about site heterogeneity, soil type (organic and mineral fractions), soil fabric, and age can significantly improve the model's accuracy. Wehling et al. (2003) reported on the characteristics of the  $G_0$  of fibrous peats at Sherman Island, California, USA, based on laboratory triaxial tests performed with high-quality Shelby tube samples from the field and on reconstituted specimens. They reported a relationship between in-situ  $G_0$  and the consolidation stress conditions that is useful for practical applications in estimating  $G_0$  at the site. Further, Hayashi and Nishimoto (2015), have proposed an empirical formula that expresses the  $G_0$  of organic clay and peats as a function of water content and effective confining pressure.  $G_0$  of peat was reported ranging from 2.2 to 10.4 MN/m<sup>2</sup> and proportional to the effective

confining stress. All these models and empirical relationships are site-specific due to the highly varied physical and mechanical properties of peat. In an overall sense, the number of past studies available on the shear stiffness properties of peat is limited compared to those available with respect to 1-dimensional compressibility and shear strength properties.

## **2.4 Summary**

Organic soils are weak in strength and soft in stiffness, their overall mechanical behavior is complex. The currently available practice guidelines (e.g., ASCE 1984; ALA 2001; PRCI 2009) provide guidance mainly with respect to the design of pipelines buried in typical sand-like and clay-like soils. The guidelines developed for these inorganic soils are primarily adopted for the design of buried pipelines in organic soils; however, due to the high uncertainties in the soil parameters for organic soils and associated significant design assumptions involved, often such approaches need to be used with significant safety factors. There is an increasing need to accurately analyze the response of pipelines buried in organic soils under anticipated operating and environmental conditions, and engineers are justifiably interested in new systematic approaches to solve design problems related to buried pipelines in organic soil terrains (Marshall and Ruban 1983; Robertson and Curle 1995; Oswell 2002; Thomas and Henderson 2004; Hendry 2011; Bedair 2013; Yang 2013).

These concerns combined with the significant variability of the strength and stiffness properties of organic soil and the long distances traversed by the pipelines, there is a strong need to provide site-specific, robust methods to determine soil restraints (i.e., soil-springs) for the assessment of soil-pipe interaction in organic soils. The mechanical (stress-strain) behavior of organic soils plays a

critical role in this process; our knowledge in this front is also limited particularly with respect to the need to obtain site-specific strength and stiffness properties required to develop soil springs.

With this background, a comprehensive research program is proposed in this thesis to characterize organic soils and advance the related SPI methodologies available. It was recognized that there is a need to: (a) Characterize organic soils using relatively simple and cost-effective methods to capture the “bulk” behavior of soft and weak organic soils; (b) understand the SPI mechanisms in organic soils by developing full-scale physical testing equipment to obtain high quality experimental data on axial and lateral loading SPI mechanisms in pipes buried in organic soil and utilize the experimental data for validating numerical modeling frameworks; (c) select a suitable constitutive model for organic soils using specialized tests that would invoke well-defined boundary value problem (e.g., pressuremeter test that simulates a well-defined cavity expansion problem) for numerical analysis to assess and validate suitable stress-strain models to represent organic soils; (d) modeling of lateral SPI using the tested physical model configurations numerically, compare the outcomes with experimental results and use this basis to validate and develop representative numerical frameworks to investigate the lateral SPI problem in detail; (e) utilize the numerical framework as per (d) above to simulate the lateral SPI problem under different organic soil strength and stiffness levels and pipe configurations and compare the lateral soil restraint p-y curves from numerical analysis with those from current practice guidelines.

As a part of this, comprehensive geotechnical investigations with an array of field sampling and testing were performed at two research sites underlain by organic soil (located in the vicinity of pipeline rights-of-way); the data obtained from these different in situ testing tools combined with detailed laboratory geotechnical testing were used to develop correlations specifically with respect

to organic soils and, in turn, obtain strength and deformation parameters for organic soils with the intent of contributing to improve the current state-of-practice design methodologies.

### **Chapter 3: Material Characterization of Organic Soils for SPI Analysis**

As discussed in Chapter 2, characterization of shear stress-strain relationship of organic soils plays a vital role in understanding SPI behavior, through the soil load development (as a result of relative ground displacement) on buried pipelines located in organic soil terrains. In order to address this, comprehensive geotechnical field investigations were carried out at some selected organic soil sites. In addition, laboratory tests were conducted to investigate the interface friction between organic soil and different pipe surface (coating) materials. The data obtained from these in situ and laboratory element testing are used to obtain representative strength and deformation parameters for organic soils, and in turn, as input to SPI interaction analyses undertaken to assess the performance of pipelines buried in organic soils. This chapter includes details of the geotechnical investigations and interpreted shear strength and stiffness properties for organic soils as appropriate – Note: Specific details related the field work are also given in Liu et al. (2018).

### **3.1 Field Geotechnical Investigation Program**

The following well-established geotechnical field investigation techniques: Seismic Cone Penetration Test (SCPT), Ball Penetration Test (BPT), Electronic Vane Shear Test (eVST) and Pressuremeter Test (PMT) were utilized in this study for the characterization of organic soils. All the field investigations were conducted with test equipment and technical support provided by ConeTec Investigations Ltd., Burnaby, B.C., Canada, under the direction and supervision of UBC research team members over several discrete days between November 2017 and January 2018.

#### **3.1.1 Site locations and overall test program**

The field geotechnical investigation program was conducted at two sites, located in the vicinity of pipeline rights-of-way; Site 01: Surrey, British Columbia, and Site 02: Wabasca, Alberta in Canada. Site 01 is located at a municipal park (Bolivar Park) in Surrey, B.C. Site 02 is located in northern Alberta along the pipeline right-of-way of the Liege Lateral Loop No. 2 – Pelican Lake Section belonging to TC Energy. Geographical locations of Site 01 and Site 02 are shown in Figure 3.1 and Figure 3.2 respectively.

The plan view of the test holes are shown in Figure 3.3(a) and Figure 3.4(a) respectively. The work was undertaken with test holes in the vicinity identifies in terms of groups: (i) Group 1-01 and Group 1-02 at Site 01; Group 2-01 and Group 2-02 at Site 02. As may be noted from the figures, at a given group the following tests were conducted: SCPT tests (one in each group), BPT tests (one in each group), and eVST tests (three in each group). It is noted that, due to technical difficulties, there were 2 unsuccessful PMTs in Test Group 1 and only 2 eVSTs at each Test Group

in Site 02. The depth locations of eVST and PMT testing at the two research sites are shown in Figure 3.3(b) and Figure 3.4(b). A summary of test equipment dimensions and test depths are presented in Table 3.1.

In addition, auger sampling was performed to collect disturbed grab-soil samples, including relatively undisturbed samples obtained using thin-walled, sharpened-edge, no-inside-clearance, stainless-steel tubes for visual inspection and laboratory testing as appropriate. Specific relevant details related to the site investigation are presented in the upcoming sections.

**Table 3.1 Summary of test equipment dimensions and test depths of the field investigation program**

Field Test	Equipment Dimensions	Test Depths: Site 01		Test Depths: Site 02	
		Test Group 1	Test Group 2	Test Group 1	Test Group 2
SCPT	15 cm <sup>2</sup> cone (4.37 cm diameter) net area ratio: 0.8	Continuous profile	Continuous profile	Continuous profile	Continuous profile
BPT	150 cm <sup>2</sup> ball (13.8 cm diameter)	Continuous profile	Continuous profile	Continuous profile	Continuous profile
eVST	Double tapered 75 x 150 mm vane	3.5 m	3.5 m	3 m	1.5 m
		5 m	5 m	5 m	4.45 m
		6.5 m	6.5 m		
PMT	Effective volume of probe: 1554 cm <sup>3</sup> (46 cm height)	3.66 m	3.5 m	1.35 m	1.5 m
		4.8 m	5.05 m	2.88 m (unsuccessful)	3.21 m
		6.25 m	6.5 m	4.52 m (unsuccessful)	4.25 m

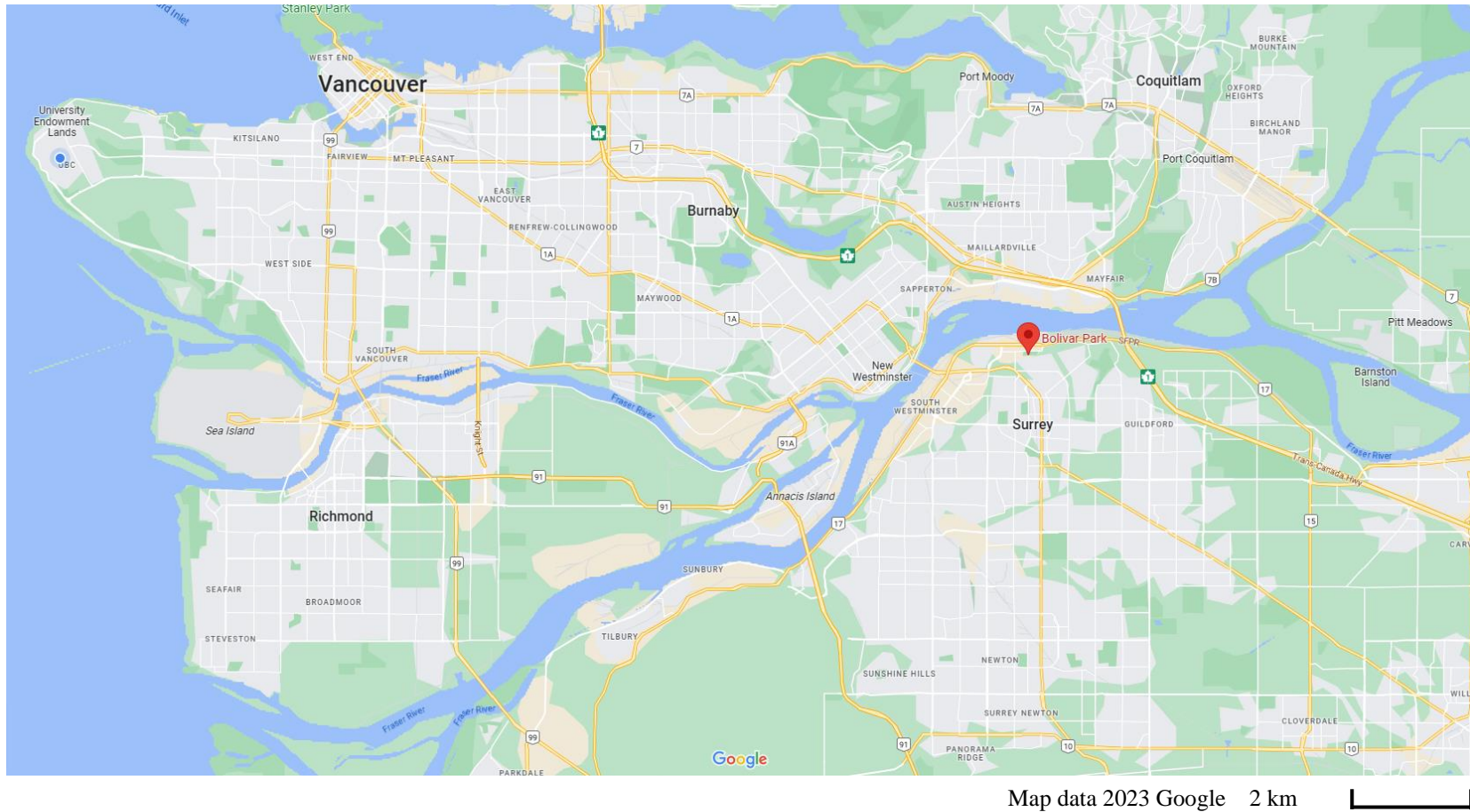


**Figure 3.1 Location of test site 01: Surrey, British Columbia, Canada from Google maps, by Google <https://www.google.ca/maps/place/Bolivar+Park/@49.2109297,122.8530789,17z>)**

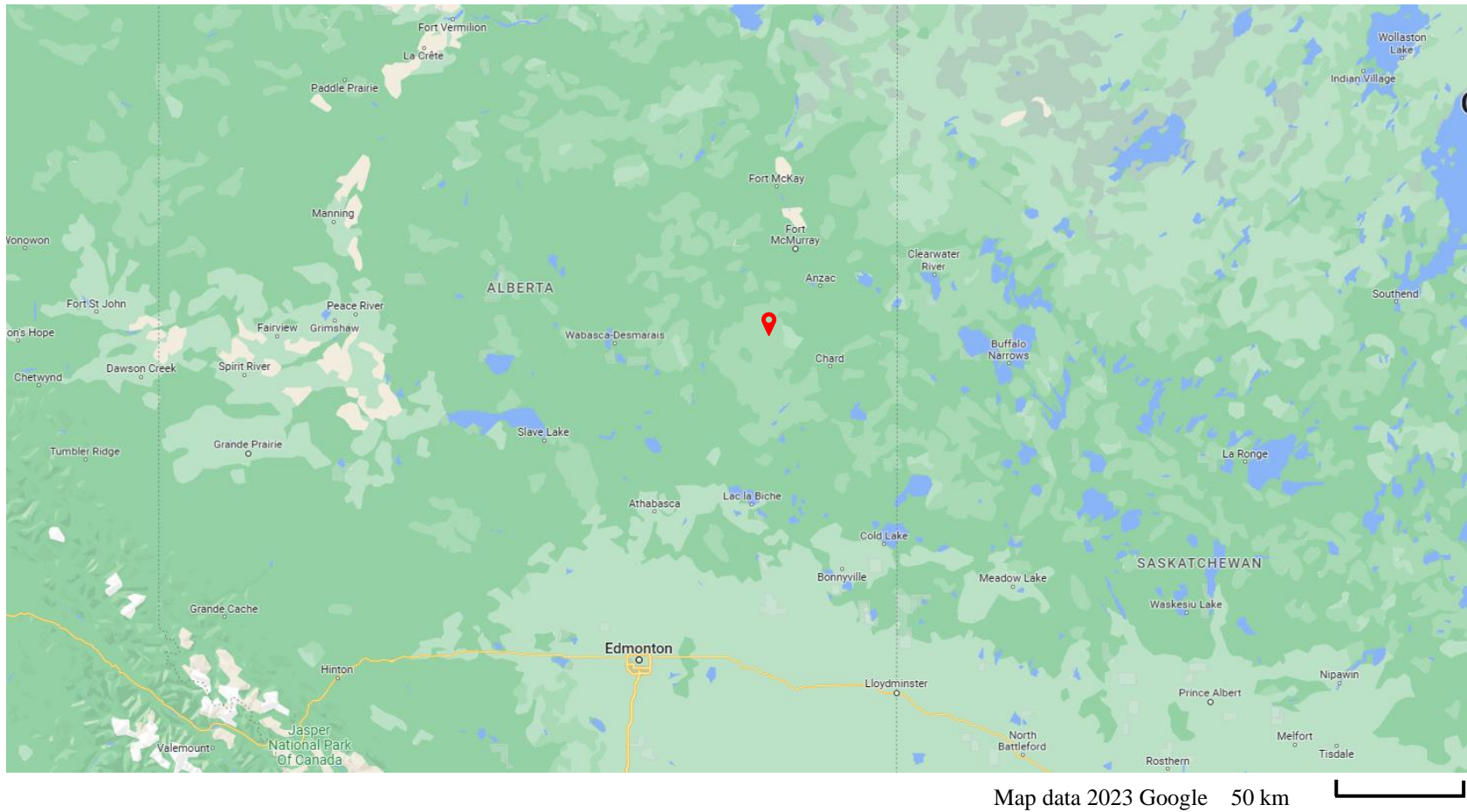
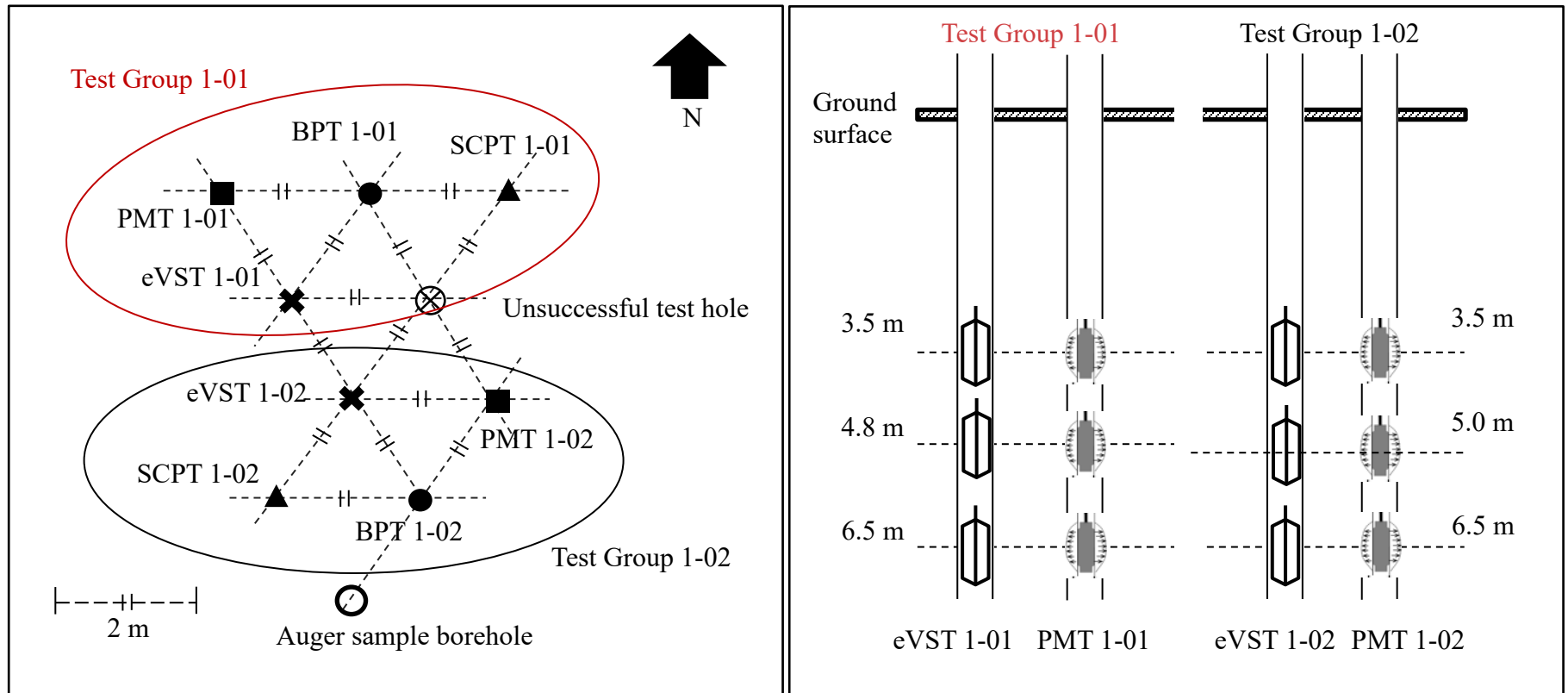


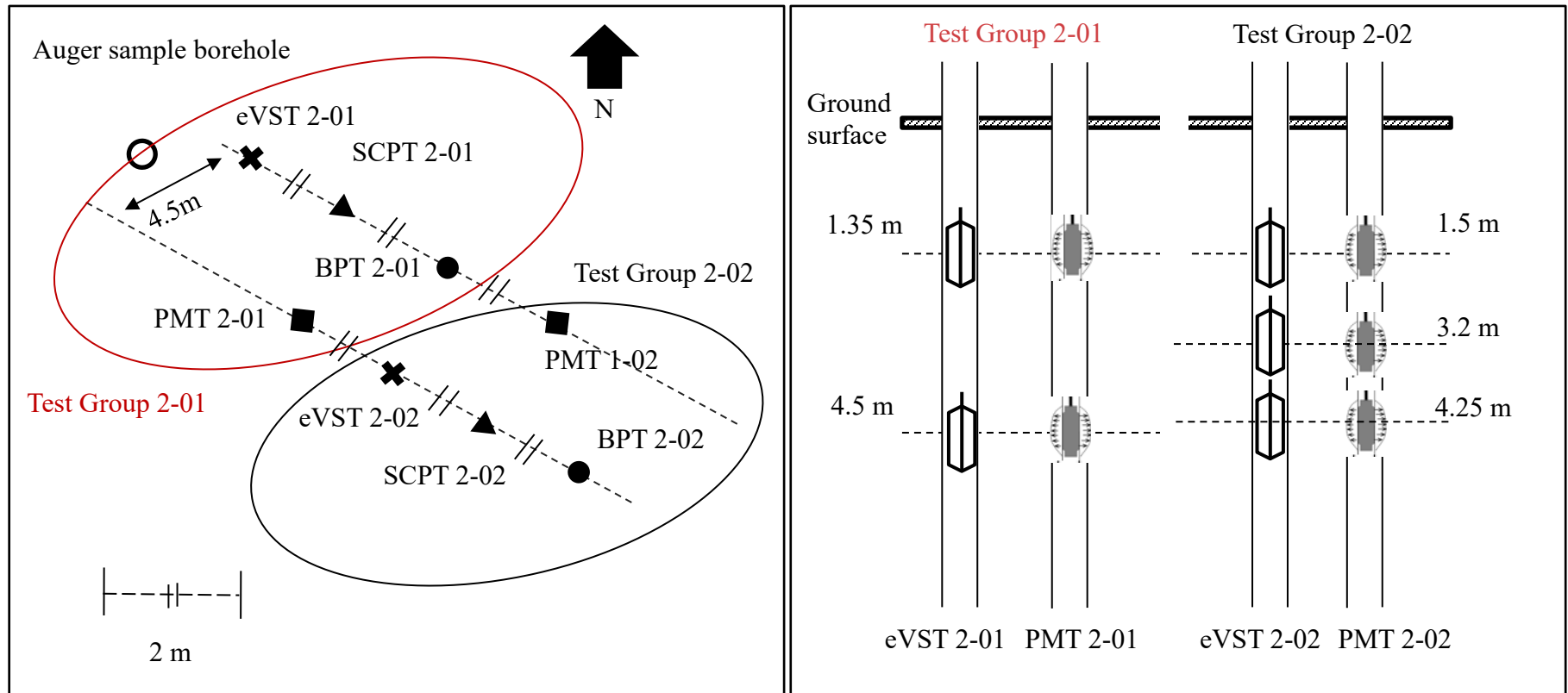
**Figure 3.2 Location of test site 02: Wabasca, Alberta, Canada from Google maps, by Google (<https://www.google.ca/maps/@55.4055596,-112.701179,6.71z>)**



(a)

(b)

Figure 3.3 Field geotechnical investigations at Site 01 in Surrey, British Columbia, Canada: (a) Test hole location layout (Plan view); (b) Depth locations of eVST and PMT testing at Test Group 1-01 and Test Group 1-02. Note: Test hole identification numbers are given beside the hole location markings



(a)

(b)

**Figure 3.4 Field geotechnical investigations at Site 02 in Wabasca, Alberta, Canada: (a) Test hole location layout (Plan view); (b) Depth locations of eVST and PMT testing at Test Group 2-01 and Test Group 2-02. Note: Test hole identification numbers are given beside the hole location markings**

### **3.1.2 Seismic cone penetration tests**

SCPT consists of a penetrometer with a cone tip, and simultaneous measurements of cone tip and sleeve resistances are recorded as the cone is pushed into the ground, at a typical rate of 2.5 cm/s. Four SCPTs were conducted at Site 01 and Site 02 at Test Group locations 1 and 2 and the variation of tip resistance ( $q_t$ ), sleeve resistance ( $f_s$ ), pore pressure ( $u_2$ ), and shear wave velocity ( $v_s$ ) with depth below the ground surface for the two sites are presented in Appendix A.1: Figures A.1 through A.4.

As noted by (Boylan et al. 2011), in addition to the soil behavior type, the variations in tip and friction sleeve resistances in organic soils also reflect the interaction of the cone with the fibers as the cone is penetrated in the ground – sometimes leading to results that are difficult to interpret compared to those from cone penetration testing in mineral soils. In soft organic soils, since the measured CPT resistance ( $q_c$ ) is relatively low, the magnitude of the standard corrections required on the  $q_c$  can form a significant portion of the measured resistance. For example, it has been reported that the soft nature of organic soil leads to cone resistance measurements lower than the accuracy of the measure resulting in zero resistance being measured (Boylan et al. 2011), making SCPT a less reliable tool in determining strength properties of soft organic soils.

### **3.1.3 Full flow ball penetrometer tests**

BPT is a full flow penetrometer test that is widely used in offshore testing, specifically investigating soils that are low in shear strength and stiffness (i.e., fluid like). Compared to SCPT, BPT uses a ball with a relatively large diameter (~14 cm) instead of a cone that in turn, would

displace a larger volume of soil during penetration. Because of the variable nature and low strength and stiffness, it is considered preferable to characterize organic soils using probing methods such as BPT that would “test” (or mobilize) a relatively large soil volume during penetration. In particular, when the BPT probe is pushed in to a weaker soft soil, the soil would essentially “flow” around the ball as a fluid while mobilizing a relatively large soil volume during the penetration of the spherical probe.

Furthermore, past studies have shown that full-flow penetrometers like T-bar and ball reduces the challenges in measuring penetration resistance in soft peat and organic soils using SCPT, due to the larger failure surface mobilized during probe penetration compared to the SCPT (Long and Gudjonsson 2004, Oung et al. 2004, Boylan and Long 2006). Long et al. (2010) have also found that the full-flow penetrometers like T-bar and ball provide a less “noisy” resistance factors than those from CPT for organic soils. It is known that penetration tests in organic soils are likely to occur under partial drained conditions which would result in overestimation of the undrained resistance present in the soil (Lunne et al. 1997); however, the use of cones larger than the standard 10 cm<sup>2</sup> cone penetrometer has demonstrated lesser effects of partial drainage on penetration resistance. Therefore, use of larger probes is beneficial in increasing the accuracy of measurements and reducing the effects of partial drainage when testing soft soils like muskeg where the effects of consolidation is dominant (Boylan et al. 2011).

As indicated in Table 3.1, BPTs were penetrated to a depth of about 6.5 m below the ground surface. The results from BPTs presenting the variation of ball tip resistance ( $q_b$ ) with depth below the ground surface are shown in Appendix A.2, Figure A.5 and A.6, for the Sites 01 and Site 02, respectively. Note: The upper material (the frozen layer at Site 01 and the sand fill at Site 02) was drilled out prior to pushing the ball penetrometer.

### 3.1.4 Electronic vane shear tests

Vane shear tests have been reasonably utilized to determine  $s_u$  of fine-grained and organic soils in site investigations practice for many decades. Its ability to obtain a direct measurement of the in situ undrained shear strength using a relatively simple method, in contrast to the difficulties in obtaining undisturbed samples of soft and weak soils for laboratory testing, has been the main reason for the popularity of vane shear tests. The vane shear test consists of a four-blade, stainless steel vane attached to a steel rod that is pushed into the ground and rotated at pre-specified rates to measure the torque at peak and remolded states as schematically shown in Figure 3.5 ( ASTM-D2573 2015). A modified electrically operated version of the field vane test (eVST) was employed to obtain undrained shear strengths of organic soil at different specific depths. As indicated in Table 3.1, the device consisted of a four-blade, stainless steel, double-tapered vane (75 mm in 150 mm in height and 45° top and bottom taper angles) attached to a steel rod. This test allowed measuring both the peak and remolded shear strengths.

Respectively, six and four eVSTs were conducted at Site 01 and Site 02 covering the depth ranges tested during the previously described field tests. Site 01: Test group 01 - at 3.5 m, 5.0 m, and 6.5 m below the ground surface and Test group 02 - at 3.5 m, 5.0 m, and 6.5 m below the ground surface. Site 02: Test group 01 - at 3.0 m and 5.0 m below the ground surface and Test group 02 - at 1.5 m, and 4.5 m below the ground surface. Appendix A.3: Figure A.7 and Figure A.8 present the variation of peak and remolded shear stress with respect to the vane rotation at different test depths and test group locations.

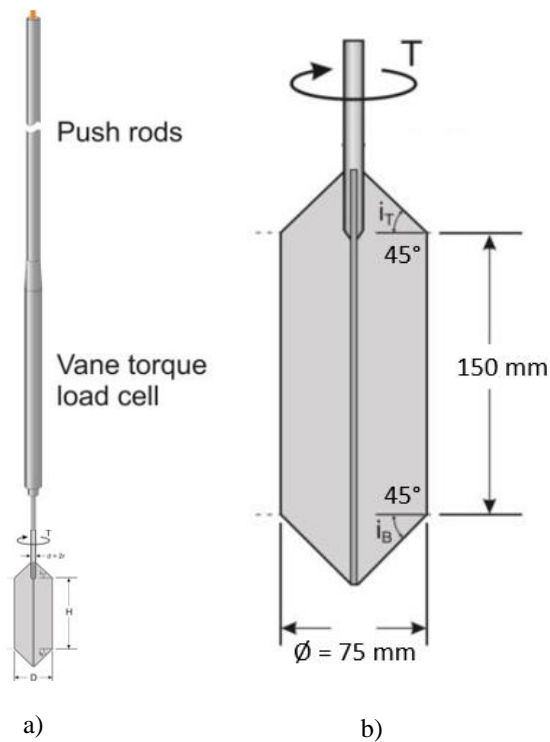


**Figure 3.5 a) Illustration of vane attached to the vane rods b) Dimensions of the vane used for testing (ConeTec 2017)**

### 3.1.5 Pressuremeter tests

A commercially available pre-bored, 70-mm diameter, pressuremeter (TEXAM pressuremeter, manufactured by RocTest Inc., Saint-Lambert, Quebec, Canada) was used in this PMT test program. PMT generates lateral deformation in the soil and mobilizes a significant volume of the soil, causing large lateral displacements. This provides a direct measure of the in-situ stress-strain relationship as the cavity expands. Lateral pressure versus radial displacement curves from PMTs were used in numerical modeling of field PMT test cases as a way of validating a selected

constitutive model to represent organic soils. This aspect is discussed in detail in Chapter 4 of this thesis.

PMTs were performed at two test locations each at Site 01 and 02 [see Figure 3.3(a) and Figure 3.4(a)]. Site 01: Test Group 01 - at 3.66 m, 4.80 m, and 6.25 m below the ground surface and Test Group 02 - at 3.5 m, 5.05 m, and 6.5 m below the ground surface [see Figure 3.3 (b)]. Site 02: Test Group 01 - at 1.35 m and 4.52 m below the ground surface and Test Group 02 - at 1.5 m, 3.21 m and 4.25 m below the ground surface [see Figure 3.4 (b)]. Appendix A.4: Figures A.9 and A.10 and Figures A.11 and A.12 illustrates typical PMT curves showing lateral pressure vs radial displacement at Site 01 and Site 02 at different test depths respectively [These figures are extracted from UBC site investigations report prepared by ConeTec Investigations Ltd. (ConeTec 2017)]. The needed corrections were performed by ConeTec Investigations Ltd. in accordance with ASTM D4719 (2007).

### **3.2 Geotechnical Laboratory Element Tests**

Laboratory element Direct Simple Shear (DSS) and Direct Shear (DS) tests were conducted on bulk organic soil samples retrieved from the two test sites in Surrey, British Columbia and Wabasca Alberta, Canada. DSS and DS tests were conducted to determine organic soil shear strength properties and interface shear properties between organic soil and pipe materials respectively. Following sub-sections discuss the two types of tests, material used, and the tests performed.

### 3.2.1 Direct simple shear tests

Laboratory monotonic Direct Simple Shear (DSS) tests were performed on reconstituted specimens prepared from bulk samples extracted from Site 01 to further confirm the undrained shear strength properties of the organic soil derived from in-situ testing. The DSS device at the University of British Columbia geotechnical research laboratory was used for the testing herein; the device is a modified Marshall-Silver-NGI-type DSS device (Silver and Seed 1971), and it follows the simple shear testing methodology of the NGI-type DSS apparatus described by Bjerrum and Landva (1966).

Organic soils from Site 01 extracted as bulk samples was tested using DSS device. organic soil was prepared for the DSS tests by placing a uniformly mixed bulk sample in a consolidation cell under a vertical seating load of 5 kPa. Specimens for the DSS tests were extracted using a stainless-steel ring (see Figure 3.6) from the consolidation cell. This step was conducted to place the soft organic soil samples on the DSS device in an effective manner. Laboratory geotechnical characterization as per index properties of the tested organic soil, determined by the research team working on the same research program from the UBC Okanagan Campus (Siddiqua and Elmouchi, 2020, Elmouchi 2021, Elmouchi et al. 2021), are summarized in Appendix A.5; Table A.1.

DSS tests were conducted in two phases: 1) consolidation; 2) strain-controlled monotonic shear. Monotonic DSS tests were conducted at a strain rate of 10% strain per hour (which is the standard rate used for sands and silts in UBC-DSS test device) on specimens initially consolidated in the DSS device to vertical effective consolidation stresses ( $\sigma'_{vc}$ ) of 20 and 30 kPa corresponding to 2.1 and 3.2 m depths (calculated based on the average bulk unit weight of soil) respectively. The

observed stress-strain behavior from the DSS tests conducted are presented in Appendix A.6: Figure A.13 and Figure A.14.

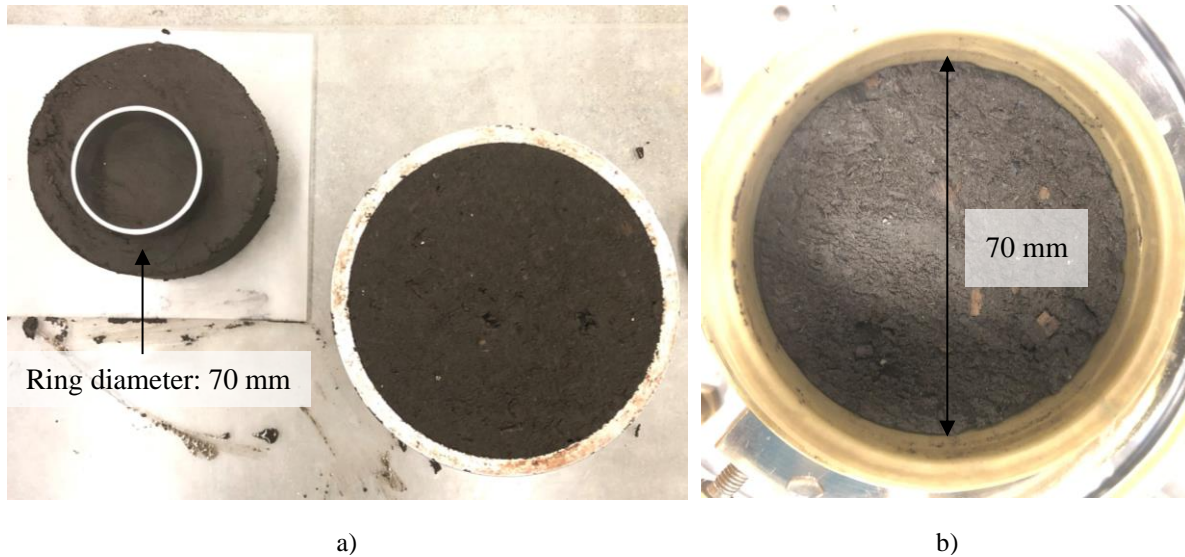


**Figure 3.6 DSS test specimen preparation a) extracting the samples into a stainless-steel ring of 70 mm diameter; b) 70 mm diameter sample placed inside the DSS membrane.**

### **3.2.2 Interface direct shear tests**

A series of direct shear tests was conducted to investigate the interface shear properties between organic soil and pipe surfaces. Laboratory element-level testing of soil-solid interfaces using the commonly used direct shear apparatus (DSA) was performed to investigate interface shear strength properties between soil and different construction materials. In addition to the development of useful geotechnical data, the resulting interface frictional properties served as input for assessing physical modeling SPI experiments, as well as associated numerical modeling. Experimental aspects including the direct shear apparatus and procedure, tested pipe material and soil and

specimen preparation and direct shear test results are included in the following sub-sections. Use of these results in SPI modeling is discussed in Chapter 7.

### **3.2.2.1 Direct shear test program**

The interface direct shear tests were conducted in general accordance with ASTM D3080/D3080M (2011) by modifying a conventional direct shear apparatus. The ability to test element level uniform specimens while providing a definitive shearing mechanism at the soil-solid interface is a clear advantage of using this shearing approach (Negussey et al. 1989, O'Rourke et al. 1990). The device accommodated remolded organic soil specimens of 100 mm x 100 mm in plan area, and ~20 mm in initial height. The required modification to the conventional DS device is relatively simple, where a solid test surface was inserted in the lower half of the box as indicated in Figure 3.7. The soil tested was contained in the top half of the box allowing the soil to rest against the solid test surface during shear.

The specimens were initially consolidated to vertical stress levels of 10 kPa, 20 kPa, 50 kPa and 100 kPa prior to shearing. The vertical displacement of the specimen was measured using an LVDT during the consolidation phase and throughout the test. The top half of the box was attached to a motor shaft which sheared the specimen at a shear displacement of 0.05 mm/min up to 10 mm. The displacement rate was estimated according to the with ASTM D3080/D3080M (2011) assuming the shear displacement at failure to be 10 mm for a fine-grained soil. The interface shear strength envelope was obtained using the results from a number of tests assuming a Mohr-Coulomb failure criterion. Apart from the interface shear properties, internal shear properties of

the soil were also assessed by testing organic soil alone in direct shear (i.e., without the test solid surface) for comparison purposes.

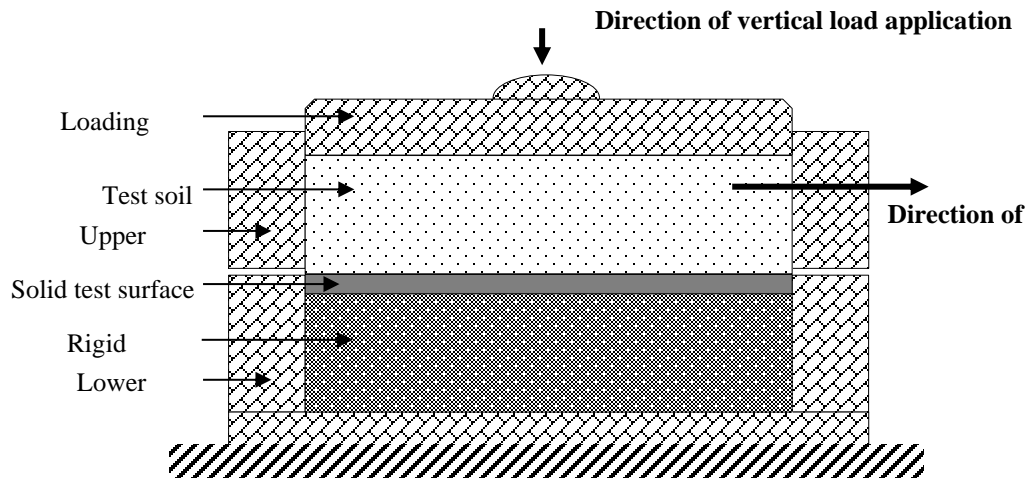


**Figure 3.7 Schematic diagram of the Direct Shear Apparatus (DSA) used to study interface properties between organic soil and pipe surfaces (Note: not to true scale)**

In this, organic soils from Site 01 extracted as bulk samples was tested using DSA. Laboratory geotechnical characterization as per index properties of the tested organic soil, determined by the research team working from the UBC Okanagan Campus (Siddiqua and Elmouchi, 2020), are summarized in Appendix A.5; Table A.1. Two solid surfaces were tested under this initial study: (a) Mild steel (MS) solid test surface: Sand blasted mild-steel plate of type CS-Type-A (6.4 mm thickness) to represent a pipe material without any coating applied; (b) Green epoxy (GE) coated (1.5 mm thick coating) mild-steel test surface; this coating is considered to represent those typically used in pipeline protection applications. According to Amarasinghe (2019) surface roughness of GE and MS solid test surfaces are  $0.15 \mu\text{m}$  and  $7.0 \mu\text{m}$ , respectively, when evaluated

using the laser confocal microscope using a gauge length of 12.5  $\mu\text{m}$ . Figure 3.8 shows the pictures of the tested solid surfaces inside the DSA.

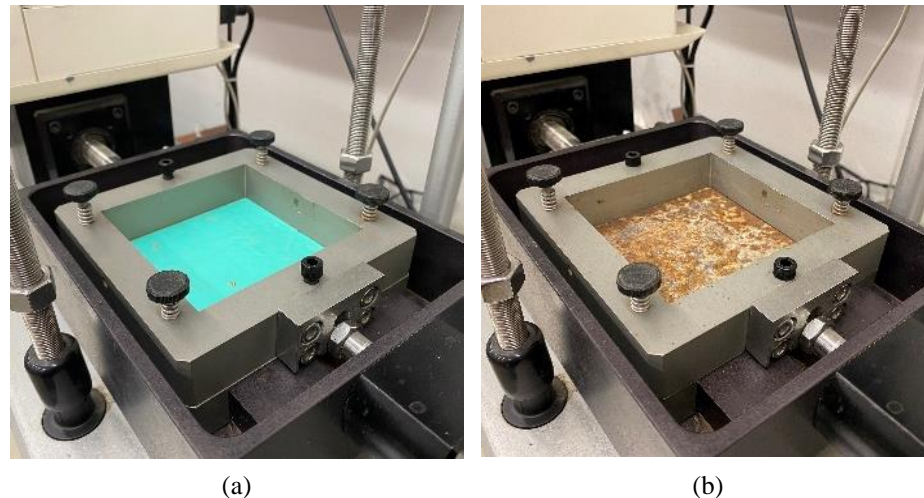


**Figure 3.8 (a) Green epoxy coating (GE) and (b) sand blasted mild steel (MS) solid surfaces tested in the DSA**

Reconstituted test specimens were prepared from bulk organic soil samples, which were stored in a moisture-controlled environment to minimize the loss of moisture and preserve the in-situ moisture content as much as possible. No water was added, and as-is soil from the bulk samples were used in the specimen preparation. Samples were reconstituted by mixing the organic soil from the bulk sample in a container to achieve a reasonably uniform specimen. Prior to soil placement inside the shear box, organic matter that were larger than 3 cm in size were removed from the reconstituted samples. The sample was then placed inside the shear box with appropriate mass and height requirements to achieve the tested wet densities in the laboratory. As indicated earlier, the lower part of the shear box has a solid pipe surface; therefore, the organic soil placed inside the upper box was resting on this solid test surface. Some gentle pressure had to be imparted manually (using fingers) to obtain a visually uniform and effective placement of soil. A photograph

of a specimen prepared in the shear box, prior to placement of the top loading platen for the application of consolidation stress, is presented in Figure 3.9. The test program is given in Appendix A.7: Table A.2.

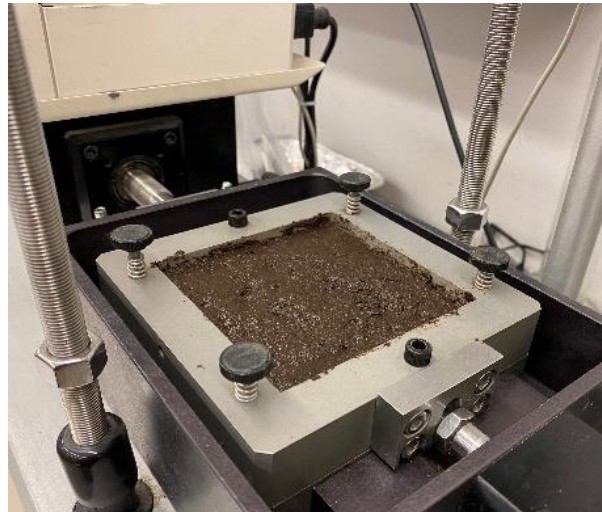


**Figure 3.9** Reconstituted organic soil specimen in the shear box prior to placement of the top loading platen

### **3.3 Interpretation of Field and Laboratory Test Results**

The data collected from the above field and laboratory investigations were interpreted to obtain the needed shear strength and stiffness properties for assessing physical modeling SPI experiments, as well as associated numerical modeling. With regard to the strength properties, the main focus was on obtaining undrained shear strength ( $s_u$ ) since the assessments were mainly performed using total stress analysis. The use of total stress approaches were considered more appropriate, compared to effective stress methodology. As indicated in Section 2.3, the use of effective stress approaches invariably requires good modeling of shear-induced pore water pressure, which is an extremely difficult task for complex organic soils; this has been one of the key reasons for the use

of total stress approaches in most industry applications with research undertaken by leading researchers working on organic soils.

This section initially presents the methods used for determining undrained shear strength ( $s_u$ ) from the field tests; SCPT<sub>u</sub>, BPT<sub>u</sub>, eVST, and PMT. Site-specific, interpreted results are shown in the latter sections. Comparison of  $s_u$  results include the  $s_u$  determined based on laboratory direct simple shear tests as well. Furthermore, interface friction properties are presented based on laboratory direct shear tests.

### **3.3.1 Undrained shear strength properties**

The undrained soil strength ( $s_u$ ) values derived from the field and laboratory investigations, and their mutual comparisons are presented herein. In this regard, due consideration was given to published information available from previous research on organic soils (Boylan et al. 2011; Weemees et al. 2006).

The profiles of  $s_u$  from the SCPTs was determined using the empirical approach given in Equation 3.1 (Robertson et al. 1986), considering a resistance factor ( $N_{kt}$ ) and net penetration resistance ( $q_{net}$ ). It has been suggested that  $N_{kt}$  can typically range from 10 to 20 (Powell and Quaterman 1988), and a value of 12.5 was used for the organic soil studied in this thesis with consideration given to plasticity index, sensitivity, and degree of consolidation of the site (Liu et al 2018).

$$s_u = q_{net}/N_{kt} \quad 3.1$$

The  $s_u$  profile from the BPTs was determined using an essentially identical empirical approach as described by Equation 3.2; herein,  $N_{ball}$  of 11 is used based on literature and information available from the extensive experience gathered by a local in situ testing contractor (Weemees et al. 2006). The selected  $N_{kt}$  and  $N_{ball}$  values fall in the reported range by Boylan et al., (2011) for organic soils.

$$s_u = q_{net}/N_{ball} \quad 3.2$$

The data from field eVSTs were also used to estimate  $s_u$  values; they were calculated according to ASTM D2573 (2015) with respect to the vane shear tests conducted at different test depths and different test group locations (see Figures 3.3 and 3.4). This method of interpretation produces a single value for peak undrained shear strength at a given depth of interest based on the maximum value of torque, vane diameter, height of the vane and angles of taper at the vane top and bottom. Furthermore,

from PMT was interpreted using either empirical approaches or cavity expansion theory derivations combined with soil stress strain model. In the current study, values of  $s_u$  from PMT data are determined using the approach proposed by Gibson and Anderson (1961) assuming the soil is elastic-perfectly plastic.

Undrained shear strengths determined from different field tests described above are shown in Figure 3.10 and 3.11 for Site 01 and Site 02, respectively. These figures presents results from laboratory DSS tests on organic soils from Site 01 as well. Interpreted  $s_u$  from SCPT data shows significant variability at both sites – from 10 kPa to 40 kPa for the Test Group 01 and 10 kPa to 75 kPa for the Test Group 02 at Site 01 and 5 kPa to 60 kPa for both Test Groups 01 and 02 at Site 02. However, the  $s_u$  values (20 kPa – 50 kPa for both Test Groups at Site 01 and 10 kPa – 60 kPa

for both Test Groups in Site 02) interpreted from BPTs display fewer local variations compared to the SCPT results; this is in accord with observations by Boylan et al., (2011). With the relatively small diameter, the SCPT  $q_{net}$  values (hence the  $s_u$ ) detect the presence of organic fibers, soil consistency, etc., with an increased sensitivity compared to the  $q_{b-net}$  from BPT probe that has a larger footprint – i.e., the larger size of the BPT would “average” or “filter” out the localized effect response and reflects a more macro-scale response of the soil matrix.

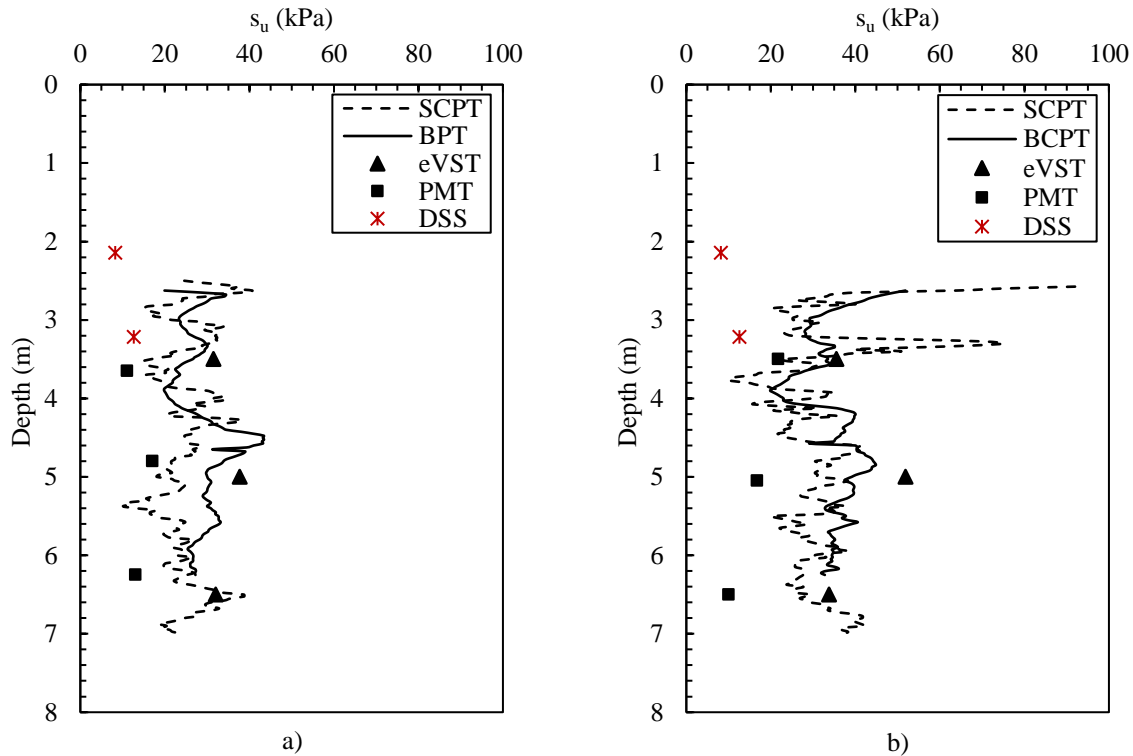


**Figure 3.10** Variation of undrained shear strength,  $s_u$  with depth based on SCPT, BPT, eVST, PMT field tests and laboratory DSS tests at Site 01: (a) Test Group 01 (b) Test Group 02 [ConeTec 2017) and reported in Elmouchi (2021)]

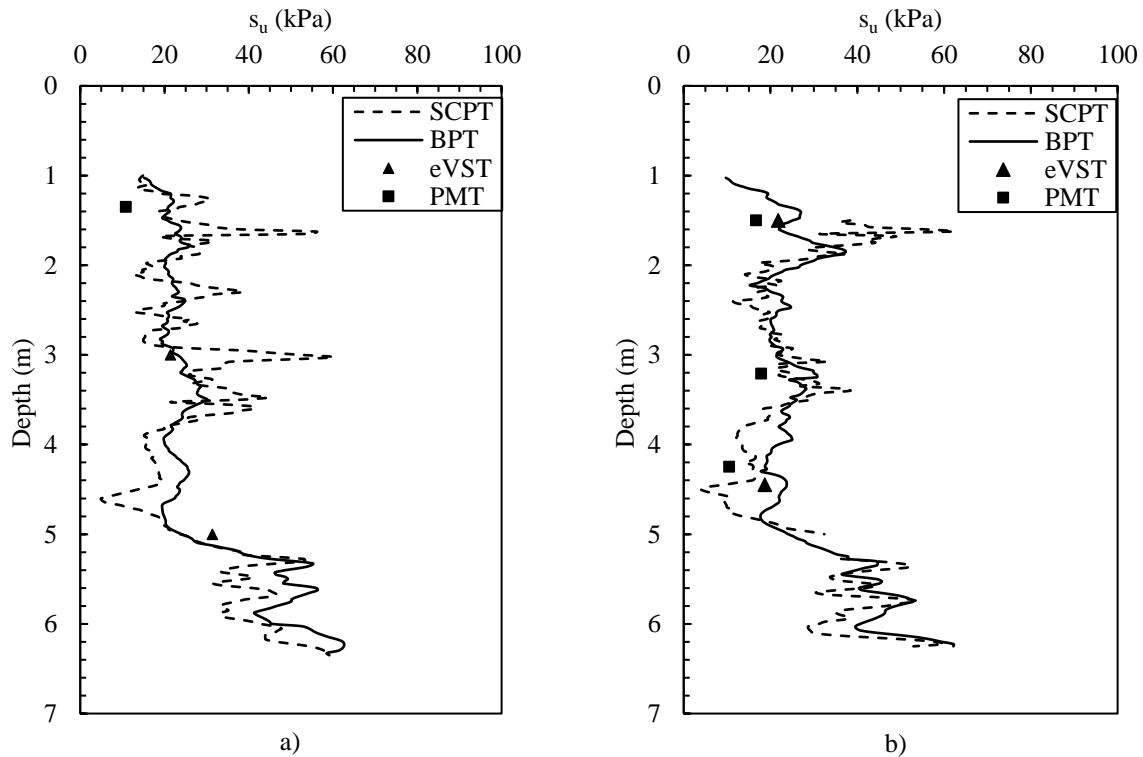


**Figure 3.11** Variation of undrained shear strength,  $s_u$  with depth based on SCPT, BPT, eVST and PMT field tests at Site 02: (a) Test Group 01 (b) Test Group 02 (ConeTec 2017)

It is also of interest to note that the  $s_u$  values from BPT seem to be in agreement with those from eVST. This agreement demonstrates the role that eVST could play in characterizing site undrained soil strength parameters of organic soils, further confirming the popularity of this tool by industry and academia (Mesri and Ajlouni 2007). Nonetheless, it is to be noted that the disadvantages in the use of the field vane for  $s_u$  measurements of organic soils due to uncertain failure conditions around the vane circumference has been noted by Landva (1980).

The data interpreted from PMTs from the present study seem to display generally lower  $s_u$  values compared to those from SCPT, BPT, and eVST. Due to the involved nature and complexities in

setup inside boreholes, the PMT is not a widely used testing tool; in the present instance, the interpreted  $s_u$  values from the PMT data seem to reflect the combined effects from the disturbed soils zones near the pocket walls during pre-bored PMT (Baguelin et al. 1978) and relatively undisturbed soil zones away from the walls as the PMT probe is expanded – leading to a  $s_u$  value between remolded and peak undrained shear strengths.

The  $s_u$  values derived from laboratory DSS tests conducted on reconstituted organic soils from Site 01 are also superimposed on Figure 3.10. As may be noted these  $s_u$  values are smaller compared to the counterpart values derived from the field tests; these outcomes are likely to be due to sample disturbance and change in soil fabric during specimen reconstitution for laboratory testing.

### **3.3.2 Shear stiffness properties**

The small strain shear modulus ( $G_0$ ) is a commonly used “base” parameter in quantifying the shear stiffness of soils. In order to understand the stiffness properties of the tested sites,  $G_0$  was interpreted using a number of methods based on the available test data.  $v_s$  determined from field measurements (commonly using SCPT) is one of the most reliable methods of estimating  $G_0$  at a given location. Using shear wave propagation theory, the value  $G_0$  can be estimated using Equation 3.3, where  $\rho$  is the mass density of the soil through which the waves are propagated. For the present sites, the  $G_0$  versus depth profiles were determined using  $V_s$  measured from SCPTs using a  $\rho$  value of organic soil as  $1100 \text{ kg/m}^3$  [based on findings by ElMouchi and Siddiqua (2020), ElMouchi et al. (2021) and measurements done by the author during lab testing].

$$G_0 = \rho V_s^2 \quad 3.3$$

The values of shear moduli determined from SCPT shear wave velocity measurements ( $G_0$ ) are presented in Figures 3.12 and 3.13 for Sites 01 and 02, respectively. Moreover, it was of interest to compare these  $G_0$  values with those generated from the PMTs using the approach proposed by Hughes and Robertson (1985). Based on this theory, shear modulus is calculated as half the slope of the unload-reload cycle of the pressure-radial strain curve. The values of shear moduli determined from the first unload-reload loop from PMTs ( $G_{ur}$ ) are superimposed on the same figures above. As notable from these figures, the  $G_0$  values and  $G_{ur}$  values are in good agreement as suggested by Hughes and Robertson (1985).

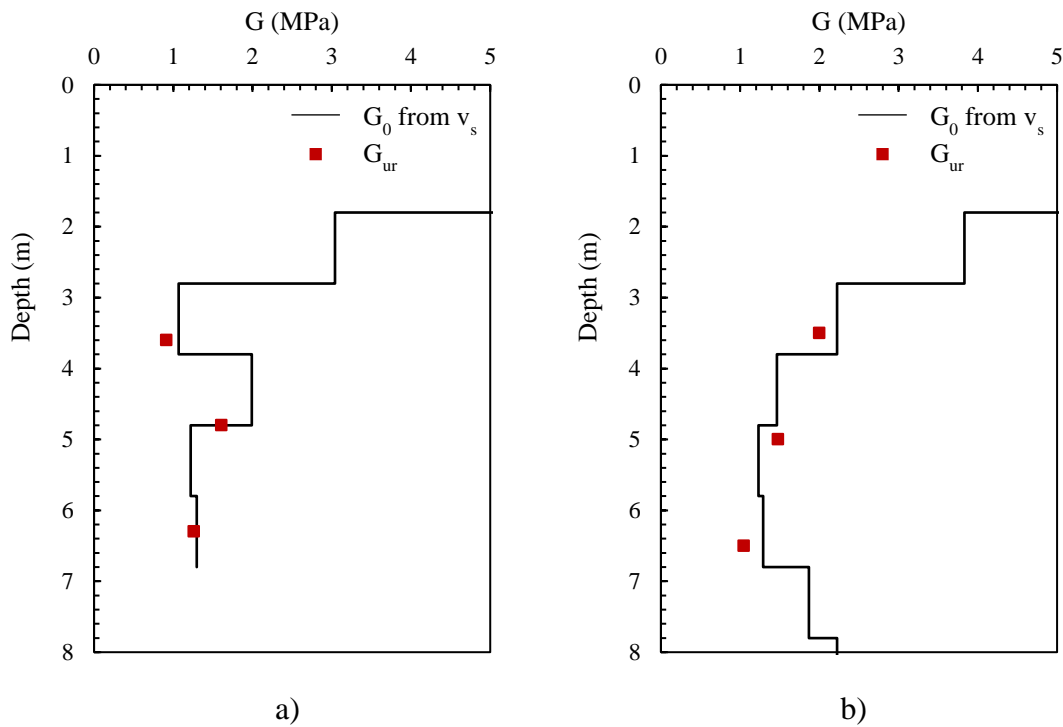


**Figure 3.12** Variation of small stress shear stiffness,  $G_0$  and  $G_{ur}$  from first unload-reload from PMT test results with depth at Site 01 in Surrey, British Columbia, Canada: (a) Test Group 01 (b) Test Group 02.

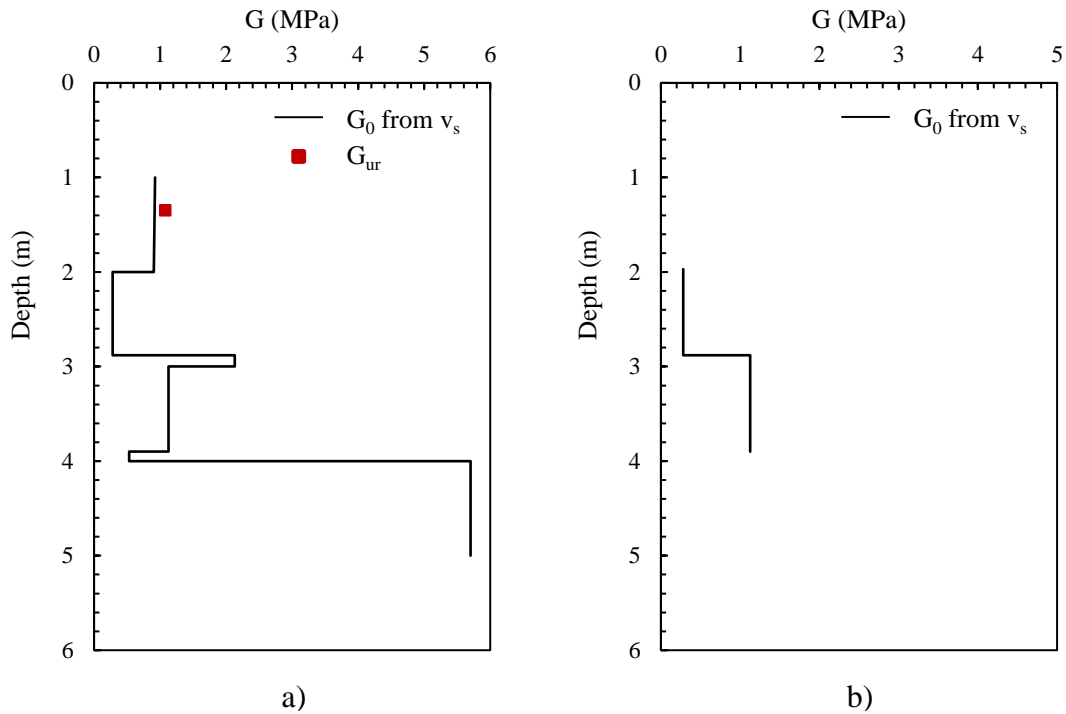
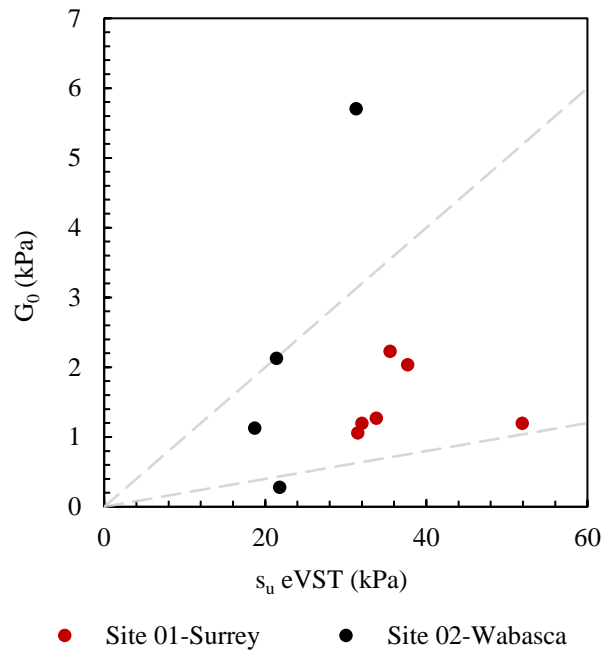


Figure 3.13 Variation of small stress shear stiffness,  $G_0$  and  $G_{ur}$  from first unload-reload from PMT test results with depth at Site 02 in Wabasca, Alberta, Canada: (a) Test Group 01 (b) Test Group 02.

### 3.3.3 Shear strength and stiffness correlations

Due to many reasons, it is commonplace to seek correlations between shear strength and stiffness in geomaterial characterization for constitutive modeling. With this background and considering the value of such correlations in setting up input parameters for numerical modeling, potential correspondence between the soil shear stiffness ( $G$ ) and strength ( $s_u$ ) derived from the previous sections was examined. In this attempt, considering the high reliability, the  $G_0$  values were derived based on measured  $v_s$  values; similarly, the noted promising performance of full-flow penetrometers (Boylan et al., 2011) in soft and weak soils, the counterpart  $s_u$  values were derived

from BPT data. The results are plotted in Figure 3.14 with dashed lines providing some bounds on  $G_0/s_u$  which represents the rigidity index of the organic soil. It appears that there is significant scatter in the plot leading to  $G_0/s_u$  ratios enveloped between  $\sim 20 - 100$ , and they are significantly low compared to those typically noted for mineral soils. In addition to the natural variability and complexity of organic soils, such wider range observed for  $G_0/s_u$  can also be partly attributed to the fact that the values in the numerator and denominator both being low in soft and weak organic soils (i.e., low values divided by low values could leading to answers with wider scatter).



**Figure 3.14  $G_0$  from  $v_s$  measurements versus  $s_u$  from eVST based on test data from two Test Sites 01 and 02**

Parameters representing shear stress and strain relationship of organic soil is needed to represent the soil domain in continuum numerical modeling of horizontal soil-pipe interaction under a different section of this thesis. In particular, the site-specific  $G_0/s_u$  ratios and shear strength

properties determined as per above are utilized to characterize the bulk behavior of organic soils with respect to the numerical SPI analysis undertaken in Chapter 6.

### **3.3.4 Interface shear properties**

The findings from direct shear (DS) testing undertaken primarily to study soil-solid interface shear characteristics are discussed in this section. The shear stress versus shear displacement curves generated from interface DS tests identified in Appendix A.7, Table A.2 on organic soil and solid GE coating and mild steel interfaces are presented in Appendix A.7, Figure A.15. Similar results from direct shear tests conducted on organic soil alone are presented in Appendix A.7, Figure A.16.

The mobilized peak shear stresses from the DSA tests were extracted from the shear stress versus displacement plots (summarized in Appendix A.7, Table A.3). It was noted that there was no distinct peak or post-peak shear stress behavior visible in almost all of the DSA tests; as such, for a given test, the highest shear stress recorded within the applied shear displacement range was selected as the peak shear stress.

The shear behavior in terms of the resistances mobilized at the interfaces of organic soil-GE coating and organic soil-bare mild steel (MS) were compared. The shear resistance at the organic soil and GE coating interface is lesser than that of the MS and organic soil interface. It is reasonable to claim that this is due to the higher surface roughness level in the sand-blasted mild steel surface compared to the GE-coated surface (as well noted from the surface roughness values of GE and MS solid test surfaces; 0.15  $\mu\text{m}$  and 7.0  $\mu\text{m}$ , respectively).

The shear resistance observed in tests involving organic soil alone, provided an opportunity to plot shear strength envelopes and estimate the internal friction angle for organic soil. Comparison of the resulting shear resistance for similar normal effective stresses at different interfaces with organic soil alone from Site 01 shows that the developed shear resistance within organic soil alone is higher than that observed at the tested organic soil – solid surfaces. Figure 3.15 presents the typical shear strength envelopes for the organic soil – GE coating interface, organic soil – MS interface and organic soil alone. As Mohr-Coulomb failure criterion is a widely accepted simple model representing soils in geotechnical engineering practice, it was used to obtain interface and internal friction angles for the tested organic soil – interfaces and organic soil alone in this study.

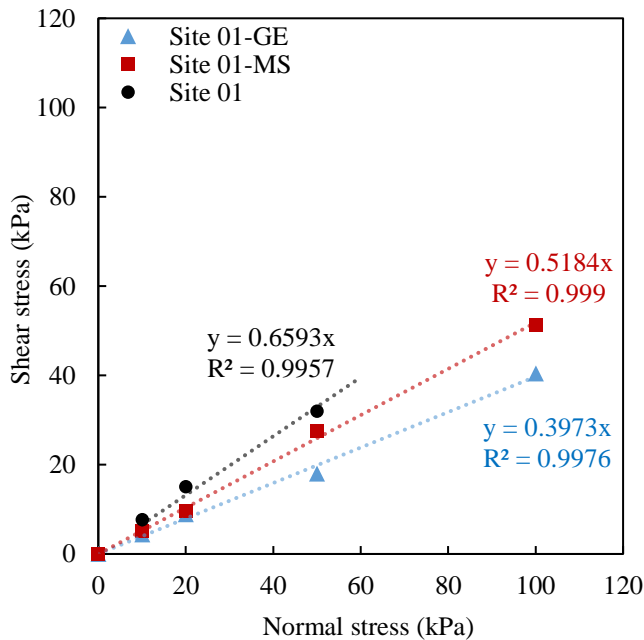


**Figure 3.15 Shear stress vs normal stress strength envelopes; a) organic soil - GE and organic soil – MS interfaces, and organic soil alone from Site 01 in Surrey, British Columbia, Canada**

The results show that the shear behavior of organic soil can be represented using frictional properties. According to Figure 3.15, the interface friction angles between Site 01 organic soil – GE coating and organic soil – sand blasted MS are  $21.7^\circ$  and  $27.4^\circ$  respectively. Further, the internal angle of friction in organic soil alone from Site 01 is  $33.4^\circ$ . Higher friction angle in sand blasted MS than that of GE coating from interface DSA tests is anticipated because the higher surface roughness of soil-solid test surface is expected to provide more traction against interface slippage. In essence, it is evident that the angle of interface friction increases with the increasing surface roughness for organic soil and solid test surface interfaces. This is in line with the previous understandings developed mainly based on interface shear tests conducted on various mineral soil-solid interfaces.

### **3.4 Summary**

Although the performance of organic soils in terms of compressibility has been well studied to address general foundation design and stability problems, very little work has been undertaken explicitly. Understanding of the mechanical behavior of organic soils plays a vital role in governing the “soil-pipe interaction” (SPI) that takes place in pipelines buried in such soils. For this reason, a detailed geotechnical field and laboratory experimental program comprising Seismic Cone Penetration Test (SCPT), Ball Penetration Test (BPT), Electronic Vane Shear Test (eVST) and Pressuremeter Test (PMT) was undertaken at two selected test sites known to be underlain by organic soils located in Surrey, British Columbia and Wabasca, Alberta, Canada. The testing work was conducted to cover soil conditions within a depth around 7 m below the ground surface at the test sites – a depth extent considered suitable since most pipelines since are located within about

2 m from the ground surface. Laboratory test program consisting of: direct shear (DS) tests to study the interface shear properties of organic soil-solid pipe material surfaces; and direct simple shear (DSS) tests on reconstituted organic soil to determine the undrained shear strength ( $s_u$ ) was also undertaken.

The shear strength and stiffness data generated from the field experiments and the interface shear properties obtained from lab tests were utilized to characterize the mechanical behavior of organic soil. The information is intended to develop parameters needed to represent organic soils in numerical modeling of soil-pipe interaction, as discussed in Chapter 7 in detail. Furthermore, the pressure versus radial expansion curves obtained from the pressuremeter tests are utilized to validate a stress-strain relationship for adequate and meaningful representation of bulk behavior of organic soil with respect to SPI analysis which is discussed in Chapter 6.

## Chapter 4: Soil-Pipe Interaction Physical Modeling Aspects

The assessment of the response of pipelines subject to ground movements involves understanding the mechanics of a complex soil-pipe interaction (SPI) problem. High quality data derived from physical model tests mimicking controlled SPI boundary value problems, providing the basis for validation of numerical and/or analytical approaches, play an important role in developing this understanding.

Generally, in remote areas when the pipelines cross organic soils, trenches are backfilled using the material excavated from the trench. Therefore, the study of direct interaction between the pipe and organic soils becomes relevant, and in turn, raising the need to undertake physical modeling of pipelines directly buried in organic soil backfills.

The large full-scale physical modeling soil chamber at the Advanced Soil-Pipe Interaction Research (ASPIRe™) facility at UBC that was designed to accommodate SPI studies on buried pipelines in mineral soils provided the technical basis and inspiration for developing smaller devices to specifically address the present research requirements (Anderson et al. 2005; Karimian 2006; Monroy-Concha 2013). The large full-scale physical modeling soil chamber is approximately 2.45 m x 3.8 m in footprint, and it could subject relative axial, lateral, and oblique ground movements on buried pipelines possessing up to 2 m of soil cover.

Unlike mineral soils such as sands and clays, organic soils exhibit numerous challenges in handling and soil preparation for testing in a full-scale experimental setup due to its inherent soft and non-uniform nature. It became evident that preparing large specimens comprising organic soil (involving complex soil placement and compaction approaches) with controlled uniformity will be difficult and involve many people. Also, fabrications and improvements needed in the large test

chamber demanded special technical support and additional time. Since these research tasks were scheduled to be undertaken during the global pandemic years, it involved numerous health and safety issues that needed to be addressed and additional obstacles related to material supply and delivery complications. Therefore, the use of the large soil chamber was considered impractical. As such, new test chambers with reduced sizes (involving reduced volume of organic soil) were built to perform the SPI (axial and lateral loading) testing contemplated for the current research as presented below.

Two testing chambers, designed and constructed at the University of British Columbia, as a part of this thesis, were used to investigate force-displacement behavior of buried pipeline configurations subjected to axial and lateral loading systematically representing typical field loading conditions encountered in organic soil terrains. The basic principles of loading mechanisms, specimen set up, and data acquisition approaches in the new devices essentially followed those developed as a part of the design of the larger soil chamber. The first test chamber is an improved version of the testing apparatus that was used for axial soil-pipe interaction by Amarasinghe (2019), accommodating settlement of the pipe specimen during full-scale tests; this was suitably modified to meet the axial pullout testing requirements in the current thesis. The second testing apparatus was newly designed and built to simulate SPI tests when buried pipelines (up to 200 mm in diameter) in organic soil are subjected to relative lateral soil displacements.

This chapter describes the experimental aspects related to the above two full-scale test apparatus that allowed studying the soil restraint development on buried steel pipe specimens in organic soils when subjected to relative axial and lateral ground displacements, respectively. Details about the design of the test chambers, tests setup, loading mechanisms, and data acquisition approaches of the systems are described in detail in the following sections.

#### 4.1 Axial SPI Test chamber

The test apparatus developed to conduct axial SPI of internal size 1.5 m x 0.8 m in plan view, and 0.75 m in height is capable of testing pipes of up to 160 mm in diameter (Figure 4.1 shows the perspective view of the soil chamber). A pipe of 2.4 m length can be tested in the axial configuration up to a maximum axial displacement of 0.5 m while 1.2 m of the pipe is in contact with the soil. The device allows for free vertical movement of the pipe during consolidation of the soil accommodated through mobile side walls. Pipes can be tested in both partially buried and fully buried configurations.



Figure 4.1 Perspective view of the axial soil-pipe interaction test apparatus

The design of the soil box was based on several considerations pertaining to practicality as well as pipeline and organic soil behavior mechanisms, and they include: a) relatively smaller box dimensions (compared to ASPIRe™ soil chamber) allowing a practical box size which is less challenging to fill organic soil in layers when preparing the soil bed for testing; b) free vertical movement of the pipe during consolidation of the soil allowed through the design of movable side walls; c) minimal effects from the end walls and side walls during axial pullout tests based on the pipe diameter tested (NPS 4); and d) minimum side friction accommodated through laminated inside walls. The original version of this test chamber that was designed and built by Amarasinghe (2019) was improved by adding a reinforced structure to withstand the stress conditions based on the proposed test program and finalizing the loading mechanism of the test chamber. Figure 4.2 shows modifications of the axial SPI test apparatus – before and after adding reinforcement. Based on the structural beam deflection-based calculations, the maximum deflection of the side walls was estimated to be less than 3 mm, and this translates to about 0.75% horizontal strain during the setup. Considering that the axial test is conducted after the setup of the specimen and the fact that there are no additional stress changes imposed at the time of testing, it is judged that the influence of side wall stiffness would not significantly affect the axial load development on the pipe during the experiments.



**Figure 4.2** Photographs taken (a) before and (b) after installation of the aluminum structure to reinforce the axial SPI test chamber

#### **4.1.1 Loading mechanism**

The pipe specimen is axially displaced (loaded) by a worm-gear linear actuator rod and a stepper motor and gear system. The linear actuator rod attached to the pipe is mounted on a railing system for the smooth movement of the pipe. The pipe specimens are loaded in a displacement-controlled manner at a rate of 0.5 mm/s based on previous research findings on the effect of loading rate on axial load generation during full-scale tests, as discussed in section 2.1.1.

The loading system details of the axial SPI testing apparatus are shown in Figure 4.3. The system consists of a high-speed bipolar stepper motor: Model 57STH56-2804B (manufactured by Analog Devices Inc. Wilmington, Massachusetts, USA) and a gear arrangement to enhance the maximum torque; these are mounted at the end of a horizontal railing frame coupled with a linear actuator rod [see Figure 4.3 a)]. The stepper motor and gear system are capable of providing a constant

displacement rate in the range of 0.1 mm/s – 25 mm/s. The horizontal railing is firmly connected to the side walls of the test chamber as may be noted.

As shown in Figure 4.4, the load cell is firmly connected to the linear actuator rod through a platform which slides on the railing system as the pipe moves in the axial direction. The system for attaching the pipe to the load cell consists of a hook attached to the load cell which passes through a rigid horizontal rod tied at the mid-level of the pipe end (see Figure 4.4). This system provided a detachable connection at the pipe end allowing the movement of the pipe or the actuator system during test preparation preventing any damage to the system.

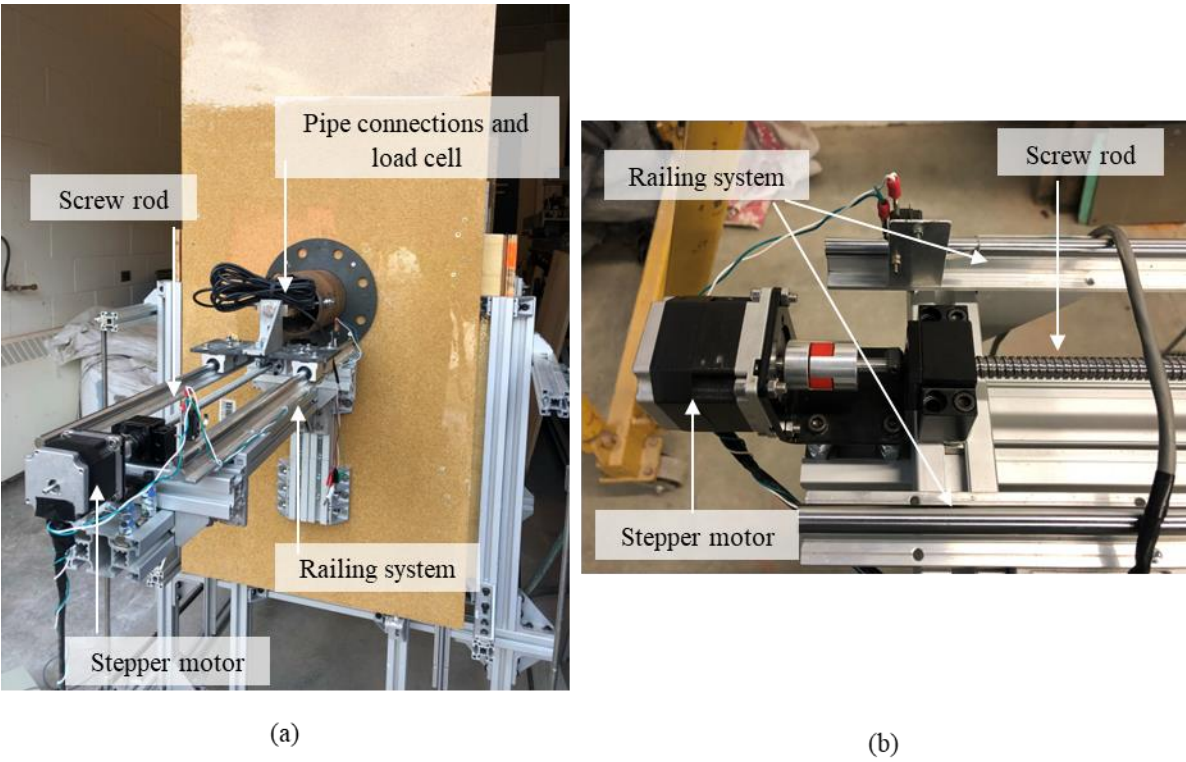


**Figure 4.3 Loading system and connections of the axial SPI test apparatus: a) Components of the loading system and b) Stepper motor and linear actuator rod connections**

Length of the pipe specimen tested in the axial SPI test apparatus is 2.4 m which was longer than the length of the box so that the pipe extends through both ends after full displacement of pipe. This ensured a constant soil-pipe test length and avoided soil disturbance at the rear end of the box during pullout. Two 170 mm circles were cut at the front and rear ends of the box to provide the entrance and exit openings for the tested pipes having diameters up to 150 mm (i.e., NPS 4 and NPS 6 pipe sizes). Two circular gaskets with 120 mm inside diameter, made from PVC were secured at these two end-openings (see Figure 4.4) to prevent soil loss during testing. Further, a foam ring which exhibited minimal resistance to pipe movement was attached to the inside face of the test chamber to prevent any leakage of soil or water when the pipe passed through the opening gasket.

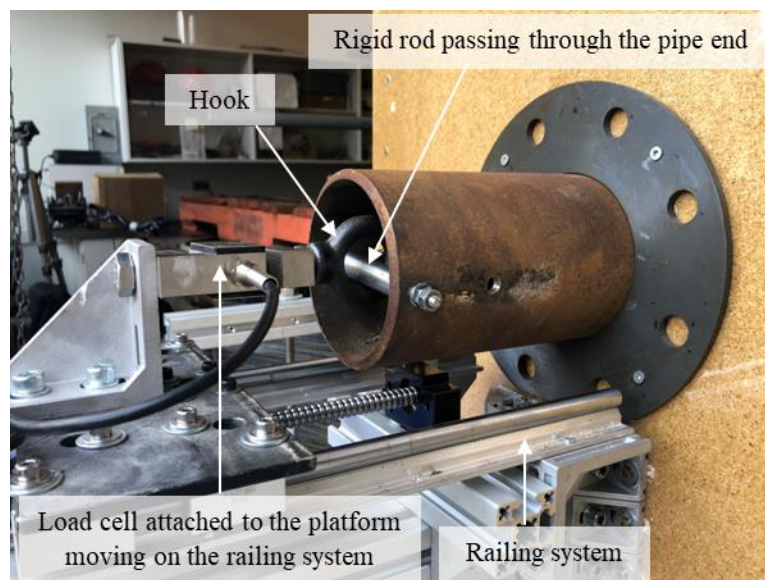


**Figure 4.4 Connection of load cell and pipe**

### **4.1.2 Instrumentation and data acquisition**

Primary measurements made during the axial displacement tests included the force acting on the pipe specimen and the displacement of the pipe relative to the soil box. Several other measurements such as soil bed density and pipe settlement were obtained to monitor the pipe and soil movements during test preparation and pipe displacement.

All measurements from the instrumentation array monitoring the test pipe were recorded at 10 samples per second. Signals from the instrumentation array were collected using a 16-channel National Instruments, Austin, TX, USA, signal conditioning board. The commercially available software package LabView Version 2, National Instruments Inc., was used for real-time acquisition of data from the two channels used for force and displacement measurements. The system was controlled using a dedicated computer system running MS Windows 10.

#### **4.1.2.1 Load measurements**

A load cell mounted on a rigid platform that moves on the railing system [see Figure 4.5 (a)] was connected to the pipe for the measurement of axial soil restraint during all axial pipe displacement tests. The load cell was an S type load cell, Model No: 3140\_0 (UBC Load cell LC78) with a maximum load capacity of 5 kN, and it is operated at an excitation voltage of 5 V; the load cell was calibrated to cover the range of expected loads. S type load cell connected to the pipe is shown in Figure 4.5 (a).

#### 4.1.2.2 Pipe displacements

Pipe displacements were measured using string potentiometers mounted on the front and rear walls of the test chamber. The cables from the string potentiometers were connected to the steel rods firmly attached to both ends of the pipe. The arrangement of sting potentiometer and the cables at the front side of the test chamber is shown in Figure 4.5 (b).

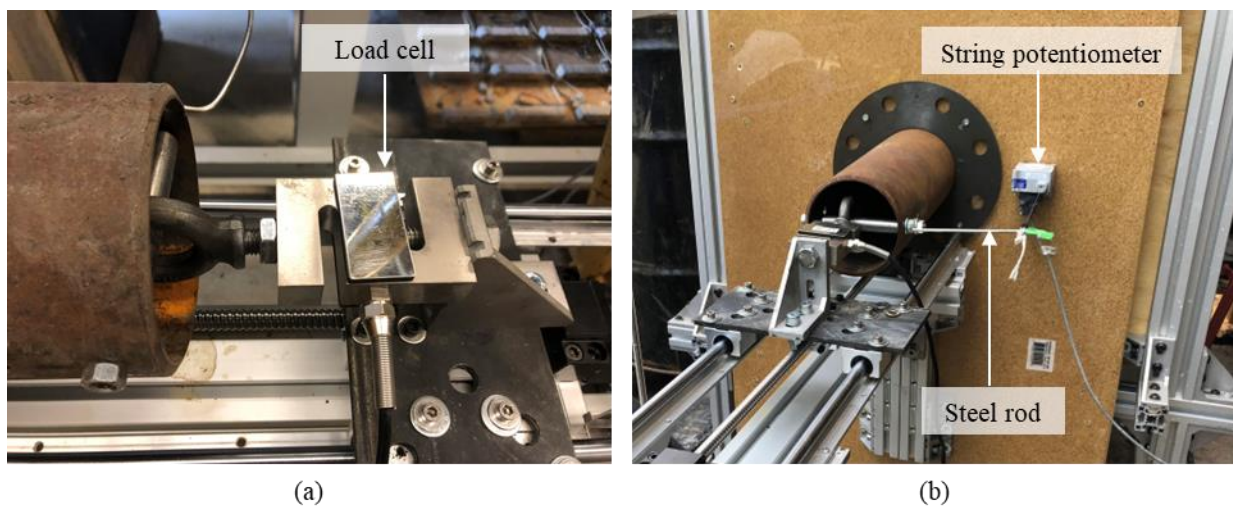


**Figure 4.5 Force and displacement measurement sensors attached to the test pipe: a) Load cell; and b) String potentiometer**

#### 4.1.3 Interface shear zone thickness and test-chamber boundary constraints

As a part of examining the axial load-displacement response, it is important to understand the test chamber boundary effects, and considerations arising with respect to the soil-pipe interface shear zone thickness, on the load developed in the pipe. The test apparatus used to conduct the axial pipe pullout tests was 1.5 m in length and 0.8 in width. The distance to the nearest side wall from the

side of the pipe (NPS 4 pipe; 114 mm in diameter) at the springline-level was 340 mm which is about three times the pipe diameter. Based on previous research studies (Roscoe 1970, Bridgwater 1980, Scarpelli and Wood 1982), the thickness of actively sheared zone has been suggested as  $10(d_{50})$ , where  $d_{50}$  is the median grain size. With respect to pipeline soil interfaces, this was further confirmed by Karimian (2006) by measuring the deformation of soil particles in the vicinity of the pipe using colored sand zones during axial pipe pullout tests in Fraser River sand. These measurements indicated that the thickness of the shear zone was 1.2 to 2.8 mm which is in line with previous research findings.

The organic soil tested in the current study was processed by removing coarser fibers and mixed to achieve a uniform soil mix; this led to the size of the fibers to be  $<5$  mm, which is less than 5% of the diameter of the tested pipe. Along with the soft nature of the tested soil and the above information on the potential shear zone thickness, it is reasonable to assume that the shear zone at the soil-pipe interface during axial pullout is likely to be less than 50 mm. Therefore, it was judged that the distance of 340 mm to the side wall from the pipe should be adequate from the point of view of minimizing boundary effects.

It is also recognized that some interaction between the shear zone and the front wall of the chamber (perpendicular to the pipe) would occur during pullout testing. Previous work by Wijewickreme et al. (2009) and Karimian (2006) with respect to axial pullout testing of pipes buried in sand has suggested that the error on the axial load from this front wall interaction is negligible; this assessment is also considered applicable for the present axial load tests involving pipes in organic soils.

#### **4.1.4 Testing program**

The new axial SPI test chamber was used to conduct eight full-scale tests using a steel pipe buried in a test organic soil bed. The tested pipe specimen was approximately 114 mm in outer diameter (NPS 4), and 2.4 m in length which had a wall thickness of 6 mm. The pipe surface was sand-blasted and was tested as a pipe without any coating application (i.e., bare pipe). The test program was aimed at conducting pipes buried in normally consolidated organic soil under five different pipe burial depth conditions. It should be noted that, in addition to the tests reported herein, several tests were performed to calibrate the instruments, measure the friction between the side walls and the pipe as a part of developing test procedures.

#### **4.1.5 Preparation of axial SPI test chamber and test procedure**

The preparation work related to a given test included several steps. First, the soil was carefully mixed in 300-liter containers using a laboratory soil mixer paddle attached to a rotor to achieve a relatively uniform soil mix; mixing was performed in a slow speed setting to minimize potential breakage of fibrous matter present within the soil. Subsequently, the mixed soil was placed in the test chamber in loose 150 – 200 mm lifts: upon placement of a given lift of soil, a gentle pressure was applied on the soil mass using a plywood sheet (0.3 m x 0.3 m) attached to a wooden handle [see Figure 4.6 (a)]; the objective was to have an evenly compacted soil deposit with an approximately level surface while recognizing the capabilities and limitations of this manual placement approach. The height of the placed lift was measured at six different points, while

containers were placed to obtain density and moisture content measurements after the test; a given lift of soil was found to reach a height of approximately 160 mm after the compression process. Once the soil level was elevated to the intended pipe invert level, the test pipe was gently lowered on to the soil bed using a crane [see Figure 4.6 (a)]; after placement, the initial vertical position of the crown along the pipe alignment was measured relative to a reference point. As the next step, the organic soil was placed, again in loose lifts, until the top surface of the soil reached the crown elevation of the pipe. Gentle pressing of the soil using a wooden tamper as shown in Figure 4.6 (a), similar to the previous lifts, were made to achieve reasonably packed soils around the pipe with good soil contact with the pipe surface. Above the pipe crown level, the organic soil was placed in loose lifts of 100 mm while applying the packing efforts similar to those described earlier until the required soil cover was attained. Again, the elevation of the final soil surface was measured at 6 different points to confirm that the specimen is in accord with the intended configuration. Figure 4.6 shows some photographs taken during the test specimen preparation work described above. Although the exact compaction approaches using construction machinery in the field is difficult to accurately replicate, the backfilling and compaction approaches used in the physical modelling setup is relevant and meaningful considering the need to have uniform test soil beds in performing controlled experimental work.

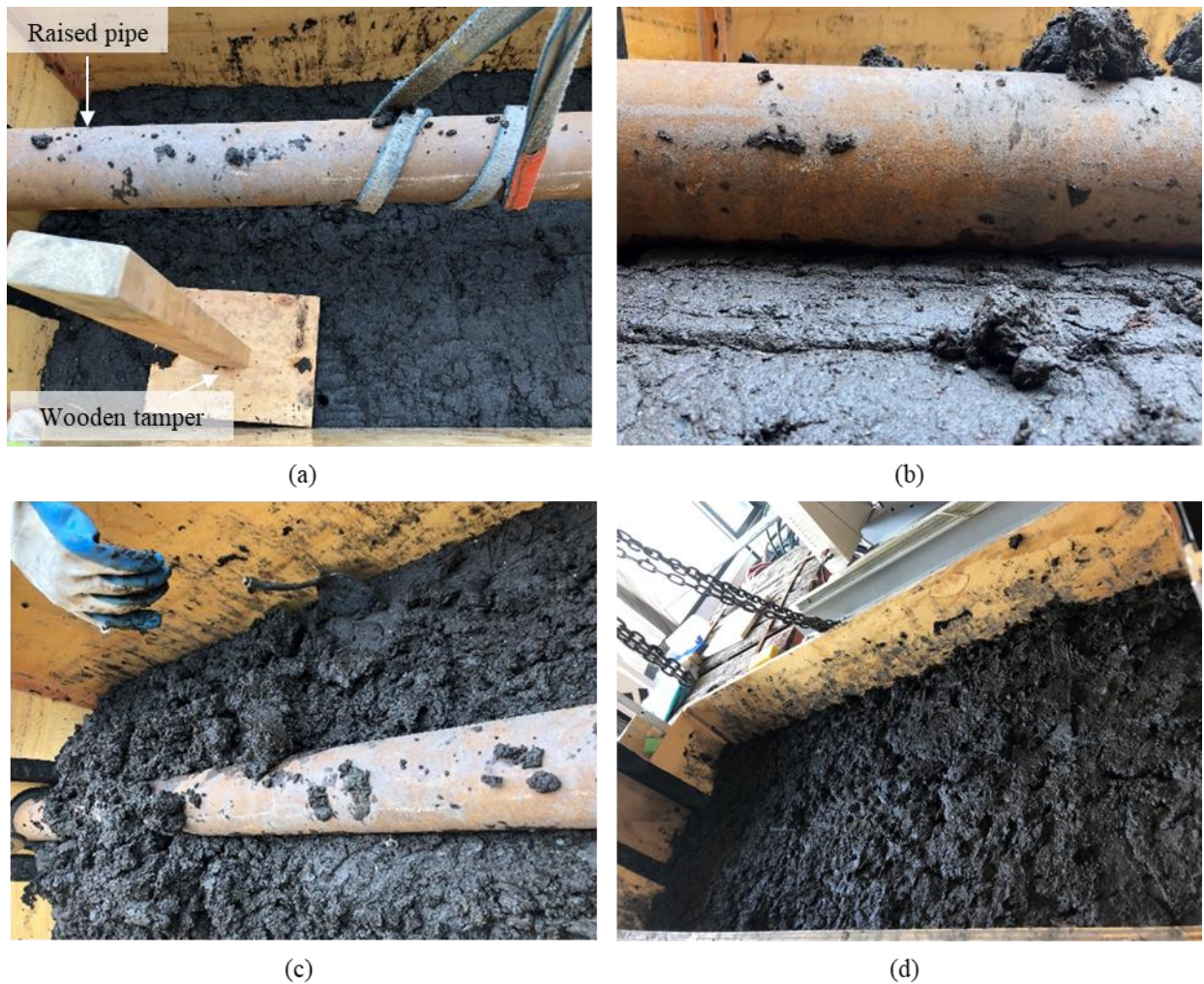


**Figure 4.6 Photographs showing different steps of the soil bed preparation prior to a test: a) Soil bed preparation before placing the pipe; b) Test pipe lowered on to the soil bed; c) Preparing the sides along the soil-pipe interface; and d) Soil cover preparation**

For the tests that required simulating pipes embedded at relatively larger depths, the corresponding higher overburden pressures, were simulated by surcharge loading of the organic soil bed. In this regard, Fraser River (FR) sand and/or tanks filled with water were placed on the surface of the organic soil bed to provide the required surcharge pressure. A cross section of the test chamber

shown in Figure 4.7 schematically illustrates such surcharge loadings employed. Prior to placing the surcharge, the soil surface was prepared as described earlier and a geotextile was placed on the organic soil cover to avoid possible material mixing. Then, FR sand (~unit weight  $16 \text{ kN/m}^3$ ) was placed in loose lifts of 50 mm up to the desired height depending on the stress requirement of the test case. Figure 4.8 shows photographs taken during the placement of geotextile and FR sand in the axial SPI test chamber. Once the sand bed was leveled, the first water tank was placed on sand after placing a plywood frame to distribute the load evenly on the sand surface. The tank was filled with water and the second water tank was placed on top of the first and filled with water the same way. Figure 4.9 shows the final set up of the axial SPI test chamber (surcharges placed) before a pipe pullout test.

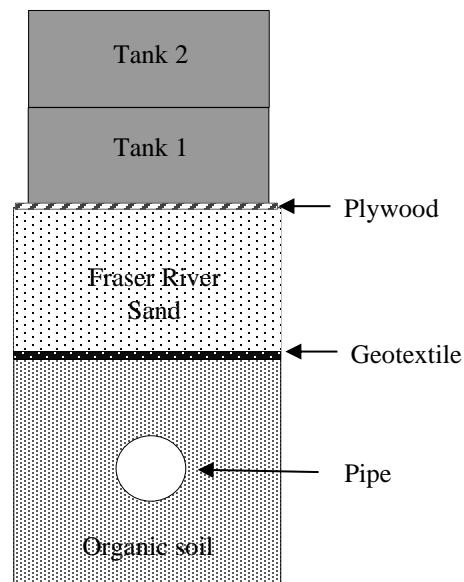


**Figure 4.7 Schematic diagram illustrating a cross section of the test chamber tested for higher overburden stress levels (Note: not true scale)**



**Figure 4.8 a) Placement of geotextile on prepared organic soil cover; and b) Preparation of FR sand bed in layers**

Due to the presence of the 200-300 mm sand bed overlying the organic soil mass, it is judged reasonable to assume that the application of equivalent overburden stress at the pipe level is uniform – i.e., the relatively higher stiffness of the water containers is not considered to impact the uniformity of the overburden stress at the pipe level due to the flexibility of the sand bed.

The soil bed was allowed to consolidate under the self-weight prior to applying the axial displacement to the pipe. After 24 hours, the position of the crown of the pipe was measured relative to a reference to check the settlement of the pipe. Two mobile side walls (see Figure 4.9) carrying the pipe were allowed to rest on four brackets attached to the soil box frame to limit further settlement of the pipe during pipe pullout.

The development of axial-soil restraint was investigated by displacing the test pipe in the axial direction at a constant rate of displacement of 0.5 mm/s. The rate of pipe displacement was selected based on previous research findings by Karimian (2006) and to match the limitations of the

actuator system of the test apparatus. Eight axial soil-pipe interaction tests were conducted on the pipe after preparing the test chamber as described above. A total axial pipe displacement of 400 mm was achieved in each test while axial force and axial displacement were measured. Experimental criteria and the results of these tests are presented in Chapter 5.



**Figure 4.9** Final set up of the SPI test chamber prior to axial displacement test

## **4.2 Horizontal SPI test chamber**

A new soil chamber was designed and fabricated for assessing SPI in buried pipelines in organics soils subjected to horizontal lateral ground displacements. The apparatus has the flexibility to perform axial displacement tests with further modifications. The design and size of the test chamber were selected considering the following factors anticipated in lateral soil failure

mechanisms in organic soil: a) smaller soil box dimensions (compared to ASPIRe™ soil chamber) allowing a more practical box size for the testing of SPI in organic soil; b) avoid the encroachment of active and passive soil zones (developed during pipe displacement) with the front and rear walls – considering the testing of pipe specimens with diameters up to 220 mm (NPS 8) – ascertained by modeling the size of the test chamber and performing numerical analysis [using FLAC-2D – Version 8 (Itasca 2016)]; and c) poly-vinyl chloride (PVC) and plexiglass facing materials were selected as materials for the side walls with the intent of to minimizing side friction during testing. The basis for suitability of these materials was determined based on detailed previous studies undertaken as a part of the ASPIRe™ soil chamber design, and they are not repeated herein (Karimian 2006; Monroy-Concha 2013). Further details on selecting the size of the box based on FLAC analysis results is presented in Appendix B.

Based on these considerations, a test chamber having a 1 m x 2 m plan footprint, and 1 m in height was chosen as the final configuration for fabrication; the chamber design was made with the support of engineering and technical staff and at UBC Civil Engineering – in essence, an NPS 8 pipe having a length of approximately 1 m can be tested with the possibility of imparting relative lateral horizontal displacements up to 0.4 m. Pipes can be tested in both, partially and fully buried configurations as needed. Figure 4.10 shows pictures taken during construction and the final assembly stages of this horizontal SPI test chamber.

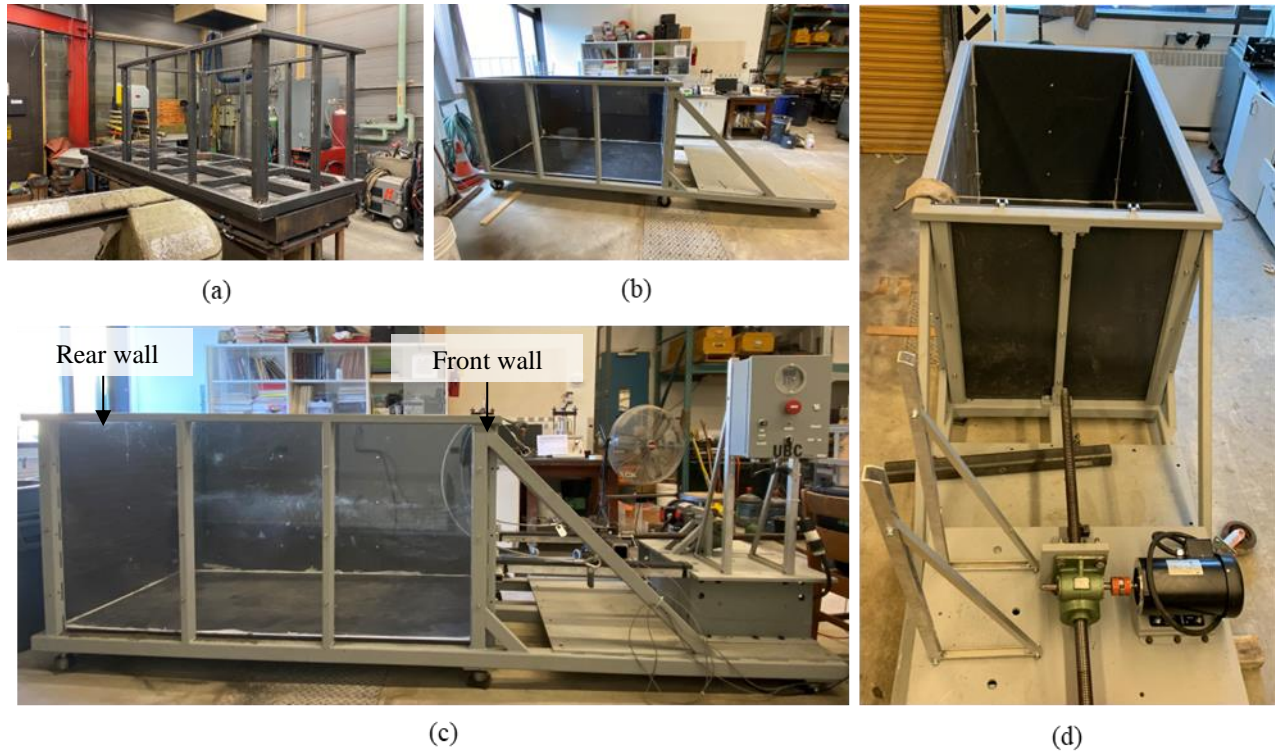


**Figure 4.10** Photographs of horizontal SPI chamber construction stages: a) Construction of the metal frame using box steel bars; b) Construction of the PVC and plexiglass walls and metal platform for equipment mounting; c) Final view of the soil chamber including the actuator system and motor controller system; and d) Installation of the actuator system consisting of an AC motor and linear actuator rod

#### 4.2.1 Loading mechanism and actuator connections

The pipe specimen is horizontally displaced by a system of pulling cables connected to a rigid steel bar and a worm-gear linear actuator rod attached to an AC motor. The steel bar rested on a railing system for smooth movement of the pipe. The pipe specimens were loaded in a displacement-

controlled manner at a rate of 3 mm/s. The available displacement rate was controlled by the capacity of the AC motor and operating limitations of the linear actuator rod.

The loading system consists of a three-phase induction motor Model MTRP-002-3BD18 (manufactured by Automation Direct Optimization Inc, Cumming, GA, USA), and a SWL 5T worm-gear linear actuator with a 24:1 gear ratio (manufactured by Qingdao Chinese Science Machinery Co. Ltd, Qingdao City, China) mounted on a loading pedestal attached to the steel floor of the horizontal SPI test chamber. Figure 4.11 shows different components of the horizontal SPI test chamber loading system. Two galvanized pulling cables, 10 mm (0.375 inch) in diameter are connected to the linear actuator rod through a rigid steel bar to maintain a uniform rate of displacement. The pulling cables are extended through two 150-mm long vertical slits on the front wall. This allowed imposing the required horizontal displacements on the test pipe specimen while providing the cables with the freedom to move in a vertical plane, as the test progresses. Two PVC sheets of 0.2 m x 0.2 m size were attached to the vertical slits on the outside of the test chamber to prevent potential leakage of soil when the pipe passed through the opening. These sheets also had the freedom to move in the vertical direction along with the cable movement. Figure 4.11 shows the location of the vertical slits covered by the PVC sheets at the opening.

As shown in Figure 4.12 (a), the load cell transducer is firmly connected to the linear actuator rod and the rigid steel bar is connected to the pulling cables. The rigid steel bar is free to slide in the horizontal direction on a platform consisting of two horizontal side bars as the pipe displaced [see Figure 4.12 (a)]. The side bars are plated with PVC so that the rigid steel bar slides with minimal friction. The pulling cables extending out of the box are attached to the rigid steel bar using built in hooks and shackles; as shown in the Figure 4.12 (b), the pipe is connected to the other end of the pulling cables (inside the test chamber) using clamps and braces on the pipes which aligned

with vertical slits on the front wall of the test chamber. The length of the cables were selected so that it provided adequate slack to make connections with the pipe during test preparation; the cables could be then adjusted to reach the required tightening corresponding to the initial reading just before commencing the test.

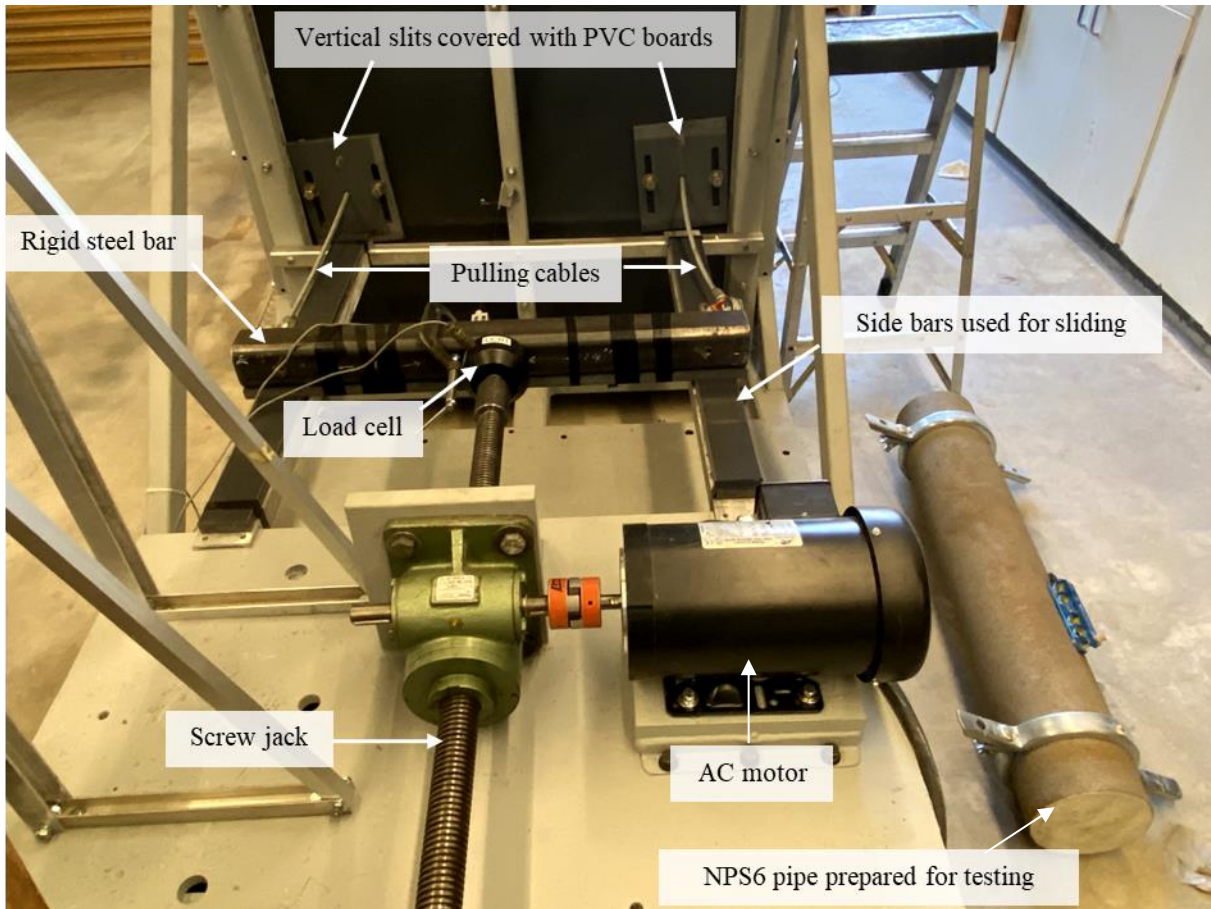


**Figure 4.11 Loading system of the horizontal SPI test chamber**

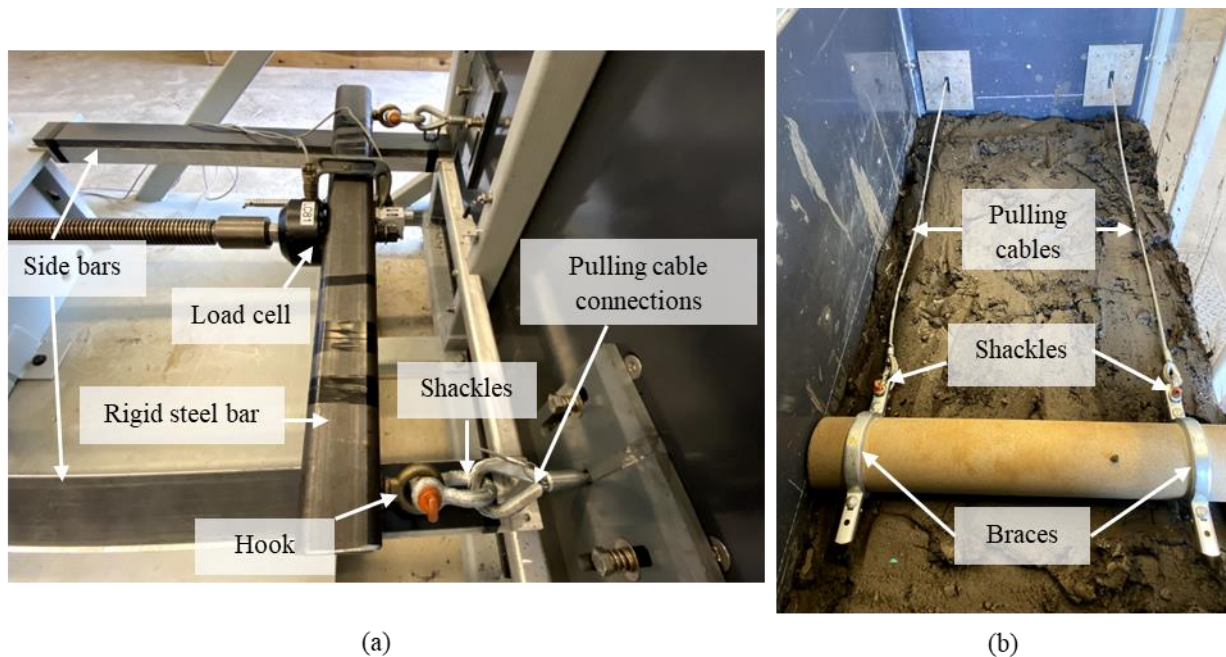


**Figure 4.12 (a) Load cell and Linear actuator rod connections outside the horizontal SPI test chamber; and (b) Pulling cable and pipe connections inside the horizontal SPI test chamber**

#### **4.2.2 Instrumentation and data acquisition**

Similar to axial displacement tests, primary measurements made during the horizontal displacement tests included the forces acting on the pipe specimen and the displacement of the pipe relative to the soil box. Several other measurements such as soil density and moisture content were obtained to establish the soil bed conditions during test preparation and pipe displacement for a given test. Apart from the above measurements, soil conditions of the prepared soil bed were assessed using a ball penetrometer, cone penetrometer, and electronic shear vane testing; these tests were conducted using test equipment and in-kind technical support provided by ConeTec Investigations Ltd. Of Richmond, B.C. This test program is further detailed in Chapter 5.

All measurements related to the force and displacement readings were recorded at 10 sps (10 samples per second). Signals from the instrumentation array were collected using a 16-channel National Instruments, Austin, TX, USA, signal conditioning boards. The commercially available software package LabView Version 2, National Instruments Inc. was used for real-time acquisition of data from the four channels dedicated for force and displacement measurements. The system was controlled using a dedicated computer system running MS Windows 10.

#### **4.2.2.1 Load measurements**

A load cell directly attached to the linear actuator rod (see Figure 4.13) connected to the pulling cables through the horizontal steel bar was used to measure the force generated due to pipe displacement, measuring the soil restraint during horizontal pipe displacement tests. The load cell was Model SW10-10K-B000 with a maximum load capacity of 4500 kg (manufactured by Transducer Techniques, LLC, Temecula, California, USA) which operated at an excitation voltage of 10 V and calibrated over the range of expected loads.

#### **4.2.2.2 Pipe displacements**

Horizontal pipe displacements relative to the test chamber were measured using three string potentiometers mounted on the front wall of the test chamber. The cables from the string potentiometers were connected to the steel bar firmly attached to the linear actuator rod. The arrangement of sting potentiometers on the front wall of the test chamber is shown in Figure 4.13.

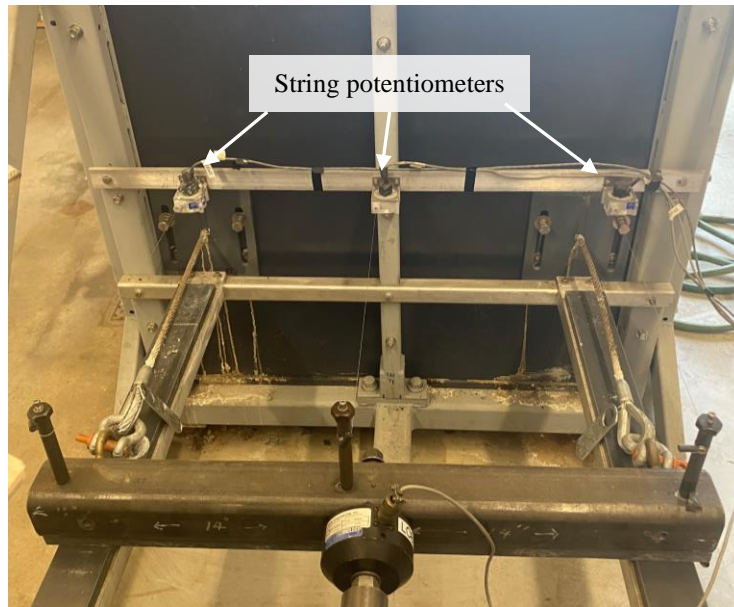


**Figure 4.13 String potentiometer placement outside the horizontal SPI test chamber**

#### **4.2.3 Effect of test chamber boundary constraints (sidewall friction)**

The lateral pipe displacement tests simulate a pipeline subjected to relative lateral horizontal soil movement in a 2-dimensional plane strain manner. The load measured from the test is then used to determine the load-displacement curves on a per-unit-length-of-pipe basis. However, mobilized frictional force between soil and vertical sidewalls of the tests chamber during pipe displacement causes additional resistance (i.e., in addition to the resistance from the soil mass around the pipe). Sidewall friction effect can be minimized by choosing appropriate material for the sidewalls of the test chamber so that the interface friction angle between side wall and the soil backfill is smaller. Past studies of full-scale pipe displacement tests have used several methods to minimize the sidewall friction. (Audibert and Nyman 1977b) has used two layers of polyethylene as sidewall

lining. (Trautmann and O'Rourke 1985) used glass and formica to reduce the effect of side wall friction and Karimian (2006) lined the side walls with stainless steel sheets.

The current study used PVC and plexiglass sheets for the sidewalls. The friction angle between the sheets and the organic soil was measured to be lower than 20°. Assuming the maximum sidewall friction for the test with the highest burial depth, the side friction was calculated for Test No. H4-8-1.9-7.3-250 (pipe diameter 220 mm and H/D 1.9). Based on the work by Karimian (2006), the failure surface is assumed to be triangular with failure angle of 30° to the horizon and the normal stress on the sidewalls is calculated based on Equation 4.1.

$$\sigma'_n = K_0 \sigma'_v \quad 4.1$$

Where  $\sigma'_n$ ,  $K_0$  and  $\sigma'_v$  are normal stress on the walls, coefficient of lateral earth pressure at rest, and effective overburden stress respectively. For a  $K_0$  of 1, the frictional force is calculated to be about 0.02 kN per meter of the pipe. This is less than 0.5% of the soil loads on the pipes that ranged from 1.5 – 9.8 kN/m. Clearly, an error of less than 0.5% and past studies on soils like sands (negligible sidewall friction even with the higher interface friction parameters compared to organic soils) suggests that the effect of sidewalls is negligible for the tested configurations of the present full-scale test series.

Another key consideration is the length of the test chamber allowing free formation of displacement zones in the chamber. Results of numerical analysis of the lateral SPI tests using different chamber lengths suggested that the computed soil restraint on pipe was not affected by the selected size of the horizontal test chamber (see appendix B).

It is recognized that a larger test chamber would have less boundary effects on the measured axial loads. Since this research task was undertaken during the global pandemic, due to the unavailability of personnel and supply chain issues, the use of the larger ASPIRe™ soil chamber (Wijewickreme et al., 2017) that would have provided more favorable conditions was not feasible.

#### **4.2.4 Testing program**

The new horizontal SPI test chamber was used to conduct a limited number of full-scale tests using sand blasted steel pipes in two different sizes. NPS 6 pipe with 168 mm (6.625 in) outer diameter and 6 mm wall thickness, and NPS 8 pipe with 219 mm (8.625 in) outer diameter and 6 mm wall thickness were tested. These pipe specimens were 0.98 m in length, which is 25 mm shorter than the width of the test chamber - thus providing nominal clearance to protect against potential jamming of the pipe inside the chamber during pipe pullout in an event of differential movement from the pulling cables. The test program was aimed at conducting eight horizontal soil-pipe interaction tests using the two pipe specimens in a normally consolidated test soil bed of organic soil under different pipe burial depth conditions.

#### **4.2.5 Preparation of horizontal SPI test chamber and test procedure**

Two states of soil bed densities (loose and dense) were planned during the horizontal pipe displacement test program. The relatively loose organic soil bed preparation followed a similar procedure discussed in Section 4.1.4 while soil layers were compacted using a steel tamper during preparation to achieve a denser soil bed for the other tests. Figure 4.14 and Figure 4.15 show

photographs of the test steps prior to the placement of pipe and after placing the pipe prior to pipe displacement test, respectively.



**Figure 4.14** Photographs showing the process of test soil bed preparation prior to pipe placement: (a) Mixing of organic soil to achieve a relatively uniform soil mix; (b) Soil mixer paddle; (c) Placing the soil in loose lifts of 6-8 inches prior to leveling; and (d) Pipe placement on the prepared soil bed (dense) before placing the soil cover



**Figure 4.15 Photographs showing the process of test soil bed preparation after pipe placement: (a) Connecting the pipe and pulling cables; (b) Placing the soil cover in loose lifts of 6-8 inches; (c) Plan view of the SPI test chamber prior to a horizontal pipe displacement test; and (d) Side view of the SPI test chamber prior to a horizontal pipe displacement test**

The soil bed was allowed to sit over night before performing the displacement test. The depth to the crown of the pipe was measured relative to a reference to check any settlement of the pipe prior

to a test. Horizontal-soil restraint was investigated by displacing the test pipe in the horizontal direction at a constant rate of displacement of 3 mm/s. Seven horizontal soil-pipe interaction tests were conducted on the pipe after preparing the test chamber as discussed above. A total horizontal pipe displacement of 400 mm was achieved in each test. The horizontal force and displacement were measured during the test phase. Experimental criteria and results are discussed in Chapter 5.

### **4.3 Summary**

Two full-scale physical test chambers were built to study the levels of mobilization of soil restraint on buried pipes due to relative ground movements in axial and horizontal directions, respectively. These new soil chambers were able to overcome the challenges identified in handling and preparation of organic soil for testing in a full-scale experimental setup due to its inherent soft and non-uniform nature, and the device dimensions were selected considering boundary effects during axial and lateral pipe displacement. Eight axial displacement tests on NPS 4 pipes and seven horizontal displacement tests on NPS 6 and NPS 8 pipes were conducted in total in the current thesis. Test parameter summary tables are presented in Chapter 5, Tables 5.1 and 5.2. The axial and horizontal restraints developed due to pipe displacement were measured and recorded along with the displacements to readily develop force-displacement relationships of pipes buried in organic soils.

## **Chapter 5: Axial and Horizontal Loading Response of Pipes Buried in Organic Soil**

This chapter presents the results generated from a series of full-scale axial and horizontal soil restraint tests conducted on pipes buried in organic soil. The experimental aspects of the testing are detailed in Chapter 4.

With respect to axial soil restraint, eight pullout tests were conducted on a NPS 4 (114 mm in diameter) steel pipe specimen buried in organic soil simulating different H/D ratios (H = burial depth to pipe centerline and D = pipe diameter). The axial SPI test chamber (see Section 4.1) was used to conduct these tests using a sand blasted (without coating material) steel pipe. The tests involved measurements of axial pipe displacement, and the applied axial load on the pipe specimen. The first section of this chapter summarizes test matrix with the parameters used and the resulting data on axial soil restraint versus pipe displacement response from the tests followed by a discussion of the results.

The second part of this chapter presents the outcomes from a series of horizontal lateral soil restraint tests conducted on pipes buried in organic soil. This physical modeling was conducted using the horizontal SPI test chamber custom designed as a part of the present research work (see Section 4.2). The tests employed NPS 6 and NPS 8 pipe specimen to simulate two organic soil bed density conditions and soil cover depths resulting in different H/D ratios. Furthermore, several in-situ geotechnical testing tools [i.e., cone penetration (CPT), electronic vane shear (eVST), and ball penetration testing (BPT)] were used to obtain in-place test-chamber-specific strengths for the organic soil materials in a given test bed. Here, again, the test measurements included pipe

displacement, and the soil restraint load on the pipe specimen. A summary of the test parameters, the observed load-displacement response, data collected from the in-situ testing of organic soil, along with any visual observations made during the testing are presented and discussed.

## 5.1 Axial Loading Response of Pipes Buried in Organic Soil

The experimental program was aimed at conducting eight axial soil-pipe interaction tests on the test pipe specimen in a normally consolidated test soil bed of organic soil.

### 5.1.1 Summary of test parameters

The test parameters and configurations pertaining to the axial pipe testing program are summarized in Table 5.1.

**Table 5.1 Summary of test parameters: axial soil-pipe interaction tests performed in organic soil**

Test ID	Pipe size	Average unit weight (kN/m <sup>3</sup> )	Average moisture content (%)	H (mm)	H/D
A1-4-2.4-260	NPS 4	10.3	260	270	2.4
A2-4-4.0-240	NPS 4	10.3	240	460	4.0
A3-4-6.0-230	NPS 4	10.5	230	700	6.0
A4-4-8.6-280	NPS 4	10.0	280	990	8.6
A5-4-10.5-260	NPS 4	10.0	260	1210	10.5
A6-4-4.0-240-2	NPS 4	10.3	240	460	4.0
A7-4-6.0-200-2	NPS 4	10.4	200	700	6.0
A8-4-10.5-240-2	NPS 4	10.3	240	1220	10.5

As may be noted, each axial displacement test is given a unique Test ID with the following labelling convention:

<X><N1>-<N2>-<N3>-<N4>-<N5>

Where:

X = Use A for axial displacement tests (i.e., denotes test type)

N1 = Test number

N2 = pipe size in NPS (Nominal Pipe Size), for example, use “4” for NPS 4 pipe.

N3 = H/D ratio

N4 = Average % moisture content of the organic soil bed

N5 = 2 if the test is a repeated test or leave blank if the test is original.

It is to be noted that the above mentioned eight tests undertaken comprised of five axial displacement tests combined with three repeat tests. The average undrained shear strength of the organic soil bed was determined to be 2 kN/m<sup>2</sup> using samples extracted during the tests using a laboratory miniature vane shear test device in accordance with ASTM D4648 (2000). It is also of relevance to note that these observed average strength values are in accord with the data derived from test-chamber-specific BPT and eVST probings performed on similar soil bed conditions during horizontal soil restraint tests as described in Section 5.2.

### **5.1.2 Axial load-displacement response**

Results of the testing program on axial soil restraints on pipes buried in organic soil are presented and discussed in this section. A series of eight tests were conducted utilizing moist organic soil

bed conditions with an average moisture content between 200% - 280% and average bulk unit weight between 10.0 kN/m<sup>3</sup> – 10.5 kN/m<sup>3</sup>. The measured load-displacement response during the axial displacement test is presented and discussed in this section.

In order to facilitate comparison of different tests, axial soil restraint is presented in the form of a normalized axial soil resistance as defined below:

$$F'_A = F_A / \gamma H \pi D L \quad 5.1$$

where,  $F_A$  is the measured axial load on pipe,  $\gamma$  is the bulk unit weight of organic soil,  $H$  is the depth to centerline of pipe,  $D$  is the pipe diameter and  $L$  is the length of test pipe specimen. The value of  $F'_A$  represents the average shear force around the pipe normalized with respect to the total stress from the soil overburden at the centerline of the pipe specimen. Similar normalization approach is common in previous research work to describe lateral soil forces.

The measured load-displacement response of the axial displacement tests are presented in Appendix C.1. The observed response of normalized axial soil restraint ( $F'_A$ ) versus axial displacement during the set of axial loading tests conducted in organic soil is presented in Figure 5.1. All the tests are conducted by monotonically loading in one direction until a displacement of 300 mm - 400 mm is reached. The observed load responses are illustrated – the tests depicted by dashed lines in Figure 5.1 are those for the repeated tests – correspondence with the original test shown by the continuous lines is achieved with the usage of similar color in the graph.

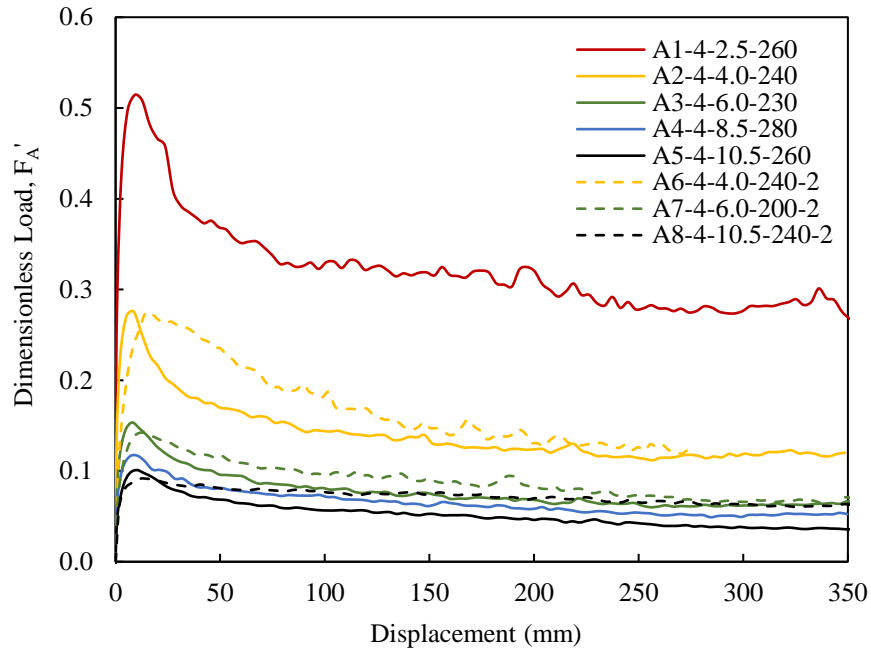


**Figure 5.1 Response of normalized axial soil restraint versus displacement during axial loading tests conducted in organic soil**

As notable from Figure 5.1, the peak  $F'_A$  decreases with increasing H/D ratio – i.e.,  $F'_A$  decreasing from ~0.1 to ~0.5 as H/D increased from 2.5 to 10.5. In all the eight cases, the  $F'_A$  was achieved at an axial displacement of about 10 mm. The post-peak  $F'_A$  values for all the tests approached a plateau when axial displacements were in excess of about 250 mm. Identifying the causes for the post-peak drop of axial load is not straightforward. Based on the general understanding of soil behavior, it is possible that the re-orientation of organic fibers as well as the fine-grained mineral soil particles at large strain levels may be partly responsible for this observation. Additional research would be necessary to study the associated mechanisms.

### 5.1.3 Discussion of test results

The  $F'_A$  versus displacement response observed for the tests conducted at H/D values of 4, 6, and 10.5 are compared with those obtained for the counterpart repeated tests in Figure 5.2. The observed agreement between the peak axial soil loads demonstrates reasonable repeatability of the preparation of soil-pipe specimens and testing approach. However, significant deviations (up to 45%) of the axial load was notable beyond the peak load value. As mentioned earlier, these deviations may be due to the complexities and the mechanisms that take place at the interface at larger displacements.

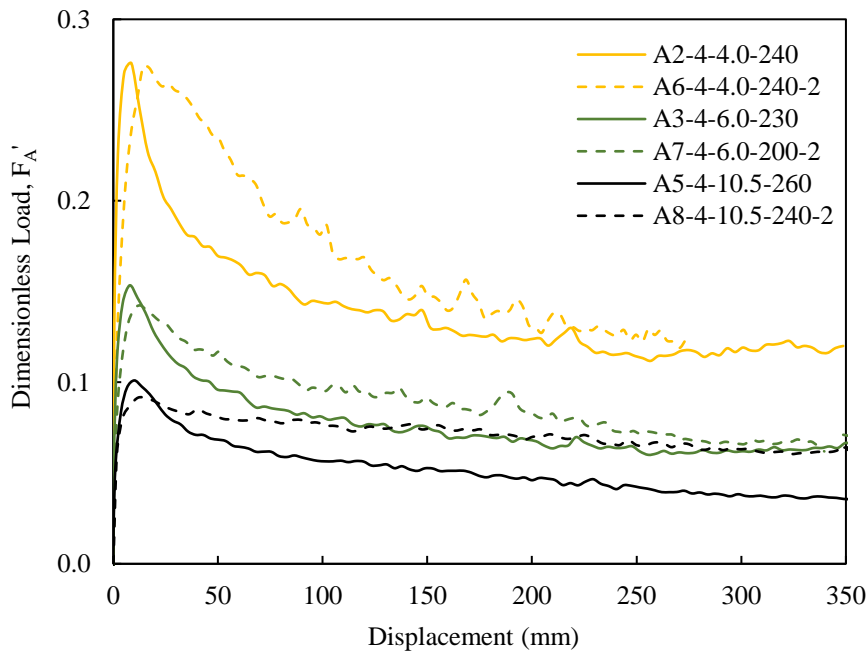


**Figure 5.2 Comparison of normalized axial soil restraint versus displacement response of repeated and original tests of the axial pipe displacement test series**

It is also of interest to compare the variation of  $F'_A$  versus axial displacement response obtained from the above physical modeling with those computed according to PRCI (2009) practice guidelines. In this regard, it is important to note that the current PRCI guidelines do not have provisions for organic soils; as such, these curves were generated based on the soil springs recommended for clayey soils - which is the commonly used practice approach for developing soil springs for organic soils. Hence, bi-linear curves of  $F'_A$  (based on Equation 5.1) versus axial displacement were developed using  $T_u$  determined based on PRCI-based Equation 5.2.

$$T_u = \pi D \alpha s_u \quad 5.2$$

Where,  $T_u$  is the peak axial load on pipe,  $D$  is the pipe diameter,  $\alpha$  is the adhesion factor which is 1 for undrained shear strength lower than about 5 kPa, and  $s_u$  is the undrained shear strength representative of the backfill.  $s_u$  values identical to those measured during full-scale testing were used in the equations to generate counterpart curves as per PRCI guidelines (2009). Moreover, the axial displacement at the peak axial soil restraint,  $T_u$  ( $\Delta_t$ ) was taken as 10 mm for soft clay (PRCI 2009).

The PRCI-based bi-linear  $F'_A$  load-displacement responses (computed using the approach proposed for soft clayey soil surrounding) corresponding to each full-scale test cases presented in Table 5.1 are compared with the corresponding measured axial load-displacement responses in Figures 5.3 through 5.7. Although the pipe displacement at the peak soil restraint is in good agreement with those based on PRCI guidelines, the PRCI-based load-displacement curve consistently exhibit much higher peak axial resistance than those from the full-scale test.

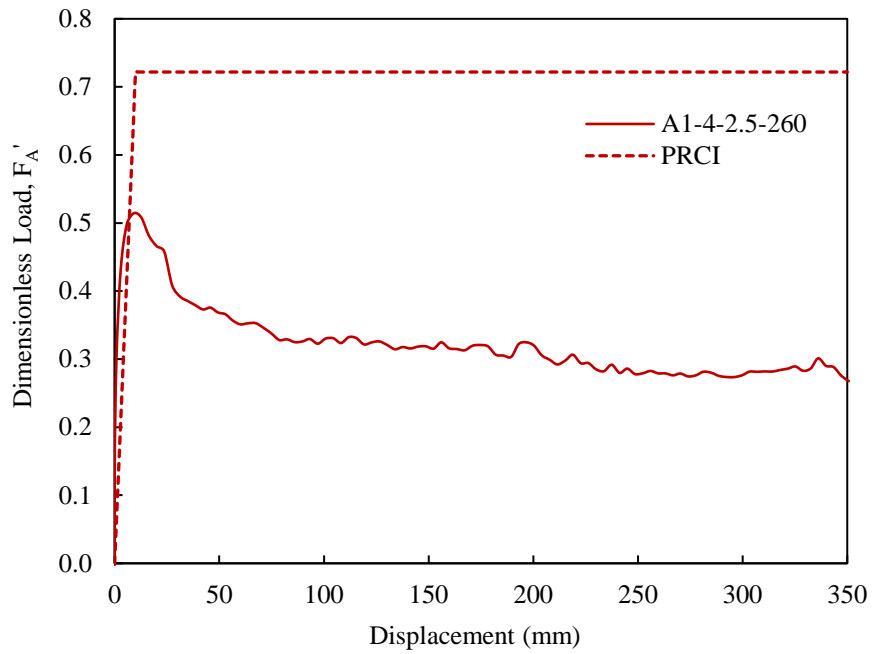


**Figure 5.3 Response of normalized axial soil restraint versus displacement during test A1-4-2.5-260 and the corresponding curve determined based on PRCI (2009) guidelines.**

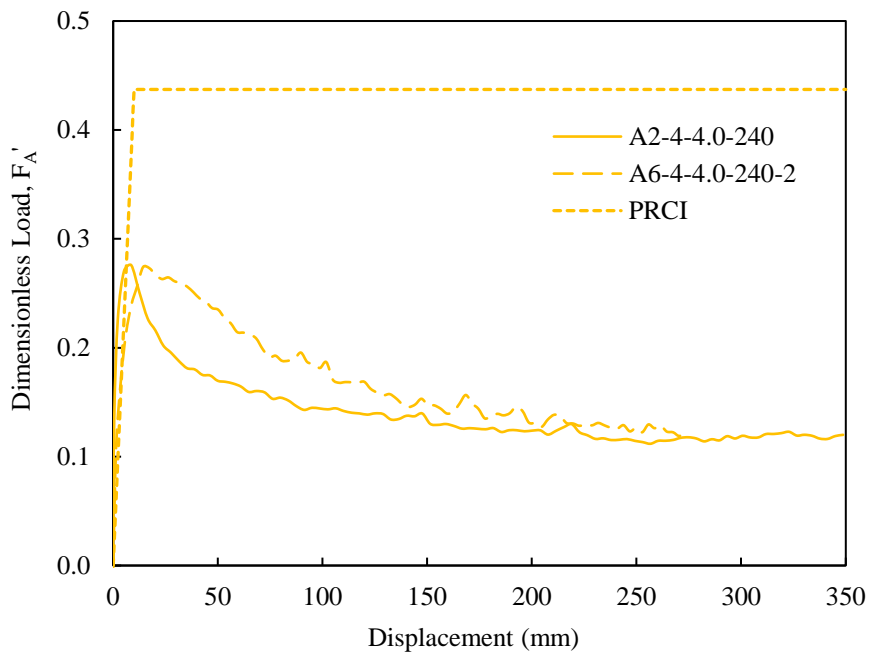


**Figure 5.4 Response of normalized axial soil restraint versus displacement during tests A2-4-4.0-240 and A6-4-4.0-240-2 and the corresponding curve determined based on PRCI (2009) guidelines.**

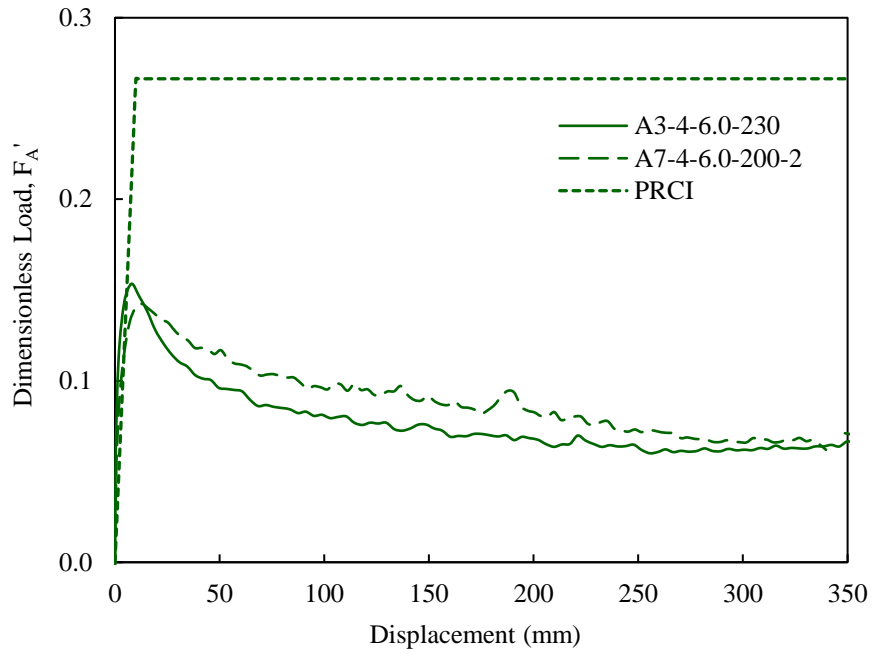


**Figure 5.5** Response of normalized axial soil restraint versus displacement during tests A3-4-6.0-230 and A7-4-6.0-200-2 and the corresponding curve determined based on PRCI (2009) guidelines

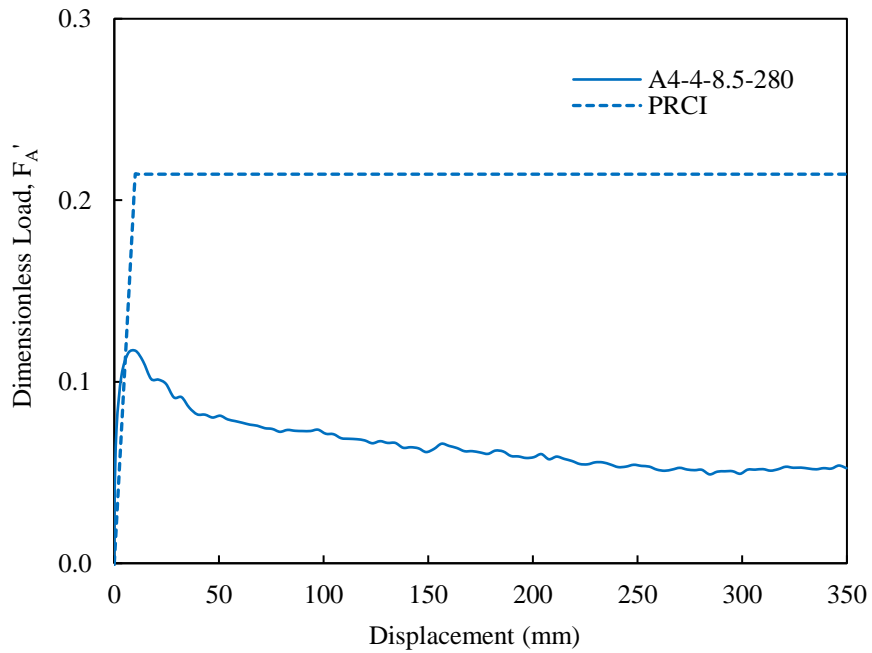


**Figure 5.6** Response of normalized axial soil restraint versus displacement during test A4-4-8.5-280 and the corresponding curve determined based on PRCI (2009) guidelines

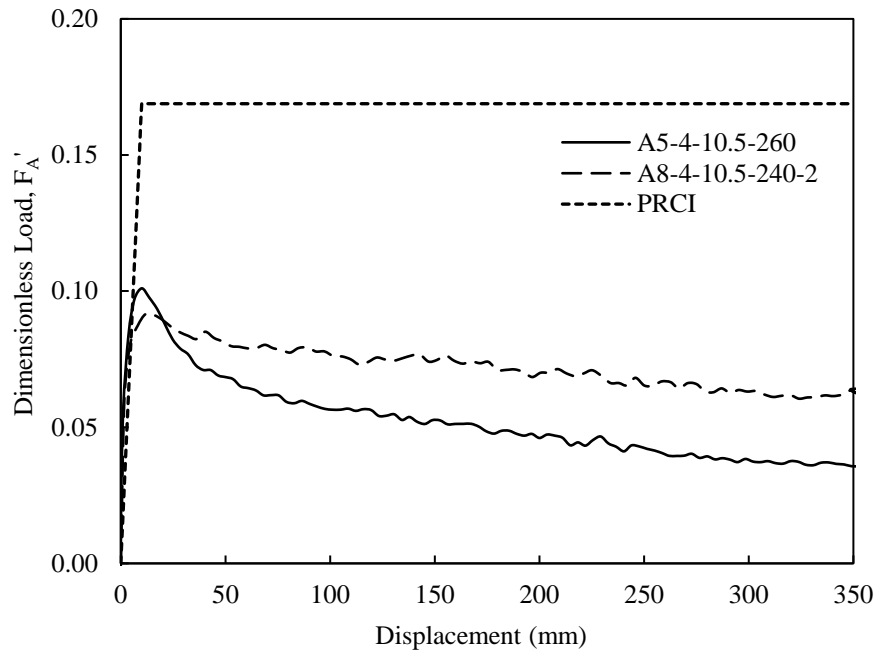


**Figure 5.7 Response of normalized axial soil restraint versus displacement during tests A5-4-10.5-260 and A8-4-10.5-240-2 and the corresponding curve determined based on PRCI (2009) guidelines.**

This difference can be viewed in a more meaningful and quantitative manner by plotting the peak  $F'_A$  values as shown in Figure 5.8; as per the trendline in Figure 5.8, the PRCI-based peak  $F'_A$  value should be reduced by about 0.67 to obtain agreement with the experiments.

This finding is of interest to the pipeline design practice. For example, under potential ground movements, lower axial soil restraint means larger anchoring length mobilization which may be desirable in cases when buried pipelines span over long distances in organic soil terrain; on the other hand, the lower axial restraint may not be favorable when pipelines located near elbows, tee junctions, or connections to valve and compressor stations, etc. are subjected to ground movements. It is recognized that the observations have been made using a limited number of tests; as such, additional research is warranted to investigate this aspect further as a way of making

definitive comments on the validity (or not) of using current PRCI guidelines developed for clayey soils to obtain soils springs for pipelines buried in organic soils.

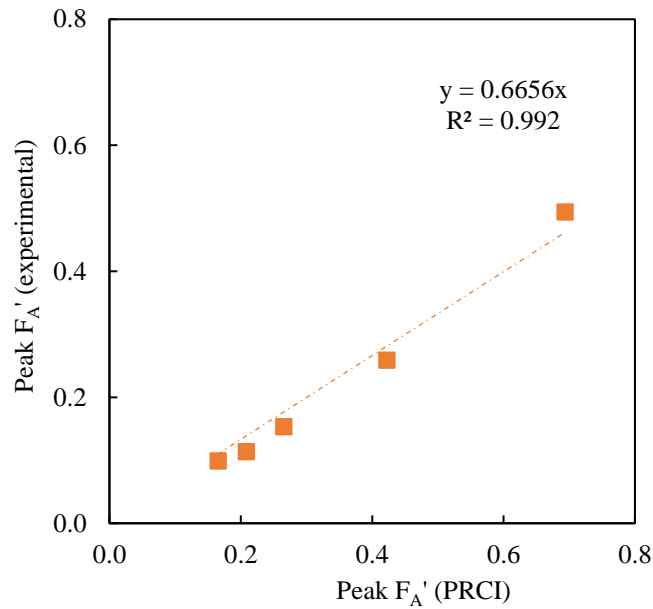


**Figure 5.8 Comparison of the normalized peak axial soil restraint from PRCI guidelines (2009) and full-scale experiments presented in Figures 5.3 through 5.7.**

## **5.2 Horizontal Loading Response of Pipes Buried in Organic Soil**

This section describes the results derived from horizontal lateral soil restraint tests conducted on buried steel pipes in organic soils. As described in Chapter 4, the experimental program involved conducting seven horizontal soil-pipe interaction tests on pipe specimens of NPS 6 (168 mm in diameter) and NPS 8 (219 mm in diameter) buried in normally consolidated test organic soil bed.

### 5.2.1 Summary of test parameters

The horizontal soil restrain testing program, along with the testing parameters, are summarized in Table 5.2.

**Table 5.2 Test parameter summary of horizontal soil-pipe interaction tests**

Test ID	Pipe size	H/D	H (mm)	Undrained shear strength (kPa)	Average moisture content (%)	Average unit weight (kN/m <sup>3</sup> )
H1-6-1.9-1.5-360*	NPS6	1.9	325	1.5	360	9.9
H2-6-3.5-2.0-340*	NPS6	3.5	585	2	340	10.0
H3-6-2.9-5.9-270	NPS6	2.9	485	5.9	270	9.9
H4-8-1.9-7.3-250	NPS8	1.9	410	7.3	250	10.2
H5-8-1.6-9.8-210	NPS8	1.6	360	9.8	210	10.1
H6-8-1.6-9.8-200*	NPS8	1.6	360	9.8	200	10.4
H7-6-1.9-9.8-220	NPS6	1.9	325	9.8	220	10.4

*\*Note: As described in Section 5.2.2, test-chamber-specific BPT, eVST, and CPT penetration tests were performed during these physical model tests.*

Horizontal Test ID labelling follow a similar order given in section 5.1.1 with additional details as follows.

Where;

<X><N1>-<N2>-<N3>-<N4>

Where:

X = Use H for horizontal displacement tests (i.e., denotes test type)

N1 = Test number

N2 = pipe size in NPS (Nominal Pipe Size), for example, use “4” for NPS 4 pipe.

N3 = H/D ratio

N4 = Average  $s_u$  at pipe centerline depth measured/inferred based on in-place strength tests

N5 = Average % moisture content of the organic soil bed.

As noted, seven tests were conducted utilizing moist organic soil bed conditions with an average moisture content between 200% - 360% and average bulk unit weight between  $9.9 \text{ kN/m}^3$  –  $10.4 \text{ kN/m}^3$  – based on six soil sample measurements per test. The tests were conducted to achieve a maximum displacement of ~400 mm at a loading rate of 3 mm/s. The lower and the upper bounds of the average moisture content and unit weight are associated with the lower and upper bound shear strength parameters, respectively. The undrained shear strength of the prepared soil bed ranged from 1.5 – 9.8 kPa based on the test-chamber-specific shear strength data. Details of the test methods and test results of the in-situ BPT, eVST and CPTs performed are presented in Appendix C.2.

### **5.2.2 Characterization of organic soil in chamber-specimens using test-specific penetration testing**

Tests No. H1-6-1.9-1.5-360 and H2-6-3.5-2.0-340 simulated horizontal loading response of pipes buried in relatively less dense organic soil bed as discussed in Section 4.3.4; on the other hand, Test No. H6-8-1.6-9.8-200 was performed in a relatively denser organic soil (which was compacted using a steel tamper during preparation of soil bed). Test-chamber-specific eVST, BPT and CPT probings were performed to characterize the shear strength properties of the organic soil during the above three pipe displacement tests. Data from these test-chamber-specific work was considered as valuable in obtaining strength and deformation parameters for the numerical

simulations of the pipe displacement tests as described in Section 2.1. In this process, one of the important considerations was how the boundaries of the soil chamber would affect the outcomes from the above testing. The radius of the BPT was about 70 mm and the closest horizontal distance to the boundary wall of the chamber was about 0.4 m (about 5.5 times the radius of the BPT). On the other hand, radius of the eVST was 30 mm, making the horizontal distance to the closest boundary about 13 times the radius. The work undertaken by Griffiths and Lane (1990) showed that the vane shear test typically induces a localized failure mechanism primarily adjacent to its circumference with negligible stress influence from the vane beyond three times its radius. Moreover, the pressuremeter analysis undertaken in Chapter 6 indicated that the horizontal displacement due to the pressuremeter test also diminishes to less than 6% at a distance of 13 times its radius. Based on this, it became apparent that the use of eVST data would be more preferable to assess the shear strength of materials in the test chamber. It is also to be noted that laboratory element testing of reconstituted peat was not practical due to its very soft consistency. Although CPTs were conducted, they were not considered in assessment of  $s_u$  of the organic soil in the test chamber due to the reasons discussed in Section 3.1.2.

The test-chamber-specific eVST data indicated that the undrained shear strength at the pipe level of the soil chamber for tests H1-6-1.9-1.5-360 and H2-6-3.5-2.0-340 are 2 kPa and 1.5 kPa, respectively (see Figures C.7, C.8, C.12 and C.13). For the Test H6-8-1.6-9.8-200, which was performed in a relatively dense organic soil bed, the eVSTs indicated a  $s_u$  value of 9.8 kPa at the pipeline spring level (see Figures C.16 and C.17) .

Due to high cost of in-situ test programs and unavailability of expert personnel to perform in-place shear strength characterization tests for each of the full-scale pipe displacement tests, four of the pipe displacement tests had to be performed without obtaining test-chamber-specific shear strength

data. Therefore,  $s_u$  values of the organic soil for these tests had to be rationally inferred based on the knowledge of the similar compaction approaches used in specimen preparation along with moisture content comparisons. In this regard, it was noted that the soil bed preparation approach used for the Tests No. H5-8-1.6-9.8-210 and H7-6-1.9-9.8-220 was essentially identical to that employed for Test No. H6-8-1.6-9.8-200; this was further corroborated by the similarity in moisture contents ranging from 200 – 220% amongst the three tests. Based on this congruence, it was considered justifiable to attribute the measured undrained shear strength of 9.8 kPa (Test No. H6-8-1.6-9.8-200) for the data interpretations and numerical analyses associated with the Tests No. H5-8-1.6-9.8-210 and H7-6-1.9-9.8-220.

Tests No. H3-6-2.9-5.9-270 and H4-8-1.9-7.3-250 had test bed moisture content levels (~250-270%) that fell “half-way” between those attained for the tests that had test-chamber-specific  $s_u$  measurements (i.e., Tests No. H1-6-1.9-1.5-360, H2-6-3.5-2.0-340 and H6-8-1.6-9.8-200). As such, it was considered reasonable to use a  $s_u$  value interpolated from those measured from test-chamber-specific probings for Tests No. H1-6-1.9-1.5-360, H2-6-3.5-2.0-340 and H6-8-1.6-9.8-200. In order to assist this process, the value of  $s_u$  inferred from test-chamber-specific probings were plotted against moisture content as shown in Figure 5.9. Using the data plot in Figure 5.9 as a correlation, the  $s_u$  for the two Tests No. H3-6-2.9-5.9-270 and H4-8-1.9-7.3-250 were found to be 5.9 and 7.3 kPa, respectively, by interpolation.

As indicated earlier, this test-chamber-specific penetration testing provided a meaningful way of obtaining and inferring undrained shear strength values for the interpretation of data and associated numerical modeling – in turn, leading to the determination of corresponding soil springs, including those based on PRCI (2009) guidelines.

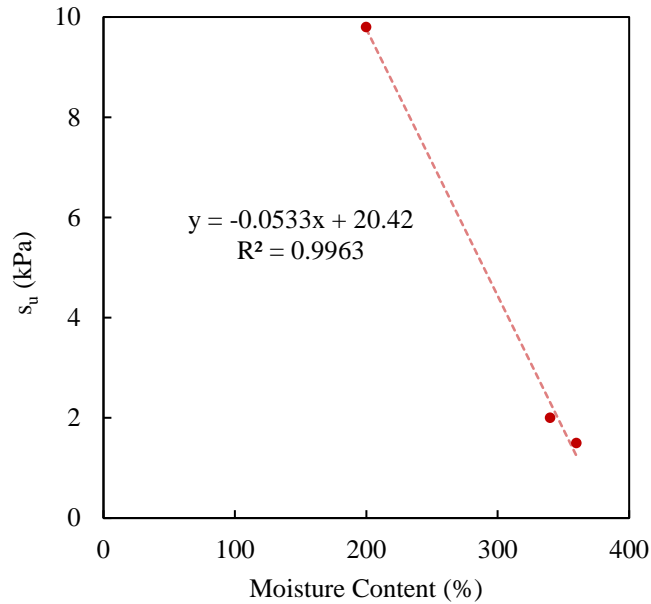


**Figure 5.9 Correlation between  $s_u$  inferred from BPT data versus moisture content of the test organic soil**

### 5.2.3 Horizontal load-displacement response

The observed load-displacement response during the horizontal displacement tests are presented in Figures 5.10 through 5.16. The counterpart horizontal load-displacement behavior calculated based on PRCI (2009) guidelines for the same test conditions (as listed in Table 5.2) are also superimposed on the same figures to assist the evaluation and discussion of the experimentally obtained data performed at the end of this section. It is important to note that, the frictional resistance of the loading system was determined by measuring the pulling force without the presence of the pipe; this frictional force correction was then applied to the measured forces.

The Tests No. H1-6-1.9-1.5-360 and H2-6-3.5-2.0-340 were performed in relatively low density organic soil bed that had  $s_u$  of 2 kPa and 1.5 kPa, respectively. The Test No. H6-8-1.6-9.8-200, performed in a relatively dense organic soil bed, had a test-chamber-specific  $s_u$  of 9.8 kPa. As

noted earlier, all of the above  $s_u$  values were obtained based on test-chamber-specific penetration testing. On the other hand, the  $s_u$  values for the other four full-scale tests performed without test-chamber-specific penetration testing were inferred by interpolation as indicated in Section 5.2.2. The values of  $s_u$  derived as described above were then used to determine p-y curves based on PRCI (2009) for comparison with the results from all the experiments.

In all the tests, except for Test No. H7-6-1.9-9.8-220, lateral soil resistance on the pipe gradually mobilized with increasing pipe displacement until an approximately plateau level was reached. In Test No. H7-6-1.9-9.8-220, the soil resistance increased with increasing pipe displacement to reach a peak, after which, the resistance dropped and reached a plateau - other than to consider this as due to experimental variability, a specific reason for the peak could not be identified.

As shown in Figures 5.10 and 5.11, Tests No. H1-6-1.9-1.5-360 and H2-6-3.5-2.0-340 conducted with relatively low density organic soil, displayed an initially softer response before building up lateral resistance leading to the peak soil load. In essence, the mobilization of lateral load required a finite displacement in all the tests, with the organic soil with lower density requiring more displacement – i.e., the displacement required for load mobilization was lesser in Test No. H6-8-1.6-9.8-200 compared to the other tests with lower density. Identification of the causative mechanism for this delayed mobilization of lateral load is not straightforward particularly with a specimen containing organic soils. It is possible that non-uniform densities with soft soil zones in the haunch area of the pipe may be one of the reasons for this observation. Achieving effective and uniform compaction in the haunch areas in the vicinity of the pipeline invert is challenging in spite of the effort taken to carefully compact in a step wise manner along the pipeline alignment – this is difficult even in the preparation of soil beds containing sand backfill, and it is further amplified when compacting soft and weak organic soils. Further, PRCI guidelines has been

developed considering mineral backfill soils, that provides for better seating of soil against the pipe, and this is likely the reason for the significant difference between the guideline and the results from the physical models.

Since Test No. H6-8-1.6-9.8-200 is essentially identical to Test H5-8-1.6-9.8-210, the measured load-displacement response for the former test is also superimposed with the test results shown in Figure 5.13 for the latter. This comparison indirectly suggests good repeatability of specimen preparation and experimental methodologies undertaken during this testing program.

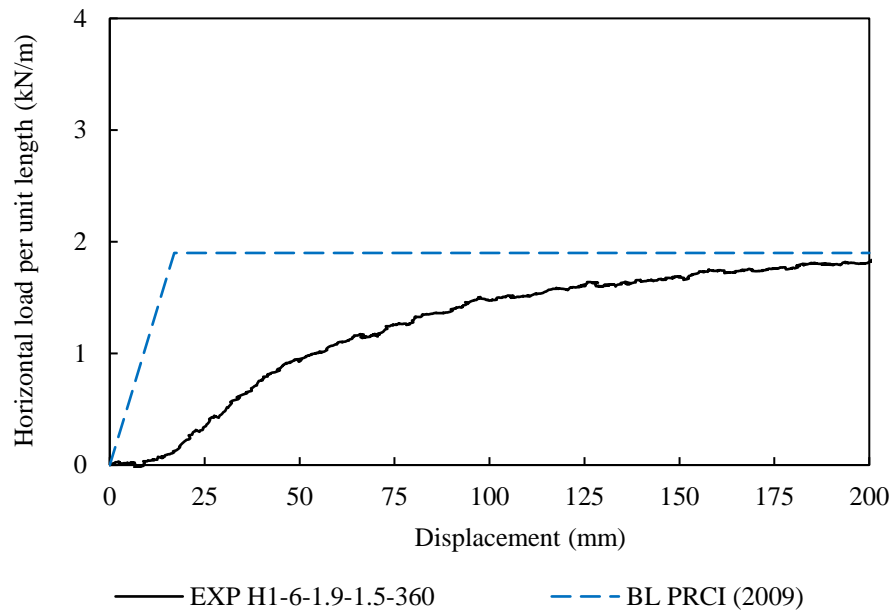


**Figure 5.10 Load-displacement response measured from Test H1-6-1.9-1.5-360 and the corresponding bi-linear curve determined based on PRCI (2009)**

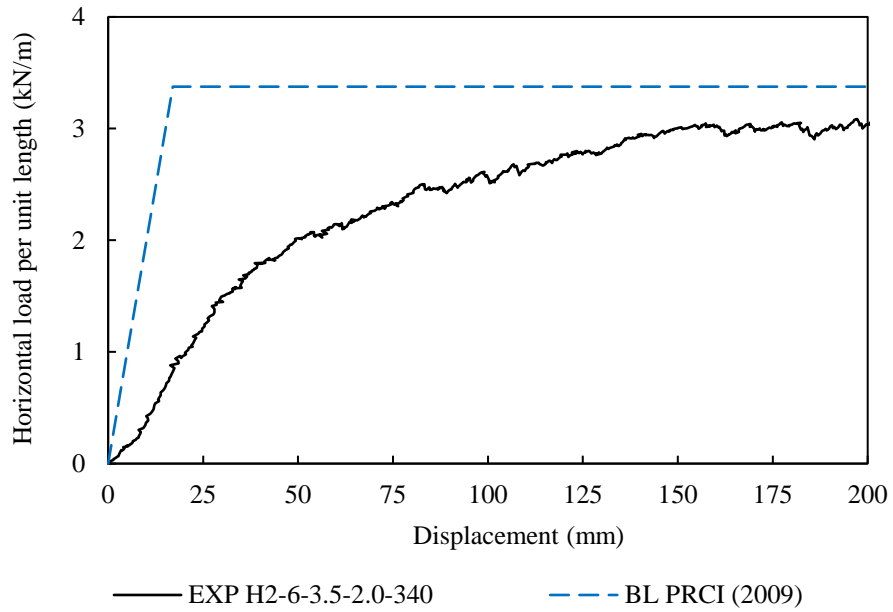


**Figure 5.11 Load-displacement response measured from Test H2-6-3.5-2.0-340 and the corresponding bi-linear curve determined based on PRCI (2009)**

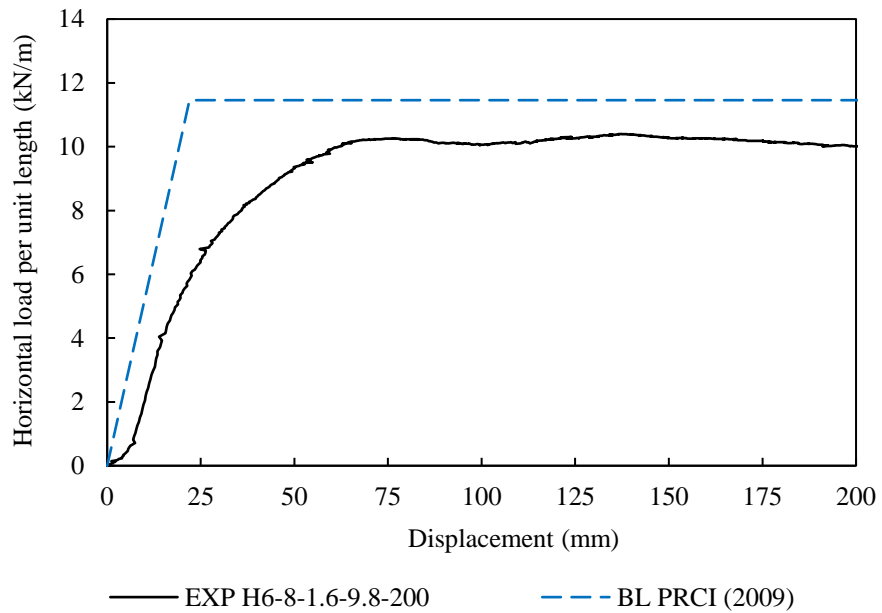


**Figure 5.12 Load-displacement response measured from Test H6-8-1.6-9.8-200 and the corresponding bi-linear curve determined based on PRCI (2009)**

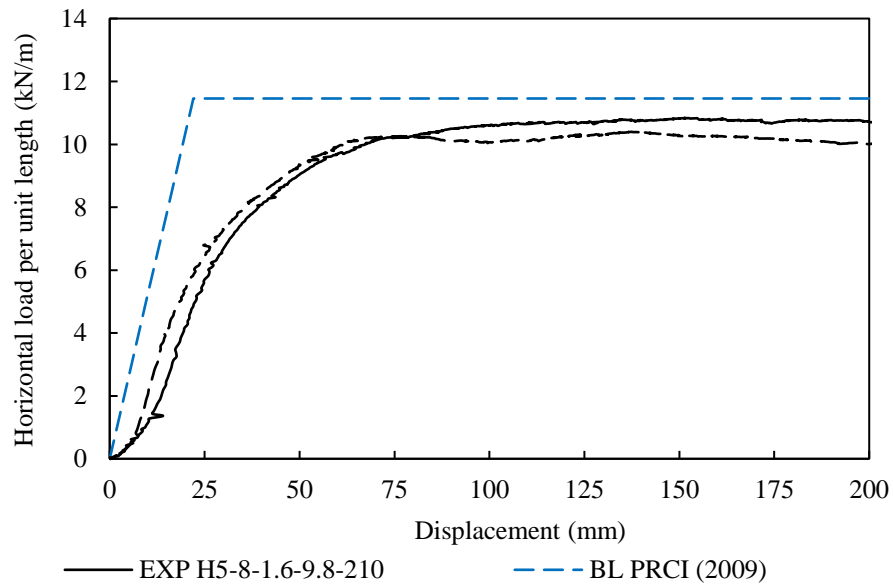


**Figure 5.13 Load-displacement response measured from Tests H5-8-1.6-9.8-210 and H6-8-1.6-9.8-200 and the corresponding bi-linear curve determined based on PRCI (2009)**

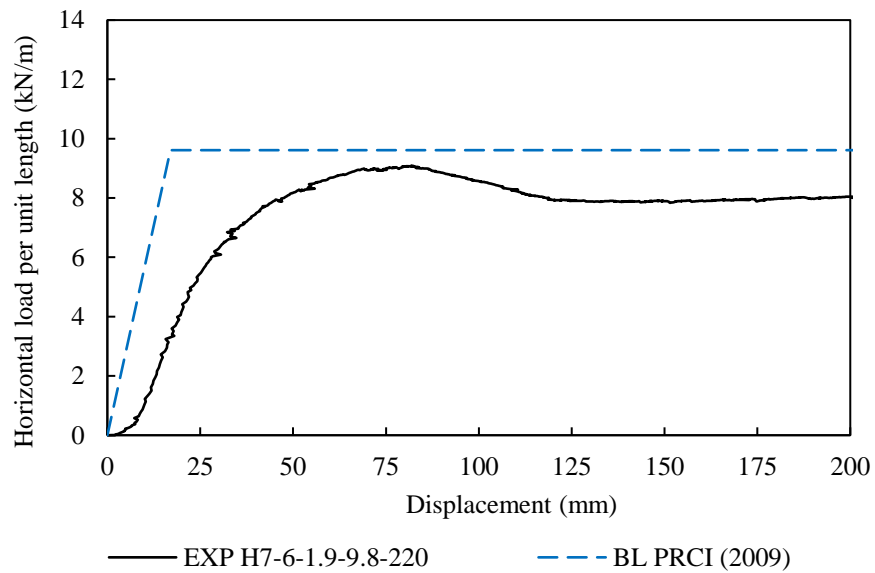


**Figure 5.14 Load-displacement response measured from Test H7-6-1.9-9.8-220 and the corresponding bi-linear curve determined based on PRCI (2009)**

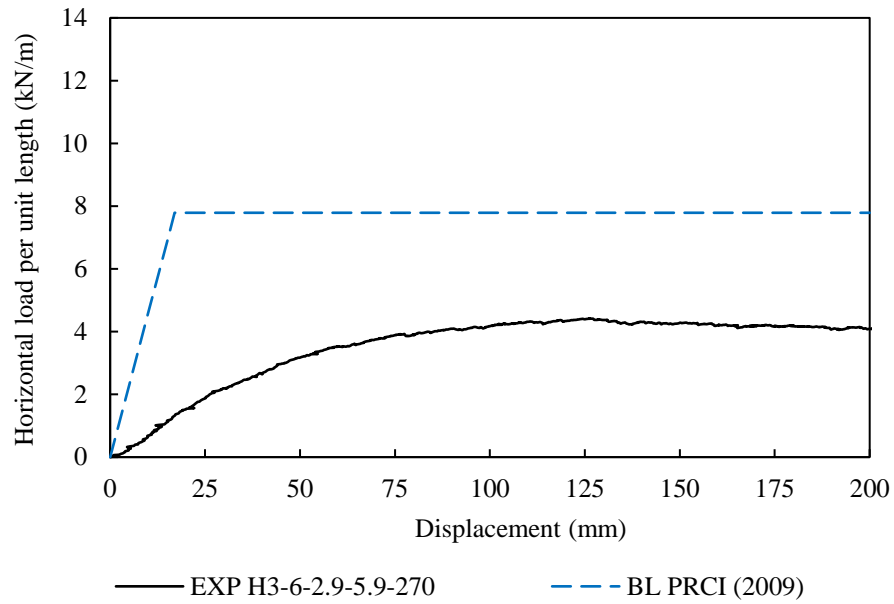


**Figure 5.15 Load-displacement response measured from Test H3-6-2.9-5.9-270 and the corresponding bi-linear curve determined based on PRCI (2009)**

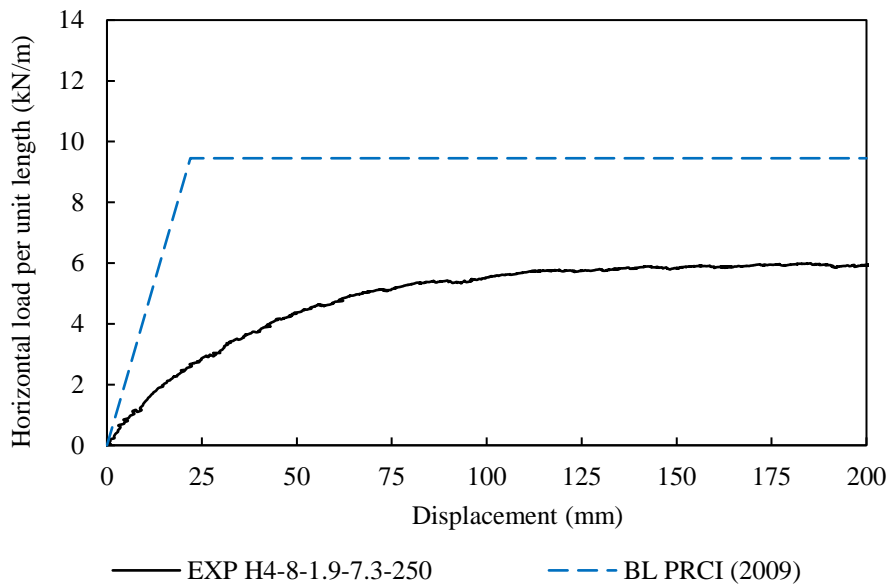


**Figure 5.16 Load-displacement response measured from Test H4-8-1.9-7.3-250 and the corresponding bi-linear curve determined based on PRCI (2009)**

As noted from the figures above, the horizontal load-displacement response calculated based on the PRCI (2009) guidelines seem to consistently over-predict the peak horizontal loads derived from the counterpart experiments. This is further examined in Figure 5.17, where the peak horizontal soil restraint measured from the experiments are compared with those calculated from PRCI (2009). As may be noted, the guidelines over predicts the peak load by around 14%. Moreover, the pipe displacement at peak soil restraint varied from 0.18D – 0.55D according to the experimental load-displacement response as opposed to 0.1D – 0.15D specified in PRCI (2009). Further comparisons and discussions of these results are made in Chapter 7.

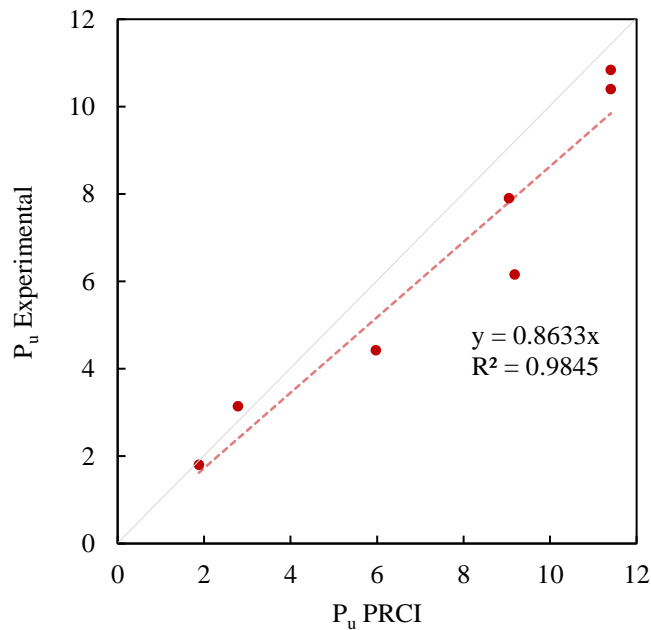


**Figure 5.17 Comparison of the peak soil restraint ( $P_u$ ) determined from PRCI guidelines (2009) and measured during full-scale experiments extracted from Figures 5.10 through 5.16**

#### **5.2.4 Visual observations during horizontal pipe displacement tests**

Taking advantage of the Plexiglas panel installed in the horizontal soil testing chamber, experimental observations were noted to discuss qualitative soil deformation patterns developed during the tests. The patterns of soil deformation from Test H6-8-1.6-9.8-200 are presented and discussed herein. Figure 5.18 a) through f) shows the side view of the deformed soil mass during test H6-8-1.6-9.8-200 from 0 to 300 mm of pipe displacement. The active zone is at the tailing side with respect to the pipe movement wedge, and a passive zone is formed in front of the pipe. Upward movement of pipe during lateral loading was measured as about 100 mm in this test. Figure 5.19 shows the surface movement, shear cracks and settlement after the pipe displacement. The observed patterns of soil deformation were noted to be similar for the other lateral soil restraint tests undertaken.

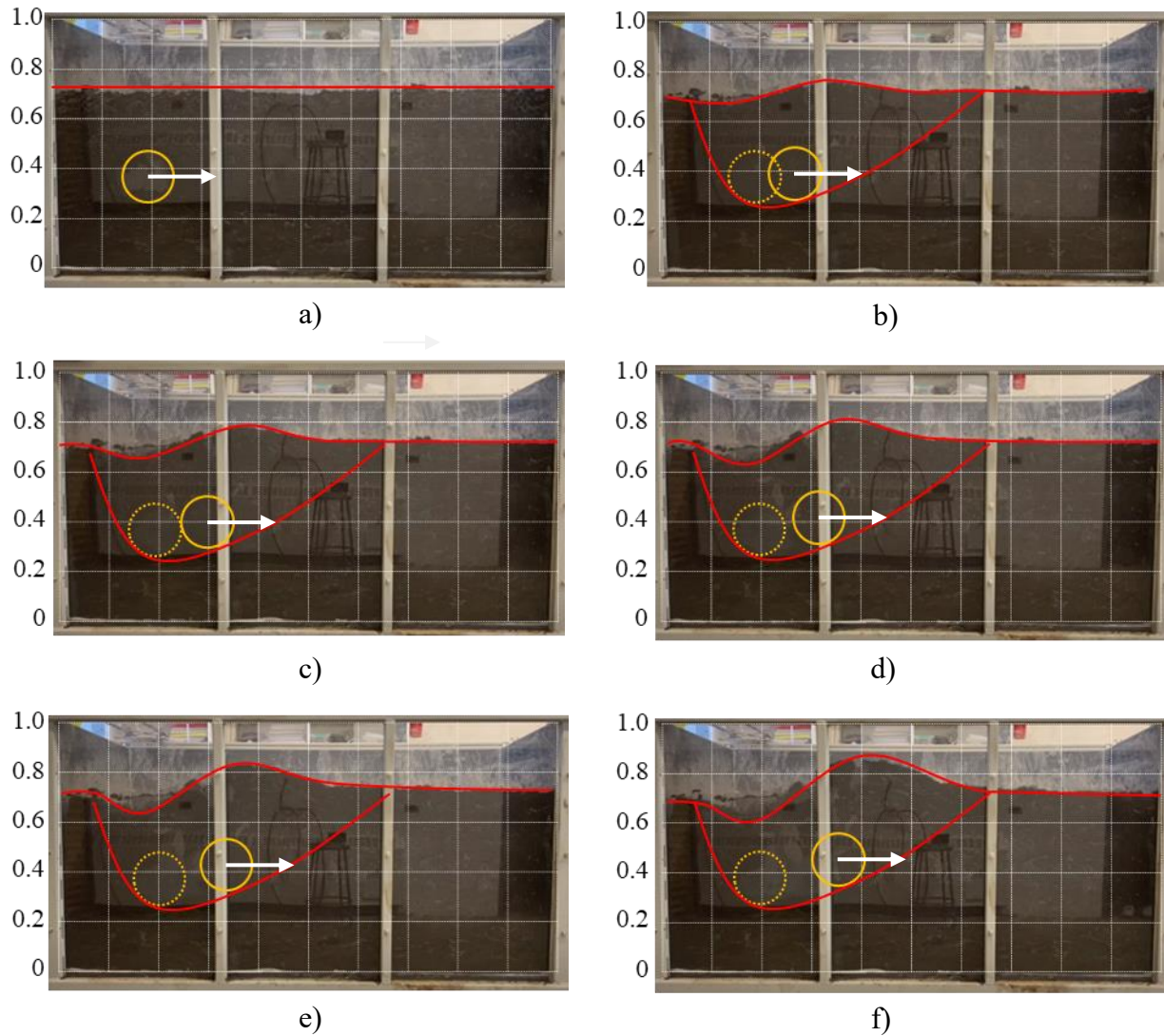


**Figure 5.18 a) – f) Backfill soil deformation during Test H6-8-1.6-9.8-200 from 0 to 300 mm of pipe displacement. Note: Arrows show the direction of pipe displacement and the lines are sketched based on the visual observations through the plexiglass during testing. The information is presented to provide an understanding of the approximate failure mechanisms developed during lateral soil restraint testing**

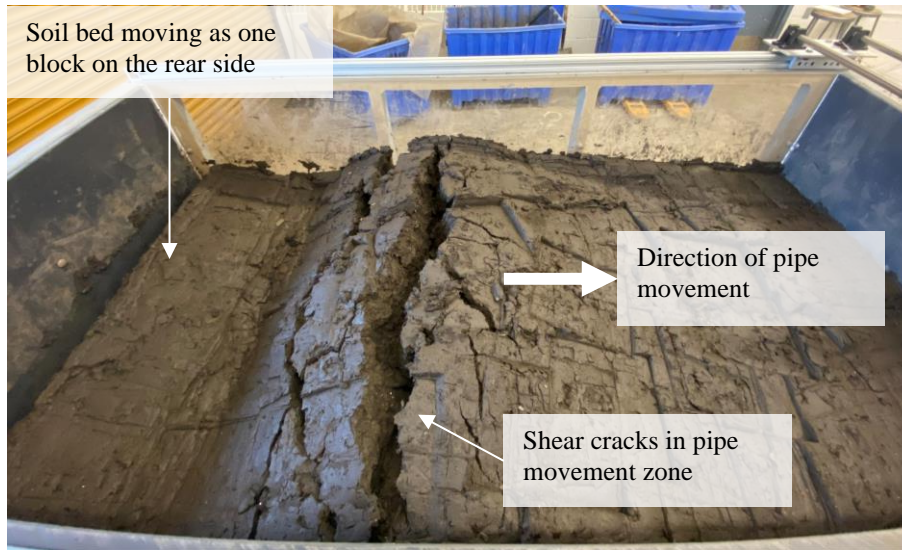


**Figure 5.19 Top soil surface deformation at the end of Test H6-8-1.6-9.8-200**

### **5.3 Summary**

Axial and lateral soil restraints developed on steel pipes subjected to relative lateral soil movements were investigated through a series of full-scale pipe displacement tests, conducted using two soil testing chambers at UBC. In order to assist the interpretation of the observed soil-pipe response, geotechnical in-place penetration testing were conducted on three selected full-scale pipe displacement tests to characterize the strength properties of the tested organic soil bed. Further visual observations of soil failure patterns and pipe position were made during horizontal pipe displacement tests.

The observed load-displacement behavior when compared with the p-y curves developed based on PRCI (2009) shows that both axial and horizontal load-displacement behavior is over predicted in the guidelines. Further, it was noted that reliable characterization of undrained shear strength of the organic soil bed is critical in determining the soil restraints. Horizontal soil restraint is further

investigated using numerical analysis methods in Chapter 7 and the full-scale tests were modeled using FLAC (2D) to investigate the load-displacement behavior and assess experimental, numerical, and guideline-based p-y curves. Chapter 7 presents an overall comparison of results and discussions of horizontal soil restraints.

## **Chapter 6: Constitutive Model for Organic Soil: Selection and Validation of a Model through Numerical Modeling of Pressuremeter**

Characterization of the behavior of organic soil and adoption of a model to support associated numerical modeling formed a key component of the scope of the current thesis. As indicated in Section 2.3.1, a total stress based (i.e., using undrained soil parameters) model was considered reasonable to particularly represent the soil constraints developed during relative lateral soil movements against pipelines.

The field pressuremeter tests that were conducted as a part of the field geotechnical testing program invoked a reasonably well-defined boundary value problem for use in the validation of the constitutive model. This chapter discusses the numerical analysis followed to select and validate the constitutive model based on the strength and stiffness characterization of bulk organic soil mass from field geotechnical characterization tools considering the high variability of the material and the long-and-wide terrain that get mobilized during relative movement of buried pipelines. It was judged that the applied pressure versus radial displacement behavior observed in field pre-bored pressuremeter (PMT) testing conducted at two field geotechnical test sites serve as a meaningful dataset to represent the bulk response of organic soil subjected to lateral loading, and in turn, as boundary value cases to be used for validating the numerical approach for this research study.

Initial sections of this chapter present some background information supporting the suitability of PMT in characterizing lateral stress-deformation followed by the rationale for the selection of a simple constitutive relationship to describe element-level behavior of organic soil. Details of the

numerical analysis performed to validate the selected constitutive model by simulating the data from field PMT tests is presented along with the results.

The validated constitutive model was then employed to numerically generate soil restraint versus ground displacement relationships (“p-y curves” or “soil springs”) for pipelines buried in organic soils – these details are presented in Chapter 7. The developed p-y relationships are compared with the counterpart curves developed using PRCI guidelines (2009) currently recommended for pipes buried in soft clayey soils - with the intent of contributing to extend the current state-of-practice design methodologies to the pipelines in organic soil.

## **6.1 Role of Pressuremeter as a Controlled Test Reflecting Mechanical Response of Soil**

The significant role of PMT as a tool to obtain the lateral stress in the ground, the stress-strain behavior, the strength and the consolidation characteristics through empirical, theoretical or analytical approaches is well accepted (Benoît and Howie 2014). PMT generates axisymmetric lateral deformation in the soil and mobilizes a bulk volume of the soil, causing relatively significant lateral displacements. In particular, a pressuremeter would specifically invoke a lateral deformation cavity expansion mechanism that can be interpreted using fundamental soil mechanics principles (Baguelin et al. 1978, Houlsby and Withers 1988). Therefore, such a tool is considered more likely to provide indices that would lead to effective correlations with engineering parameters of interest in generating p-y curves for pipeline design as well.

As PMT provides a direct measurement of the in-situ stress-deformation characteristics when the test-hole cavity expands, the tool has served as a well-suited method of assessing both stiffness and strength parameters of soil through numerical model validations. For example, PMT data have been used in determining the relation between the soil reaction (P) and the pile deflection (y), again usually called p-y curves, for laterally loaded cylindrical piles at specific depths below the ground surface (Robertson et al. 1984; Dyson and Randolph 2001; Bouafia 2007; Farid et al. 2013). Another example is where Palmer (1972) studied PMTs conducted in clay using undrained plain-strain cylindrical cavity expansion and confirmed that the assumption of undrained deformation in PMT is justified in determining a complete stress-strain relation of clay.

These considerations provided good justification for numerical modeling of field PMT test cases as a way of validating a selected constitutive model to represent organic soils. As a result, a series of field pre-bored, 70-mm diameter, PMT tests conducted using a TEXAM pressuremeter

(manufactured by RocTest Inc.) were simulated using numerical modeling. Details of the modeling work and comparisons with experimental data are given in Section 6.4.

## **6.2 Selection of Constitutive Relationship to Represent Mechanical Response of Organic Soils**

The shear behavior of peat depends on the orientation of the shearing plane relative to the alignment of the fibers present (Yamaguchi et al. 1985; O’Kelly 2017). However, with the known highly inhomogeneous and spatially variable nature of soft and weak organic soils, it is impossible to meaningfully define a representative anisotropy along a pipeline alignment. With this consideration and the need to model the response of the “bulk soil mass” that deforms during a given pipe movement, it was judged that use of a relatively simple, isotropic stress-strain relationship would be suitable for the present investigation (as opposed to the possible use of sophisticated constitutive models). Another factor is the drainage condition that should be considered in numerical modeling; as noted by Lunne et al. (1997), it is possible that partially drained conditions may prevail in organic soils even in cone penetration tests undertaken during geotechnical site characterization. In spite of this, it is of significance to note that the response of organic soils are often conducted assuming undrained soil response (Yamaguchi et al. 1985, Mesri and Ajlouni 2007, Liu et al. 2018, Trafford and Long 2020).

Based on these aspects, Mohr-Coulomb model as provided by the FLAC software manual (Itasca 2016), considering undrained conditions reflecting a shear deformation event that occurs at a relatively fast rate, was selected to represent the behavior of organic soil. Shear modulus ( $G$ ), bulk

modulus (B), undrained shear strength ( $s_u$ ), and bulk unit weight ( $\gamma$ ) of organic soil are the key material properties required as input in numerical simulations.

Soil properties for numerical analysis were derived based on site-specific data available from independent field tests and laboratory experiments conducted on samples obtained from the field as a part of the present research work. For example, the small-strain shear modulus ( $G_0$ ) was calculated using field shear wave velocity ( $v_s$ ) measurements from seismic cone penetration tests (as per Equation 6.1). In recognition that PMT test is conducted from the device installed in a pre-bored hole, the starting initial G value of the stress-strain curve was assumed to be one third of  $G_0$ ; this is in accord with the guidelines suggested by Byrne et al. (1987). The bulk modulus (B) is calculated using Equation 6.2, assuming a Poisson's ratio ( $\nu$ ) of 0.49 to model very-close-to-undrained behavior with zero volume change. The value of  $s_u$  was derived from vane shear test data which were also found to be in line with those estimated from ball penetration tests; the  $\gamma$  was directly estimated based on data from laboratory experiments conducted on samples obtained from the field.

$$G_0 = \rho V_s^2 \quad 6.1$$

$$B = \frac{2G}{3} \frac{(1+\nu)}{(1-2\nu)} \quad 6.2$$

### 6.3 Finite Difference Modeling of PMT

Eleven PMT tests performed at the two organic soil sites under the field geotechnical investigation program discussed in Chapter 3 were modeled (replicating the six and five PMT tests, respectively, completed at Site 01 and Site 02), with each represented as a numerical boundary-value problem, for validating the numerical approach proposed in a preceding section. The commercially

available FLAC-2D - Version 8 (Itasca 2016) based on the two-dimensional explicit finite difference (FD) method was used herein. In this software, a given soil domain is represented by quadrilateral elements without intermediate nodes, within an adjustable grid to fit the shape of the modeled object. Further, it is based on a “Lagrangian” calculation that is well suited to model large deformations and material collapse. The Mohr-Coulomb stress strain model, as described in the previous section above, was used as the constitutive model for this purpose.

### **6.3.1 Development of mesh configurations**

The field PMT testing was numerically modelled as a plane strain axi-symmetric boundary value problem. The Finite Difference (FD) mesh (with the assistance of the FLAC mesh generation module) was defined to provide a finer discretization throughout the model. Key parameters such as analysis time, geometry, accuracy of results, and convergence were considered in finalizing the mesh configuration. While a larger mesh size is more time efficient, it might yield inaccurate results or might not converge to a unique value. On the other hand, using a finer mesh guarantees more accurate results, but increases the analysis time. Using a very fine mesh in areas that are subjected to relatively high strains may result in instability of the model and distorted elements.

After examining several mesh configurations for convergence and minimum analysis time, a uniform mesh of size 70 x 49 elements was selected to model a two-dimensional section of 3.5 m x 2.5 m representing the soil domain tested with PMT as shown in Figure 6.1. The mesh size allowed to reach the maximum radial displacement levels recorded in all field PMT tests. As discussed earlier, this configuration of the model was chosen after iterative modeling of different

mesh and element sizes, considering the computational time and the developed strain levels in the soil domain.

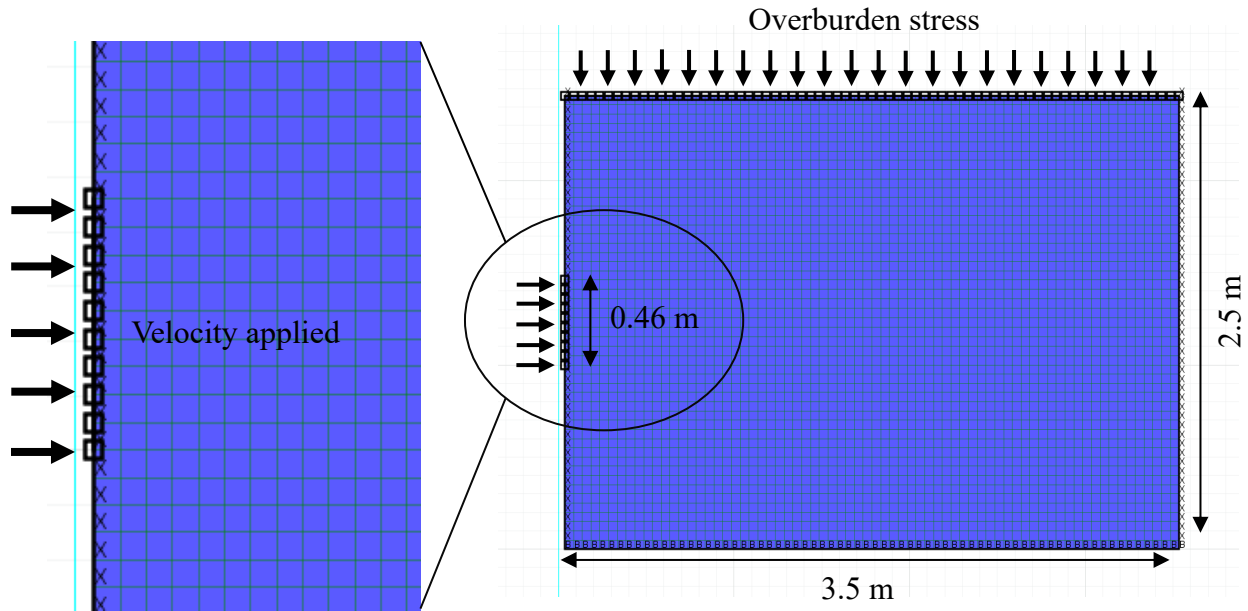


**Figure 6.1 Schematic of the two-dimensional FLAC axi-symmetric model with a uniform mesh of size 70 x 49 elements covering a 3.5 m (wide) x 2.5 m (high) area to represent the soil domain tested in pressuremeter tests**

At the bottom boundary, the nodes of the mesh are restrained from deformations along both horizontal and vertical axes (fixed), while at the two vertical boundaries (except the pressuremeter location) the nodes are restrained using roller supports to restrain any lateral deformations in the x-direction (see Figure 6.1). Nodes at the top boundary are allowed to displace freely in both horizontal and vertical directions. The model height was selected to have 1 m of depth above and below the position of the PMT, and the lateral extent of the model was selected as 100 times the initial radius of the pressuremeter to ensure that the boundaries are well outside the plastic zone (Yan 1986). The pressuremeter deformation was simulated by applying a constant rate of displacement at the nodes along the probe height of 0.46 m (at the mid depth of the mesh, as

illustrated in Figure 6.1). The PMTs conducted at different depths were simulated by applying a corresponding equivalent overburden stress on the top boundary of the mesh. An in-situ stress condition following isotropic consolidation was assumed as the initial condition for the entire mesh. All the dimensions, boundary conditions and the above discussed features are illustrated in Figure 6.1.

### **6.3.2 Soil parameters for numerical modeling of PMT**

As mentioned in Section 6.2, data from comprehensive geotechnical field investigations that were performed at two sites known to be underlain by organic soils, were utilized for the generation of soil parameters for the present analysis. The input soil parameters  $G$ ,  $B$ ,  $s_u$ , and  $\gamma$  used for each of the FLAC PMT test cases are summarized in Table 6.1. Note: (i) Laboratory experiments conducted on samples obtained from the two field sites indicated bulk densities between  $9.3 \text{ kN/m}^3$  and  $11.0 \text{ kN/m}^3$  for organic soil; based on this the use of an average value of  $10.8 \text{ kN/m}^3$  ( $1100 \text{ kg/m}^3$ ) for all the analyses cases were considered reasonable; (ii) The  $s_u$  and  $G$  values with respect to numerical modeling of a given field PMT test were interpreted directly using the spatially nearest eVST and shear wave velocity measurements, respectively, from the field geotechnical investigation results.

The numerical analysis was conducted in two steps. Initially, the model was executed to simulate gravity to establish the in-situ stress conditions. In the second step, analysis was performed with a uniform displacement rate applied along the length of PMT boundary in the model to mimic the expansion of the pressuremeter membrane with the injection of fluid in field PMT. Figure 6.2

shows the horizontal displacement contour plot after the application of pressuremeter deformation for Model PMT 1-01 350; Site 01 - Test Group 01 at 3.50 m depth below the ground surface.

**Table 6.1 Summary of input soil parameters used for each of the PMT simulations in FLAC 2D**

Model ID	$\gamma$ (kN/m <sup>3</sup> )	$s_u$ (kPa)	G (MPa)	B (MPa)
Site 01 in Surrey, British Columbia, Canada				
PMT 1-01 350	10.8	31.5	0.35	17.5
PMT 1-01 480	10.8	38	0.68	33.7
PMT 1-01 650	10.8	32	0.40	19.8
PMT 1-02 350	10.8	35.5	0.74	36.9
PMT 1-02 505	10.8	52	0.40	19.8
PMT 1-02 650	10.8	34	0.42	21.1
Site 02 in Wabasca, Alberta, Canada				
PMT 2-01 135	10.8	21.4	0.30	15.0
PMT 2-01 452	10.8	31.3	1.92	95.4
PMT 2-02 150	10.8	21.8	0.09	4.7
PMT 2-02 320	10.8	21.8	0.38	18.6
PMT 2-02 425	10.8	18.7	0.38	18.6

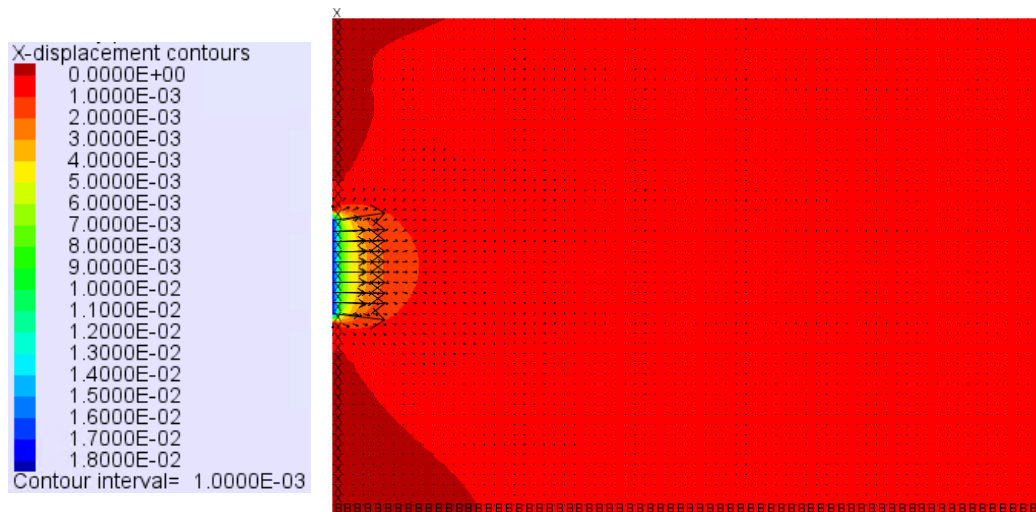


**Figure 6.2 Horizontal displacement contours after application of uniform displacement rate along the length of PMT boundary: Model PMT 1-01 350**

#### 6.4 Comparison of Test Results from Field PMT Tests and Numerical Analyses

The stress versus radial displacement relationships at the boundary of the pressuremeter derived from numerical simulations are compared with those from field PMTs at the Sites 01 and 02 are shown in Figure 6.3 through 6.8 and Figure 6.9 through 6.13, respectively. The plots in Figures 6.3 through 6.5, correspond with the field PMT tests conducted in Site 01-Test Group 01 at depths of 3.50 m, 4.80 m, and 6.50 m below the ground surface, respectively. These results show close-to-identical trends between the numerical predictions and field behavior. Similarly, Figures 6.6 through 6.8 correspond with the field PMTs of Site 01- Test Group 02 performed at 3.50 m, 5.05 m and 6.50 m test depths, respectively. Some of the results from numerical simulations agree well with those from field PMT tests whereas others show deviations.

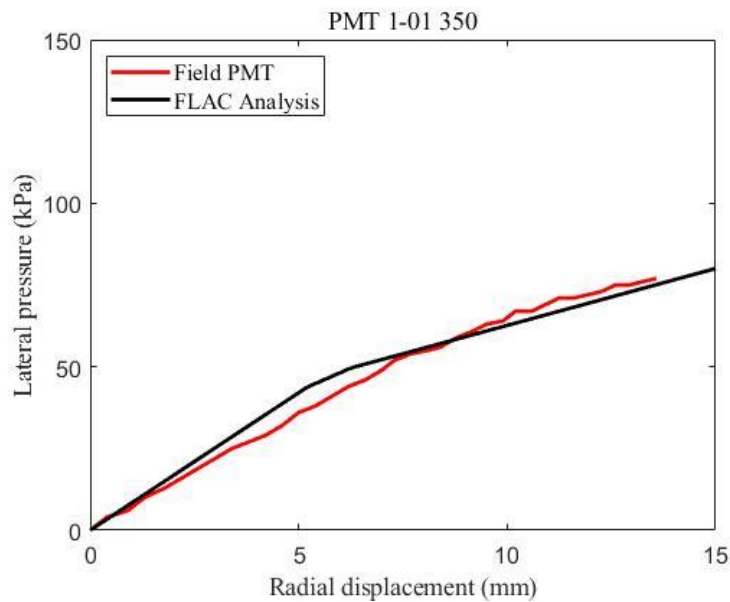


**Figure 6.3 The lateral pressure versus radial displacement comparison of field PMT and FLAC analyses at Site 01: Test Group 01 at 3.50 m depth below the ground surface**

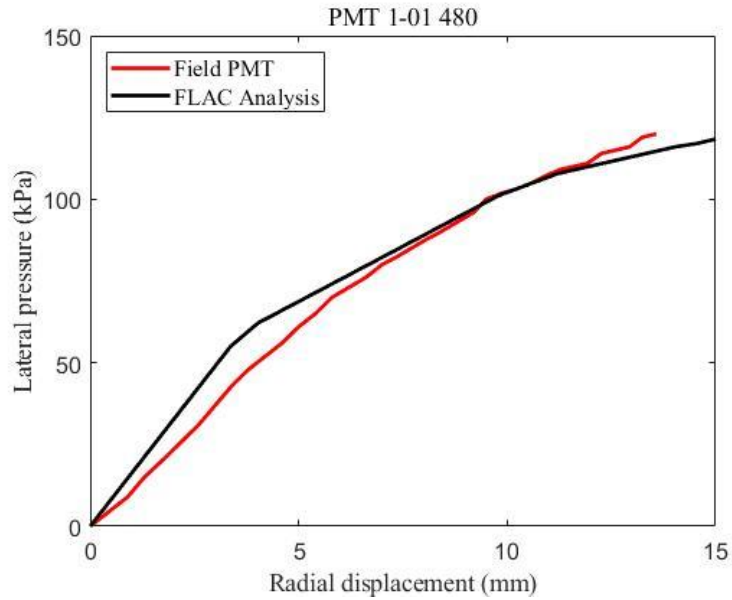


**Figure 6.4** The lateral pressure versus radial displacement comparison of field PMT and FLAC analyses at Site 01: Test Group 01 at 4.80 m depth below the ground surface

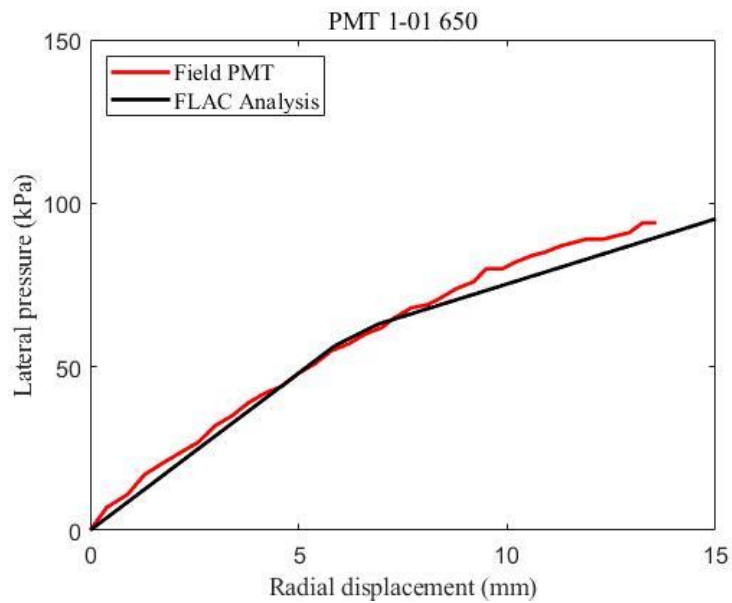


**Figure 6.5** The lateral pressure versus radial displacement comparison of field PMT and FLAC analyses at Site 01: Test Group 01 at 6.50 m depth below the ground surface

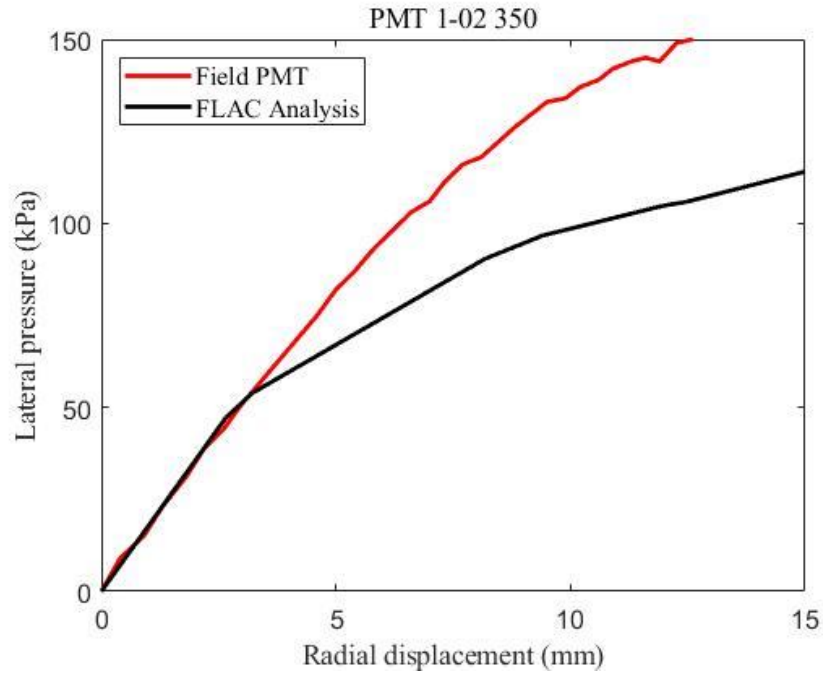


**Figure 6.6** The lateral pressure versus radial displacement comparison of field PMT and FLAC analyses at Site 01: Test Group 02 at 3.50 m depth below the ground surface

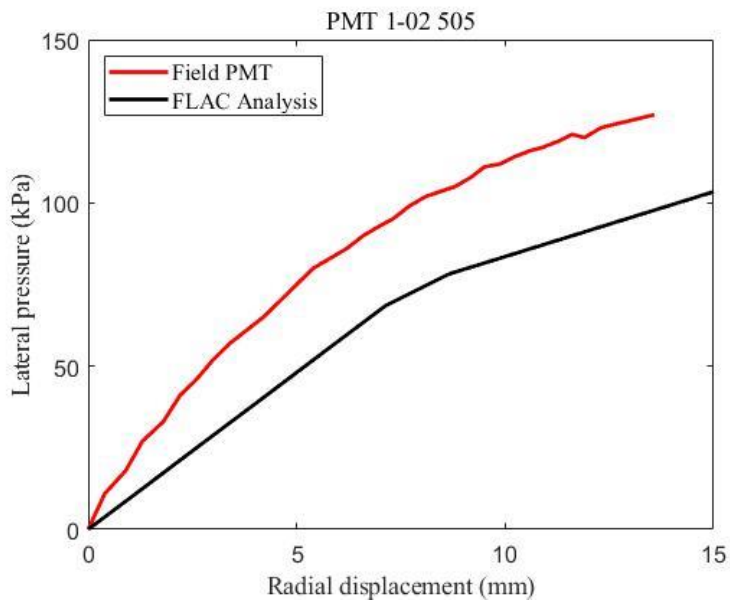


**Figure 6.7** The lateral pressure versus radial displacement comparison of field PMT and FLAC analyses at Site 01: Test Group 02 at 5.05 m depth below the ground surface

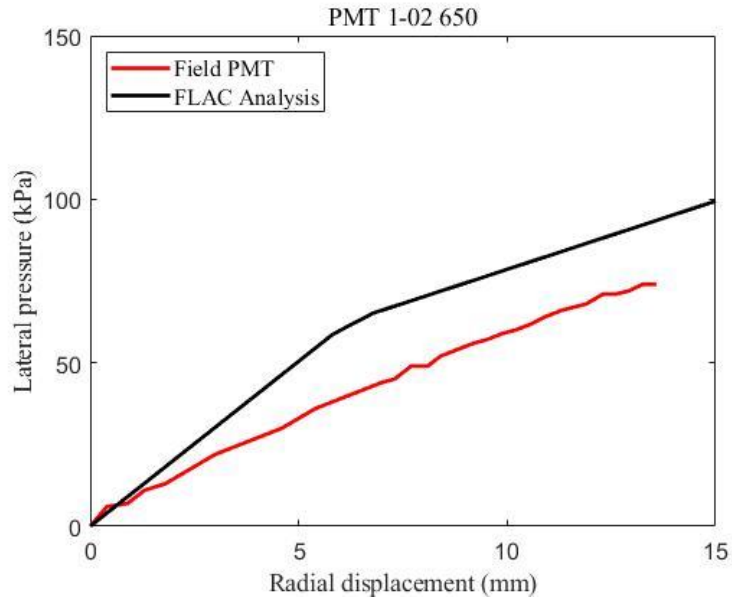


**Figure 6.8 The lateral pressure versus radial displacement comparison of field PMT and FLAC analyses at Site 01: Test Group 02 at 6.50 m depth below the ground surface**

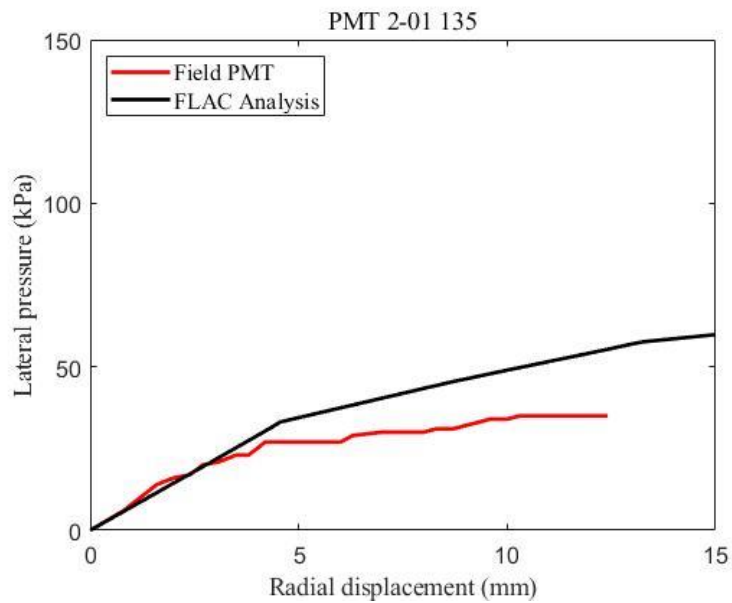


**Figure 6.9 The lateral pressure versus radial displacement comparison of field PMT and FLAC analyses at Site 02: Test Group 01 at 1.35 m depth below the ground surface**

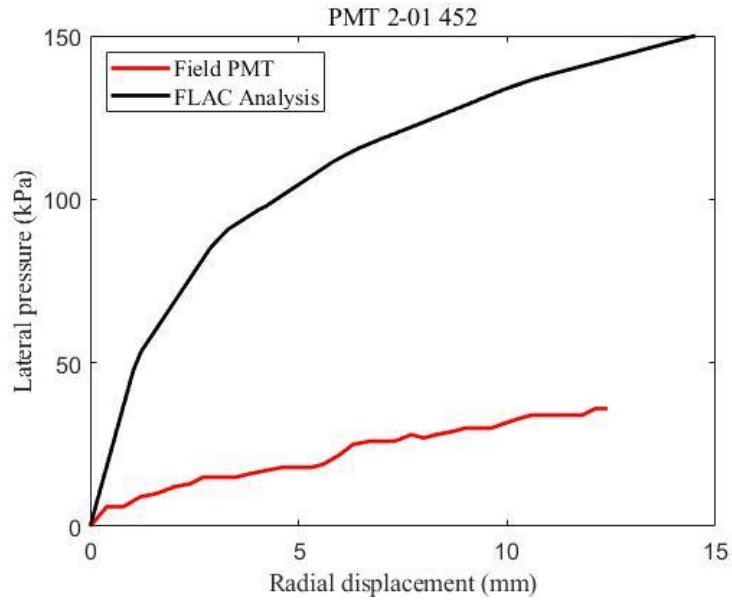


**Figure 6.10** The lateral pressure versus radial displacement comparison of field PMT and FLAC analyses at Site 02: Test Group 01 at 4.50 m depth below the ground surface

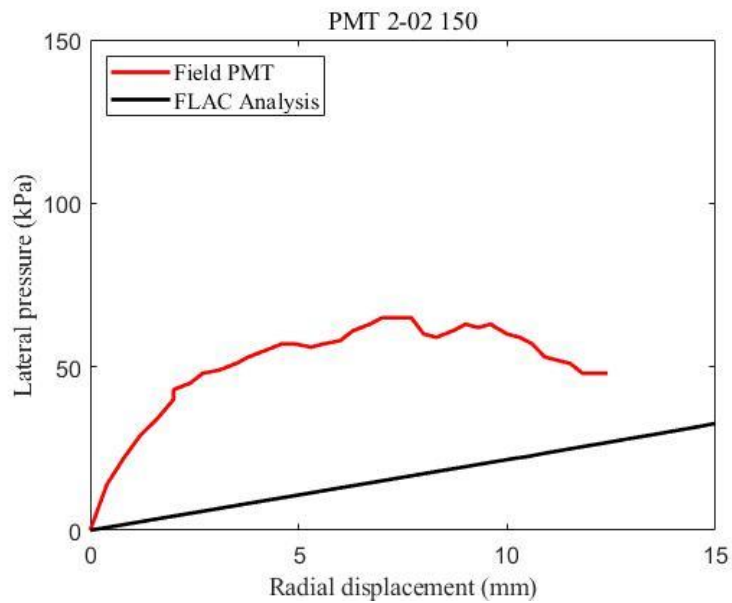


**Figure 6.11** The lateral pressure versus radial displacement comparison of field PMT and FLAC analyses at Site 02: Test Group 02 at 1.50 m depth below the ground surface

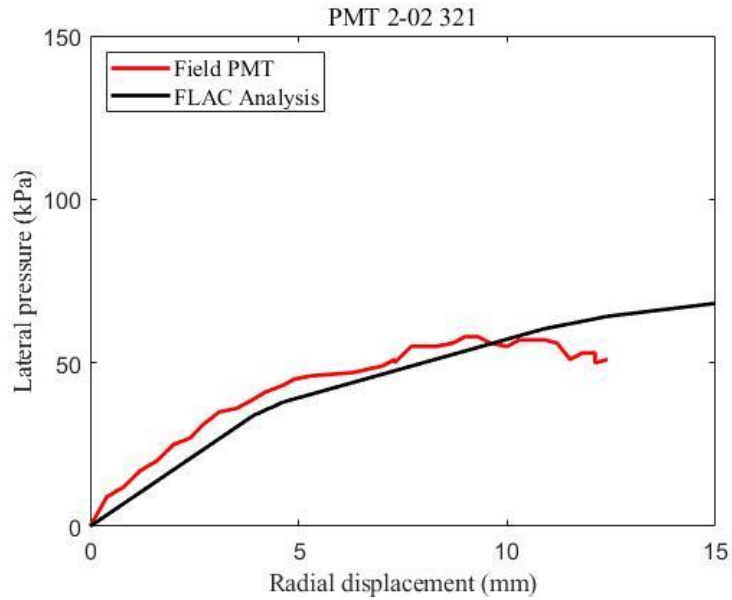


**Figure 6.12** The lateral pressure versus radial displacement comparison of field PMT and FLAC analyses at Site 02: Test Group 02 at 3.20 m depth below the ground surface

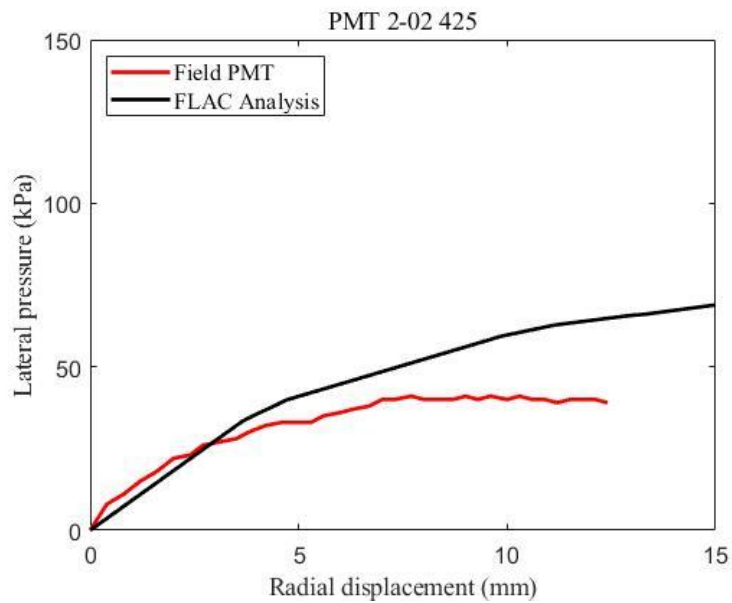


**Figure 6.13** The lateral pressure versus radial displacement comparison of field PMT and FLAC analyses at Site 02: Test Group 02 at 4.25 m depth below the ground surface

Comparisons presented in Figures 6.3 through 6.5 showing the three PMTs completed at Site 01-Test Group 01 indicate that field and numerical analyses results show good agreement between each other, while the numerical analyses for Site 01-Test Group 02 show up to  $\pm 40\%$  deviation from the field pressuremeter curves. Out of the six PMT tests completed at Site 02, the PMT test at the deepest level (4.50 m) of Test Group 01 was not successful due to technical difficulties. Hence, there are only five PMTs in total for Site 02. Comparisons presented in Figures 6.9, 6.12, and 6.13 show reasonable agreement between numerical simulations and field test results. However, Figures 6.10 and 6.11 show significant discrepancy in this comparison process. This discrepancy between the results may be attributable to the significant variability of soil stiffness and strength in the highly fibrous nature of the soils encountered at Site 02, Wabasca, Alberta. Visual observations of solid stem auger soil samples retrieved during the field investigations, indicated that the organic soil at this site contained significantly more plant and fibrous matter compared to those from Site 01, Surrey, British Columbia. This highly fibrous nature of soil could have affected the field PMT results as well as the other field testing which were used to get the soil strength and stiffness properties as independent input in the FLAC models.

In an overall sense, the comparisons shown in Figures 6.3 through 6.13 indicated that the use of isotropic Mohr-Coulomb model would be justifiable and appropriate in meaningfully representing the behavior of amorphous organic soils in continuum based numerical analysis while more research is needed to conclude the applicability of the Mohr-Coulomb model in highly fibrous organic soil deposits. This assessment is reasonable knowing that the use of sophisticated constitutive soil models is not warranted due to the substantial spatial variability and non-homogeneity of the strength and stiffness properties of organic soils (which exist especially along long-distance pipeline alignments). Moreover, it is not practical and economical to conduct

geotechnical investigations at frequent horizontal distances to effectively delineate these variabilities, and this is why any required analyses for pipeline designs are typically carried out using “average” soil parameters.

## **6.5 Summary**

A simple Mohr-Coulomb constitutive model was found suitable to numerically represent the element-level behavior of amorphous organic soils for numerical simulation of SPI; this was validated by a detailed finite difference numerical analysis of field pressuremeter tests using commercially available FLAC-2D - Version 8 (Itasca 2016) and comparing the lateral pressure versus radial displacement behavior with the corresponding data obtained from the field. Material properties used in the numerical analyses were interpreted directly from the field and laboratory geotechnical investigation results. The selected constitutive model will be used to study the horizontal soil restraints on pipes during ground movements to obtain horizontal soil restraint versus displacement curves (p-y curves or soil springs) pipelines buried in organic soil – for different pipe diameters and soil stiffness and strength property combinations in Chapter 7.

## Chapter 7: Numerical Modeling of Lateral Soil-Pipe Interaction

This chapter presents the detailed numerical finite difference analyses undertaken to generate soil restraint versus pipe displacement relationships (p-y curves or “soil springs”) for pipelines buried in organic soils. The modeling was performed assuming a total-stress-based approach (i.e., undrained soil behavior) using an isotropic Mohr-Coulomb constitutive relationship; the rationale for selecting this model to numerically describe the stress-strain response of organic soils is presented in Chapter 6.

First, a two-dimensional numerical model (FLAC analysis mesh) was established to represent the lateral soil restraint configuration of pipe buried in organic soil adopted in physical full-scale testing (as presented in Chapter 5). The soil strength and deformation parameters for the stress-strain model were derived from the in-place penetration test data during pipe displacement testing. The horizontal soil restraint versus displacement curves (p-y curves or soil springs) computed from the numerical model were compared with the counterpart load-displacement behavior measured during full-scale tests. This process allowed validation of a numerical model that meaningfully represents and captures the soil-pipe interaction (SPI) mechanisms manifested during physical modeling. Using the validated numerical framework, it was possible to derive the lateral soil springs for a range of pipeline diameter (D) and burial depth (H) combinations.

This chapter presents the details and results of the above-mentioned validation and parametric analyses undertaken using FLAC numerical modeling. The resulting load-displacement curves are compared with the counterpart curves developed using PRCI guidelines (2009) currently recommended for pipes buried in soft clayey soils with the intent of contributing to improve the current state-of-practice design methodologies.

## **7.1 Numerical Modeling of SPI During Full-Scale Horizontal Pipe Displacement**

### **7.1.1 Development of mesh configurations**

The mesh configuration for SPI modeling was selected after examining several alternate mesh configurations. It was important to have the size and geometric conditions of the model including boundary conditions to meaningfully represent the full-scale tests. As described in Section 4.3, the size of the physical modeling chamber is 2 m (length) x 1 m (width) x and 1 m (height). During the tests, the initial position of the center of the pipe was located 330 mm above the base of the chamber and 300 mm from the south wall.

Some key parameters such as time for analysis, geometry, accuracy of the results and convergence were considered in designing the mesh. It was recognized that, while a larger mesh size is more time efficient, it could affect the accuracy of the results or might not converge to a unique value. On the other hand, using a finer mesh guarantees more accurate results, but increases the analysis time. Using a very fine mesh in areas that are subjected to relatively high strains may result in instability of the model and distorted elements. Furthermore, previous numerical simulations conducted by Karimian et al. (2006) at UBC provided good insight to decide on the adequacy of the lateral mesh size and selection of boundary conditions. As the overall response of the soil-pipe system depends on boundary conditions, loading characteristics, and mechanical properties of each element, grid-sensitivity was checked as a part of selecting a discretization leading to reasonable numerical convergence. The bottom boundary of the finite difference mesh is restrained from any movements along both x and y axes (fixed), while all the vertical boundaries are restrained from

any lateral movement in the x-direction using roller supports. No displacement boundary conditions were applied on the ground surface (i.e., nodes allowed free movement at the ground surface).

Seven FLAC FD meshes had to be set up to meet the full-scale test simulations; for each case, this required examining several mesh configurations for convergence and minimum analysis time. The number of elements in the seven models varied depending on the H/D ratios ranging from 2400-4500. A uniform mesh size of 20 mm and 25 mm for NPS6 and NPS8 respectively were used in the analysis. The mesh sizing was adequate for imparting more than 300 mm of pipe displacement within a reasonable execution time along with good convergence of results without causing distortion of elements and “bad” geometry issues in the model. The analyses were run in small strain mode. Resulting load-displacement curves using different modes (small strain, large strain and automatic remeshing) were compared before choosing small strain mode and the difference between the results were identified to be negligible. This was further discussed with FLAC/Itasca (Itasca 2016) experts to confirm the use of small strain mode as opposed to large strain and automatic remeshing options. Figure 7.1 illustrates a typical mesh configuration; this example shows the dimensions and extent of the mesh (30 x 80) considered for modeling the full-scale test H6-8-1.6-9.8-200 – a test using an NPS 6 pipe and with an H/D ratio of 1.6. Table 7.1 summarizes H and D values of the mesh configurations in the full-scale test simulations.

**Table 7.1 Summary of mesh configurations used in the FLAC 2D modeling of full-scale horizontal pipe displacement**

Model ID	Pipe	D (mm)	H (mm)	H/D
F H1-6-1.9-1.5-360	NPS6	168	324	1.9
F H2-6-3.5-2.0-340	NPS6	168	584	3.5
F H3-6-2.9-5.9-270	NPS6	168	484	2.9
F H4-8-1.9-7.3-250	NPS8	219	410	1.9
F H5-8-1.6-9.8-210	NPS8	219	360	1.6
F H6-8-1.6-9.8-200	NPS8	219	360	1.6
F H7-6-1.9-9.8-220	NPS6	168	324	1.9

In the numerical modeling, the pipe was represented by a series of beam elements (about 26 - 32 elements) to approximately form a circular shape with weight and stiffness of the beam elements matching that of the pipe test specimen. With the selected deformation modulus for the pipe [density = 7850 kgm<sup>-3</sup> and Young's modulus of steel (E) 200 GPa], the pipe behaves like a rigid body when compared with the stiffness of the soil. A pipe wall thickness of 10 mm was considered based on the pipe diameter considering guidelines from CSA Z662:19 (2019).

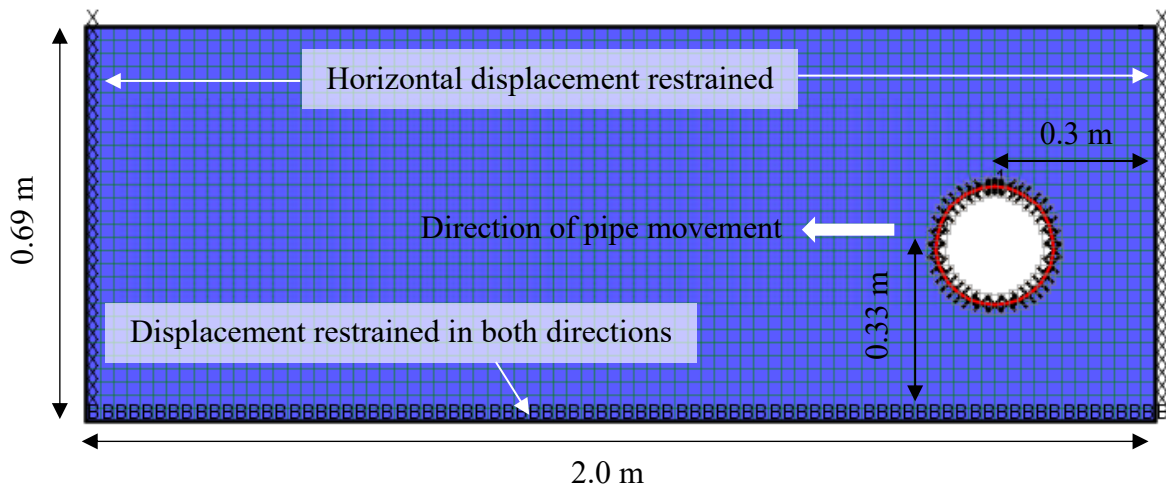


**Figure 7.1 Example schematic of dimensions and extent of the (30 x 80) mesh considered for the 2D FLAC model for lateral pipe displacement analysis of NPS6 pipe and H/D ratio of 1.6 (Model: F H6-8-1.6-9.8-200)**

### 7.1.2 Soil parameters for numerical analysis

Characterization of organic soil for numerical modeling purposes was achieved through test-chamber-specific in-place shear strength characterization tests during full-scale horizontal pipe displacement tests discussed in Section 5.2.2. Test-chamber-specific and inferred shear strength properties from the BPT and eVST data were used in numerical simulations of full-scale horizontal pipe displacement tests. Table 7.2 summarizes the input soil properties used in numerical analyses. A  $G_0/s_u$  ratio of 30 was used in calculating  $G_0$  based on the test-chamber-specific and inferred  $s_u$  data because  $G_0/s_u$  of 30 is the lowest ratio observed from field geotechnical program (presented in Section 3.3.3) giving a soft reconstituted soil bed. Similar to PMT analyses,  $G$  of organic soil was assumed to be one third of  $G_0$ ; this is in accord with the guidelines suggested by Byrne et al. (1987), and  $B$  was calculated using Equation 6.2, assuming a Poisson's ratio ( $\nu$ ) of 0.49 to model close-to-undrained behavior with zero volume change. Average unit weight determined during the full-scale tests were used in numerical simulations.

**Table 7.2 Soil strength and stiffness parameters used in the numerical simulations of full-scale horizontal pipe displacement.**

Model ID	$s_u$ (kPa)	$G$ (kPa)	$B$ (MPa)
F H1-6-1.9-1.5-360	1.5	15	0.74
F H2-6-3.5-2.0-340	2	20	0.99
F H3-6-2.9-5.9-270	5.9	59	2.93
F H4-8-1.9-7.3-250	7.3	73	3.63
F H5-8-1.6-9.8-210	9.8	98	4.87
F H6-8-1.6-9.8-200	9.8	98	4.87
F H7-6-1.9-9.8-220	9.8	98	4.87

### 7.1.3 Modeling of soil-pipe interface

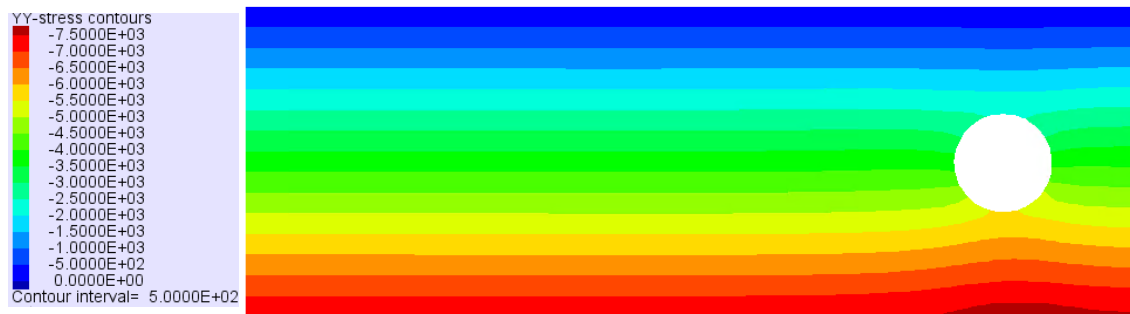
Structural beam elements were used to represent the pipe and they were separated from the soil mass using unglued interface elements. Simulation of SPI for the lateral load tests required interface shear strength value for the pipe and organic soil. Because of the mechanisms involved during lateral pipe movement, obtaining a representative shear strength parameter for the interface between pipe and organic soil is not straightforward. As such, it was decided to examine the results from full-scale axial pipe displacement tests as well as from PRCI guidelines. Based on the axial testing given in Section 5.1, interface shear strength value of  $0.67s_u$  could be inferred. This is the average adhesion factor ( $\alpha$ ) back calculated based on the peak axial load resulting from the axial pipe displacement tests. On the other hand, using charts in PRCI guidelines (2009) for normally consolidated soils, the interface shear strength would be  $1.0(s_u)$ . Owing to these considerations, interface shear strength value of  $0.67s_u$  was considered for the numerical analysis simulating physical model tests, - with some limited analyses carried out using an interface shear strength value of  $1.0(s_u)$ . It was found that the difference in the  $P_u$  values were within 10%. On average, the shear resistance values arising from  $0.67s_u$  were also comparable with the shear resistance values computed based on interface direct shear experiments presented in section 3.3.4. Therefore, it was judged reasonable to use  $0.67s_u$  for numerical analysis simulating physical model tests. The normal and shear stiffnesses for the interface were set to 3 GPa, which is approximately equal to 10 times the stiffness of the neighboring soil, as recommended in the FLAC User Manual (Itasca 2016). The soil-pipe interaction during the seven full-scale horizontal lateral pipe displacement tests was numerically modelled using the finite difference software platform FLAC 2D (Itasca 2016). Soil

behavior was represented using soil shear strength parameters obtained from in-place penetration tests performed during the pipe displacement tests.

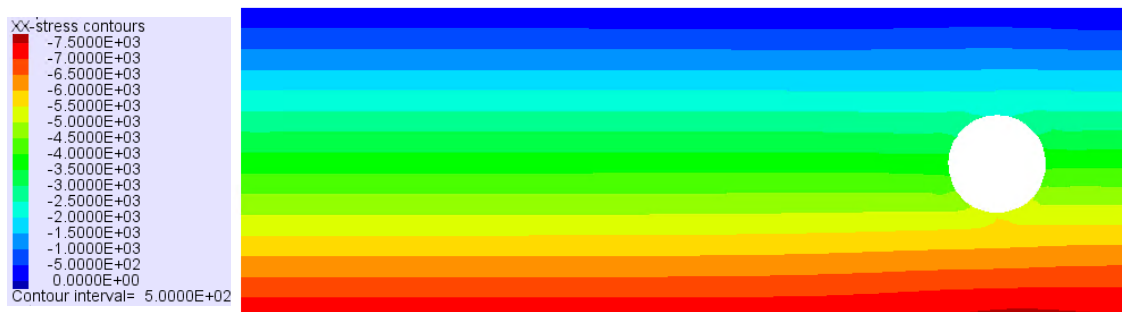
#### **7.1.4 Numerical analysis steps - application of gravity and pipe displacement**

In preparation for the analysis under pipe displacement conditions, the effect of gravity was invoked to establish the in-situ stress conditions by activating gravity mode in FLAC 2D. At this stage, the analysis was continued to achieve full equilibrium under gravitational forces before executing pipe displacement. Numerical simulations of both full-scale tests and parametric study are executed following the same order and the contours of computed horizontal and vertical stresses prior to pulling the pipe for model: F H6-8-1.6-9.8-200; NPS 6 pipe and H/D ratio of 1.6 are shown in Figure 7.2.

As may be noted from Figure 7.2 (a), the total vertical stress computed at the base of the boundary value problem is about 7.5 kPa. This is as expected for a soil deposit having a bulk density of 10.4 kN/m<sup>3</sup> and thickness of 0.72 m. The total horizontal stress computed for the base is also close to 7.5 kPa. The similarity between the vertical and horizontal stresses are likely due to the relatively low undrained shear strength specified for the soil. It is to be noted that the constitutive model does not require the specification of the coefficient of lateral earth pressure at rest ( $K_0$ ).



(a)



(b)

**Figure 7.2 Total stress contours prior to pipe displacement; a) vertical and b) horizontal for NPS 6 pipe and H/D ratio of 1.6 (Model: F H6-8-1.6-9.8-200).**

In the second step, the pipe was numerically displaced in the lateral direction, specifying a displacement boundary condition at the circumference of the pipe. A steady displacement rate of  $1 \times 10^{-8}$  m per step was applied to simulate the horizontal displacement of pipe based on the rate of convergence. In that manner, seven numerical models are simulated and validated with the load-displacement behavior results arising from the full-scale tests. The outcomes are presented and discussed in the next section.

### 7.1.5 Comparison of numerical and experimental load-displacement behavior

The soil springs (p-y curves) developed using the numerical simulations and the counterpart observations from the seven physical modeling tests are compared in Figures 7.3 through 7.9. Note: A review and discussion of the factual results from the physical modeling tests are presented in Chapter 5, and therefore, they are not repeated herein. The  $P_u$  values obtained from numerical simulations from the same results plotted against those obtained from numerical simulations of full-scale tests is presented in Figure 7.10 (corresponding  $P_u$  values are listed in Table 7.3). It can be seen that, in five of the cases out of seven, the numerical model predictions are within 90% of the ultimate failure soil load ( $P_u$ ) experienced by the pipe during physical modeling. The other two cases that involved relatively denser organic soil conditions, the numerical modeling seem to overpredict the  $P_u$ .

On the other hand, the early parts of the soil restraint versus pipe displacement curve between the physical modeling experiments and numerical modeling (until the  $P_u$  value is reached) did not display good agreement. Considering the difficulties to quantify soil non-uniformities and associated stiffness variability in test beds, other experimental errors associated with testing conditions, combined with limitations in numerical modeling may well have contributed to these deviations. It is also of relevance to note that the prediction of deformations are more challenging compared to estimation of failure loads in the solution of geotechnical boundary value problems, and the difficulties faced with respect to the above SPI analysis cases with good numerical formulations is not unusual.

Additional analysis was undertaken to examine the sensitivity of the ultimate lateral soil restraint ( $P_u$ ) for the tests H3-6-2.9-5.9-270, H4-8-1.9-7.3-250, H5-8-1.6-9.8-210 and H6-8-1.6-9.8-200

(shown in Figures 7.6, 7.7, 7.8, and 7.5 respectively), and the results are shown in Figures D.19, D.20, D.21 and D.22 respectively. As may be noted the  $s_u$  values were adjusted by 20% to align the resulting  $P_u$  with the experimental results. This variation is considered to be well within the expected variabilities particularly in organic soils. No analysis was undertaken to match the numerical outcomes with the experimental data for the initial parts of the load-displacement responses due to the non-representative nature of the soil restraints mobilized at smaller displacements as per Section 5.2.3.

In an overall sense, it became clear that the numerical model is able to capture the failure mechanisms manifested during physical modeling in a meaningful manner and in turn, predict the peak lateral soil restraint ( $P_u$  value). Based on this, it was considered reasonable that this numerical model could provide a rational basis to numerically investigate and generate lateral soil restraint p-y curves for configurations involving different pipeline burial conditions and pipe diameters – see section 7.2.1 for the implementation of this numerical work.

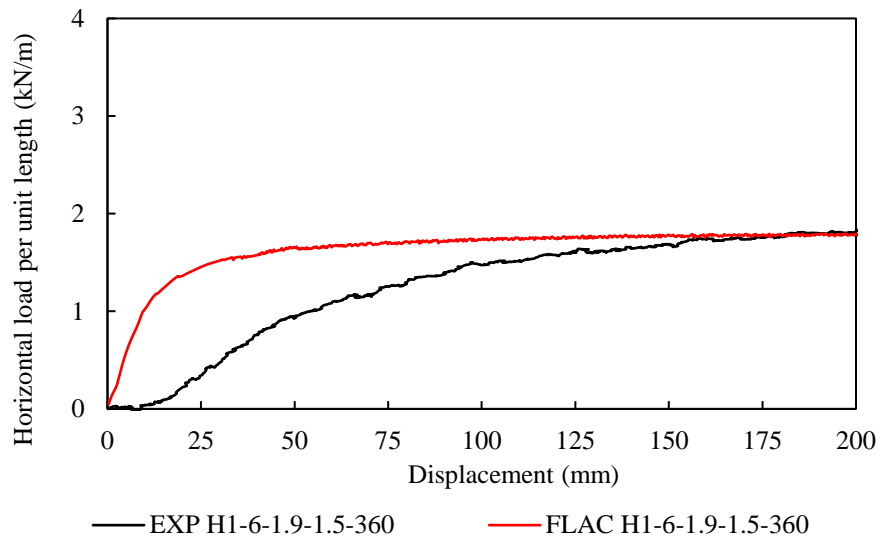


**Figure 7.3 Comparison of lateral load-displacement behavior from FLAC analyses and full-scale test results;  
Test configuration: H1-6-1.9-1.5-360**

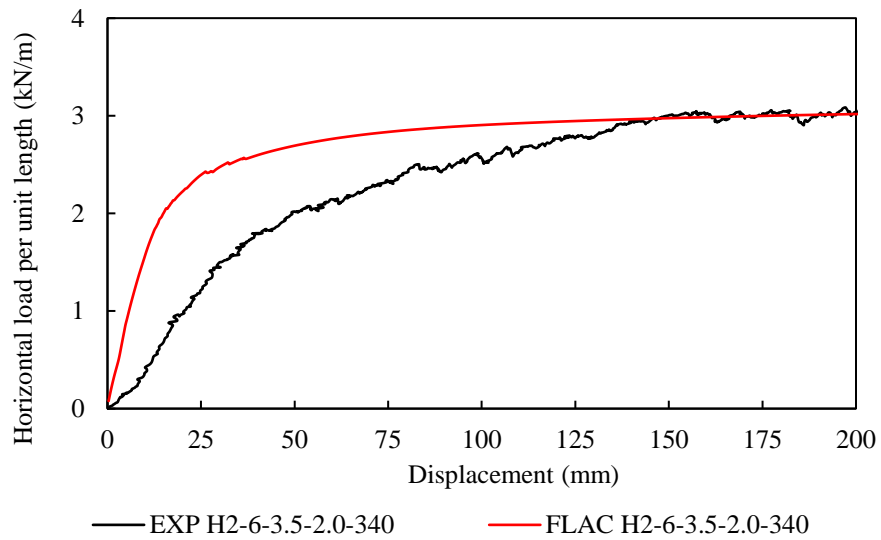


**Figure 7.4 Comparison of lateral load-displacement behavior from FLAC analyses and full-scale test results;  
Test configuration: H2-6-3.5-2.0-340**

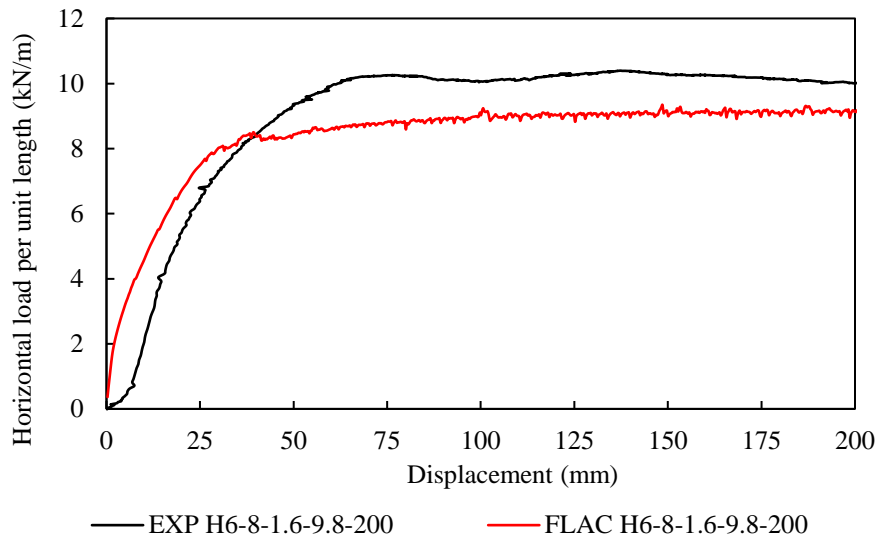


**Figure 7.5 Comparison of lateral load-displacement behavior from FLAC analyses and full-scale test results;  
Test configuration: H6-8-1.6-9.8-200**

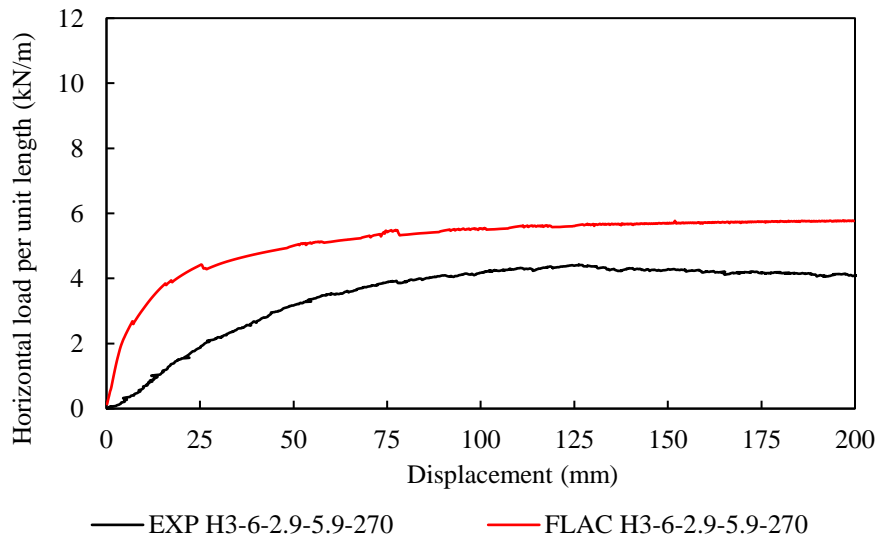


**Figure 7.6 Comparison of lateral load-displacement behavior from FLAC analyses and full-scale test results;  
Test configuration: H3-6-2.9-5.9-270**

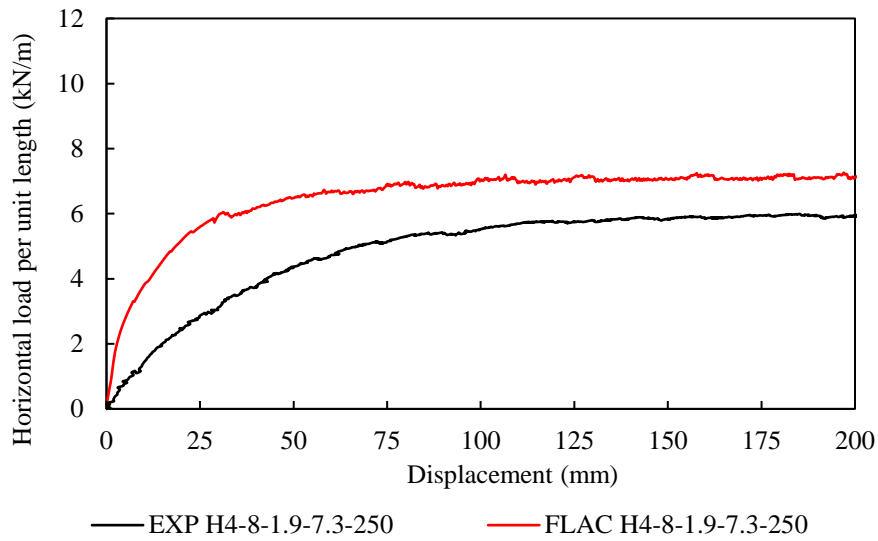


**Figure 7.7 Comparison of lateral load-displacement behavior from FLAC analyses and full-scale test results;  
Test configuration: H4-8-1.9-7.3-250**

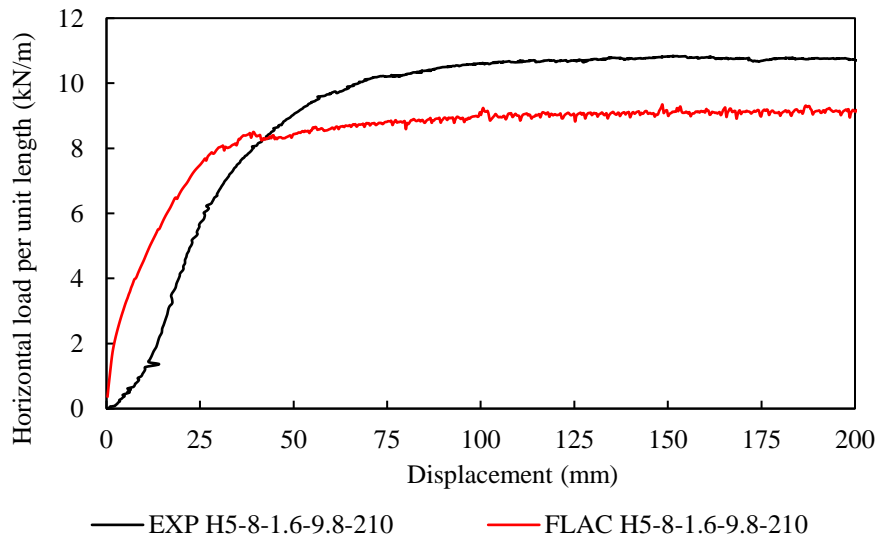


**Figure 7.8 Comparison of lateral load-displacement behavior from FLAC analyses and full-scale test results;  
Test configuration: H5-8-1.6-9.8-210**

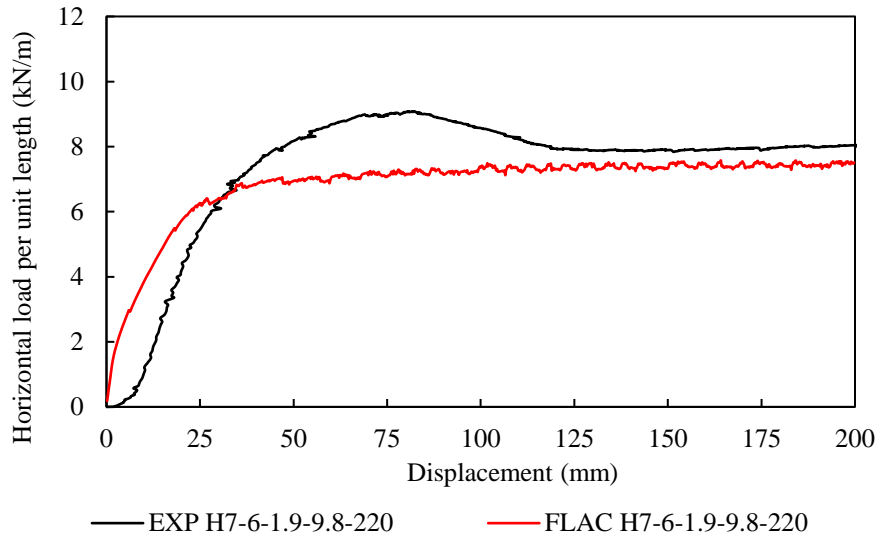


**Figure 7.9 Comparison of lateral load-displacement behavior from FLAC analyses and full-scale test results;  
Test configuration: H7-6-1.9-9.8-220**

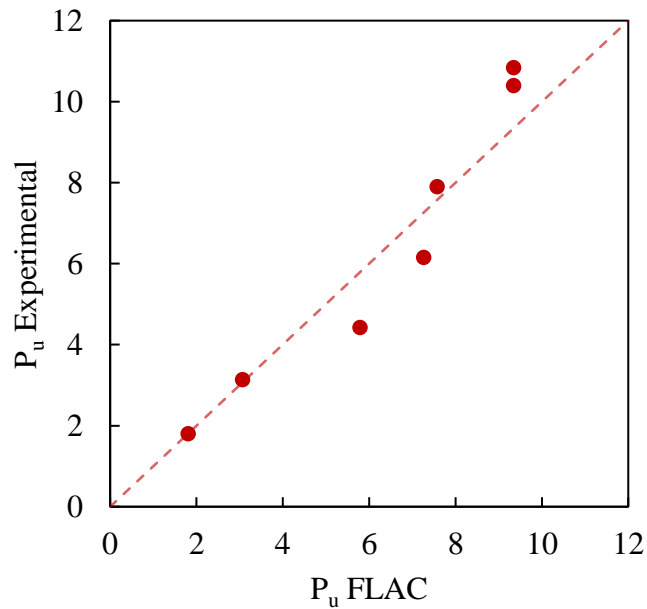


**Figure 7.10 Comparison of the peak soil restraint ( $P_u$ ) from full-scale experiments and FLAC analyses cases presented in Figures 7.3 through 7.9**

**Table 7.3 Summary of peak lateral soil restraint ( $P_u$ ) from full-scale test results and FLAC modeling of full-scale tests**

Model ID	$P_u$ experimental	$P_u$ FLAC
F H1-6-1.9-1.5-360	1.80	1.80
F H2-6-3.5-2.0-340	3.14	3.07
F H3-6-2.9-5.9-270	4.42	5.79
F H4-8-1.9-7.3-250	6.15	7.26
F H5-8-1.6-9.8-210	10.83	9.34
F H6-8-1.6-9.8-200	10.40	9.34
F H7-6-1.9-9.8-220	7.90	7.57

## 7.2 Assessment of the Findings in Relation to Design Practice Guidelines

The validated numerical model from the above section was used as a tool to develop p-y curves corresponding to a variety of soil parameter and geometric pipeline configurations. These outcomes were then compared with the counterpart soil springs generated from pipeline design guidelines.

As mentioned at the outset of this thesis, Pipeline Research Council International (PRCI 2009) provides current practice guidelines to develop soil springs to estimate soil loads on buried pipelines subject to ground movements. These guidelines are provided for applications in commonly encountered coarse-grained and fine-grained mineral soil conditions. However, the current PRCI guidelines do not have provisions for organic soils, and as such, the equations intended for fine-grained (total stress based) are often used by engineers to address problems associated with buried pipelines in organic soils.

With this backdrop, it is of value to use the findings from the numerical modeling research to examine the applicability of the PRCI equations (recommended for fine-grained soils) for organic soils. This was accomplished by developing PRCI-based p-y curves for organic soils for the soil

parameters and geometric pipeline configuration cases (a total of twenty four cases) and comparing with the corresponding p-y curves arising from numerical modeling. Further comparisons between the PRCI-based p-y curves for organic soils and numerical modeling of the full-scale tests are also included in this discussion.

### **7.2.1 Predictions of lateral soil restraint versus displacement curves using numerical analysis**

Full-scale physical modeling of buried pipelines provides reliable results for prediction of soil loads on pipe. However, considering the cost and time restraints associated, and the large number of variables affecting soil behavior and various geometrical configurations of buried pipes with regard to the burial depth and pipe size, it is not practical to conduct extensive full-scale physical modeling to explore this multiplicity of cases. Numerical analysis provide an alternate opportunity to investigate these aspects at relatively low cost, time, and effort requirements.

With this background, the validated numerical model as per previous sections was used to develop the p-y curves for pipes buried in organic soils under different undrained soil strength and stiffness properties and various pipe geometrical configurations. In this regard, twenty four numerical analyses cases as described below were conducted with different pipe burial depths, pipe diameters and organic soil properties covering the strength and stiffness parameter ranges determined during the field investigation program (see Chapter 3 for details related to the field investigation program).

### 7.2.1.1 Development of mesh configurations

Four mesh configurations were selected for the numerical predictions of pipe displacement consisting of 24 model cases. Four pipe diameters (324 mm, 610 mm, 914 mm, and 1219 mm in diameter, respectively, corresponding to NPS 12, 24, 36, and 48 were modeled (NPS = Nominal Pipe Size, diameter expressed in inches). The two-dimensional geometry shown in Figure 7.11 represents an example of dimensions and extent of the mesh (64 x 120) considered for the modeling of NPS 12 pipe and H/D ratio of 2 (Model ID: 2\_D12\_LD\_MC). The number of elements in each model was between 7600 – 8500. Similar to the full-scale test simulations, this mesh size allowed more than 300 mm of pipe displacement in all conditions. Table 7.4 summarizes the H and D values of the chosen mesh configurations.

**Table 7.4 Summary of mesh configurations used in the FLAC 2D predictions of lateral soil restraint**

Model ID	Pipe	D (mm)	H (mm)	H/D
2_D12_LD_MC	NPS 12	324	648	2
2_D24_LD_MC	NPS 24	610	1219	2
2_D36_LD_MC	NPS 36	914	1829	2
2_D48_LD_MC	NPS 48	1219	2438	2

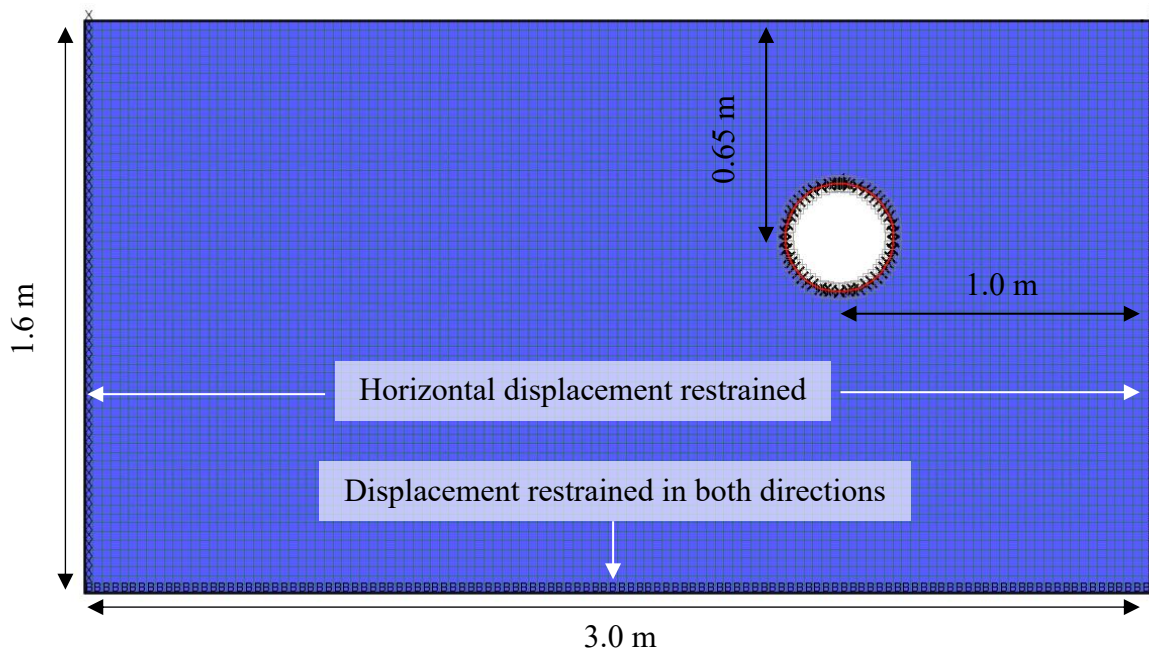
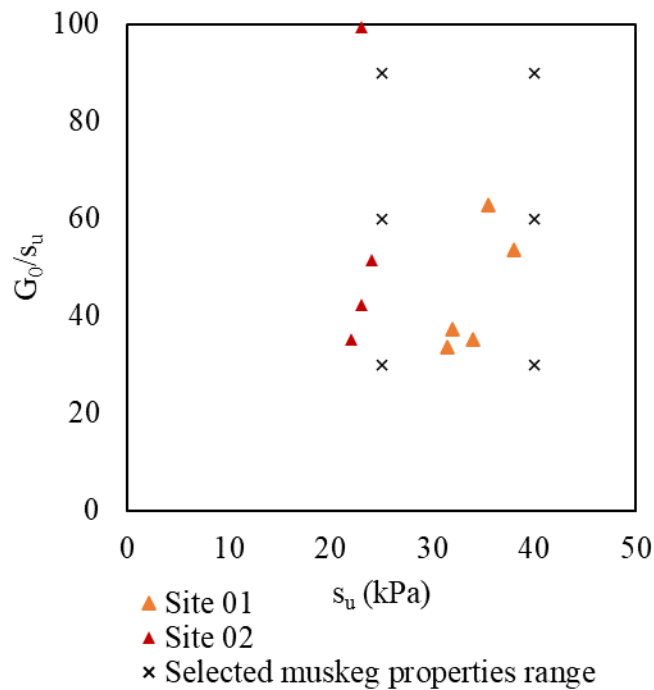


Figure 7.11 Example schematic of dimensions and extent of the (64 x 120) mesh considered for the two-dimensional FLAC model for lateral pipe displacement analysis of NPS12 pipe and H/D ratio of 2 (Model ID: 2\_D12\_LD\_MC).

### 7.2.1.2 Soil parameters for numerical analysis

It was considered reasonable to conduct the numerical simulations considering an array of cases comprising different soil shear stiffness ( $G$ ) and strength ( $s_u$ ) combinations, which are the key input material parameters required for the chosen isotropic Mohr-Coulomb model based on the PMT analysis in Chapter 6. These combinations were selected to reflect the properties of organic soils that were encountered during the geotechnical investigations at the Sites 01 and 02 discussed in Chapter 3. In addition, Exploration of this range of parameters will also serve as a way of assessing the sensitivity of stiffness and strength of organic soil on the load-displacement curves. Six

combinations of  $G_0/s_u$  and  $s_u$  as shown in Figure 7.12, and summarized in Table 7.5, were selected as the input soil parameters for the numerical modeling (Note:  $G_0/s_u$  which represents the rigidity index of the organic soil is a well-recognized normalizing approach in representing soil properties). The  $G_0/s_u$  and  $s_u$  derived from site-specific data from the two test sites (at the locations of PMT numerical simulations described earlier) are also shown in the same figure. Similar to numerical analyses of pressuremeter testing presented in Chapter 6,  $G$  of organic soil was taken as one third of small strain shear modulus ( $G_0$ ) and  $B$  was calculated using Equation 6.2, assuming a Poisson's ratio ( $\nu$ ) of 0.49 to model close-to-undrained behavior with zero volume change (Yan 1986). Bulk density of organic soil was considered as  $1100 \text{ kg/m}^3$  keeping in accord with those used in the modeling of PMT in section 6.3.2.



**Figure 7.12**  $s_u$  versus  $G_0/s_u$  plots based on test data from two test sites and  $s_u$ - $G_0/s_u$  combinations as soil input parameters for FLAC simulations of lateral pipe displacement.

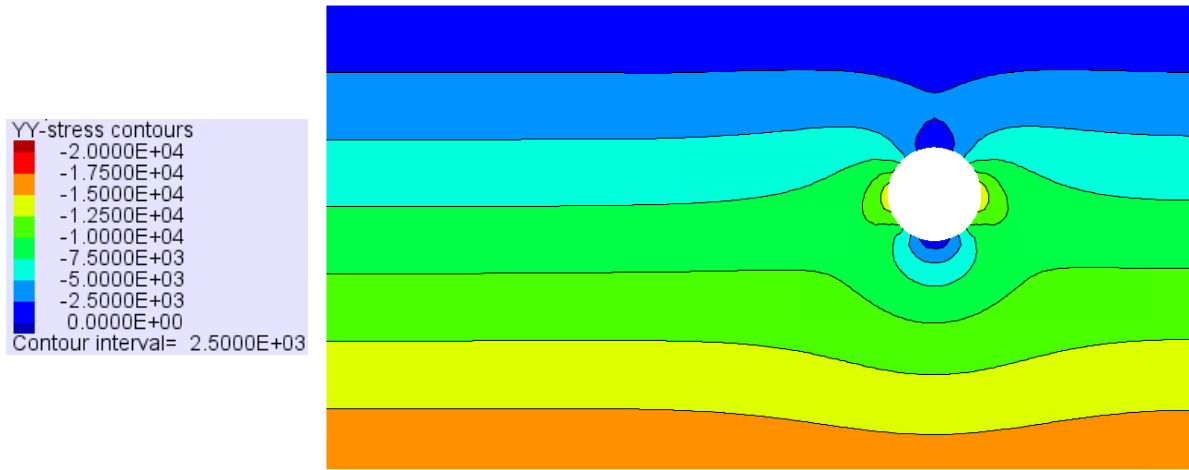
**Table 7.5 Soil strength and stiffness parameters used in FLAC 2D predictions of lateral soil restraint**

	Set A			Set B		
	Case 1	Case 2	Case 3	Case 1	Case 2	Case 3
$s_u$ (kPa)	25	25	25	40	40	40
$G_0/s_u$ Ratio	30	60	90	30	60	90
$G_0$ (MPa)	0.75	1.5	2.25	1.2	2.4	3.6
$G$ (MPa)	0.25	0.5	0.75	0.4	0.8	1.2
$B$ (MPa)	12.42	24.83	37.25	19.87	39.73	59.6

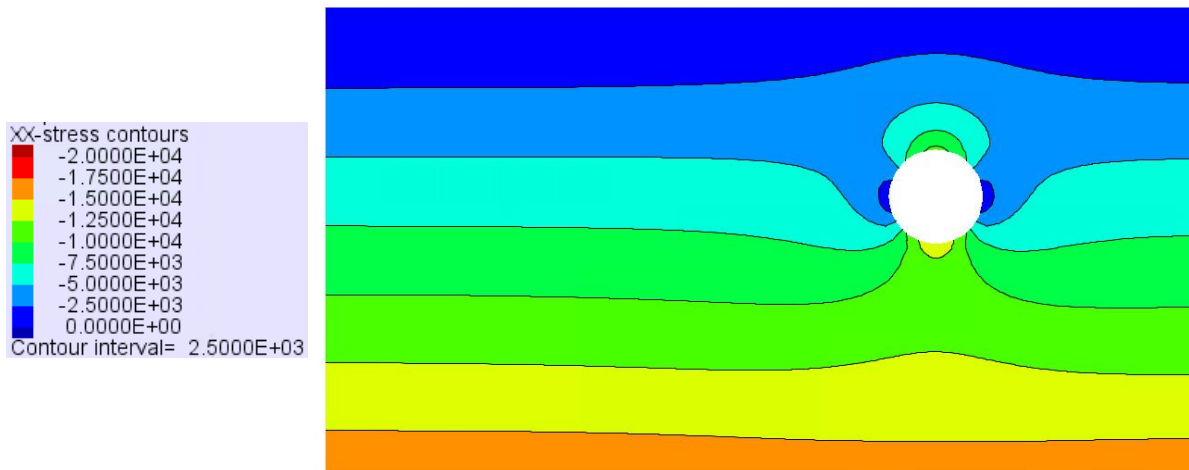
### **7.2.1.3 Modeling of soil-pipe interface and stress state prior to pipe displacement**

As discussed in Section 7.1.3, soil-pipe interface was modeled similar to the full-scale test models using structural beam elements representing the pipe and unglued interface elements following the same procedure to simulate lateral SPI.

As before, the steps of executing the model under gravity and displacing the pipe at a steady displacement rate of  $1 \times 10^{-8}$  per step was applied to simulate the horizontal displacement of pipe as elaborated in Section 7.1.4. the contours of computed horizontal and vertical stresses prior to pulling the pipe for model : 2\_D12\_LD\_MC; NPS 12 pipe and H/D ratio of 2 are shown in Figure 7.13. The twenty-four numerical predictions arising from the four mesh configurations and the six strength-stiffness combinations for organic soil in this manner were simulated and the outcomes are presented and discussed in the next section.



(a)



(b)

Figure 7.13 Total stress contours prior to pipe displacement; a) vertical and b) horizontal for NPS 12 pipe and H/D ratio of 2 (Model: 2\_D12\_LD\_MC).

## 7.2.2 Development of equivalent bi-linear soil springs from numerically computed p-y curves

The PRCI-based p-y curves are bi-linear, and this curve is essentially defined by knowing the break point ( $\Delta_p/D, P_u$ ) where  $P_u$  is the maximum lateral soil restraint on the pipe, and  $\Delta_p/D$  is the normalized pipe displacement at which  $P_u$  occurs (Note:  $\Delta_p$  is the pipe displacement at which  $P_u$  occurs and  $D$  is pipe diameter). To make a straightforward comparison between the PRCI-based and numerically and experimentally generated p-y curves, it was considered meaningful to have the latter p-y curves represented in a bi-linear fashion using the following steps and as schematically shown in Figure 7.14: Step-1) Identify the maximum lateral soil restraint ( $P_u$ ) from the numerically-generated curve (essentially by visual examination of the curve); Step-2) Find the point of intersection (identified as Point Q) between  $0.5P_u$  and the numerically-generated curve; and 3) Extend the straight line joining the origin (Point O) of the graph and Point Q until that intersects with the horizontal line drawn at  $P = P_u$  at Point R. In essence, the bi-linear representation of the numerically generated p-y curve would be depicted by the curve OQRZ - which allows ready comparison with those derived from PRCI guidelines.

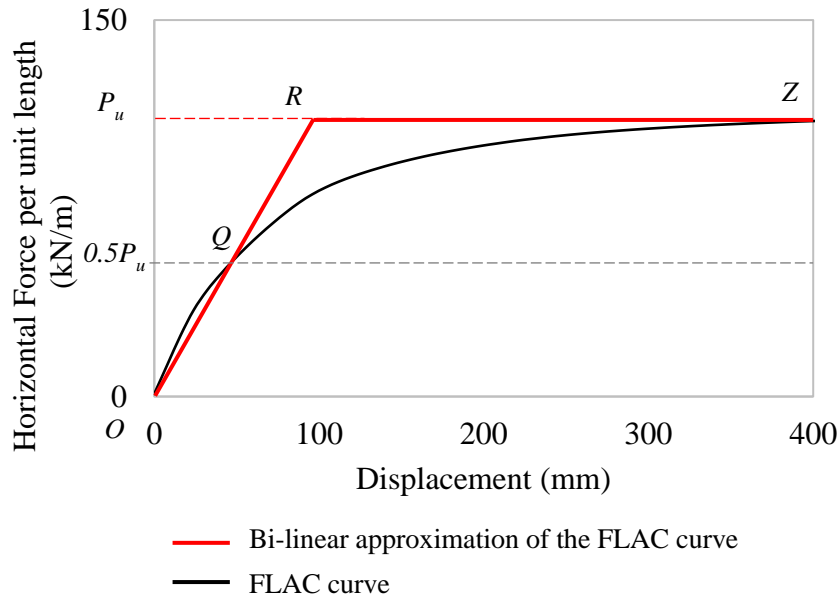


**Figure 7.14** Schematic showing steps required to obtain bi-linear approximation of lateral soil restraint versus pipe displacement curves from FLAC analyses (Example used herein for the Set A Case 1:  $s_u = 25$  kPa and  $G_0/s_u = 30$ ;  $H/D = 2$  and NPS36)

### 7.2.3 Numerical predictions of load-displacement behavior

A comparison between the horizontal p-y (soil spring) curves developed using the numerical predictions and PRCI guidelines (2009) are presented in Appendix D.1 (Figures D.1 through D.12). Further, the p-y curves generated based on the numerical models of the horizontal full-scale tests (a total of six cases since one case out of the total considered is a repeat test) were compared with the corresponding PRCI-based p-y curves for organic soils in Appendix D.2 (Figures D.13 through D.18). Following the same steps in Section 7.2.2 and Figure 7.14, numerically generated p-y curves were represented in a bi-linear form. The soil strength parameters ( $s_u$  values) identical to those used in the numerical model, presented in Table 7.2 and Table 7.5 were applied in the

equations to generate these curves. The counterpart bi-linear curves developed as per the procedures outlined in Section 7.2.2 are overlaid on the same figures, respectively. The peak soil restraint ( $P_u$ ) and the normalized pipe displacement at which  $P_u$  occurs ( $\Delta_p/D$ ) derived from PRCI guidelines and numerical simulations are summarized in Tables D.1 and D.2

Comparison between the curves shown in a given plot (Figures D.1 through D.18) indicate that the value of  $P_u$  from the bi-linear soil springs developed using PRCI guidelines are consistently higher than those respectively computed from the numerical simulations. These higher estimations of  $P_u$  from PRCI guidelines (2009) can be potentially attributed to the reason that the PRCI guidelines have been developed to address SPI in soft clayey soils as opposed to very soft and weak organic soils. With all the analysis data, the trendline between  $P_{u-num}$  versus  $P_{u-PRCI}$  in Figure 7.15, suggests a gradient of 0.77. This suggests that, if the PRCI guidelines (2009) assuming soft clayey soil conditions are used to obtain soils springs for organic soils, the PRCI-based  $P_u$  value should be modified with a reduction factor of 0.77 for the organic soils (as per Equation 7.4).

$$P_{u(Muskeg)} = 0.77P_{u(PRCI)} \quad 7.1$$

Further, it is of value to note that the peak soil restraint is dependent mainly on the  $s_u$  of the soil, irrespective of the  $G_0/s_u$  ratio which relates to the rigidity index of the organic soil. This observation is in line with the  $s_u$  based method given in PRCI (2009) guidelines to calculate horizontal soil restraint.

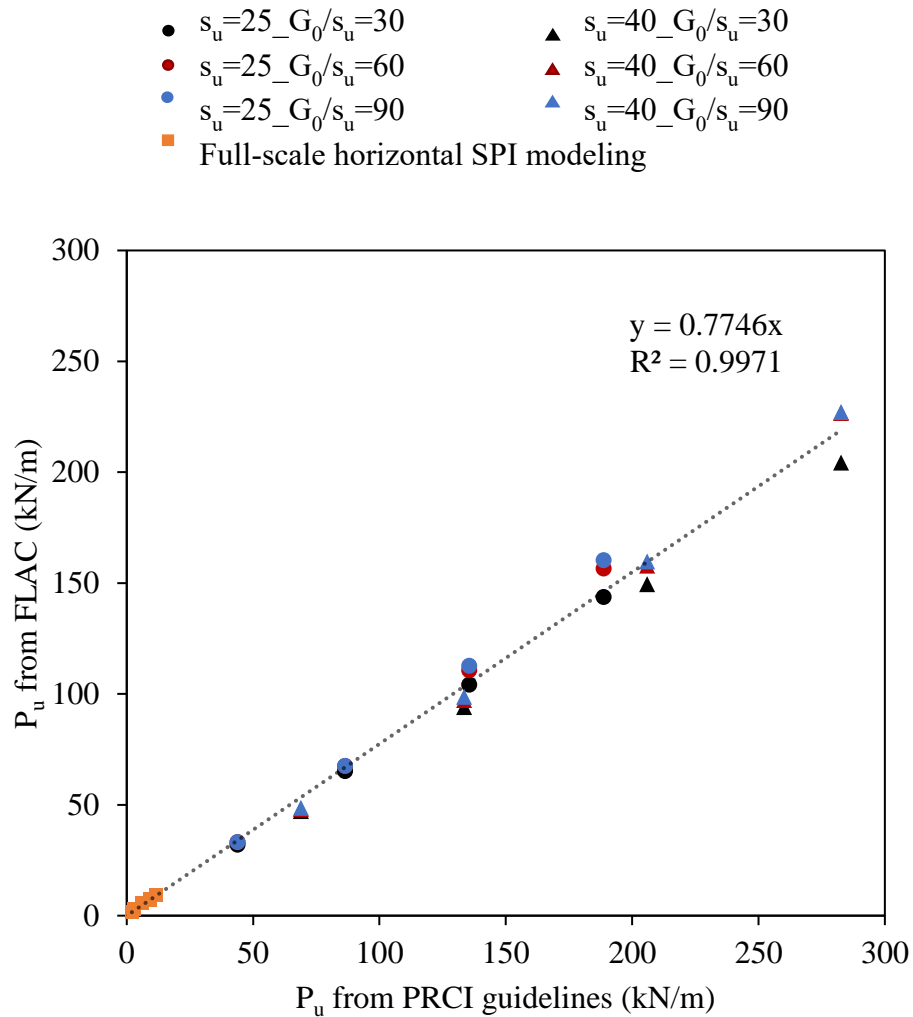


**Figure 7.15 Comparison between the peak soil restraint ( $P_u$ ) determined based on PRCI guidelines (2009) and numerical parametric analyses.**

Unlike for the value of  $P_u$ , no distinguishable relationship was identifiable between the  $\Delta_p$  values generated from numerical analysis and PRCI-based equations. PRCI (2009) guidelines specify a  $\Delta_p$  value ranging from 0.1D to 0.15D for pipes buried in soft clayey soils. The results from the

numerical analyses predict a  $\Delta_p$  value ranging from  $0.03D$  to  $0.15D$  which satisfies the upper bound given in the guidelines.

However, when  $\Delta_p/D$  from numerical analysis is plotted against the pipe diameter,  $D$ , as shown in Figure 7.16, it was noted that  $\Delta_p/D$  is well correlated with pipe diameter and stiffness/strength ratio of organic soil.  $\Delta_p/D$  decreases with  $D$  for a given organic soil stiffness/strength ratio and  $\Delta_p/D$  decreases as that ratio increases. Further, it shows that pipes buried in stiffer organic soil reach the peak soil restraint faster, which is in line with the material behavior. Therefore, it is of value to consider the effect of organic soil stiffness when determining  $\Delta_p/D$  rather than choosing an arbitrary value between  $0.1D - 0.15D$  as suggested in PRCI (2009). Additional analysis could be undertaken to study further to obtain more insight.

The above findings seem to provide a way to generate the bi-linear p-y curves for pipes buried in organic soils by modifying those specified by PRCI guidelines (2009) for soft clayey:

1. Modify the PRCI-based  $P_u$  by applying a reduction factor of 0.77 to obtain the  $P_u$  for organic soils; and
2. Determine  $\Delta_p/D$  using the curves given in Figure 7.16 based on the pipe diameter,  $D$ , and the stiffness/strength ratio for organic soils (use interpolation for other cases).

In general, accurate quantification of organic soil strength and stiffness properties is difficult due to the complex and varied nature of the soil. If the undrained shear strength ( $s_u$ ) is determined using field test methods such as ball penetration test, reasonable prediction of p-y curves for pipes buried in organic soil can be made using the available data on  $G_0/s_u$  ratio ranges.

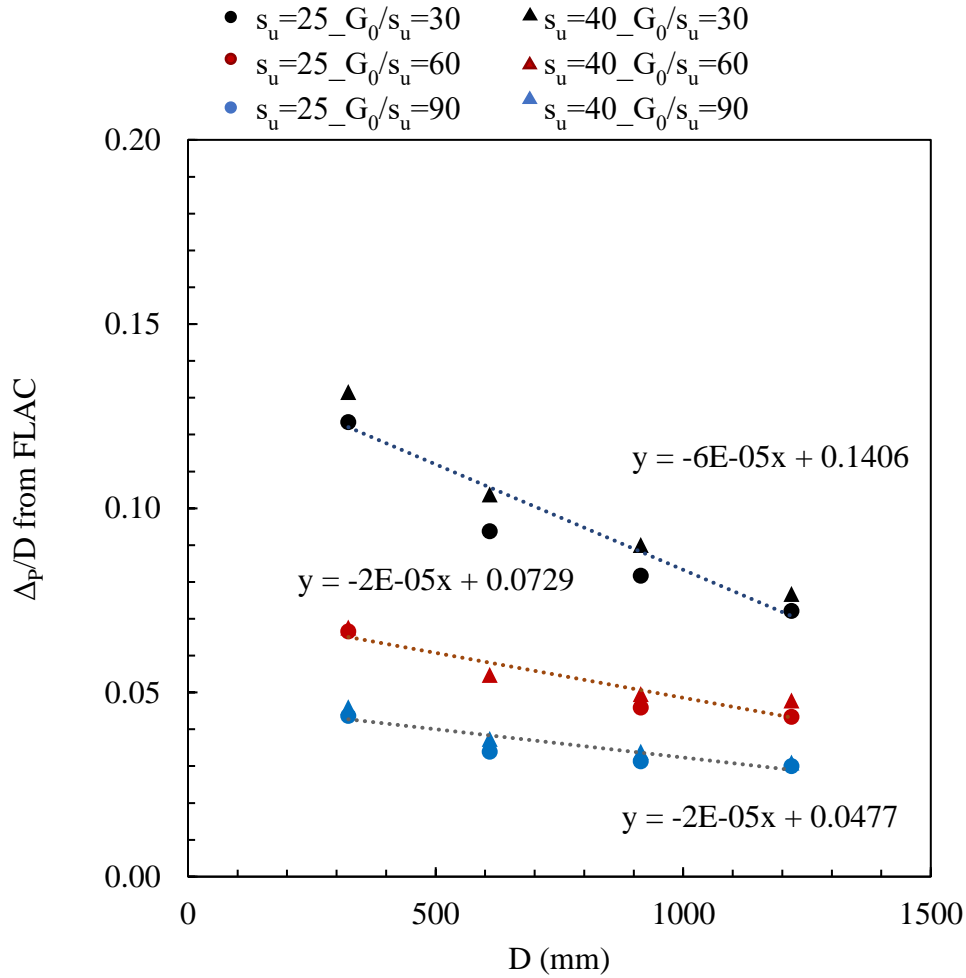


Figure 7.16 Graphical representation of correlations between  $\Delta_p/D$  and pipe diameter (D) from numerical analyses

### 7.3 Summary

Detailed numerical finite difference analyses were conducted to examine soil-pipe interaction (SPI) of pipelines buried in organic soils using Mohr-Coulomb constitutive model to represent the element-level behavior of the soil. First, a numerical model was established to simulate lateral SPI of pipes buried in organic soil using the data from physical full-scale testing (presented in Chapter

5) as a basis. Soil parameters for the numerical analysis were obtained from in-place penetration test data during pipe displacement testing. Horizontal soil restraint versus displacement curves (p-y curves or soil springs) were obtained for buried pipelines in organic soil and compared with the counterpart load-displacement behavior measured during full-scale tests. This allowed validation of a numerical model that meaningfully represent and capture the physical mechanisms manifested during physical testing.

Using the validated numerical framework, a series of pipeline configurations (pipeline depth, diameter) were simulated to obtain a comprehensive understanding of SPI. One of the key outcomes of this analysis is the soil restraint versus displacement response of pipelines subjected to relative lateral movements in organic soils. Comparison of families of curves derived from this work with those derived from current PRCI guidelines (2009) indicates that the PRCI guidelines provide soil springs with  $P_u$  values higher than those estimated from numerical simulations - i.e.,  $P_u$  from FLAC analyses  $\approx 0.77P_u$  from PRCI. In an overall context, the present work suggests that lateral soil restraints on pipes buried in organic soils can be approximated by modifying the approaches specified by PRCI guidelines (2009) for soft clayey soils.

## **Chapter 8: Summary, Conclusions and Recommendations**

### **8.1 Overview**

A large proportion of the northern Canadian lands is covered with soft and weak organic soils (muskeg), and significant lengths of the energy (oil and gas) transmission pipelines are located in these terrains. Relative ground movements occurring due to operational and environmental reasons have been recognized as a threat to the structural integrity and safety of buried oil and gas pipeline systems in these soils. The engineering design and/or assessment of pipelines against these demands essentially involves soil-pipe interaction (SPI) analysis, and this work is faced with many challenges due to the lack of current understanding of the mechanical behavior of organic soils as well as difficulties in characterizing highly variable soils along pipeline corridors. The relationships to express soil restraint development on buried pipelines subjected to relative ground movements (often called p-y curves or soil springs) are essential to undertake SPI analysis. Currently, there are no specific guidelines to obtain soil springs for buried pipelines in organic soils. Due to this absence, the current design provisions given in PRCI (2009) for pipelines in fine-grained mineral soils are often used by the engineering profession, with significant conservatism, for SPI analysis in organic soils.

While extensive research work has already been undertaken to study compressibility and strength of organic soils, the current fundamental understanding of the performance of buried pipelines in such soils when subjected to ground movements is very limited. In addition to performing laboratory element level testing to study the stress-strain response of organic soils, it is essential to conduct physical modeling experimentation to obtain insights on mechanisms and generate

critical data on soil restraint development to address this complex real life SPI problem; at present, based on the available published literature, there is no evidence of any systematic physical modeling and associated analysis undertaken on this topic.

With this background, a systematic study was launched at UBC to advance the understanding of the behavior of organic soils and the associated response of pipelines buried in such soils. The research program was supported by key pipeline industry partners (owner-operator firms) along with Collaborative Research and Development (CRD) funding from the Natural Sciences and Engineering Research Council of Canada. The present thesis forms a key part of the scope of work tasks undertaken with respect to this research program. In particular, the following specific tasks were performed: (i) characterization of organic soils to obtain engineering parameters for numerical SPI analysis, and development of material-specific empirical (or semi-empirical) correlations between strength and stiffness properties based on the field test data; (ii) developing two full-scale physical testing equipment to obtain high quality experimental data on axial and lateral loading SPI mechanisms in pipes buried in organic soil; (iii) selection of a suitable constitutive model to simulate the lateral soil-pipe interaction of pipes buried in organic soils; (iv) numerical analysis of lateral SPI and validation of the developed SPI model to justify its suitability for engineering evaluations using full-scale physical model testing results; (v) examining the suitability of the current PRCI (2009) guidelines to derive “soil springs” to represent the SPI in organic soils.

The following sections present and summarize the key findings and contributions arising from this research work and recommendations for future research.

## **8.2 Summary of the Key Findings and Contributions**

### **8.2.1 Characterization of organic soil using field and laboratory test program**

The main intent herein was to obtain soil shear strength and stiffness parameters for SPI analysis of pipelines subject to relative ground movements. Data derived from comprehensive geotechnical investigation programs [consisting of seismic cone penetration testing (SCPT), ball penetration testing (BPT), electronic vane shear testing (eVST), and pressuremeter testing (PMT) along with laboratory testing] conducted on soils from two test sites underlain by organic soils were examined to address the above intent.

The work was initiated with the understanding that an in situ geotechnical probe that would invoke macro-scale response in soft and weak organic soil deposits would be prudent - to obtain strength and deformation parameters to interpret the bulk mass deformations that get mobilized when ground movements occur relative to pipelines. It was found that BPT with a larger cross-sectional footprint (150 cm<sup>2</sup>) mobilizing a significant volume of the soil surrounding is effective as a probing tool for investigating organic soil along pipeline corridors – i.e., the larger cross-section of the BPT “filters” out the smaller-scale response (that otherwise would arise, for example, from cone penetration testing) and reflects a more average macro-scale response of the soil matrix. The results are in accord with observations by Boylan et al., (2011). Further, the undrained shear strength ( $s_u$ ) values interpreted from BPT using an  $N_{ball}$  factor of 11 (Weemees et al. 2006) were in good agreement with those from electronic vane shear testing (eVST). In an overall sense, the findings confirmed that the BPT testing would be one of the simple and effective tools to explore organic

soils along energy pipeline right-of-way corridors in northern parts of British Columbia and Alberta, Canada.

Preliminary correlations between  $s_u$  and initial shear modulus ( $G_0$ ) were developed based on  $G_0$  determined from site-specific seismic shear wave velocity testing data and  $s_u$  from BPT data. The resulting  $G_0/s_u$  ratios for the tested organic soil sites were found to range between 20 and 100, compared to the ratios in the order of 1000 and higher that typically exist with respect to fine-grained mineral soils; this was anticipated due to the soft nature of organic soil with low stiffness properties. Considering the in situ testing data from two sites, it was demonstrated that  $G_0/s_u$  ratios generated from site-specific correlations, combined with  $s_u$  values obtained from BPT testing, can be utilized to effectively represent the soil stress-strain behavior of organic soil in numerical modeling undertaken herein (as shown in Chapter 6 for validating a stress-strain relationship for representation of bulk behavior, followed by Chapter 7 where numerical analysis of horizontal soil-pipe interaction was undertaken).

### **8.2.2 Apparatus for lateral and axial SPI physical modeling**

Two new full-scale physical test chambers were built to study the levels of mobilization of soil restraint on buried pipes due to relative ground movements in axial and horizontal directions, respectively. Through this contribution to experimentation technology, the highly specialized equipment capabilities at the Advanced Soil-Pipe Interaction Research (ASPIRe™) facility at UBC were enhanced in a unique and complementary way for the testing of buried pipelines in organic soils.

These new soil chambers were able to overcome the challenges identified in handling and organic soil preparation for testing in a full-scale experimental setup due to its inherent soft and non-uniform nature, and the device dimensions were selected considering boundary effects during pipe displacement. The design analysis details and experience gained from the fabrication of the large soil test chamber that has a 2.4 m x 3.8 m footprint (Karimian 2006, Wijewickreme et al. 2017) were valuable in the design of these new devices.

The new test chambers were utilized towards conducting axial and lateral soil-pipe interaction controlled experiments. The data derived from the devices were used for validation of numerical approaches used to determine SPI analysis of pipes buried in organic soils (as per Chapters 4 and 5, and Sections 8.2.4 and 8.2.5 below).

#### Axial SPI Physical Modeling Apparatus

The axial SPI test apparatus of internal size 1.5 m x 0.8 m plan view and 0.75 m in height was capable of testing pipes of up to 160 mm in diameter. Pipe length in the order of 2.4 m can be axially loaded up to a maximum displacement of 0.5 m with a constant 1.2 m contact length with the soil in the chamber. The main feature of this test chamber is the mobile side walls (at the front and rear end of the chamber) that are free to move vertically; this allowed the embedded pipe to settle (without restraint) in harmony with the significant vertical movements that would occur due to the consolidation of the substantially compressible organic soil mass – the axial pullout testing would commence after consolidation is completed.

## Lateral SPI Physical Modeling Apparatus

A new test chamber was designed and built to investigate the lateral SPI. This test apparatus has a chamber of internal size 1 m x 2 m plan view and 1 m in height; the device is capable of testing pipes up to 220 mm (~8 inch) in diameter and approximately 1 m in length, with the ability to impart maximum horizontal displacement of up to 0.4 m. The size of the test chamber was selected allowing a practically viable box size that would allow preparing a weak compressible organic soil bed for testing. The side walls that were made using Plexiglass and PVC were used to minimize side friction during testing; the side walls of the test chamber were well braced against lateral movements using steel members, in essence, designed to serve as almost rigid boundaries with any lateral displacements due to the lateral soil pressures. This also included the development of a new AC motor-based loading mechanism and control system.

### **8.2.3 Selection of a Constitutive Model for Numerical Analysis**

Numerical analyses were performed to select a constitutive model to represent the mechanical behavior of organic soils. The results from several pre-bored pressuremeter tests (PMTs) conducted at two field geotechnical test sites served as controlled test boundary value cases for this numerical modeling.

By comparing the horizontal stress versus radial displacement response derived from field PMTs with those from numerical simulations, it was demonstrated that the use of isotropic Mohr-Coulomb formulation is justifiable and appropriate for representing the stress-strain behavior of organic soils of this study in a continuum-based numerical analysis. This assessment was

considered reasonable knowing that the use of sophisticated constitutive models would not be warranted due to the substantial spatial variability and non-homogeneity of the strength and stiffness properties of organic soils (which exist especially along long-distance pipeline alignments).

#### **8.2.4 Axial soil restraint on buried pipelines**

Full-scale axial pipe displacement test series conducted using a sand blasted steel pipe (NPS 4 pipe size) buried in organic soil provided opportunity to develop original experimental datasets on axial SPI in organic soil; in particular, the data enabled investigating the effect of overburden stress level on the axial soil-pipe interaction force development and generating experimental data to compare with those derived from pipeline design guideline recommendations. Load-displacement response comparisons between full-scale test results and PRCI (2009) guidelines revealed that the bi-linear soil springs developed using PRCI guidelines (for fine-grained soils) are consistently higher than those respectively achieved from laboratory full-scale tests. These higher estimations of peak axial soil restraint from PRCI guidelines (2009) can be attributed to the reason that these guidelines have been developed to address SPI in soft clayey soils as opposed to very soft and weak organic soils. It was found that, for the organic soils studied herein, the PRCI-based peak axial soil restraint ( $T_u$ ) assuming soft clayey soil conditions needs to be modified with a reduction factor of 0.67 to match with the  $T_u$  values obtained from experimental modeling undertaken in the present work – in turn, shedding valuable insights on the suitability of employing PRCI (2009) guidelines for generating axial soil springs for pipes buried in organic soils.

### 8.2.5 Lateral soil restraint on buried pipelines

Seven horizontal lateral pipe soil restraint tests were conducted on pipes buried in organic soil using NPS 6 and NPS 8 pipe specimens with two organic soil bed density conditions and different soil cover depths simulating a range of H/D ratios. According to the test-chamber-specific eVST probing results,  $s_u$  of the loose organic soil bed was interpreted around 1.5 – 2 kPa and the relatively denser organic soil bed had a shear strength of 9.8 kPa. For the pipe displacement tests that were performed without test-specific shear strength data, the  $s_u$  values of the organic soil was rationally inferred based on compaction approaches along with moisture content comparisons. Using these test-chamber-specific and inferred shear strength properties, the physically tested SPI system was modeled as a numerical boundary value problem.

When the soil springs (p-y curves) developed using the numerical simulations and the counterpart observations from the seven physical modeling tests were compared, the ultimate failure soil load ( $P_u$ ) values obtained from five physical modeling fell within 85-98% of the  $P_u$  predicted from the numerical models. The other two cases that involved relatively higher pipe depth conditions, the numerical modeling seemed to underpredict the  $P_u$ . Sensitivity analysis indicated that agreement between the  $P_u$  from numerical models and experiments could be achieved for these tests when  $s_u$  were changed within 20% from the originally used from test-chamber-specific  $s_u$  values.

The initial parts of the soil restraint versus pipe displacement curves between the physical modeling experiments and numerical modeling did not display good agreement; although the exact reason is not known, it appears possible that the potential non-uniformities in density and associated stiffness variability in test beds, particularly in the haunch area of the pipe, combined

with limitations in numerical modeling may have contributed to the differences in these observed deviations.

Overall, the total-stress based numerical model as developed above was able to capture the load mobilization manifested during physical modeling in a satisfactory manner and in turn, predict the peak lateral soil restraints ( $P_u$  values) well. It was judged that such a numerical model could provide a rational basis to numerically investigate and generate lateral soil restraint p-y curves for configurations involving different pipeline burial conditions and pipe diameters and to assess the suitability of using PRCI (2009) guidelines to generate soil springs for pipelines buried inorganic soils - which is one of the objectives of this thesis.

#### **8.2.5.1 Comparison of bi-linear lateral soil springs from numerical analysis versus PRCI guidelines**

Detailed numerical finite difference analyses were conducted to examine lateral SPI of pipelines buried in organic soils. In this regard, a systematic numerical parametric study was performed considering a series of pipeline configurations (pipeline depth, diameter) to obtain a comprehensive understanding of SPI.

The new research findings indicated that soil springs from PRCI guidelines (2009) assuming fine-grained soil conditions should be modified with a reduction factor of 0.77 to represent the lateral SPI in buried pipelines in organic soils studied herein. These higher estimations of  $P_u$  from PRCI guidelines (2009) can be attributed to the reason that the PRCI guidelines have been developed to address SPI in soft clayey soils as opposed to organic soils with very low stiffness and strength. Further, it is of value to note that the peak lateral soil restraint is dependent mainly on the  $s_u$  of the

soil, independent of the  $G_0/s_u$  ratio which represents the rigidity index of the organic soil. This observation, in principle, is in accord with the solely  $s_u$  based equation given in PRCI (2009) guidelines to calculate horizontal soil restraint.

Unlike for the value of  $P_u$ , no distinguishable relationship was identifiable between the  $\Delta_p$  values generated for lateral soil restraints from numerical analysis and PRCI-based equations. However,  $\Delta_p/D$  from numerical analysis is well correlated with pipe diameter and rigidity index of organic soil.  $\Delta_p/D$  decreases with  $D$  for a given rigidity index and  $\Delta_p/D$  decreases as it increases.

These findings provide an approach that will generate the bi-linear lateral loading p-y curves for pipes buried in organic soils by modifying those specified by PRCI guidelines (2009) for soft clayey soils; The approach consists of reducing the PRCI-based  $P_u$  by a factor of 0.77 to obtain the  $P_u$  for organic soils and determine  $\Delta_p/D$  based on the pipe diameter,  $D$ , and the rigidity index for organic soils.

In general, accurate quantification of organic soil strength and stiffness properties is difficult due to the complex and varied nature of the soil. If the undrained shear strength ( $s_u$ ) is determined using relatively simple in-situ test methods such as eVST or BPT, reasonable prediction of lateral restraint p-y curves applicable for pipes buried in organic soil in the field can be made using the available data on  $G_0/s_u$  ratio ranges.

#### **8.2.6 Recommended procedure of developing p-y curves based on the research findings**

Based on the research findings herein, a step-wise approach as given below can be considered for modifying the PRCI-based curves to develop p-y curves for SPI assessment of pipelines buried in organic soils.

- Conduct field tests, specifically full-flow ball penetrometer tests to capture the bulk behavior of soft and weak organic soil. The present research has indicated that utilizing such field test methods would serve as relatively straightforward and effective methods for investigating organic soils within energy pipeline right-of-way corridors, to obtain shear strength properties (i.e., undrained shear strength,  $s_u$ ).
- It would be important to conduct field sampling to obtain water content and organic content parameters to characterize the organic soils.
- Subsequently, utilize the obtained shear strength and stiffness parameters to establish p-y curves in accordance with the PRCI (2009) guidelines:

Axial soil restraint bi-linear curves for pipes buried in organic soils:

- Reduce the PRCI (2009) based peak axial soil restraint ( $T_u$ ) assuming soft clayey soil conditions with a reduction factor of 0.67.
- Assume axial displacement at  $T_u$  value ( $\Delta_t$ ) to be identical to those given by PRCI (2009) for soft clays.

Lateral soil restraint bi-linear curves for pipes buried in organic soils:

- Reduce the PRCI (2009) - based ultimate lateral load ( $P_u$ ) by applying a reduction factor of 0.77 to ascertain the  $P_u$  specifically for organic soils.
- Determine the relative displacement at  $P_u$  ( $\Delta_p/D$ ) based on the pipe diameter ( $D$ ) and the  $G_0/s_u$  ratio tailored for organic soils as per Figure 7.16 of this thesis. Note that this figure has been developed based on numerical analyses covering the pipe

diameter ranges from 324 mm (NPS 12) to 1219 mm (NPS 48) and assuming shear stiffness as a fraction of  $G_0$  – see Section 6.2.

- Special note:

Deviations/adjustments to the above approaches may be required when applying for organic soil sites in general. It is important to emphasize that the approaches have been based on systematic research performed largely considering geotechnical data from organic soil at two sites located along pipelines (in Alberta and British Columbia, Canada, respectively) along with parametric bounds for numerical analysis. In particular, the following are noted:

- water content of the soil varying from 300% to 650% and organic content ranging from 65% to 87%, respectively.
- $30 < G_0/s_u < 90$ ; and  $20 < s_u < 40$

### **8.3 Limitations and Errors Associated with the Present Study**

Similar to any experimental and numerical modeling research work, there were associated limitations and errors that needed to be considered during data interpretation and arriving at conclusions.

Some of the key errors and uncertainties associated with the full-scale physical testing of this study are judged to arise from; test chamber boundary effects, and uniformity of the tested organic soil beds (with respect to density, moisture content and fibrous matter found in the soil)

Test chamber boundary effects were minimized by selecting the size of the box to match the pipe sizes intended to test based on a numerical analysis. Numerical modeling of the horizontal SPI test chamber and a chamber with two times dimensions confirmed that the effect of the size and extent

of the box on the resultant load-displacement curves in lateral SPI analysis was minimal (presented in Appendix B). Sidewall friction was calculated based on interface friction properties measured based on direct shear tests and judged to have minimal effect. Further, the size of the pipes that can be tested using this test chamber was limited up to NPS 8 due to time, cost and personnel constraints as discussed in Chapter 4. Due to this the number of full-scale tests conducted within the scope of this study is limited, and further testing can be beneficial to improve the understanding.

As organic soil is inherently non uniform and highly spatially variable, different methods were used to minimize the nonuniformities arising due to presence of fibers during experimental work. Soil was mixed in large containers to achieve a relatively uniform mix before test soil bed preparations and same procedures were followed during all the tests (soil lift thicknesses, tamping counts). However, these non-uniformities in the organic soil needed to be taken into careful consideration when the resulting formulations are applied to SPI analysis.

Further, the behavior of organic soil in SPI is neither drained nor undrained in the field; it is a partially drained problem. As such, total stress analysis approach has limitations. At the same time, effective stress based approach need to capture the pore water pressure generation accurately, which is challenging.

The outcomes of physical modeling of SPI provided valuable input to capture the 2D SPI problem. However, the formulations arising from 2D analysis will always have limitations when applied to assess 3D SPI problems in real life. One such example is the occurrence of ground movements in oblique angles to the direction of pipe alignment during ground movements.

#### 8.4 Recommendations for Future Work

Based on the research tasks carried out during the present study, additional work on this topic can be undertaken to obtain a better understanding of SPI in organic soils and develop more refined guidelines and recommendations for design guidelines. Recommendations for future work can be listed as follows:

- Extend the investigation to sites underlain by organic soils with different organic contents, water contents and/or origin and to widen the database on strength and stiffness parameters and in turn, assess and validate current findings. Use of ball penetrometer at these sites to obtain strength parameters would further demonstrate the applicability of this technique for characterizing organic soils along pipeline corridors.
- Further investigation to explore the feasibility of obtaining shear wave velocity measurements through the use of the same ball penetrometer that is employed to obtain shear strength parameters (instead of conducting separate seismic cone penetrometer testing).
- Additional full- scale axial pullout tests to obtain data with tests on different pipe diameters, overburden ratio and backfill density levels, and in place penetrations tests to characterize the shear strength properties of the organic soil. This additional data expand the current dataset to validate a numerical model to study the axial SPI of pipes buried in organic soil.
- Additional full-scale horizontal pipe displacement tests using larger pipe diameters and higher backfill density conditions will expand the database providing extra support to

increase the current understanding and it will give additional insight in improving the numerical analysis.

- As the full-scale tests in the laboratory setup are performed in a controlled environment, it will be of great relevance to perform the pipe displacement tests in a field set up. This will allow testing of larger pipes with lesser effort of preparing the organic soil bed and generate load-displacement responses that are close to reality as it preserves the non-uniform nature of the organic soil during testing. In situ penetration tests can be performed to characterize the shear strength of the tested organic soil as well.

## **Bibliography**

- ALA. 2001. Guidelines for the design of buried steel pipe.
- Amarasinghe, R.S. 2019. Shear strength of soil-pipeline interfaces under low confining stresses and large displacements. University of British Columbia.
- Anderson, C., Wijewickreme, D., Ventura, C., and Mitchell, A. 2005. Full-scale laboratory testing of soil-pipe interaction in branched polyethylene pipelines. *Experimental Techniques*, **29**(2): 33–37. doi:10.1111/j.1747-1567.2005.tb00211.x.
- API. 2011. Recommended Practice for Geotechnical Foundation Design Consideration. Recommended Practice for Geotechnical Foundation Design Consideration,.
- ASCE. 1984. Guidelines for the seismic design of oil and gas pipeline systems. New York.
- ASTM. 2000. Standard Test Method for Laboratory Miniature Vane Shear Test for Saturated Fine-Grained Clayey Soil (D4648/D4648M – 16). ASTM International,.
- ASTM D3080/D3080M. 2011. ASTM D3080/D3080M – 11 Direct Shear Test of Soils Under Consolidated Drained. ASTM International,.
- ASTM D4719 – 07. 2007. Standard Test Methods for Prebored Pressuremeter Testing in Soils. American Society for Testing and Materials, **i**: 1–10. doi:10.1520/D4719-07.2.
- Audibert, J.M.E., and Nyman, K.J. 1977a. Soil restraint against horizontal motion of pipes. *ASCE J Geotech Eng Div*, **103**(10): 1119–1142. doi:10.1061/ajgeb6.0000500.
- Audibert, J.M.E., and Nyman, K.J. 1977b. Soil Restraint Against Horizontal Motion of Pipes.

- Journal of the Geotechnical Engineering Division, **103**(10): 1119–1142. International Center for Numerical Methods in Engineering (CIMNE), Barcelona, Spain, Barcelona, Spain. doi:10.1061/AJGEB6.0000500.
- Baguelin, F., Jézéquel, J.F., and Shields, D.H. 1978. The Pressuremeter and Foundation Engineering. *In* First Edit. Transtech Publications, Clausthal, Germany.
- Bedair, O. 2013. Engineering challenges in the design of alberta’s oil sands projects. *Practice Periodical on Structural Design and Construction*, **18**(4): 247–260. doi:10.1061/(ASCE)SC.1943-5576.0000163.
- Benoît, J., and Howie, J.A. 2014. A View of Pressuremeter Testing in North America. *SOILS and ROCKS*, **37**(3): 211–231.
- Bjerrum, L., and Landva, A. 1966. Direct Simple-Shear Tests on a Norwegian Quick Clay. *Géotechnique*, **16**(1): 1–20. doi:10.1680/geot.1966.16.1.1.
- Blakeman, W. 1974. Geotechnical considerations with respect to the muskeg portions of a proposed iron ore slurry pipeline route. Montrea.
- Bouafia, A. 2007. Single piles under horizontal loads in sand: determination of P–Y curves from the prebored pressuremeter test. *Geotechnical and Geological Engineering*, **25**(3): 283–301. doi:10.1007/s10706-006-9110-7.
- Boylan, N., and Long, M. 2006. Characterisation of peat using full flow penetrometers. *In* Proceedings of the 4th International Conference on Soft Soil Engineering - Soft Soil Engineering. pp. 403–414.

- Boylan, N., and Long, M. 2009. Development of a direct simple shear apparatus for peat soils. *Geotechnical Testing Journal*, **32**(2): 126–138. doi:10.1520/GTJ101703.
- Boylan, N., and Long, M. 2014a. Evaluation of peat strength for stability assessments. *Proceedings of the Institution of Civil Engineers - Geotechnical Engineering*, **167**(5): 421–430. doi:10.1680/geng.12.00043.
- Boylan, N., and Long, M. 2014b. Evaluation of peat strength for stability assessments. *Proceedings of the Institution of Civil Engineers - Geotechnical Engineering*, **167**(5): 421–430. doi:10.1680/geng.12.00043.
- Boylan, N., Long, M., and Mathijssen, F.A.J.M. 2011. In situ strength characterisation of peat and organic soil using full-flow penetrometers. *Canadian Geotechnical Journal*, **48**(7): 1085–1099. doi:10.1139/t11-023.
- Bridgwater, J. 1980. On the width of failure zones. *Geotechnique*, **30**(4). doi:10.1680/geot.1980.30.4.533.
- Burland, J.B. 1973. Shaft friction of piles in clay—a simple fundamental approach. *Ground Engineering*, **6–3**(September): 30–42.
- Byrne, P.M., Cheung, H., and Yan, L. 1987. Soil parameters for deformation analysis of sand masses. *Canadian Geotechnical Journal*, **24**(3): 366–376. doi:10.1139/t87-047.
- Campanella, R.G., Howie, J.A., Hers, I., Sully, J.P., and Robertson, P.K. 1990. Evaluation of cone pressuremeter tests in soft cohesive soils. *Pressuremeters*,. doi:10.1016/0148-9062(91)92994-a.

- Cappelletto, A., Tagliaferri, R., Giurlani, G., Andrei, G., Furlani, G., and Scarpelli, G. 1998. Field Full Scale Tests on Longitudinal Pipeline-Soil Interaction. *In* In Proceedings of the International Pipeline Conference. American Society of Mechanical Engineers. pp. 771–778.
- Cathie, D.N., Jaek, C., Ballard, J.C., and Wintgens, J.F. 2005. Pipeline geotechnics – state-of-the-art. *In* *Frontiers in Offshore Geotechnics*. Taylor & Francis. pp. 95–114.
- Chatterjee, S., White, D.J., and Rando, M.F. 2012. Numerical simulations of pipe–soil interaction during large lateral movements on clay. *Géotechnique*, **62**(8): 693–705. doi:10.1680/geot.10.P.107.
- Chen, R.P., Zhu, B., and Ni, W.J. 2016. Uplift tests on full-scale pipe segment in lumpy soft clay backfill. *Canadian Geotechnical Journal*, **53**(4): 578–588. doi:10.1139/cgj-2015-0084.
- ConeTec. 2017. Site investigation report: Muskeg pipeline interaction research project - CRD CRDPJ 500977 - prepared at the request of D. Wijewickreme research group, UBC. ConeTec Investigations Ltd. Richmond, BC.
- CSA. 2019. Oil and Gas Pipeline System - CSA Standard Z662:19.
- D2573, A. 2015. Standard Test Method for Field Vane Shear Test in Saturated Fine-Grained Soils. American Society of Testings and Methods, **i**.
- Daiyan, N., Kenny, S., Phillips, R., and Popescu, R. 2011. Investigating pipeline-soil interaction under axial-lateral relative movements in sand. *Canadian Geotechnical Journal*, **48**(11): 1683–1695. doi:10.1139/t11-061.

- Das, B.M., and Seeley, G.R. 1975. Load-Displacement Relationship for Vertical Anchor Plates. *Journal of the Geotechnical Engineering Division*, **101**(7): 711–715. doi:10.1061/ajgeb6.0000180.
- Dhowian, A., and Edil, T. 1980. Consolidation Behavior of Peats. *Geotechnical Testing Journal*, **3**(3): 105. doi:10.1520/GTJ10881J.
- Dilrukshi, S., and Wijewickreme, D. 2020. Study of Trench Backfill Particle Size Effects on Lateral Soil Restraints on Buried Pipelines Using Discrete Element Modeling. *Journal of Pipeline Systems Engineering and Practice*, **11**(1): 1–14. doi:10.1061/(ASCE)PS.1949-1204.0000423.
- Dyson, G.J., and Randolph, M.F. 2001. Monotonic Lateral Loading of Piles in Calcareous Sand. *Journal of Geotechnical and Geoenvironmental Engineering*, **127**(4). doi:10.1061/(asce)1090-0241(2001)127:4(346).
- Elmouchi, A. 2021. Geotechnical Characterization and Stabilization of Muskeg Soils Using the Microbially Induced Calcite Precipitation Technique (MICP). The University of British Columbia (Okanagan).
- Elmouchi, A., Siddiqua, S., Wijewickreme, D., and Polinder, H. 2021. A Review to Develop new Correlations for Geotechnical Properties of Organic Soils.
- Farid, M., Salah, N.M., and Cosentino, P.J. 2013. Pencil Pressuremeter Testing to Determining P-Y Curves for Laterally Loaded Deep Foundations. *Procedia Engineering*, **54**: 491–504. Elsevier Ltd. doi:10.1016/j.proeng.2013.03.045.

- Gibson, R.E., and Anderson W. F. 1961. In-situ measurement of soil properties with the pressuremeter. *Civil Engineering and Public Works review*, **56**(568): 615–618.
- Griffiths, D. V., and Lane, P.A. 1990. Finite element analysis of the shear vane test. *Computers and Structures*, **37**(6). doi:10.1016/0045-7949(90)90022-T.
- Guo, P.J., and Stolle, D.F.E. 2005. Lateral Pipe–Soil Interaction in Sand with Reference to Scale Effect. *Journal of Geotechnical and Geoenvironmental Engineering*, **131**(3): 338–349. doi:10.1061/(ASCE)1090-0241(2005)131:3(338).
- Haan, E.J.D., and Grognet, M. 2014. A large direct simple shear device for the testing of peat at low stresses. *Proceedings of the Institution of Civil Engineers: Structures and Buildings*, **4**: 283–288. doi:10.1680/geolett.14.00033.
- Hallam, M.G. 1978. Dynamics of marine structures. *In* 2nd Editio. CIRIA Underwater Engineering Group.
- Hansen, J.B. 1961. The Ultimate design of piles against transversal loads. *Geoteknisk Institut (Danish Geotechnical Institute)*, (12): 16.
- Hayashi, H., and Nishimoto, S. 2015. Shear modulus at small strain of normally consolidated peat. *In* 15th Asian Regional Conference on Soil Mechanics and Geotechnical Engineering, ARC 2015: New Innovations and Sustainability. pp. 576–580.
- Hebib, S. 2001. Experimental investigation on the stabilisation of Irish peat. University of Dublin, Trinity College, Dublin, Ireland.

- Hebib, S., and Farrell, E.R. 2000. Laboratory Determination of Deformation and Stiffness Parameters of Stabilized Peat. *In* Soft Ground Technology. American Society of Civil Engineers, Reston, VA. pp. 182–193.
- Hendry, M.T. 2011. The geomechanical behaviour of peat foundations below rail-track structures. University of Saskatchewan, Saskatoon, Canada.
- Hobbs, N.B. 1986. Mire morphology and the properties and behaviour of some British and foreign peats. *Quarterly Journal of Engineering Geology and Hydrogeology*, **19**(1): 7–80. doi:10.1144/GSL.QJEG.1986.019.01.02.
- Houlsby, G.T., and Withers, N.J. 1988. Analysis of the cone pressuremeter test in clay. *Géotechnique*, **38**(4): 575–587. doi:10.1680/geot.1988.38.4.575.
- Hsu, T.-W. 1993. Rate Effect on Lateral Soil Restraint of Pipelines. *Soils and Foundations*, **33**(4): 159–169. doi:10.3208/sandf1972.33.4\_159.
- Hsu, T.-W., Chen, Y.-J., and Hung, W.-C. 2006. Soil Restraint to Oblique Movement of Buried Pipes in Dense Sand. *Journal of Transportation Engineering*, **132**(2): 175–181. doi:10.1061/(ASCE)0733-947X(2006)132:2(175).
- Hughes, J.M.O., and Robertson, P.K. 1985. Full-displacement pressuremeter testing in sand. *Canadian Geotechnical Journal*, **22**(3): 298–307. doi:10.1139/t85-043.
- Hughes, J.M.O., Wroth, C.P., and Windle, D. 1977. Pressuremeter tests in sands. *Géotechnique*, **27**(4): 455–477. doi:10.1680/geot.1977.27.4.455.

- Karimian, H., Wijewickreme, D., and Honegger, D. 2006a. Full-Scale Laboratory Testing to Assess Methods for Reduction of Soil Loads on Buried Pipes Subject to Transverse Ground Movement. *In International Pipeline Conference*. ASMEDC, Calgary, Alberta, Canada. pp. 91–99.
- Karimian, H., Wijewickreme, D., and Honegger, D. 2006b. Buried Pipelines Subjected to Transverse Ground Movement: Comparison Between Full-Scale Testing and Numerical Modeling. *In International Conference on Offshore Mechanics and Arctic Engineering - OMAE*. ASME. pp. 73–79.
- Karimian, S.A. 2006. Response of Buried Steel Pipelines Subjected to Longitudinal and Transverse ground movement. University of British Columbia.
- Katebi, M., Wijewickreme, D., Maghoul, P., and Roy, K. 2021. Lateral force–displacement response of buried pipes in slopes. *Géotechnique*, **1**(c): 1–13. doi:10.1680/jgeot.21.00057.
- Kishida, T., Boulanger, R.W., Wehling, T.M., and Driller, M.W. 2006. Variation of small strain stiffness for peat and organic soil. *In 8th US National Conference on Earthquake Engineering*. San Fransisco, California, USA. p. 1057.
- Landva, A., and La Rochelle, P. 1983. Compressibility and Shear Characteristics of Radforth Peats. *In Testing of Peats and Organic Soils, ASTM STP 820*. ASTM International, 100 Barr Harbor Drive, PO Box C700, West Conshohocken, PA 19428-2959. pp. 157–191.
- Landva, A.O. 1980. Vane testing in peat. *Canadian Geotechnical Journal*, **17**(1): 1–19. doi:10.1139/t80-001.

- Lea, N.D., and Brawner, C.O. 1963. Highway design and construction over peat deposits in lower British Columbia. *In Highway Research Record*.
- Liu, B. 2019. Personal communications (industry based experience provided during the present research work).
- Liu, J., Wijewickreme, D., Liu, B., and Weemees, I. 2018. Characterization of muskeg soils for soil-pipe interaction analysis – Some preliminary findings. *In 71st Canadian Geotechnical Conference, Edmonton, Alberta*. p. 7.
- Long, M. 2005. Characterisation and constitutive modelling of peat with reference to landslides. *Studia Geotechnica et Mechanica*, **27**(3–4): 67–90.
- Long, M., Boylan, N., Powell, J., O’Connor, S., and Donohue, S. 2010. Characterisation of the soils beneath the flood banks along the River Thames estuary. *In 4th International Workshop – Soil Parameters from In Situ Tests*. Poznań, Poland. pp. 395–411.
- Long, M., and Gudjonsson, G.T. 2004. T-bar testing in Irish soils. *In 2nd International Conference on Geotechnical and Geophysical Site Characterization – ISC’2*. Edited by the N. A.V. da Fonseca and P.W. Mayne. Millpress, Rotterdam. Porto, Portugal. pp. 719–726.
- Lunne, T., Robertson, P., and Powell, J. 1997. Cone Penetration Testing in Geotechnical Practice., 1997. Blackie Academic and Professional, ..,.
- MacFarlane, I.C. 1969. Engineering characteristics of peat. *In Muskeg Engineering Handbook*. University of Toronto Press, Canada. pp. 78–126.

- Marshall, R.C., and Ruban, T.F. 1983a. Geotechnical aspects of pipeline construction in Alberta. Canadian Geotechnical Journal, **20**(1): 1–10. doi:10.1139/t83-001.
- Marshall, R.G., and Ruban, T.F. 1983b. Geotechnical Aspects of Pipeline Construction in Alberta. Canadian geotechnical journal, **20**: 1–10.
- Merifield, R.S., Sloan, S.W., and Yu, H.S. 2001. Stability of plate anchors in undrained clay. Géotechnique, **51**(2): 141–153. doi:10.1680/geot.51.2.141.40290.
- Mesri, G., and Ajlouni, M. 2007. Engineering Properties of Fibrous Peats. Journal of Geotechnical and Geoenvironmental Engineering, **133**(7): 850–866. doi:10.1061/(ASCE)1090-0241(2007)133:7(850).
- Mitigating Losses from Land Subsidence in the United States. 1991. *In* Mitigating Losses from Land Subsidence in the United States.
- Monroy-Concha, M. 2013. Soil restraints on steel buried pipelines crossing active seismic faults. University of British Columbia.
- Neely, W.J., Stuart, J.G., and Graham, J. 1973. FAILURE LOADS OF VERTICAL ANCHOR PLATES IN SAND. ASCE J Soil Mech Found Div, **99**(SM9): 669–685. doi:10.1061/jsfeaq.0001925.
- Negusse, D., Wijewickreme, W.K.D., and Vaid, Y.P. 1989. Geomembrane interface friction. Canadian Geotechnical Journal, **26**(1): 165–169. doi:10.1139/t89-018.
- O’Kelly, B.C. 2017. Measurement, interpretation and recommended use of laboratory strength

- properties of fibrous peat. *Geotechnical Research*, **4**(3): 136–171.  
doi:10.1680/jgere.17.00006.
- O’Kelly, B.C., and Zhang, L. 2013. Consolidated-Drained Triaxial Compression Testing of Peat. *Geotechnical Testing Journal*, **36**(3): 20120053. doi:10.1520/GTJ20120053.
- O’Rourke, T.D., Druschel, S.J., and Netravali, A.N. 1990. Shear strength characteristics of sand-polymer interfaces. *Journal of Geotechnical Engineering*, **116**(3): 451–469.  
doi:10.1061/(ASCE)0733-9410(1990)116:3(451).
- Oliveira, J.R.M.S., Almeida, M.S.S., Almeida, M.C.F., and Borges, R.G. 2010. Physical Modeling of Lateral Clay-Pipe Interaction. *Journal of Geotechnical and Geoenvironmental Engineering*, **136**(7): 950–956. doi:10.1061/(asce)gt.1943-5606.0000311.
- Oswell, J.M. 2002. Geotechnical aspects of northern pipeline design and construction. *Proceedings of the International Pipeline Conference, IPC, A*: 555–562. doi:10.1115/IPC2002-27327.
- Oung, O., Van der Vegt, J.W.G., and Tiggeleman, L. 2004. Adapted T-bar penetrometer versus CPT to determine undrained shear strengths of Dutch soft soils. *Proc. 2nd Int. Conf. on Geotechnical and Geophysical Site Characterisation*,.
- Ovesen, N.K. 1964. Anchor slabs, calculation method and model tests. *Bulletin 16*. Kongens Lyngby, Denmark: The Danish Geotechnical Institute,.
- Palmer, A.C. 1972. Undrained plane-strain expansion of a cylindrical cavity in clay: a simple interpretation of the pressuremeter test. *Géotechnique*, **22**(3): 451–457.

- Paulin, M.J., Phillips, R., Clark, J.I., Trigg, A., and Konuk, I. 1998. A full-scale investigation into pipeline/soil interaction. *In International Pipeline Conference - ASME*. pp. 779–787.
- Popescu, R., Phillips, R., Konuk, I., Guo, P., and Nobahar, A. 2002. Pipe-soil interaction: large scale tests and numerical modelling. *Physical Modelling in Geotechnics*,: 917–922. doi:10.1201/9780203743362-166.
- Powell, J., and Quaterman, R. 1988. The interpretation of CPT in clays with particular reference to rate effects. *In Penetration Testing, ISOPT-1; Proc. int. symp. Orlando*. pp. 903–910.
- PRCI 2009. . Guidelines for constructing natural gas and liquid hydrocarbon pipelines through areas prone to landslide and subsidence hazards. *In Design, Materials, and Construction Committee of Pipeline Research Council International, Inc.*
- Radforth, N.W. 1969. Muskeg as an engineering problem. *In Muskeg Engineering Handbook. Edited by I.C. MacFarlane. University of Toronto Press, Toronto*. pp. 3–30.
- Randolph, M., and Gourvenec, S. 2011. Offshore geotechnical Engineering. *In 1st editio. CRC Press*.
- Robertson, P.K., Campanella, R.G., Gillespie, D., and Greig, J. 1986. Use of piezometer cone data. pp. 1263–1280.
- Robertson, P.K., Hughes, J.M.O., Campanella, R.G., and Sy, A. 1984. Design of laterally loaded displacement piles using a driven pressuremeter. *In ASTM Special Technical Publication*.
- Robertson, R., and Curle, R. 1995. Screw anchors economically control pipeline buoyancy in

- muskeg. *Oil & Gas Journal*, **93**(17): 49–54.
- Roscoe, K.H. 1970. The influence of strains in soil mechanics. *Geotechnique*, **20**(2). doi:10.1680/geot.1970.20.2.129.
- Rowe, R.K., and Davis, E.H. 1983. Discussion: The behaviour of anchor plates in sand. *Géotechnique*, **33**(1): 73–74. doi:10.1680/geot.1983.33.1.73.
- Roy, K., Hawlader, B., Kenny, S., and Moore, I. 2016. Finite element modeling of lateral pipeline-soil interactions in dense sand. *Canadian Geotechnical Journal*, **53**(3): 490–504. doi:10.1139/cgj-2015-0171.
- Scarpelli, G., and Wood, D.M. 1982. Experimental observations of shear band patterns in direct shear tests. *Deformation and failure of granular materials. IUTAM symposium, Delft, 1982.*
- Silver, M., and Seed, H. 1971. Deformation Characteristics of Sands under Cyclic Loading. *Journal of the Soil Mechanics and Foundations Division*, **97**(8): 1081–1098. American Society of Civil Engineers. doi:10.1061/JSFEAQ.0001648.
- Tali, R.G. 1983. Analytical modeling of the performance of muskeg deposits under loading. McGill University, Montreal, Quebec.
- Thomas, L.N., and Henderson, J. 2004. An Integrated Approach to Pipeline Buoyancy Control and Implementation. *In 2004 International Pipeline Conference, Volumes 1, 2, and 3. ASME*DC. pp. 2369–2378.
- Trafford, A., and Long, M. 2020. Relationship between Shear-Wave Velocity and Undrained

- Shear Strength of Peat. *Journal of Geotechnical and Geoenvironmental Engineering*, **146**(7): 1–10. doi:10.1061/(ASCE)GT.1943-5606.0002298.
- Trautmann, C.H. 1983. Behaviour of pipe in dry sand under lateral and uplift loading. Cornell University, Ithaca, NY, USA.
- Trautmann, C.H., and O'Rourke, T.D. 1985. Lateral Force-Displacement Response of Buried Pipe. *Journal of Geotechnical Engineering*, **111**(9): 1077–1092. doi:10.1061/(ASCE)0733-9410(1985)111:9(1077).
- Viergever, M.A. 1985. Cone penetration with enlarged tip in cohesive soils. Proc. 11th international conference on soil mechanics and foundation engineering, San Francisco, August 1985. Vol. 2, (Balkema),.
- Wang, J., and Yang, Z. 2016. Axial friction response of full-scale pipes in soft clays. *Applied Ocean Research*, **59**. doi:10.1016/j.apor.2016.05.010.
- Weemees, I., Howie, J., Woeller, D., Sharp, J., Cargill, E., and Greig, J. 2006. Improved Techniques for the in-Situ Determination of Undrained Shear Strength in Soft Clays. *In* 59th Canadian Geotechnical Conference. Vancouver, B.C., Canada. pp. 89–95.
- Wehling, T.M., Boulanger, R.W., Arulnathan, R., Harder, L.F., and Driller, M.W. 2003. Nonlinear Dynamic Properties of a Fibrous Organic Soil. *Journal of Geotechnical and Geoenvironmental Engineering*, **129**(10): 929–939. doi:10.1061/(ASCE)1090-0241(2003)129:10(929).
- White, D., Bruton, D.A.S., Bolton, M., Hill, A.J., Ballard, J.-C., and Langford, T. 2011.

SAFEBUCK JIP - Observations of Axial Pipe-soil Interaction from Testing on Soft Natural Clays. doi:10.4043/21249-ms.

Wijewickreme, D. 2019. Personal communications (industry based experience provided during the present research work).

Wijewickreme, D., Karimian, H., and Honegger, D. 2009. Response of buried steel pipelines subjected to relative axial soil movement. *Canadian Geotechnical Journal*, **46**(7): 735–752. doi:10.1139/T09-019.

Wijewickreme, D., Monroy, M., Honegger, D.G., and Nyman, D.J. 2017. Soil restraints on buried pipelines subjected to reverse-fault displacement. *Canadian Geotechnical Journal*, **54**(10): 1472–1481. doi:10.1139/cgj-2016-0564.

Yamaguchi, H., Ohira, Y., Kogure, K., and Mori, S. 1985. Undrained Shear Characteristics of Normally Consolidated Peat Under Triaxial Compression and Extension Conditions. *Soils and Foundations*, **25**(3): 1–18. doi:10.3208/sandf1972.25.3\_1.

Yan, L. 1986. Numerical studies of some aspects with pressuremeter tests and laterally loaded piles. University of British Columbia.

Yang, H. 2013. A Systematic Limit-State Design Approach for Finite Element Analysis of Buried Oil Transporting Pipeline. *Journal of Water Resources Planning and Management*, **136**(5): 1–10.

Yimsiri, S., Soga, K., Yoshizaki, K., Dasari, G.R., and O'Rourke, T.D. 2004. Lateral and Upward Soil-Pipeline Interactions in Sand for Deep Embedment Conditions. *Journal of Geotechnical*

and Geoenvironmental Engineering, **130**(8): 830–842. doi:10.1061/(ASCE)1090-0241(2004)130:8(830).

## **Appendices**

### **Appendix A Field and Laboratory Test Results**

This section presents the field and laboratory test results plots and test results summaries from seismic cone penetration, ball penetration, electronic vane shear, pressuremeter, direct simple shear and direct shear tests.

## A.1 Seismic Cone Penetration Test Results

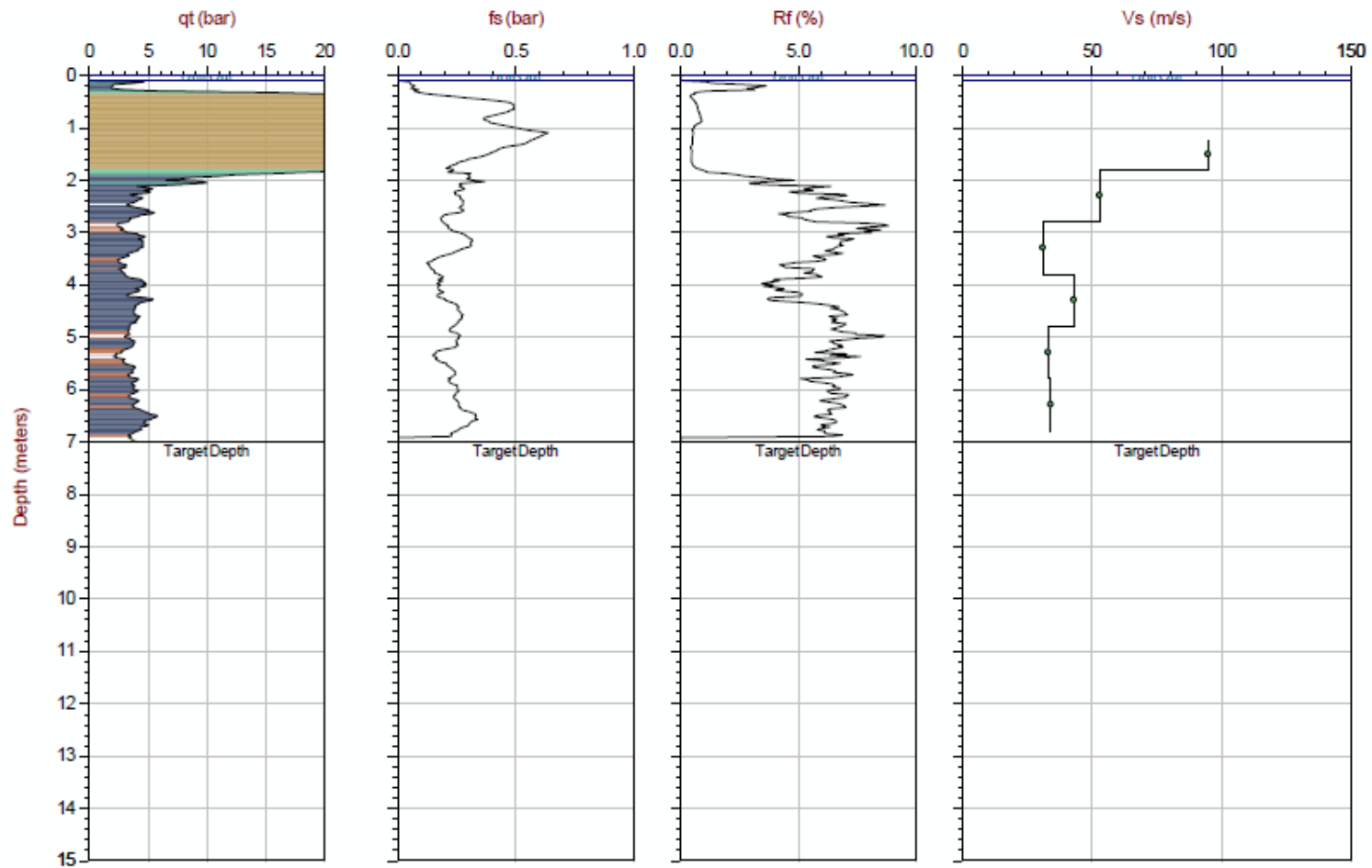
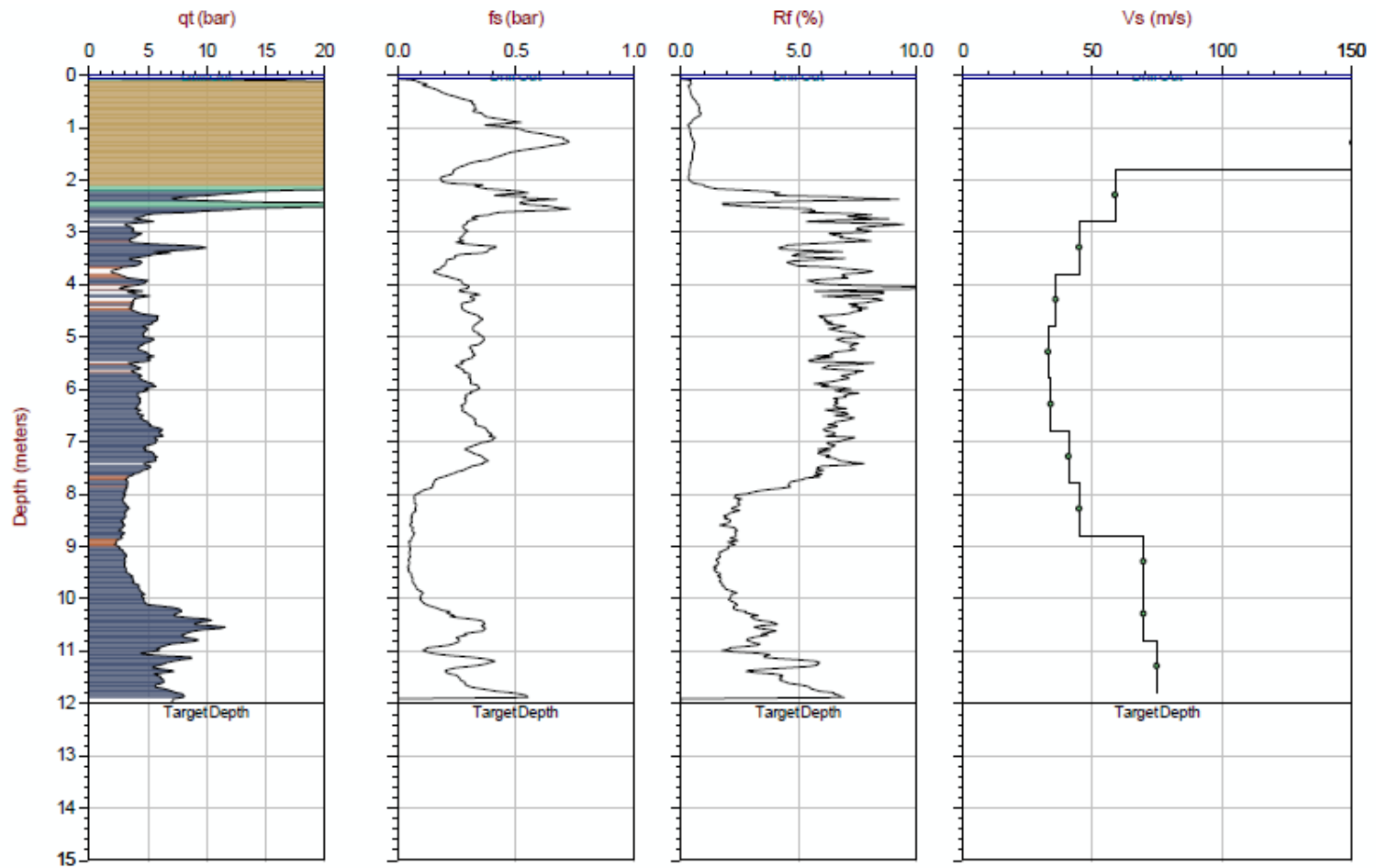
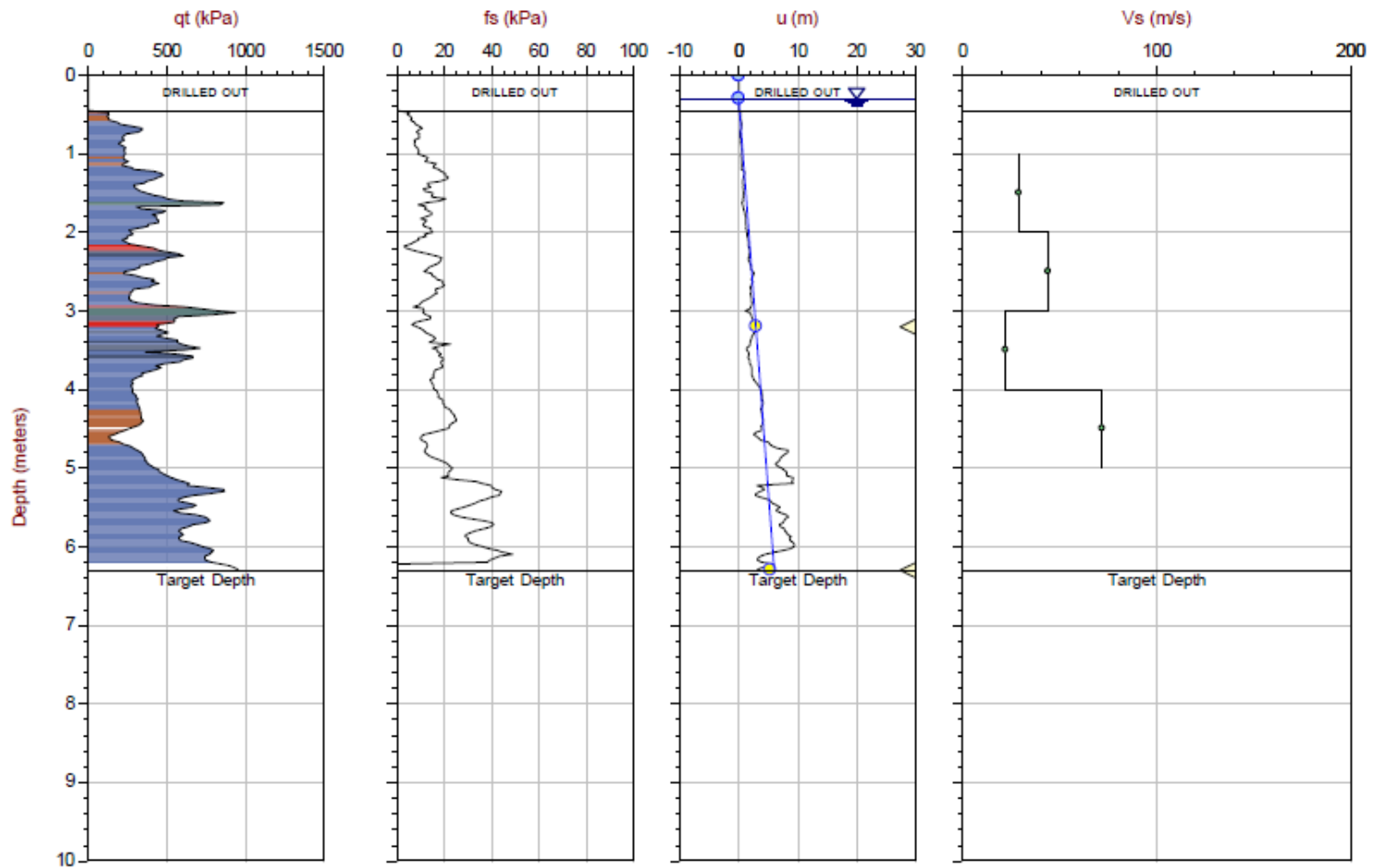


Figure A.1 The variation of tip resistance ( $q_t$ ), sleeve resistance ( $f_s$ ), pore pressure ( $u_2$ ), and shear wave velocity ( $v_s$ ) with depth below the ground surface at Site 01 in Surrey, British Columbia, Canada: Test Group 01 (UBC 2017)



**Figure A.2 The variation of tip resistance ( $q_t$ ), sleeve resistance ( $f_s$ ), pore pressure ( $u_2$ ), and shear wave velocity ( $v_s$ ) with depth below the ground surface at Site 01 in Surrey, British Columbia, Canada: Test Group 02 (UBC 2017)**



**Figure A.3 The variation of tip resistance ( $q_t$ ), sleeve resistance ( $f_s$ ), pore pressure ( $u_2$ ), and shear wave velocity ( $v_s$ ) with depth below the ground surface at Site 02 in Wabasca, Alberta, Canada: Test Group 01 (UBC 2017)**

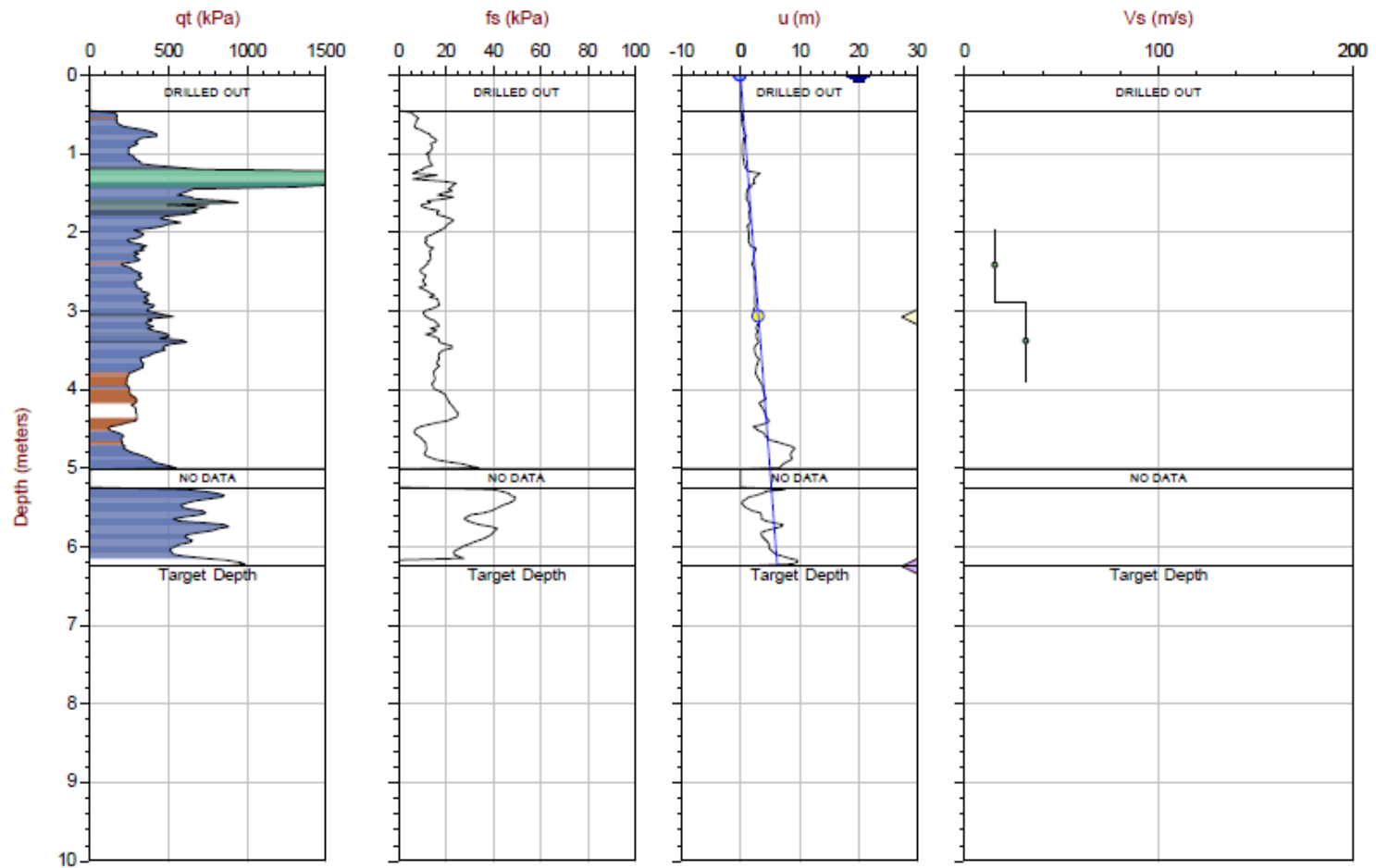


**Figure A.4 The variation of tip resistance ( $q_t$ ), sleeve resistance ( $f_s$ ), pore pressure ( $u_2$ ), and shear wave velocity ( $v_s$ ) with depth below the ground surface at Site 02 in Wabasca, Alberta, Canada: Test Group 02 (UBC 2017)**

## A.2 Ball Penetration Test Results

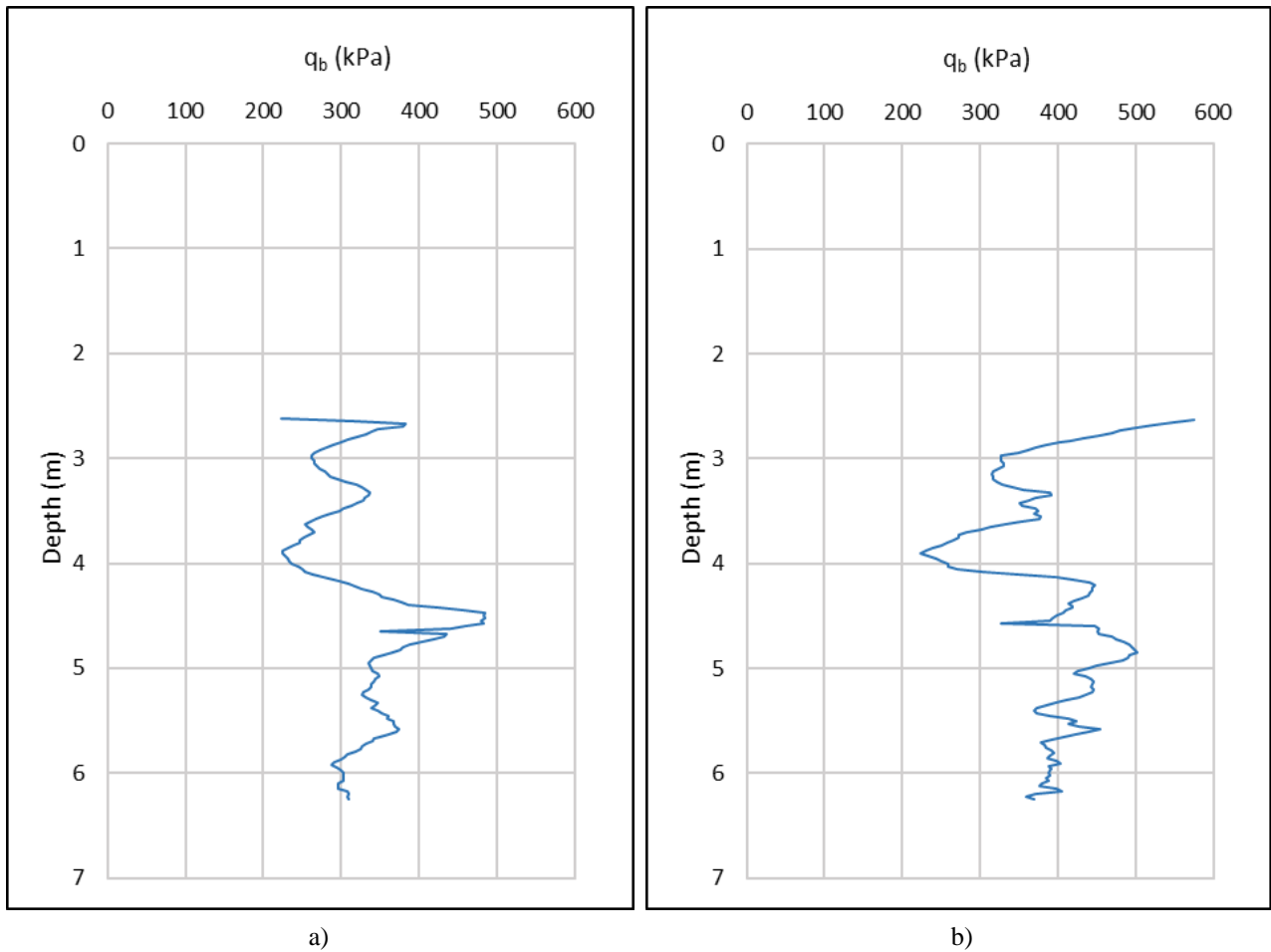


**Figure A.5** The variation of ball tip resistance ( $q_b$ ) with depth below the ground surface at Site 01 in Surrey, British Columbia, Canada: a) Test Group 01; b) Test Group 02 (UBC 2017)

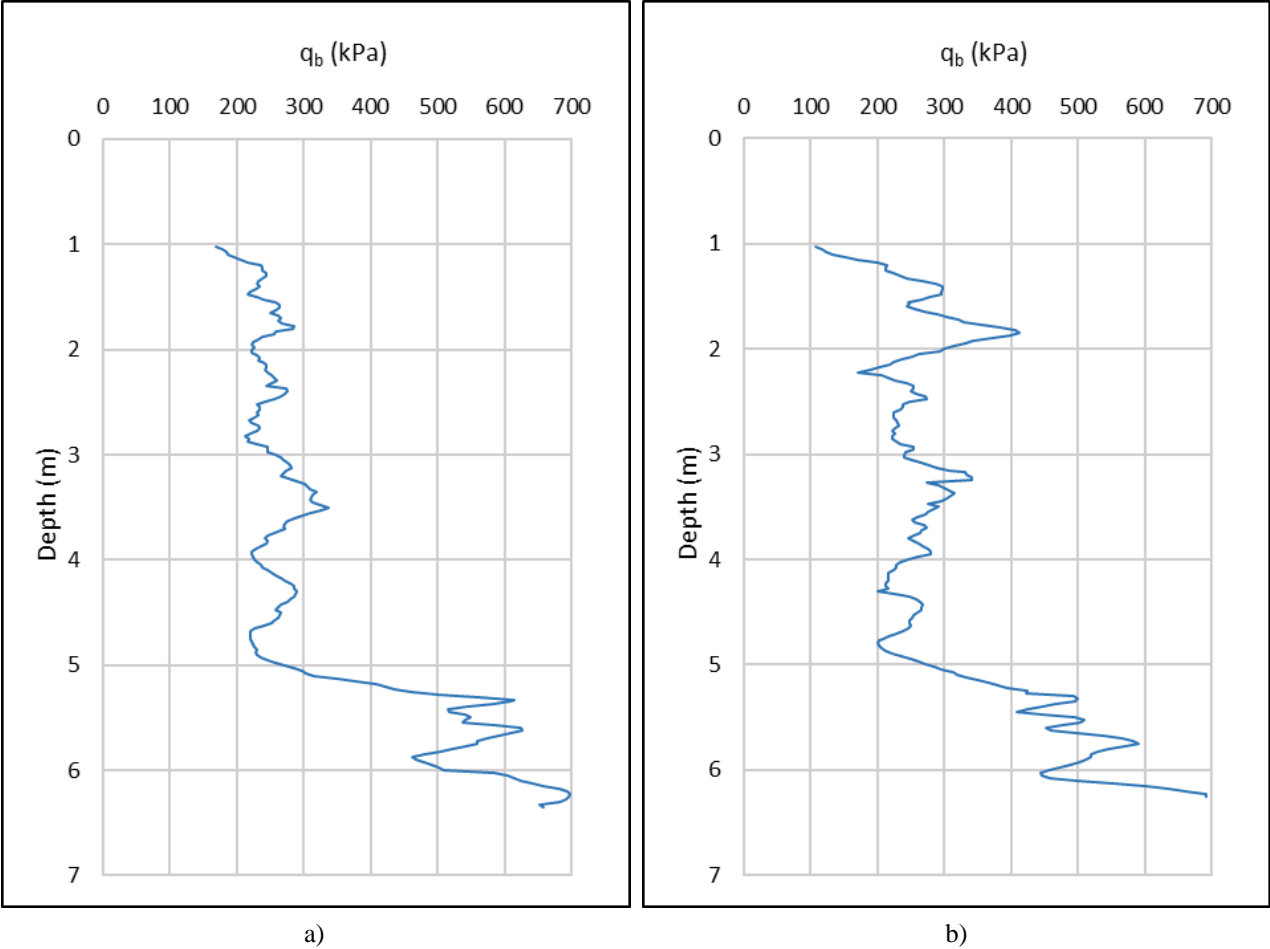
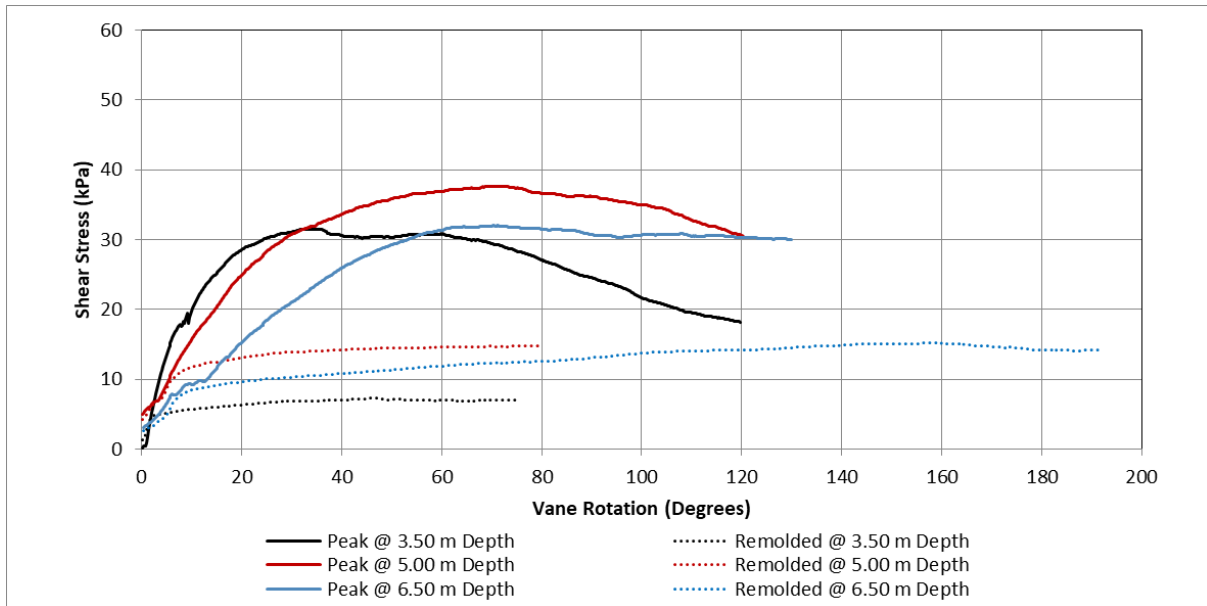
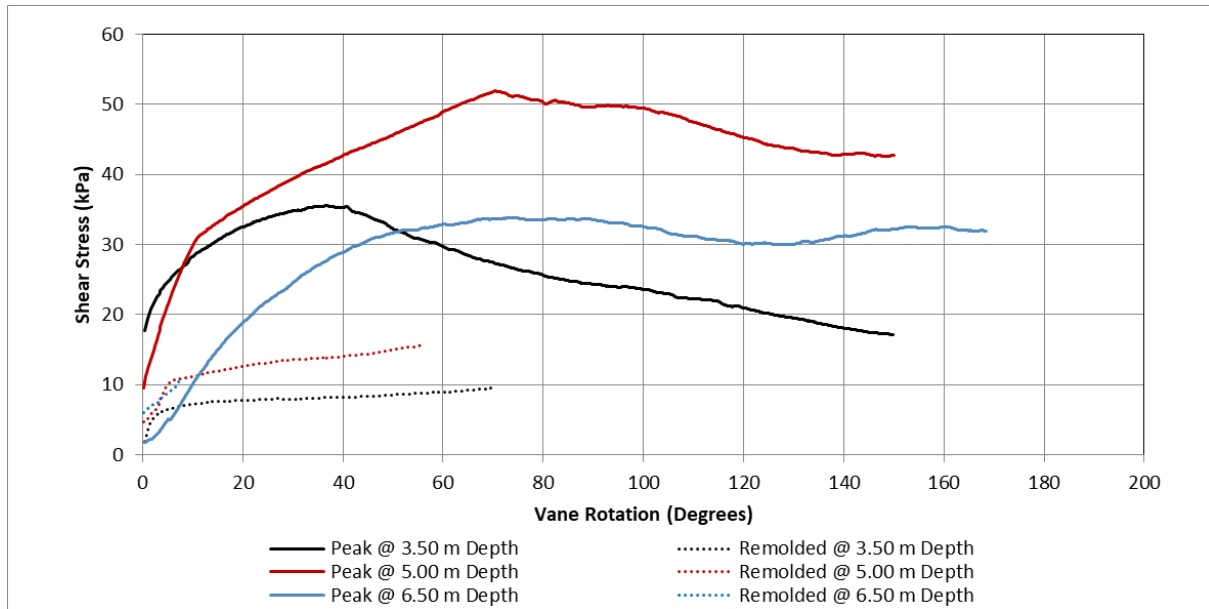


Figure A.6 The variation of ball tip resistance ( $q_b$ ) with depth below the ground surface at Site 02 in Wabasca, Alberta, Canada: a) Test Group 01; b) Test Group 02 (UBC 2017)

### A.3 Electronic Vane Shear Test Results

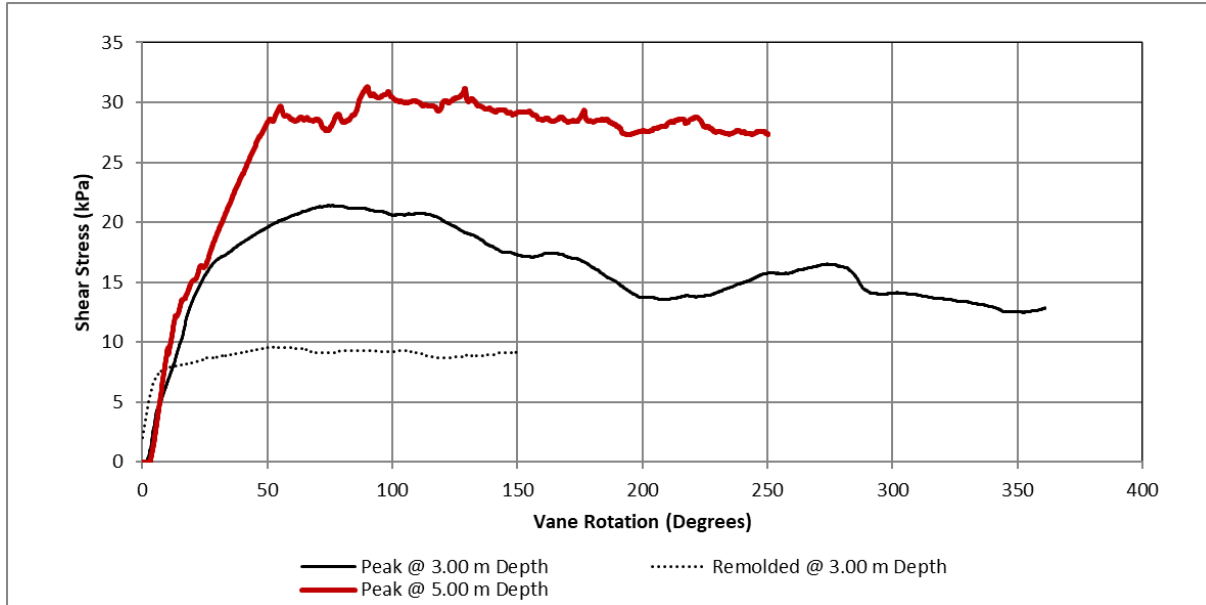


(a)

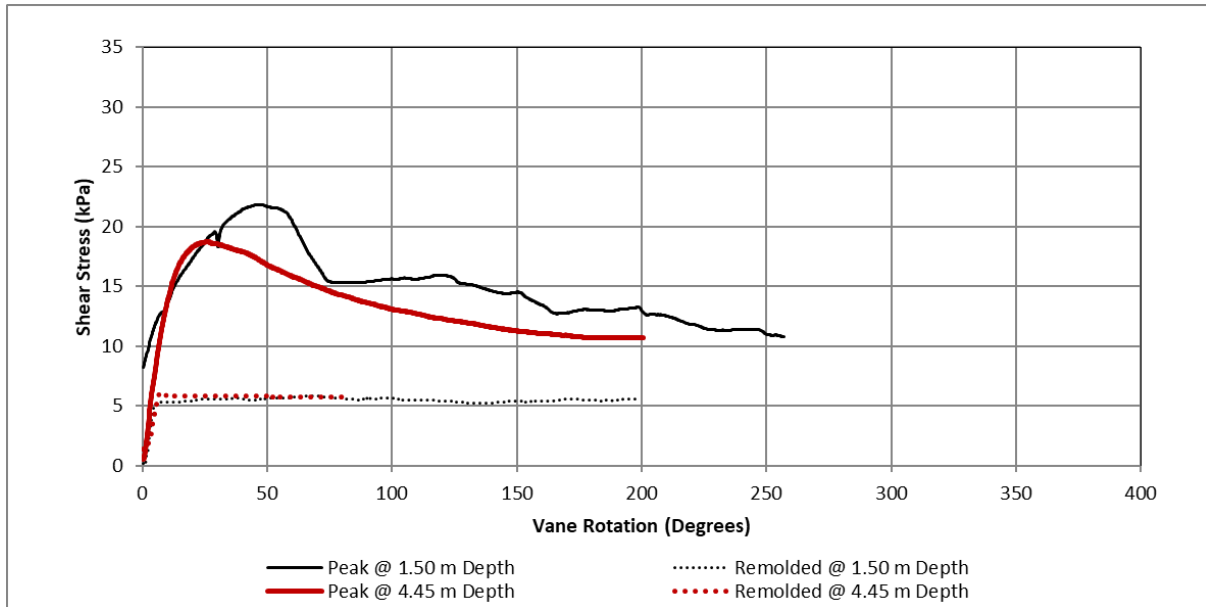


(b)

Figure A.7 The variation of peak and remolded shear stress with the vane rotation based on eVSTs conducted at Site 01 in Surrey, British Columbia, Canada: (a) Test Group 01; (b) Test Group 02 (UBC 2017)



(a)



(b)

**Figure A.8 The variation of peak and remolded shear stress with the vane rotation based on eVSTs conducted at Site 02 in Wabasca, Alberta, Canada: (a) Test Group 01; (b) Test Group 02 (UBC 2017)**

## A.4 Pressuremeter Test Results

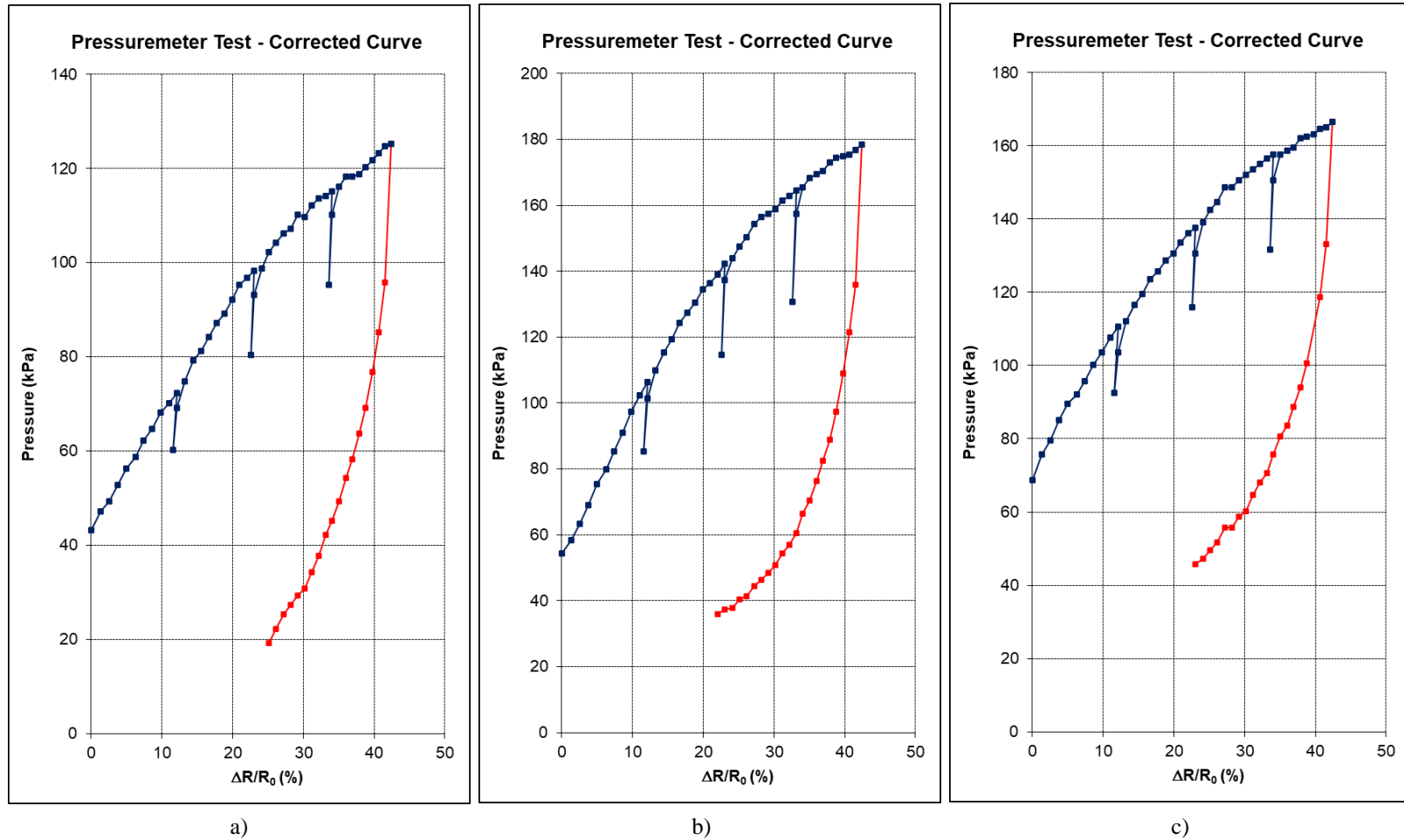


Figure A.9 Lateral pressure vs radial displacement curves generated from pressuremeter tests conducted at Site 01 in Surrey, British Columbia, Canada: (a) Test Group 01 at 3.50 m; (b) Test Group 01 at 4.80 m; (c) Test Group 01 at 6.50 m depths below the ground surface (UBC 2017)

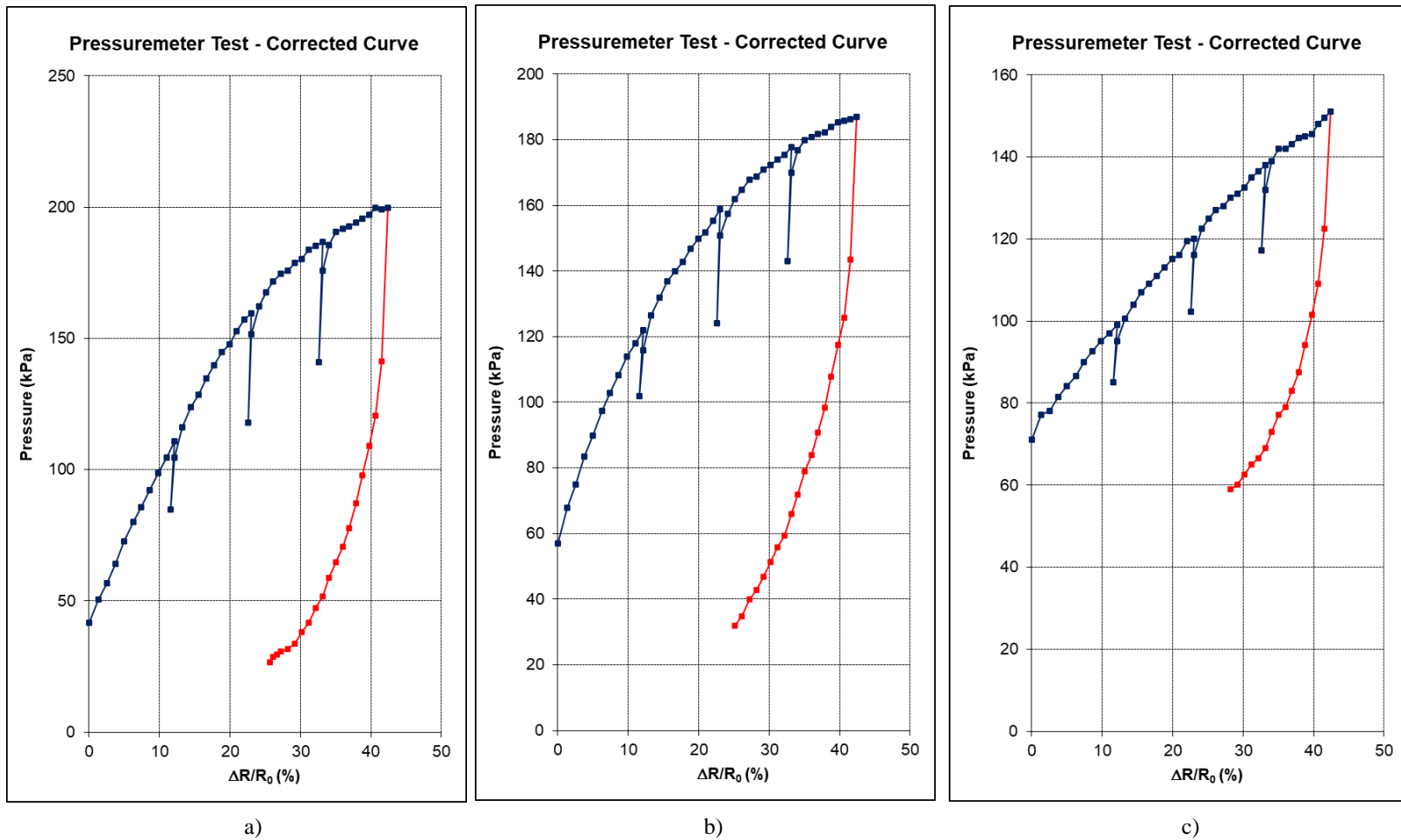


Figure A.10 Lateral pressure vs radial displacement curves generated from pressuremeter tests conducted at Site 01 in Surrey, British Columbia, Canada: (a) Test Group 02 at 3.50 m; (b) Test Group 02 at 5.05 m; (c) Test Group 02 at 6.50 m depths below the ground surface (UBC 2017)

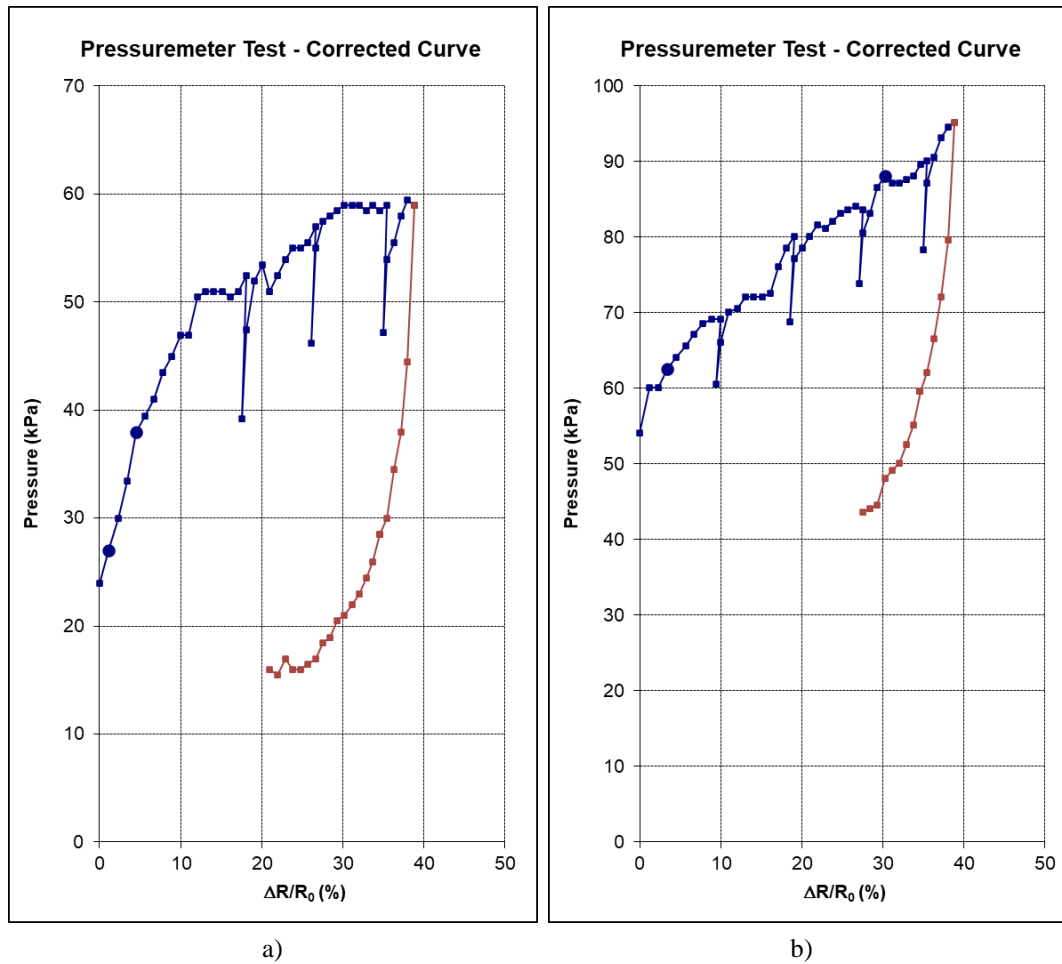


Figure A.11 Lateral pressure vs radial displacement curves generated from pressuremeter tests conducted at Site 02 in Wabasca, Alberta, Canada: (a) Test Group 01 at 1.35 m; (b) Test Group 01 at 4.52 m depths below the ground surface (UBC 2017)

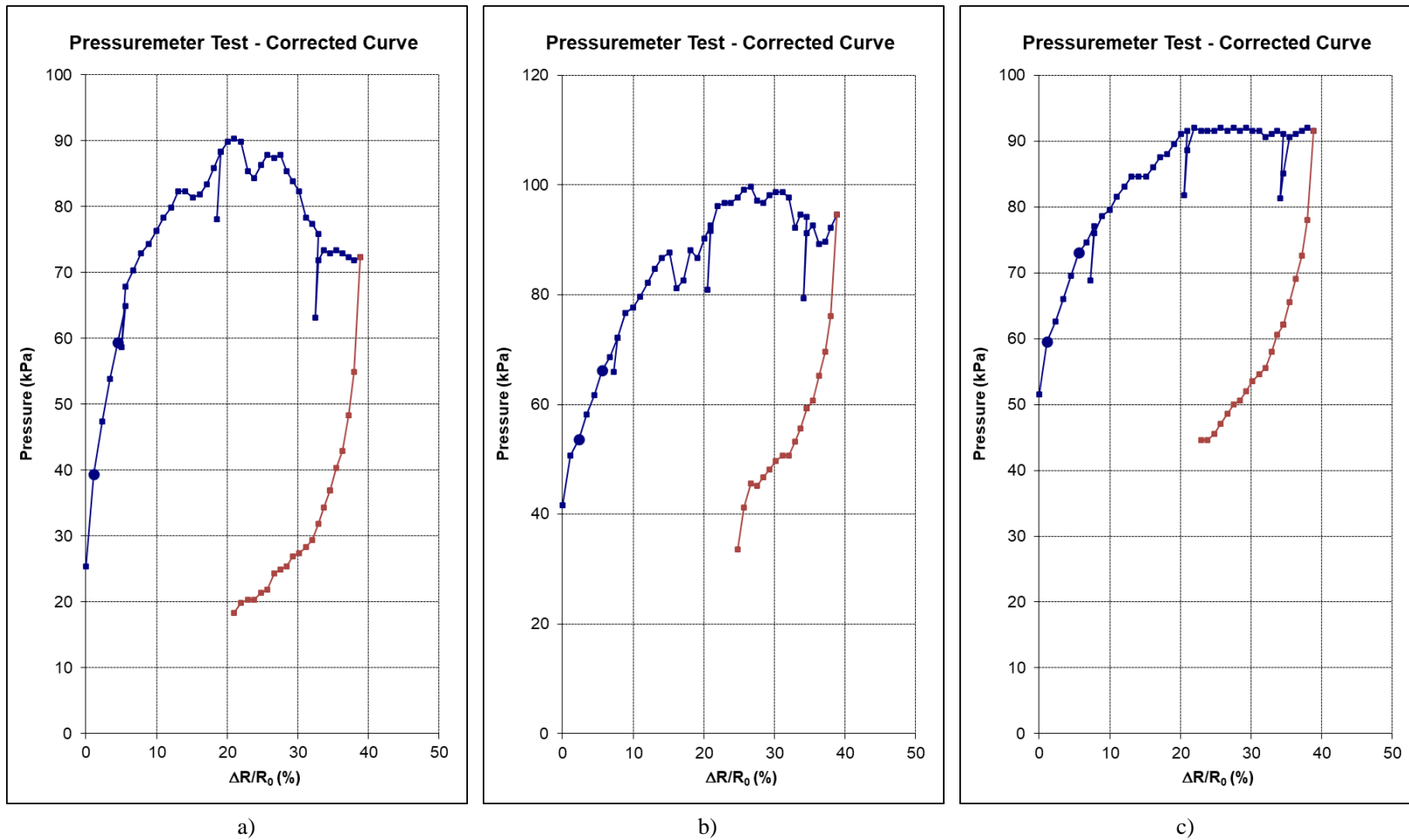


Figure A.12 Lateral pressure vs radial displacement curves generated from pressuremeter tests conducted at Site 02 in Wabasca, Alberta, Canada: a) Test Group 02 at 1.50 m; (b) Test Group 02 at 3.21 m; (c) Test Group 02 at 4.25 m depths below the ground surface (UBC 2017)

## A.5 Laboratory Index Properties of the Tested Organic Soil

**Table A.1 Index properties of organic soil tested in laboratory test program from Site 01 in Surrey, British Columbia, Canada, and Site 02 in Wabasca, Alberta, Canada**

Soil property	Site 01 in Surrey, British Columbia, Canada	Site 02 in Wabasca, Alberta, Canada
Water content (%)	370 ± 20	350 ± 20
Ash content (%)	35 ± 4	13 ± 4
Organic content (%)	65 ± 4	87 ± 4
Fiber content (%)	47 ± 4	55 ± 4
Wet density (g/cm <sup>3</sup> )	1.01	1.1
Dry density (g/cm <sup>3</sup> )	0.75	0.55
Specific gravity	1.96	1.88

## A.6 Direct Simple Shear Test Results

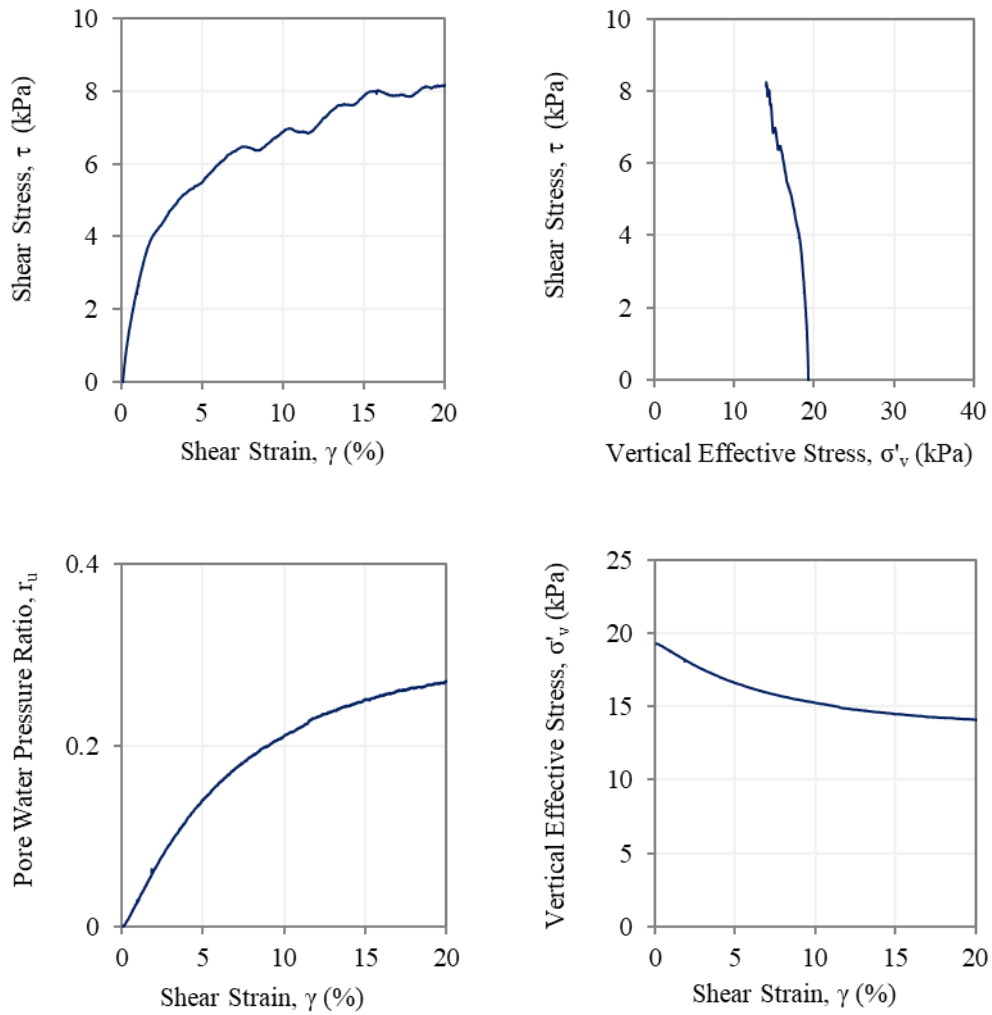
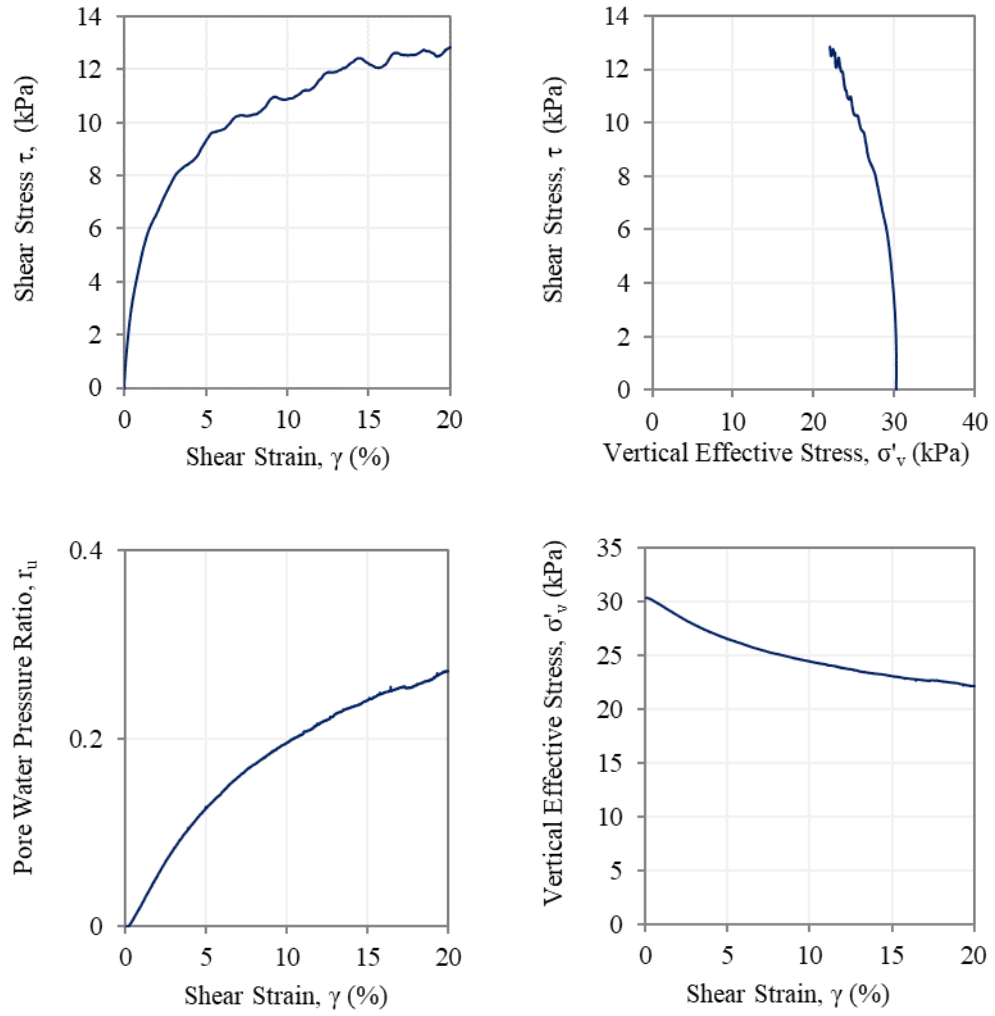


Figure A.13 DSS Monotonic shear test results at vertical effective stress 20 kPa

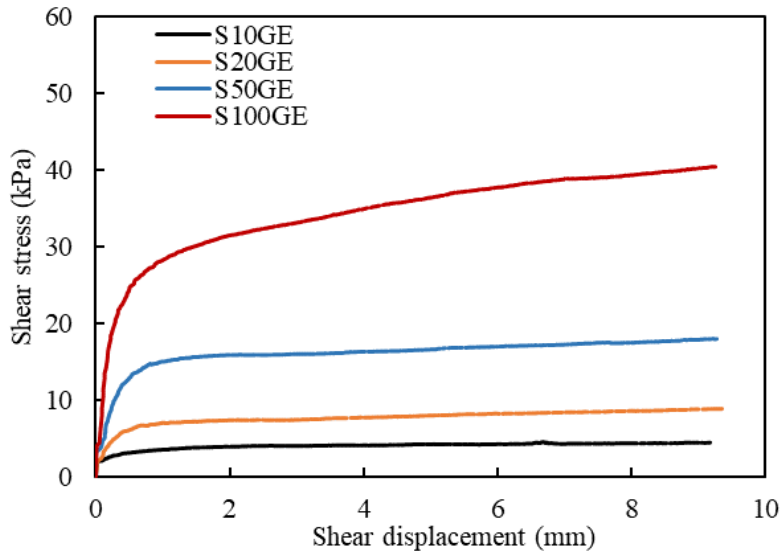


**Figure A.14 DSS Monotonic shear test results at vertical effective stress 30 kPa**

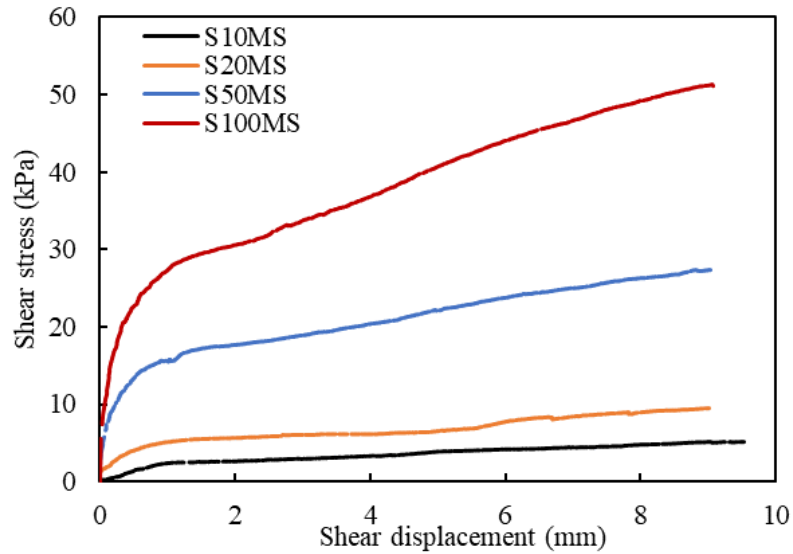
## A.7 Direct Shear Test Program and Test Results

**Table A.2 Direct Shear test program**

Test type	Test ID*	Vertical effective consolidation stress, $\sigma'_{vc}$ (kPa)
	Site 01 in Surrey, British Columbia, Canada	
	Interface friction properties	
Interface direct shear tests: Organic soil – GE coating solid test surface	S10GE	10
	S20GE	20
	S50GE	50
	S100GE	100
Interface direct shear tests: Organic soil – MS solid test surface	S10MS	10
	S20MS	20
	S50MS	50
	S100MS	100
Direct shear tests: organic soil	Internal friction properties	
	S10	10
	S20	20
	S50	50



a)



b)

**Figure A.15 Shear stress vs shear displacement at 10, 20, 50 and 100 kPa from interface direct shear tests on; a) Organic soil from Site 01 in Surrey, British Columbia, Canada – GE coating solid test surface and b) Organic soil from Site 01 in Surrey, British Columbia, Canada – MS solid test surface**

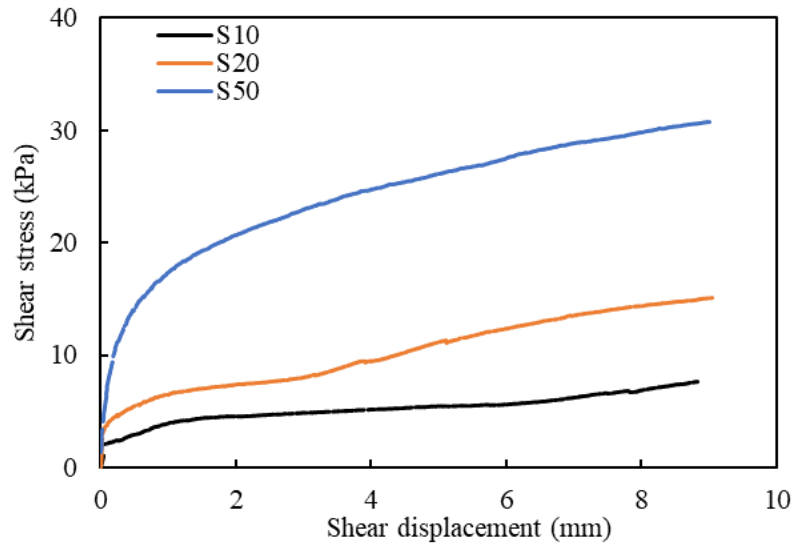


**Figure A.16 Shear stress vs shear displacement at 10, 20 and 50 kPa of direct shear tests on organic soil at Site 01 in Surrey, British Columbia, Canada**

**Table A.3 Summary of laboratory direct shear test results**

	Initial wet density	Initial moisture content	Vertical stress	Peak shear stress
	g/cm <sup>3</sup>	%	kPa	kPa
Site 01 Surrey, British Columbia, Canada	Interface friction properties: Green epoxy coating - Organic soil			
	1.14	295	10	4.4
	1.15	328	20	8.9
	1.15	307	50	18
	1.16	335	100	40.4
	Interface friction properties: Mild steel - Organic soil			
	0.11	300	10	5.2
	0.11	292	20	9.6
	0.11	300	50	27.5
	0.12	268	100	51.2
	Internal friction properties: Organic soil			
	1.18	298	10	7.7
	1.16	223	20	15.1
	1.2	280	50	32

## **Appendix B Effect of Horizontal SPI Test Chamber Size**

Details of FLAC 2D numerical modeling utilized to assess the impact of boundary conditions/size of the horizontal test chamber during the design and fabrication stage of the test chamber is discussed in this section.

## **B.1 Assessment of Effect of the Horizontal SPI Test Chamber Size Using Numerical Analysis**

This section contributes directly to the development of the horizontal soil-pipe interaction full-scale testing chamber presented in Section 4.2. FLAC 2D numerical modeling was utilized to assess the impact of boundary conditions/size of the horizontal test chamber during the design and fabrication stage of the test chamber.

Two FLAC mesh configurations were developed to assess the impact of test chamber size (including front and rear wall boundaries, along with the bottom boundary) on pipe load-displacement behavior. These configurations represent a larger box dimensionally, mirroring the largest pipe diameter and highest H/D ratio tested in the horizontal test chamber. Full-scale Test No H4-8-1.9-7.3-250 with a 220 mm pipe diameter and H/D of 1.9 was modelled as Case 1 and Test No H2-6-3.5-2.0-340 with a 168 mm pipe diameter and H/D of 3.5 was modelled as Case 2. The results from numerical analyses were directly compared with those obtained from the numerical models that represented the full-scale Tests No H4-8-1.9-7.3-250 and H2-6-3.5-2.0-340 (presented in Section 7.1.5). It is important to note that the two models were analyzed with identical soil and interface properties (soil properties are used similar to respective FLAC simulations), element sizes and boundary conditions (presented in Section 7.1.1). The resulting load versus displacement curves for the two cases are presented in Figures B.1 and B.2.

In addition to soil loads on pipe, the contours of horizontal total stresses in the soil domain for the two cases are also compared in Figures B.3 and B.4 respectively. As noted in these figures, the horizontal stress levels at the left boundary of the box are higher than that of the right boundary. This can be attributed to the horizontal forces getting developed in the direction of pipe

displacement. Further, this type of a stress development pattern was observed by Karimian (2006) in his numerical modelling to assess the box size requirements with respect to the larger ASPIRe™ soil chamber (Wijewickreme et al., 2009) at UBC.

Based on Figures B.1 and B.2, the development of horizontal forces in the horizontal test chamber are in good agreement with the model simulating a larger box size. It can be concluded that, for burial depths and pipe diameters tested, the end and front walls in the physical model are located at an acceptable distance from the pipe location and that the results can be extended to field conditions.

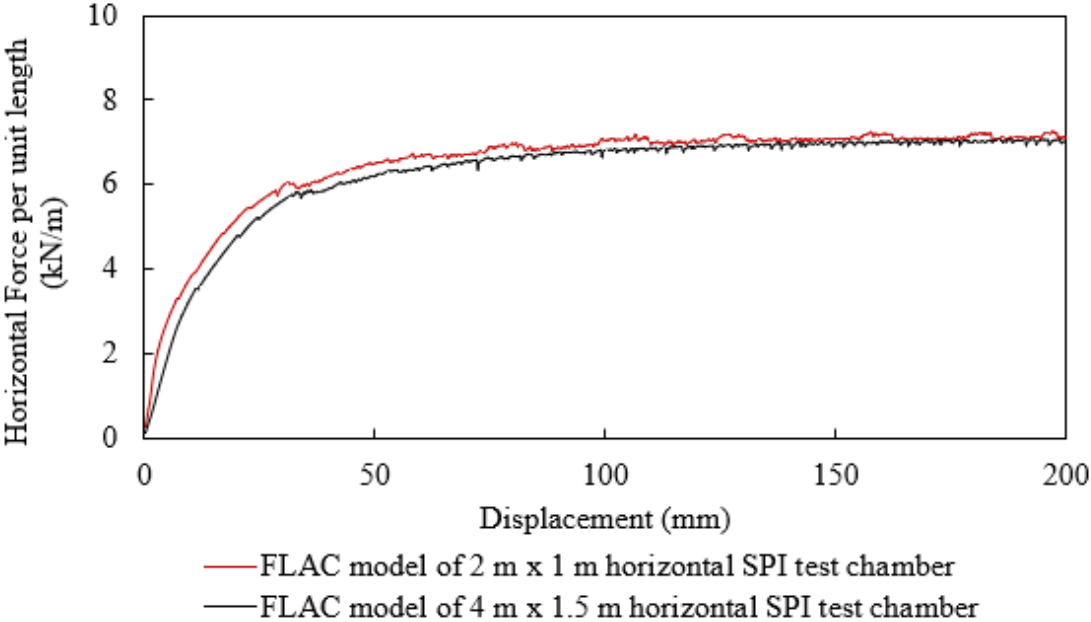


**Figure B.1 Comparison of load-displacement behavior using test chambers with different dimensions based on numerical simulations for NPS 8 pipe, H/D 1.9; Test No H4-8-1.9-7.3-250**

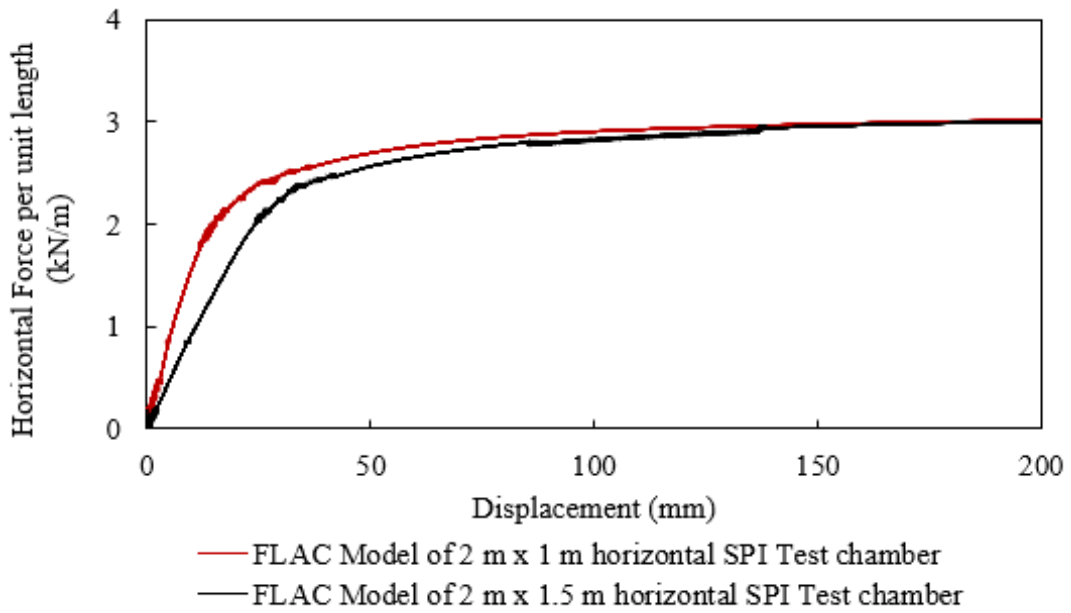


**Figure B.2 Comparison of load-displacement behavior using test chambers with different dimensions based on numerical simulations for NPS 6 pipe, H/D 3.5; Test No H2-6-3.5-2.0-340**

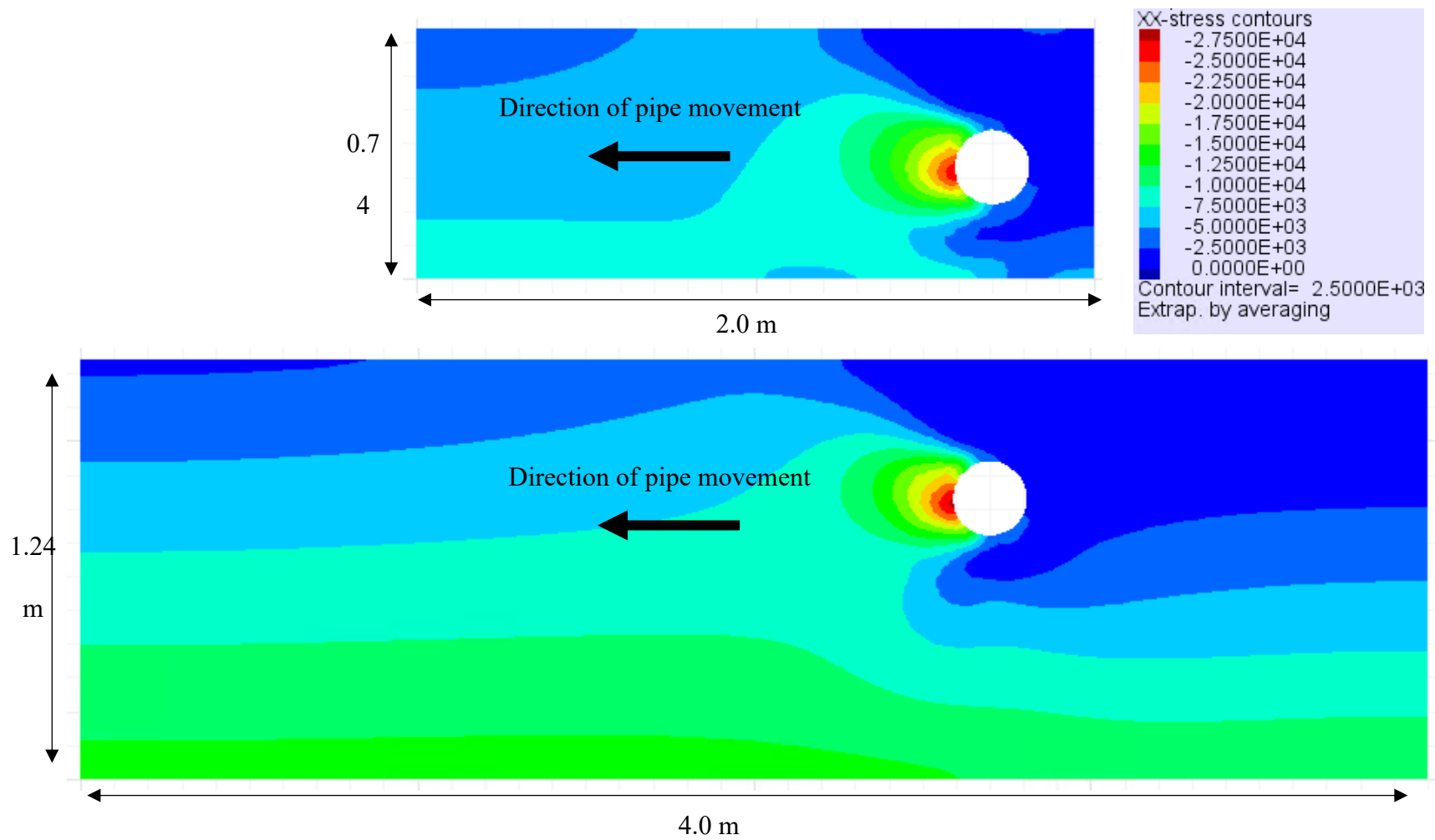


**Figure B.3 Horizontal total stress contours after 100 mm of horizontal pipe displacement: (a) Numerical model of full-scale Test No H4-8-1.9-7.3-250 and (b) Numerical model simulating a horizontal SPI test chamber of 4 m in length and 1.5 m in height**

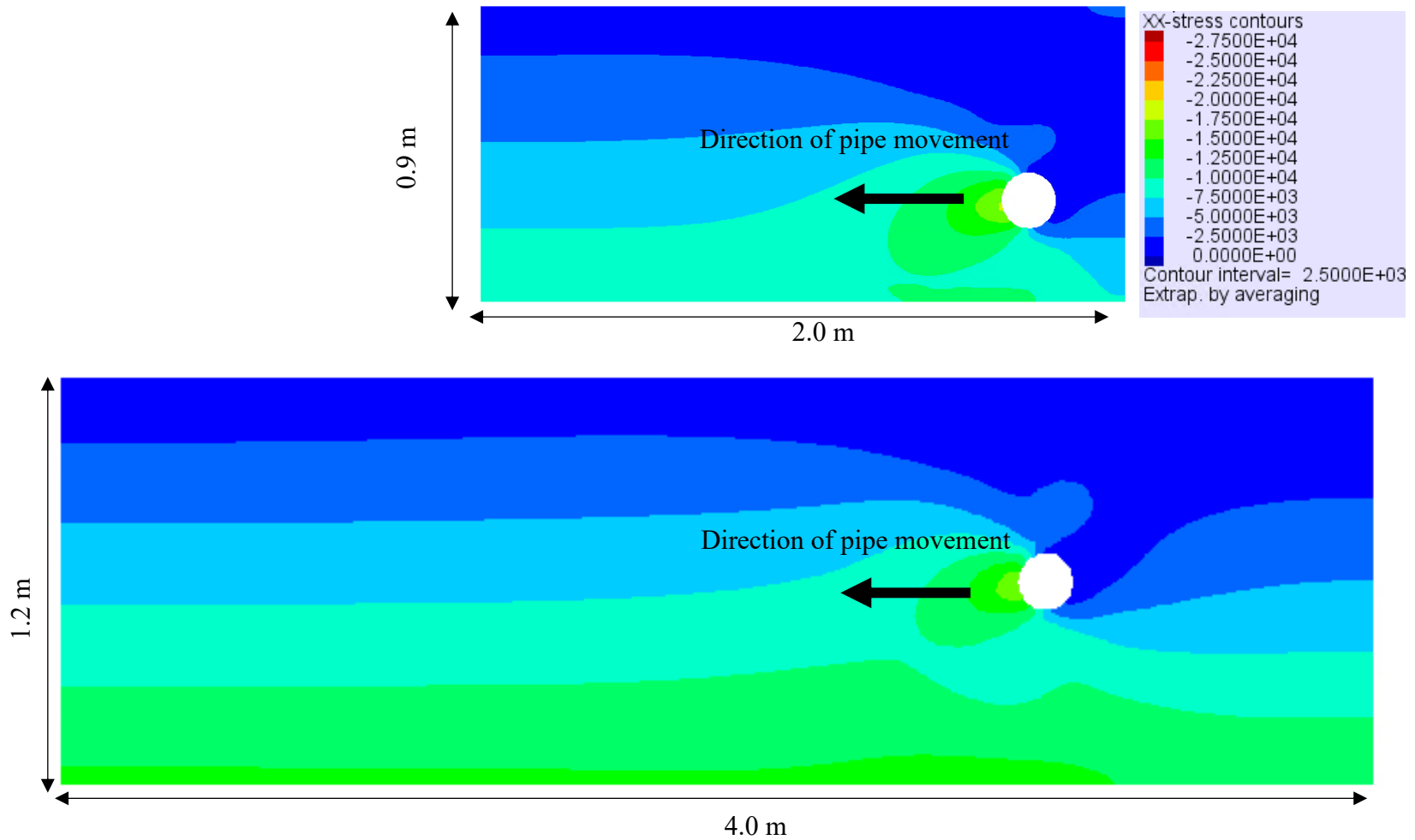


Figure B.4 Horizontal total stress contours after 100 mm of horizontal pipe displacement: (a) Numerical model of full-scale Test No H2-6-3.5-2.0-340 and (b) Numerical model simulating a horizontal SPI test chamber of 4 m in length and 1.5 m in height

## **Appendix C Full-Scale Physical Modeling Test Results and Photographs**

Appendix C compiles measured load-displacement behavior from axial pipe pullout tests and test-chamber-specific in place penetration test results and photographs during physical model tests.

### C.1 Axial Load versus Displacement Response Measured from Full-Scale Tests

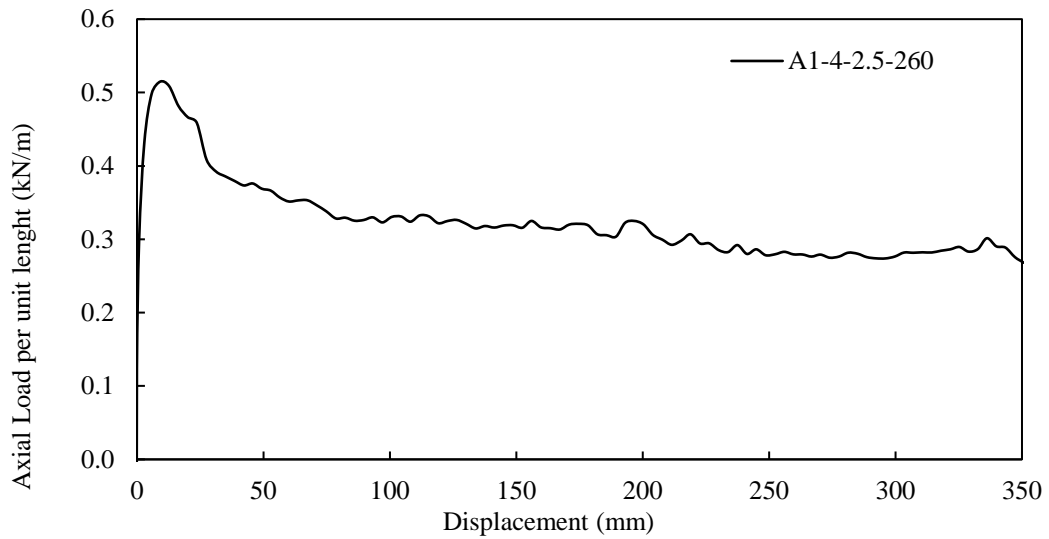


Figure C.1 Response of axial pullout load versus displacement during test A1-4-2.5-260

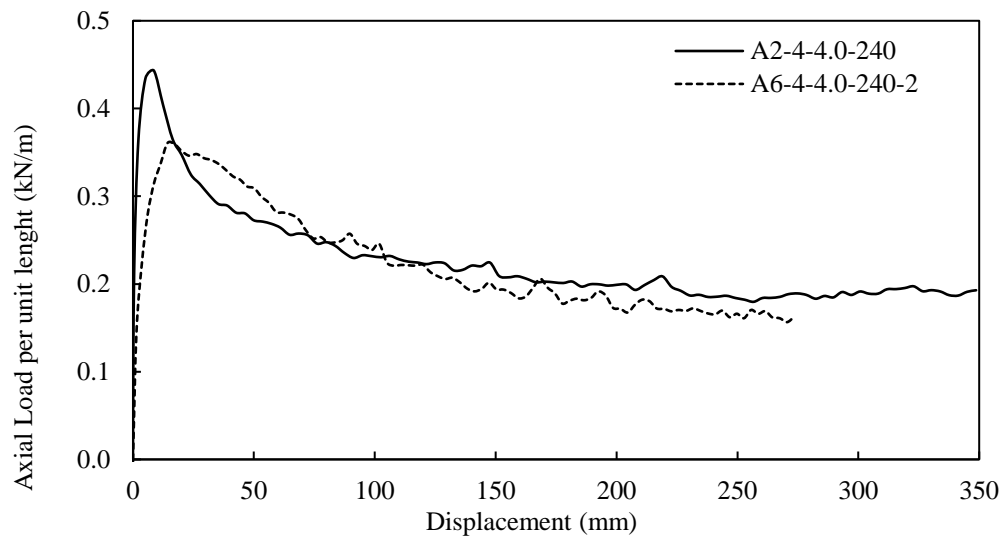
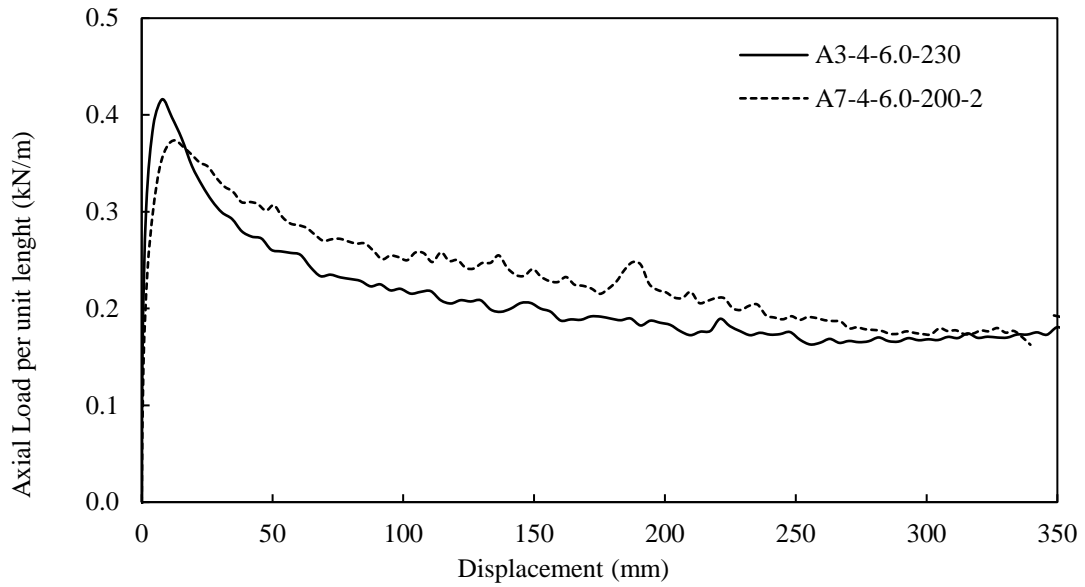
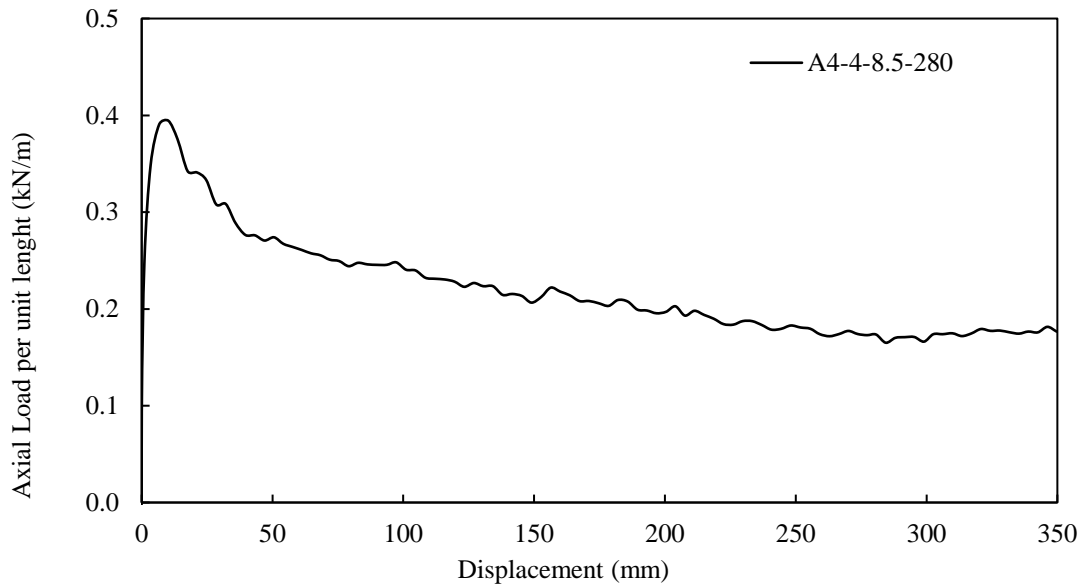


Figure C.2 Response of axial pullout load versus displacement during tests A2-4-4.0-240 and A6-4-4.0-240-2



**Figure C.3** Response of axial pullout load versus displacement during tests A3-4-6.0-230 and A7-4-6.0-200-2



**Figure C.4** Response of axial pullout load versus displacement during test A4-4-8.5-280

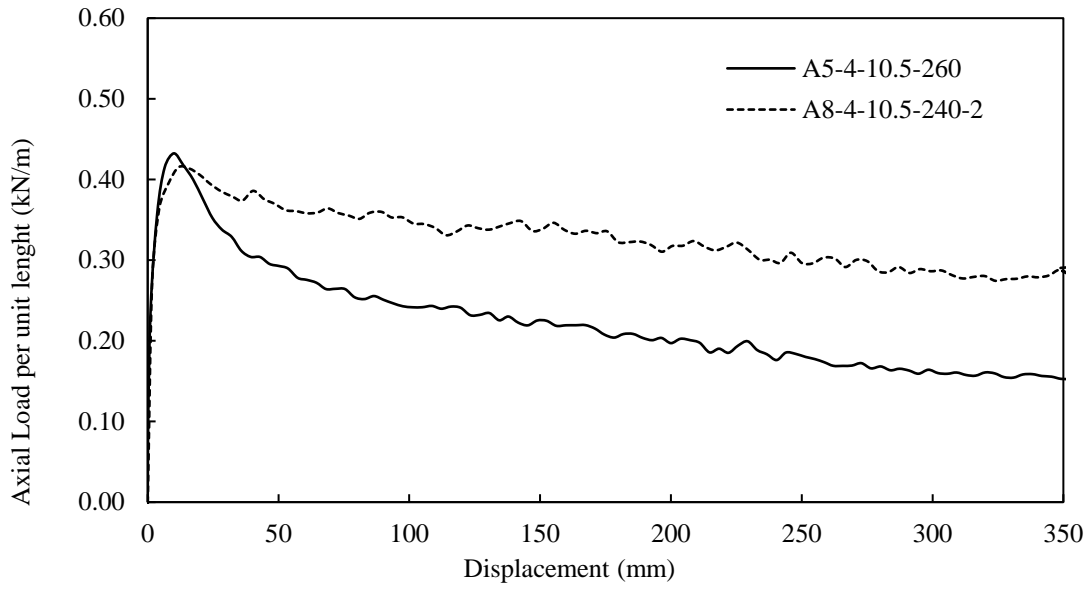


**Figure C.5 Response of axial pullout load versus displacement during tests A5-4-10.5-260 and A8-4-10.5-240-**

## C.2 Test Specific In-place Penetration Tests

The undrained shear strength of the organic soil beds prepared during full-scale horizontal pipe displacement tests were determined based on the test-chamber-specific shear strength data measured using BPT, eVST and CPT. Details of the test methods and test results of the in-situ BPT, eVST and CPTs performed are presented herein. All the field investigations were conducted with test equipment and technical support provided by ConeTec Investigations Ltd., Burnaby, B.C., Canada, under the direction and supervision of UBC research team members over several discrete days between September 2022 and December 2022. Among the horizontal pipe displacement tests, shear strength data were measured during Tests No. H1-6-1.9-1.5-360 and H2-6-3.5-2.0-340 and H6-8-1.6-9.8-200. The test plan consisted of 2 BPTs, 2CPTs and 4 eVSTs per full-scale test. However, some tests were not successful and the summary of test equipment dimensions and test depths are presented in Table C.1. In-situ test details presented in Section 3.1 discusses the BPT, CPT and eVST tests in detail.

The results from BPTs: the variation  $s_u$  with depth below the ground surface, eVSTs: variation of measured shear stress with the angle of vane rotation at peak and remolded states and CPTs: the variation of tip resistance ( $q_t$ ), sleeve resistance ( $f_s$ ) and pore pressure ( $u_2$ ) with depth below the ground surface are schematically shown in Figures C.6 through C.19. Further, Pictures taken during the test program are presented in Figures C.20 through 23.

**Table C.1 Summary of test equipment dimensions and test depths of in-place BPT, eVST and CPT tests**

		BPT	eVST		CPT
		150 cm <sup>2</sup> ball (13.8 cm diameter)	Double tapered 60 x 120 mm (45°, 45°)		15 cm <sup>2</sup> cone (4.37 cm diameter) net area ratio: 0.8
H1-6-1.9-1.5-360	Test Location 1	Continuous profile	0.31 m	0.59 m	Continuous profile
	Test Location 2	Continuous profile	0.43 m	0.58 m	Continuous profile
H2-6-3.5-2.0-340	Test Location 1	Continuous profile	0.3 m	0.54 m	Continuous profile
	Test Location 2	Continuous profile	0.3 m	0.6 m	Continuous profile
H6-8-1.6-9.8-200	Test Location 1	N/A	0.3 m	N/A	Continuous profile
	Test Location 2	N/A	0.3 m	N/A	Continuous profile

**In-place penetration test results – Full-scale Test No H1-6-1.9-1.5-360**

*Ball Penetration Tests*

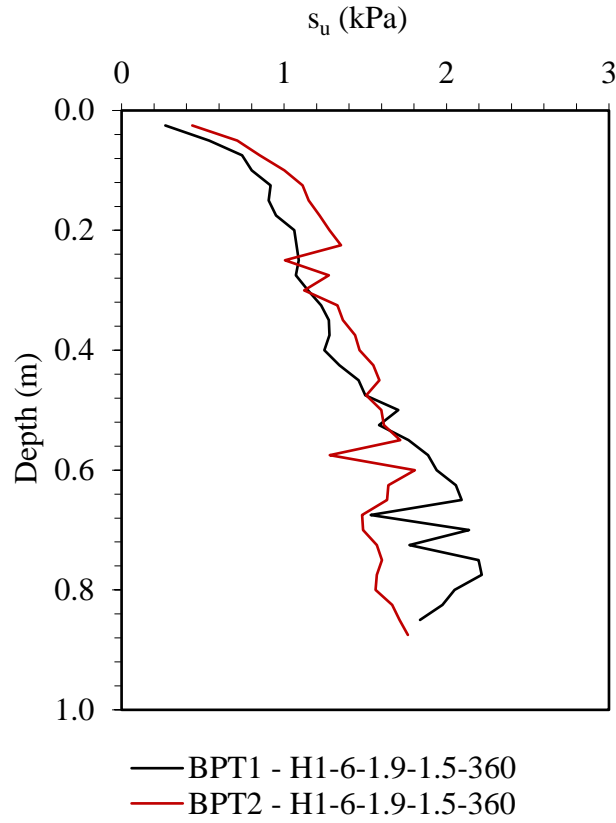


**Figure C.6 Variation of  $s_u$  with depth during BPT: H1-6-1.9-1.5-360 – Test Locations 1 and 2**

Electronic Vane Shear Tests

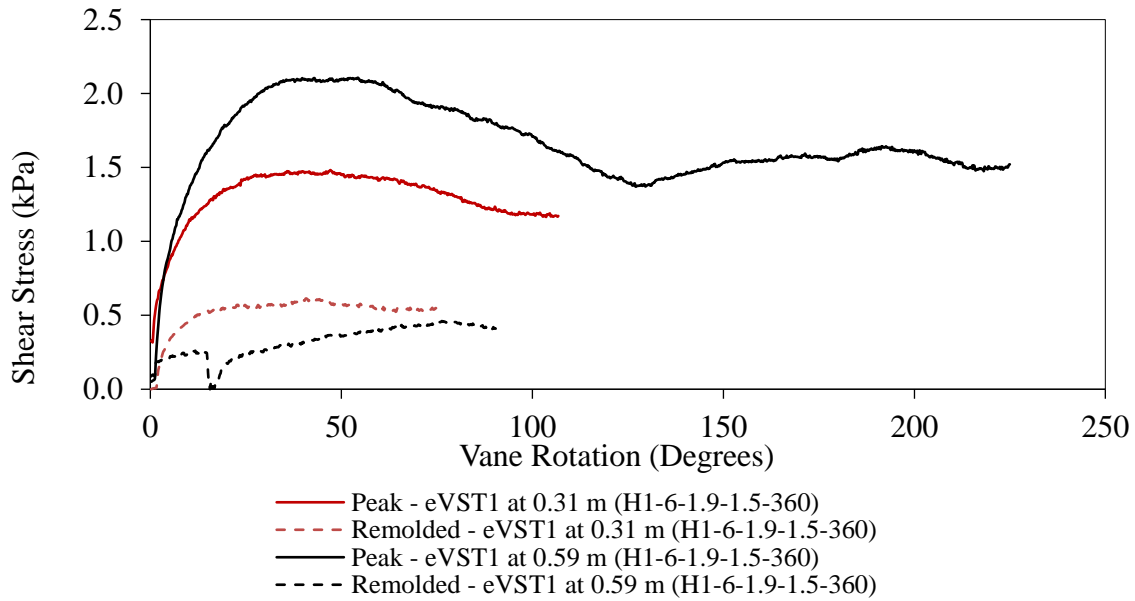


Figure C.7 Variation of shear stress with vane rotation during eVST at peak and remolded stages: H1-6-1.9-1.5-360 – Test Location 1

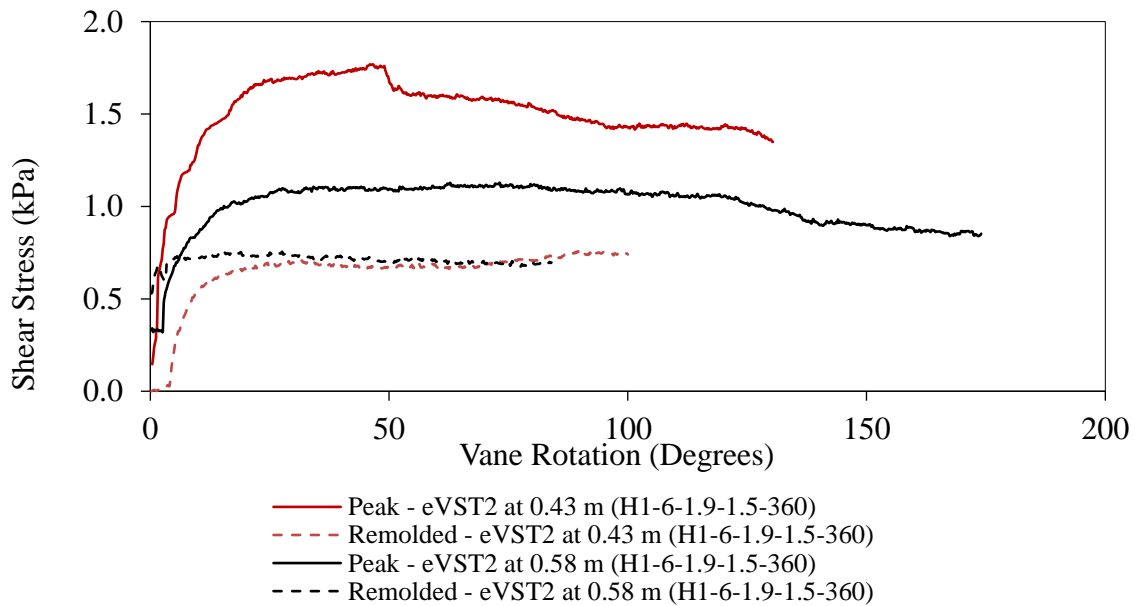


Figure C.8 Variation of shear stress with vane rotation during eVST at peak and remolded stages: H1-6-1.9-1.5-360 – Test Location 2

Cone Penetration Tests

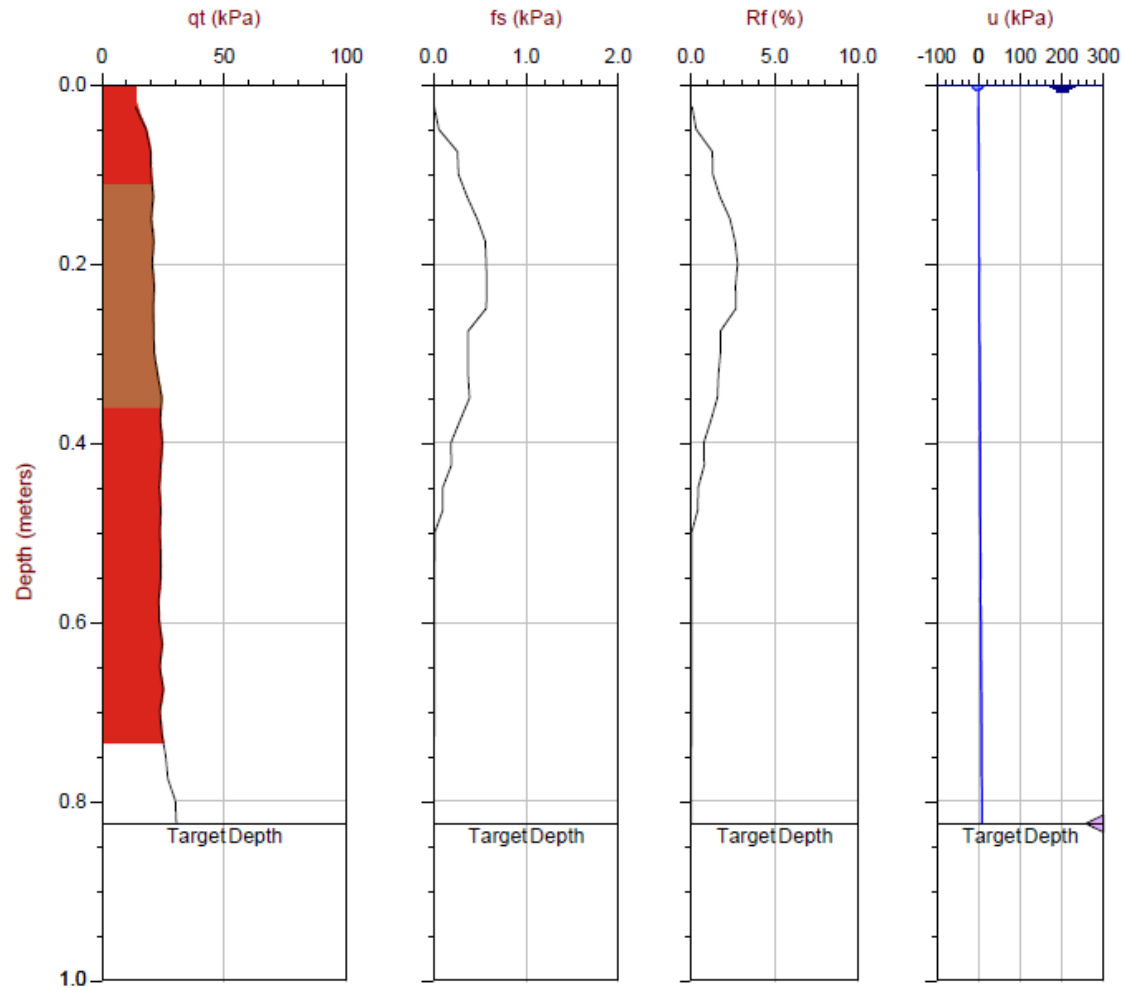
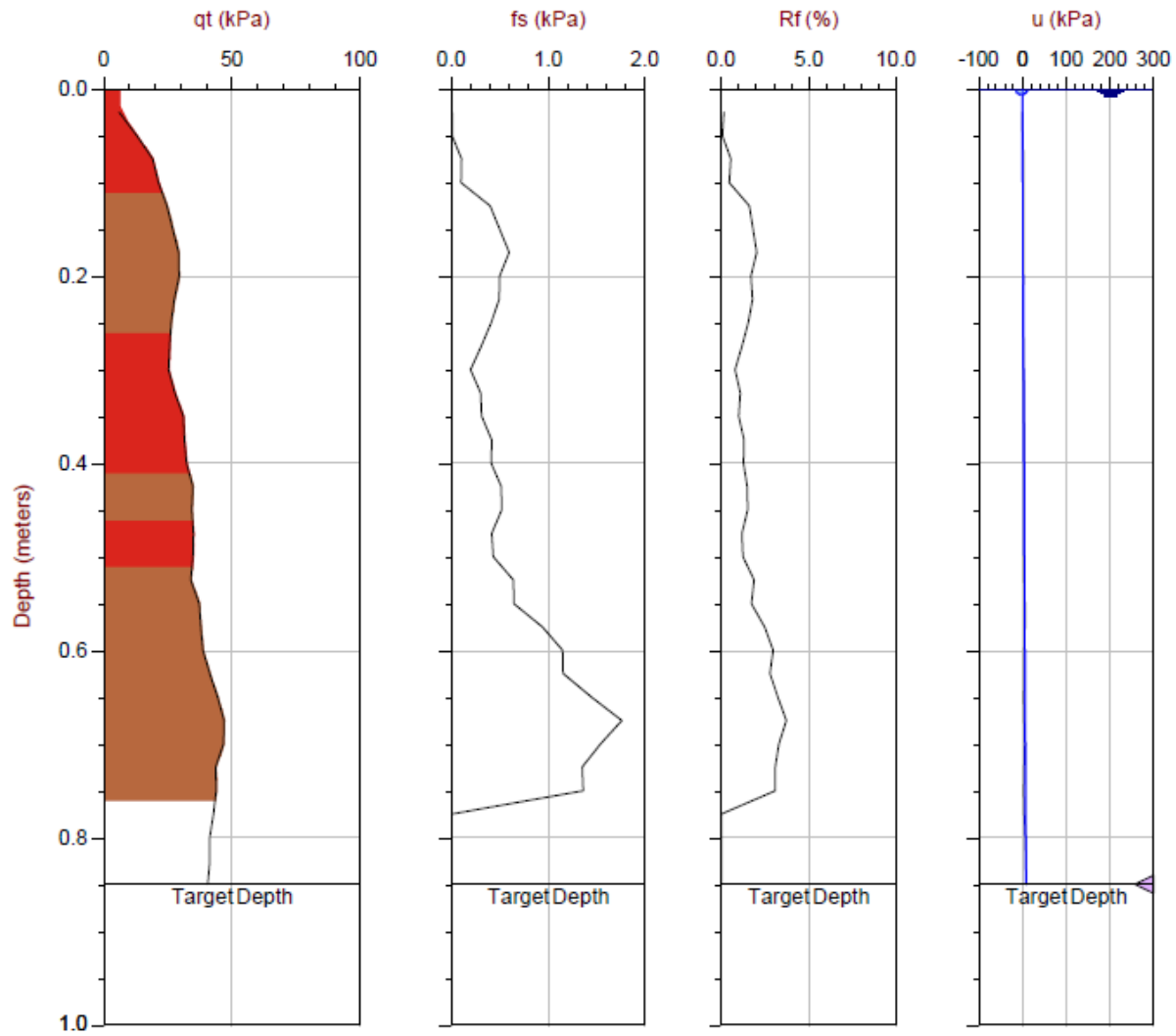


Figure C.9 The variation of tip resistance ( $q_t$ ), sleeve resistance ( $f_s$ ), friction ration ( $R_f$ ) and pore pressure ( $u$ ) with depth below the ground surface during CPT: H1-6-1.9-1.5-360 – Test Location 1



**Figure C.10 The variation of tip resistance ( $q_t$ ), sleeve resistance ( $f_s$ ), friction ratio ( $R_f$ ) and pore pressure ( $u$ ) with depth below the ground surface during CPT: H1-6-1.9-1.5-360 – Test Location 2**

**In-place penetration test results – Full-scale Test No H2-6-3.5-2.0-340**

*Ball penetration Tests*

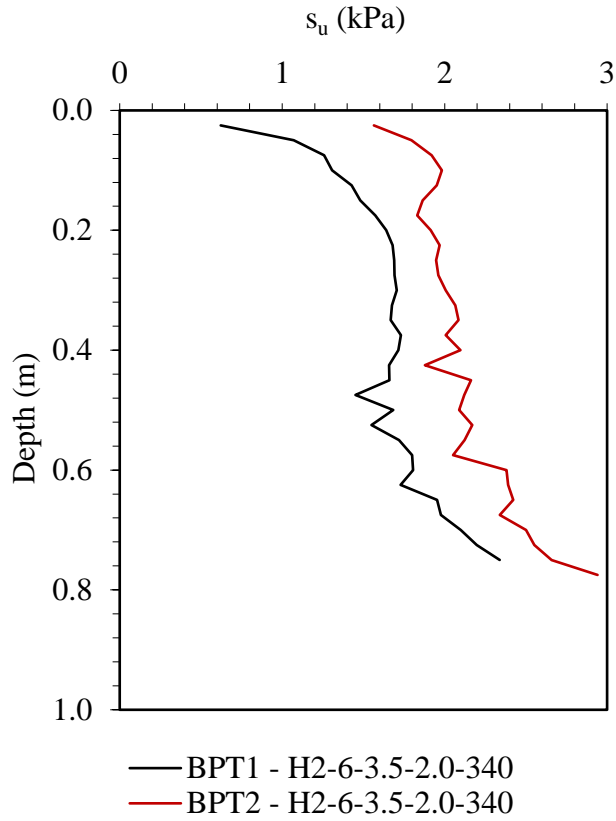


**Figure C.11 Variation of  $s_u$  with depth during BPT: H2-6-3.5-2.0-340 – Test Locations 1 and 2**

Electronic Vane Shear Tests

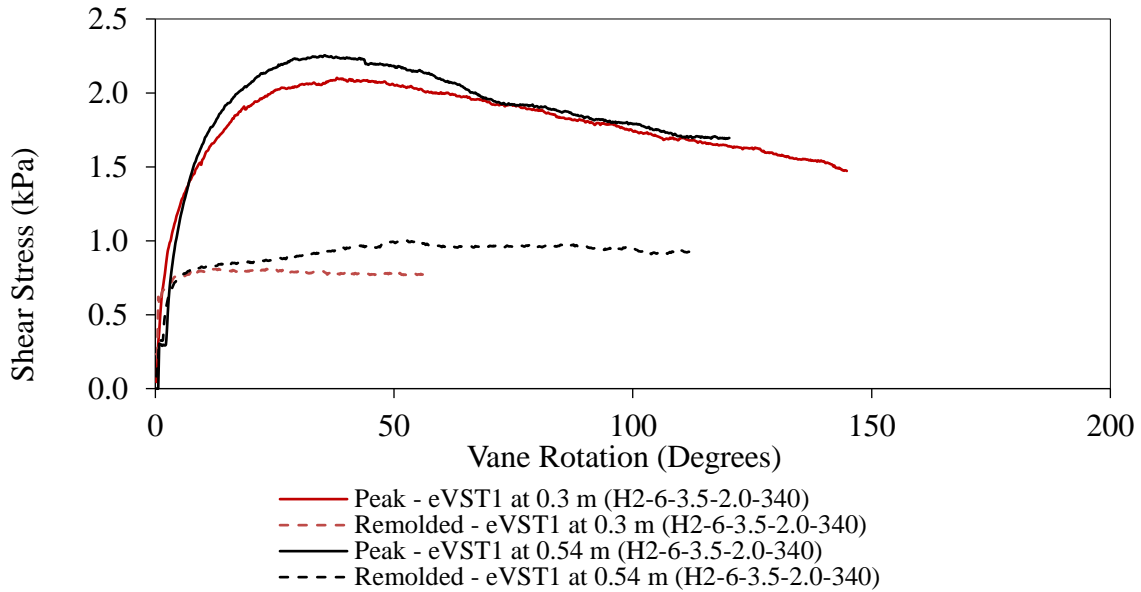


Figure C.12 Variation of shear stress with vane rotation during eVST at peak and remolded stages: H2-6-3.5-2.0-340 – Test Location 1

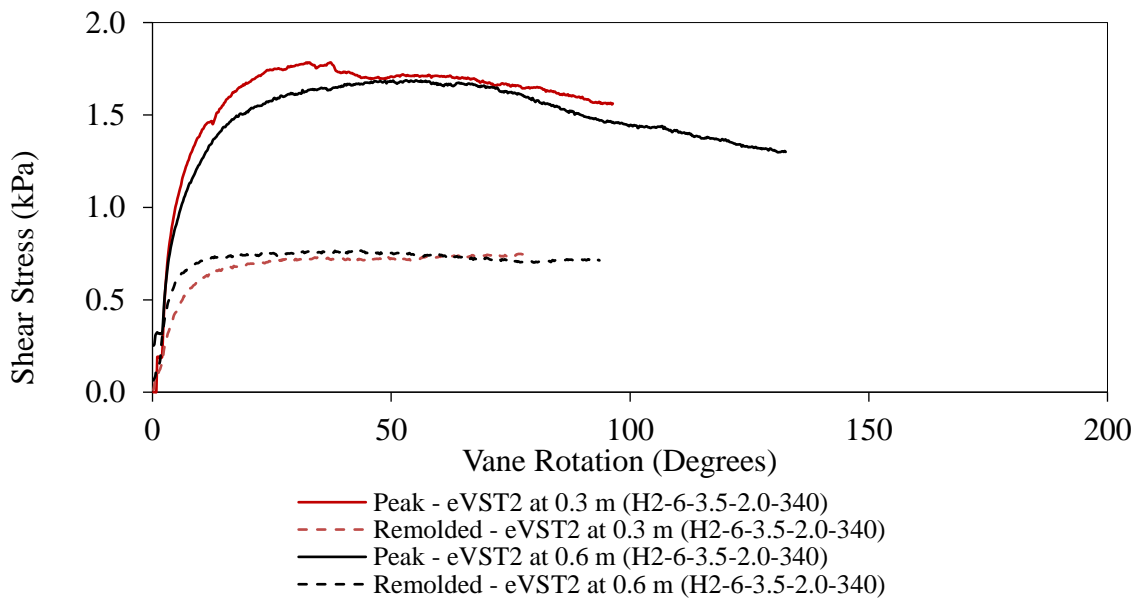
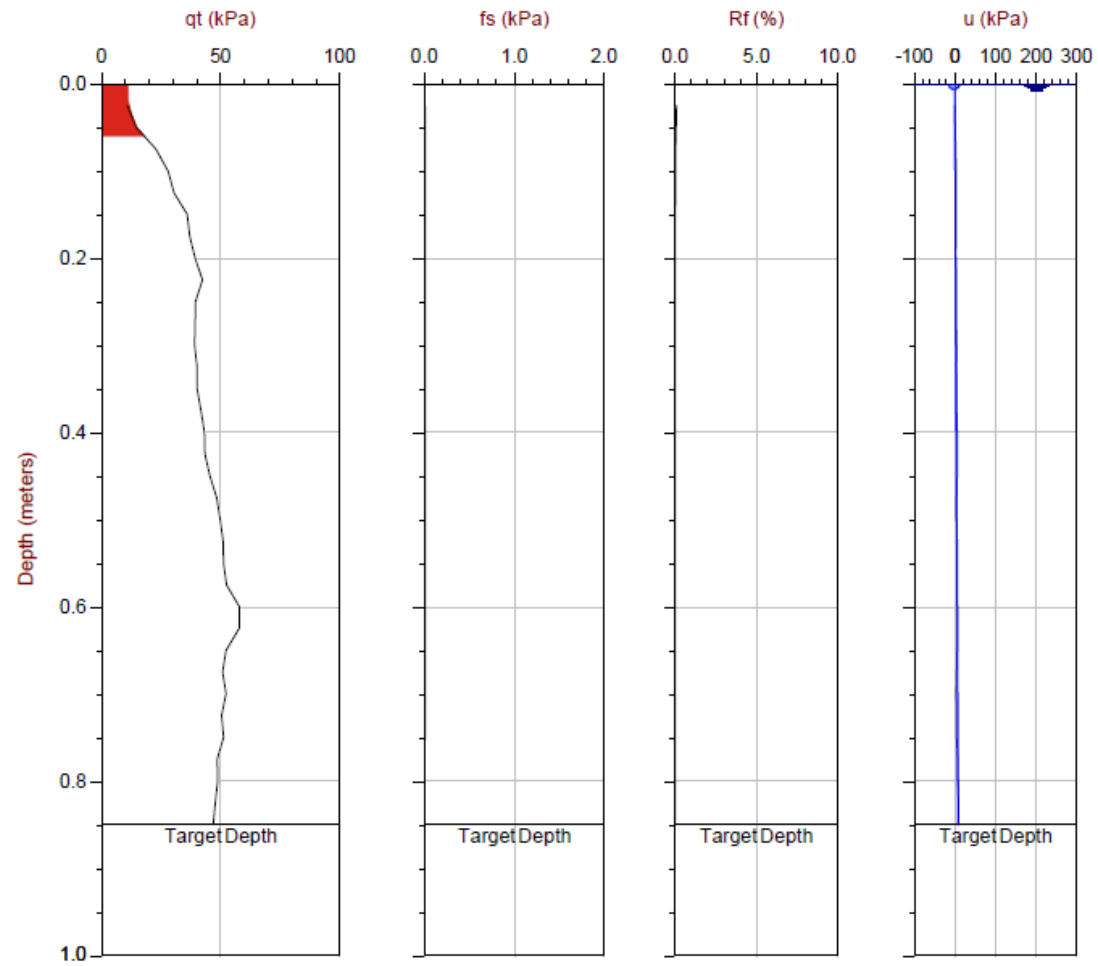


Figure C.13 Variation of shear stress with vane rotation during eVST at peak and remolded stages: H2-6-3.5-2.0-340 – Test Location 2

*Cone Penetration Tests*



**Figure C.14** The variation of tip resistance ( $q_t$ ), sleeve resistance ( $f_s$ ), friction ratio ( $R_f$ ) and pore pressure ( $u$ ) with depth below the ground surface during CPT: H2-6-3.5-2.0-340 – Test Location 1

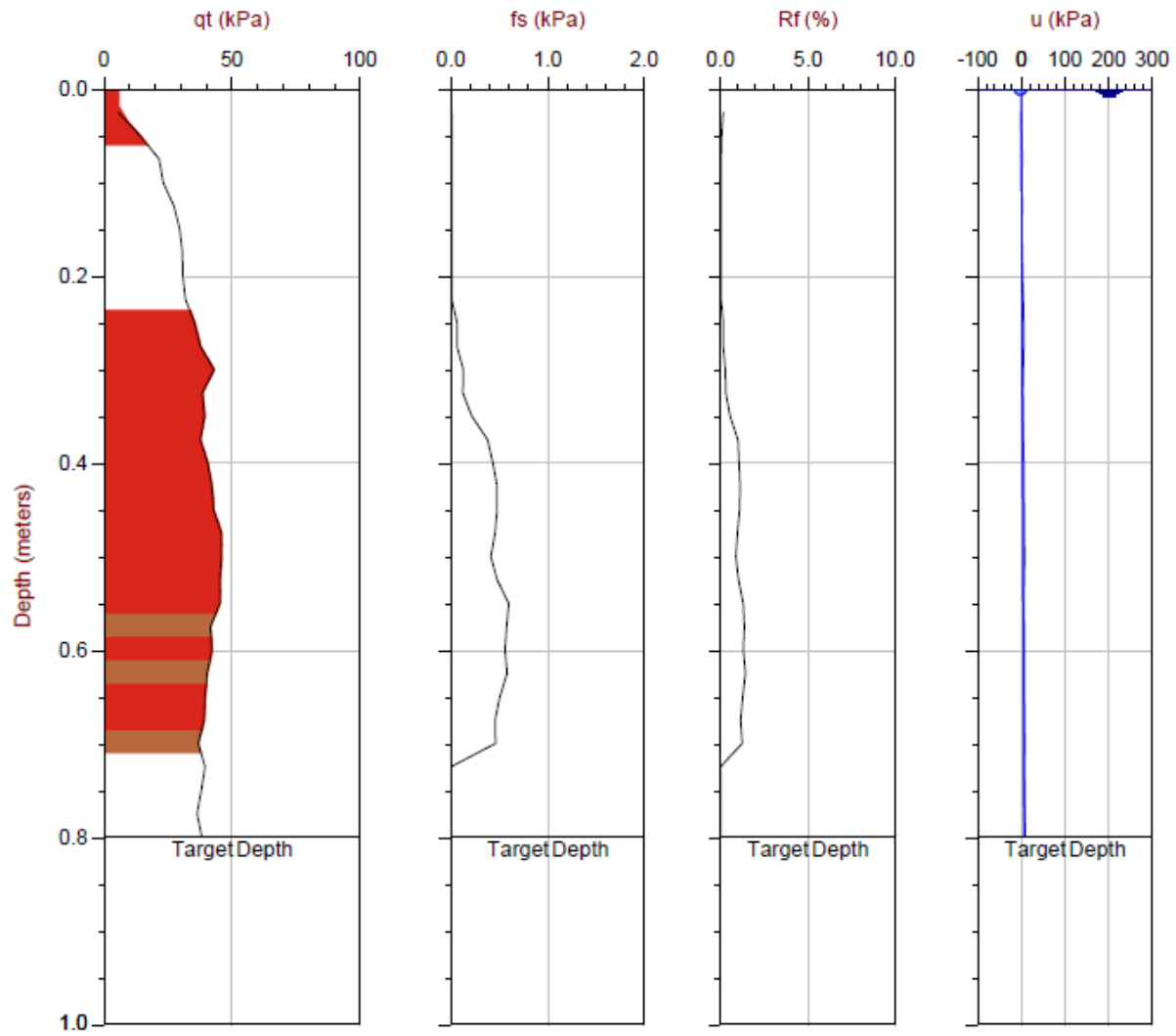


Figure C.15 The variation of tip resistance ( $q_t$ ), sleeve resistance ( $f_s$ ), friction ratio ( $R_f$ ) and pore pressure ( $u$ ) with depth below the ground surface during CPT: H2-6-3.5-2.0-340 – Test Location 2

## In-place penetration test results – Full-scale Test No H6-8-1.6-9.8-200

### Electronic Vane Shear Tests

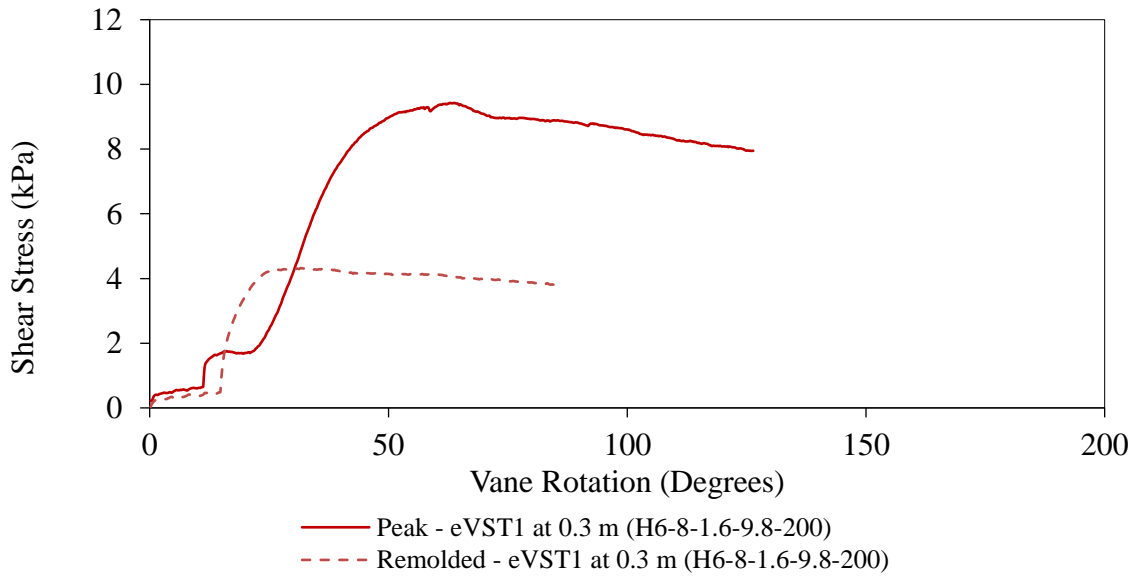


Figure C.16 Variation of shear stress with vane rotation during eVST at peak and remolded stages: H6-8-1.6-9.8-200 – Test Location 1

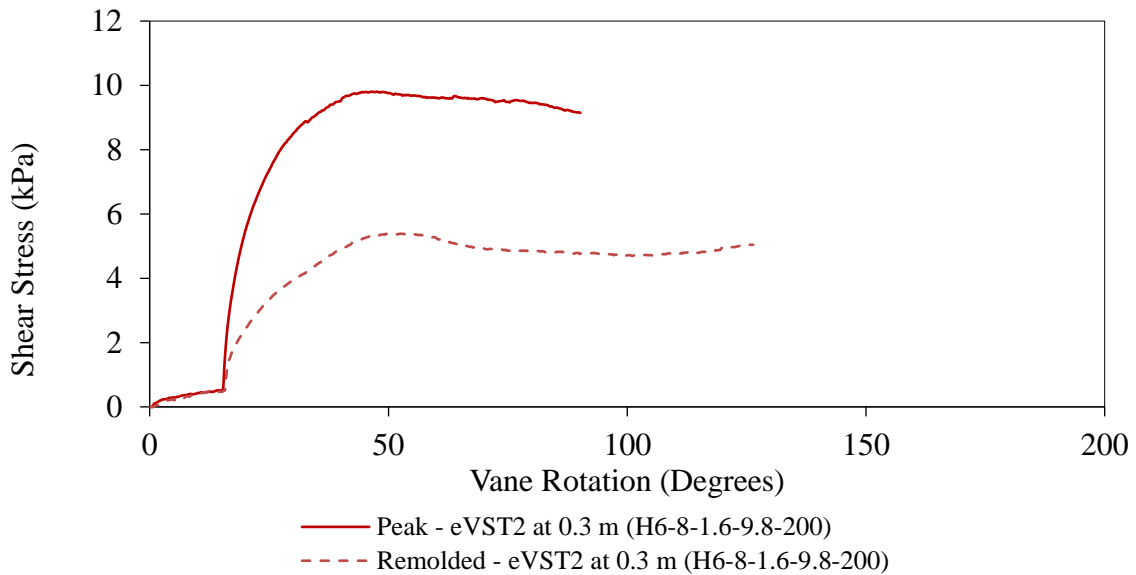


Figure C.17 Variation of shear stress with vane rotation during eVST at peak and remolded stages: H6-8-1.6-9.8-200 – Test Location 2

Cone Penetration Tests

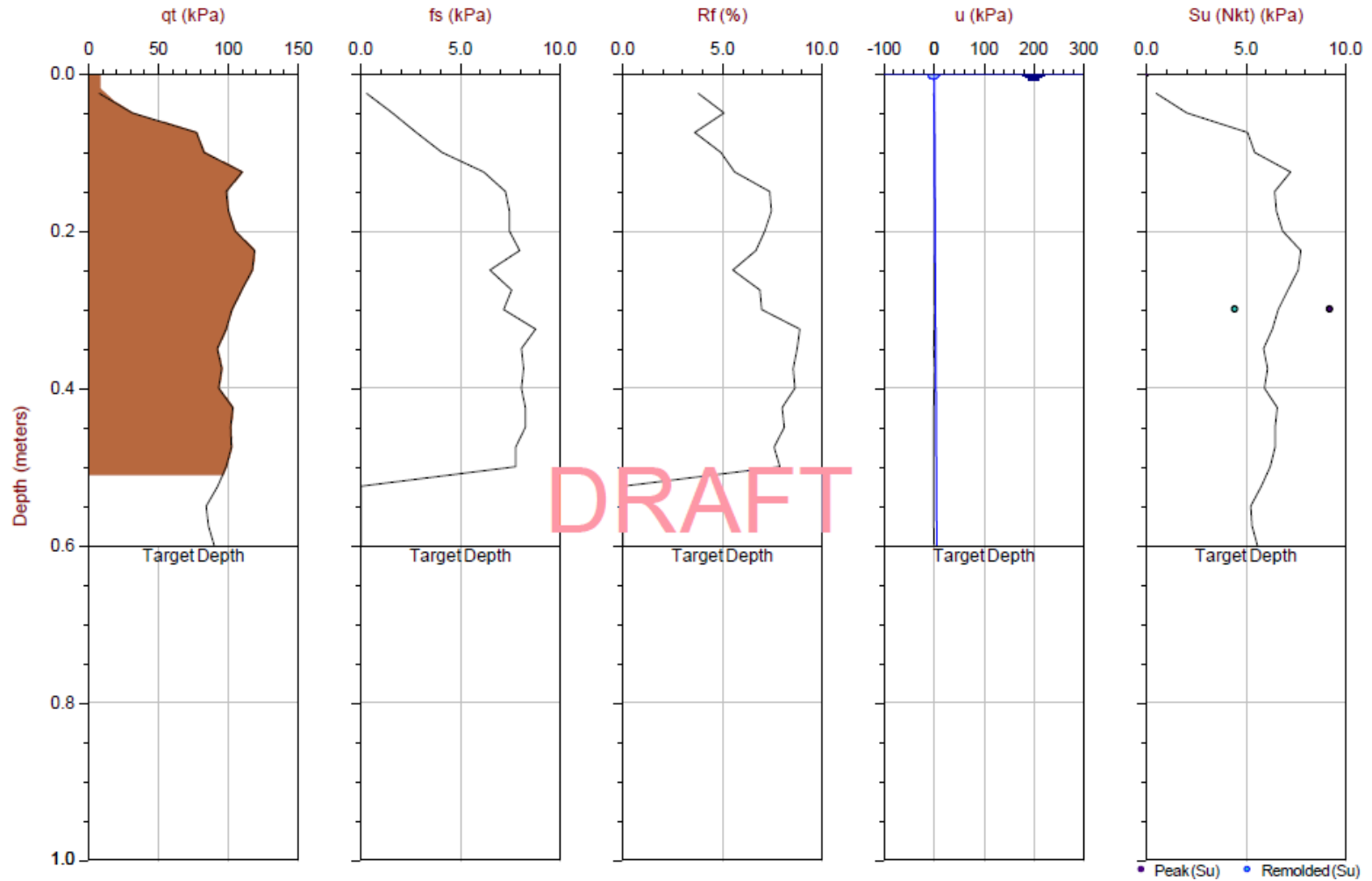


Figure C.18 The variation of tip resistance ( $q_t$ ), sleeve resistance ( $f_s$ ), friction ration ( $R_f$ ), and pore pressure ( $u$ ) and undrained shear strength ( $s_u$ ) with depth below the ground surface during CPT: H6-8-1.6-9.8-200 – Test Location 1

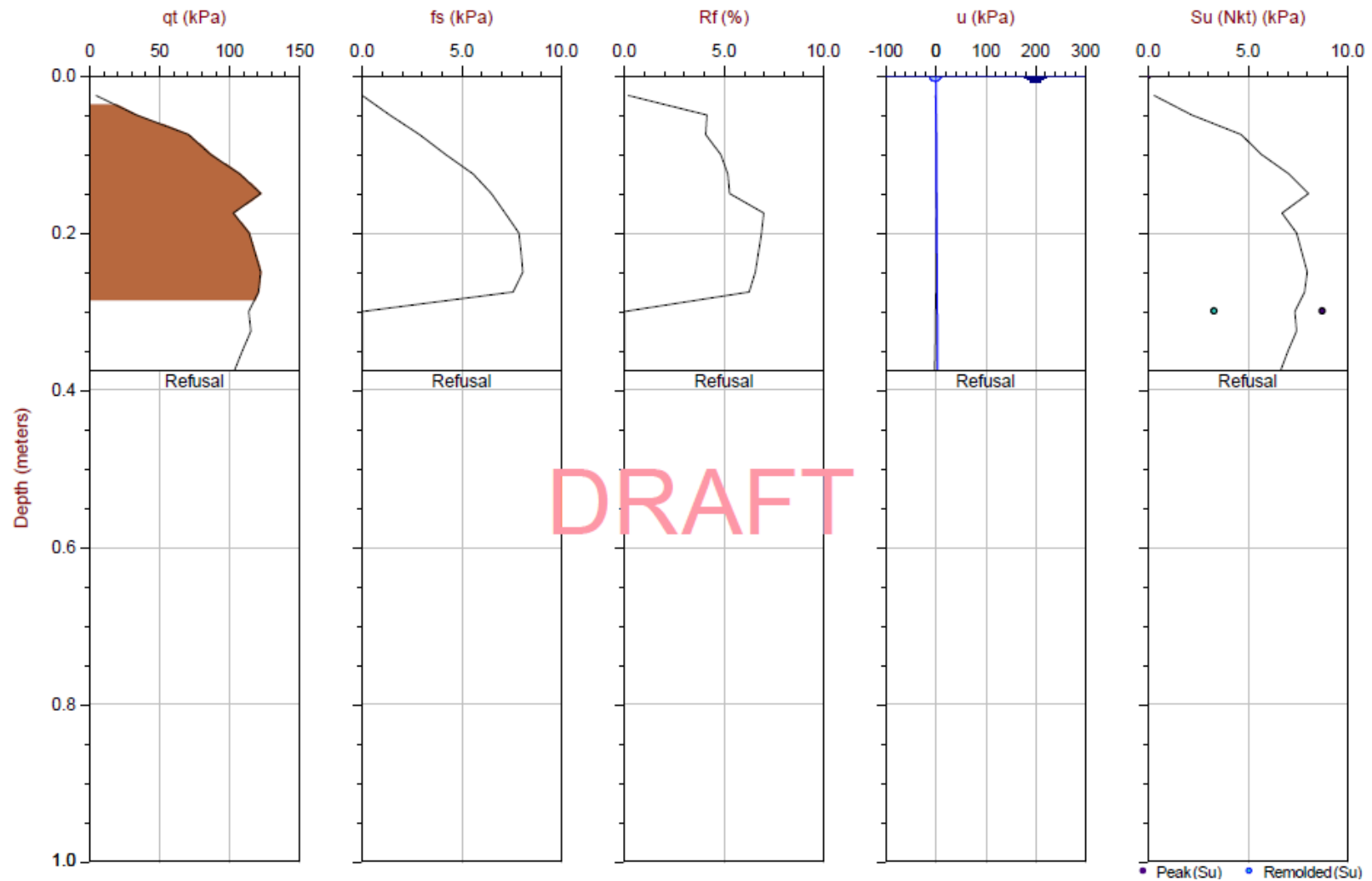


Figure C.19 The variation of tip resistance ( $q_t$ ), sleeve resistance ( $f_s$ ), friction ratio ( $R_f$ ), and pore pressure ( $u$ ) and undrained shear strength ( $s_u$ ) with depth below the ground surface during CPT: H6-8-1.6-9.8-200 – Test Location 2

### C.3 Photographs Illustrating In-Place Penetration Tests



(a)



(b)



(c)

Figure C.20 (a), (b) Square frame moving on linear railings (moving in x, y directions) which is built at UBC to mount the torque head connected to the vane and (c) Torque head mounted on the mobile frame prior to testing



(a)

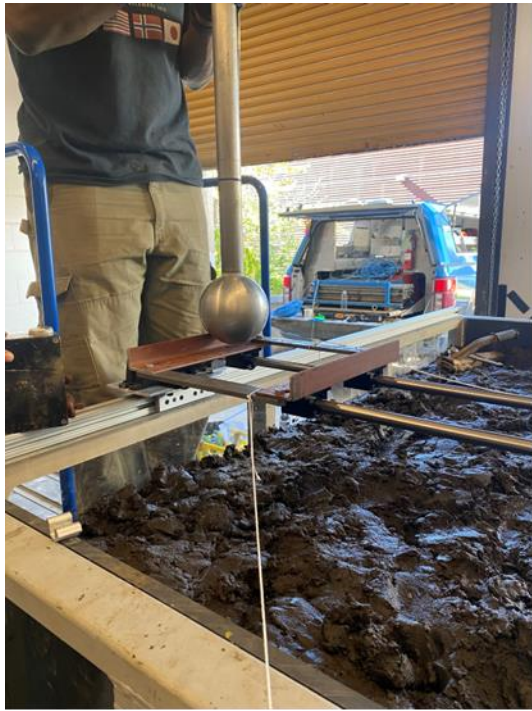


(b)



(c)

Figure C.21 (a) Double tapered 60 x 120 mm ( $45^\circ$ ,  $45^\circ$ ) vane head used for the vane shear tests; (b) and (c) vane mounted on the frame prior to penetrating into the organic soil bed



(a)



(b)



(c)

**Figure C.22 (a), (b) 150 cm<sup>2</sup> ball penetrometer prior to performing the test and (c) ball tip extraction after completion of a test**



(a)



(b)



(c)

**Figure C.23 (a) 15 cm<sup>2</sup> (4.37 cm diameter) cone tip used for the cone penetration tests; (b) cone penetrometer mounted on the platform prior to performing the test; (c) cone penetrating into the organic soil bed**

## **Appendix D P-y Curve Comparisons**

### **D.1 Comparison of P-y Curves Generated Based on the Numerical Predictions and PRCI Guidelines (2009)**

A comparison between the bi-linear horizontal p-y (soil spring) curves developed using the numerical predictions and PRCI guidelines (2009) are presented in this section.

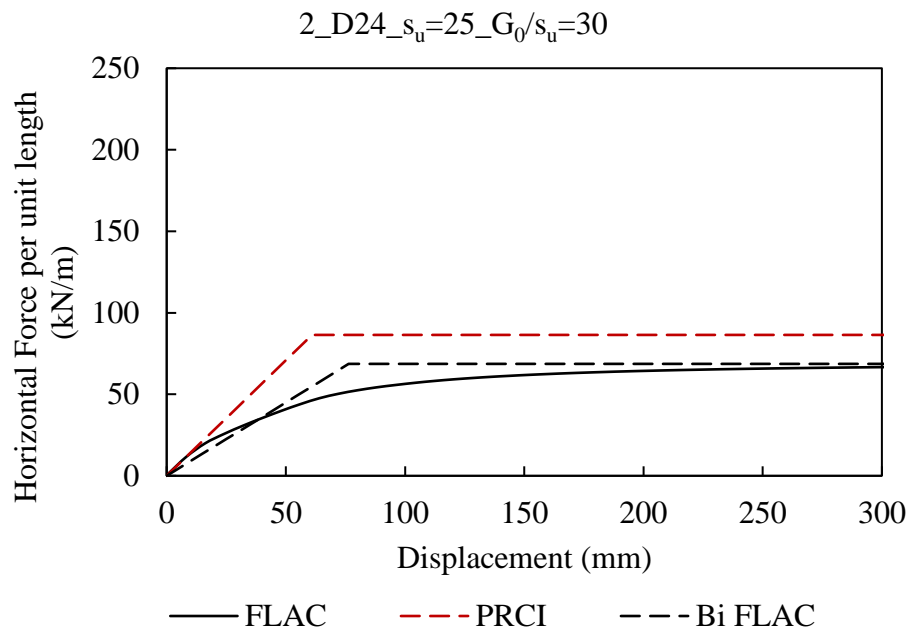
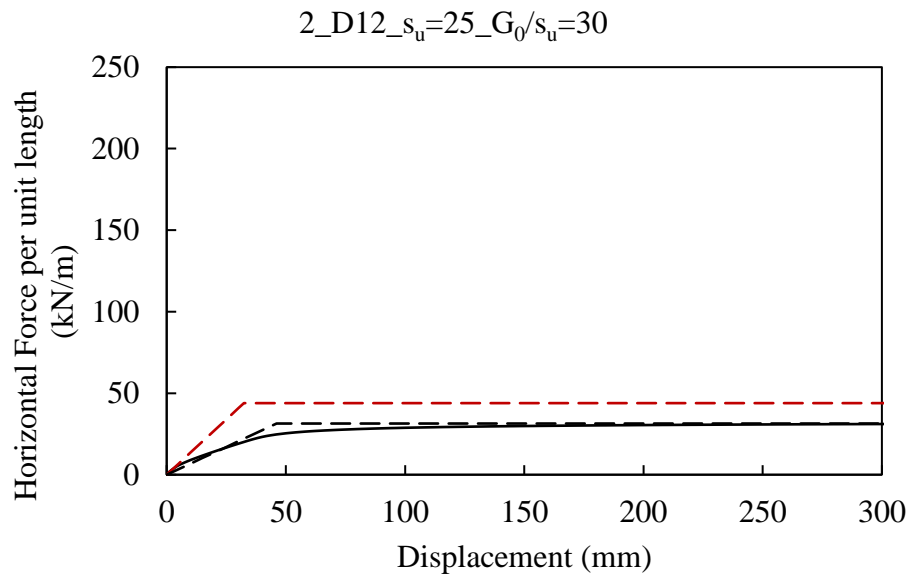


**Figure D.1 Horizontal force per unit length versus pipe displacement ( $\Delta_p/D$ ) from FLAC analyses and PRCI guidelines (2009). Analysis Case: Set A Case 1 ( $s_u = 25$  kPa,  $G_0/s_u = 30$ ,  $H/D = 2$ ): (a) NPS 12 pipe; (b) NPS 24 pipe**

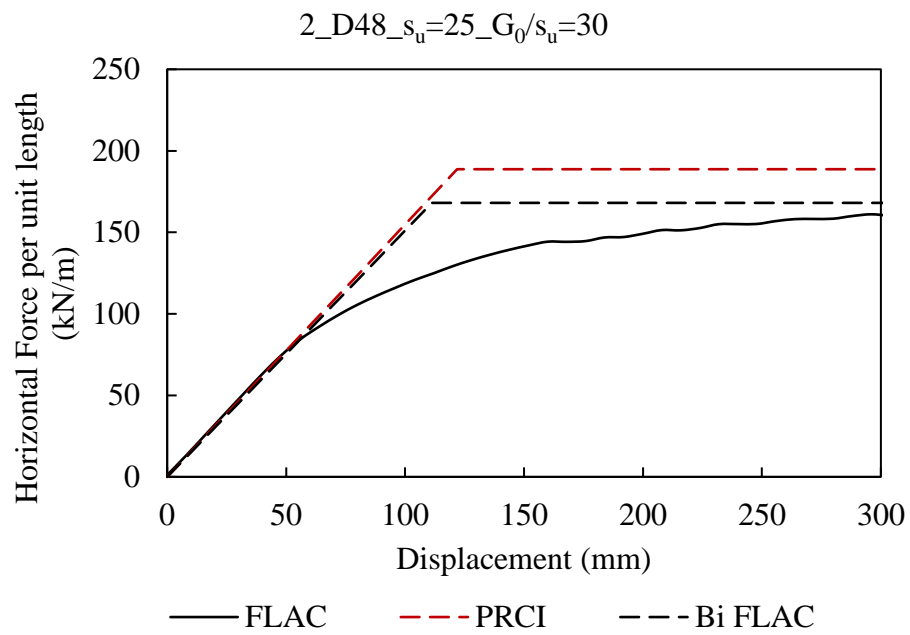
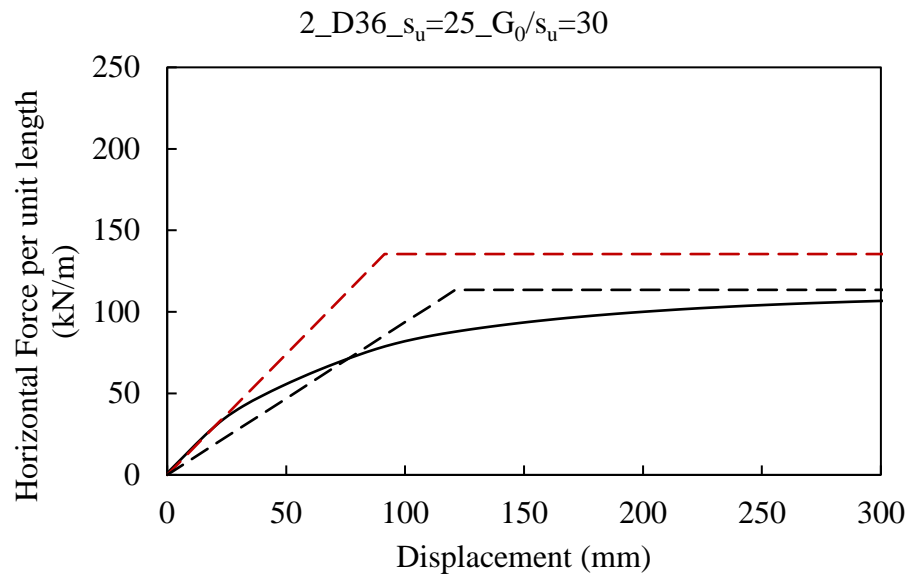


**Figure D.2 Horizontal force per unit length versus pipe displacement ( $\Delta_p/D$ ) from FLAC analyses and PRCI guidelines (2009). Analysis Case: Set A Case 1 ( $s_u = 25$  kPa,  $G_0/s_u = 30$ ,  $H/D = 2$ ): (a) NPS 36 pipe; (b) NPS 48 pipe.**

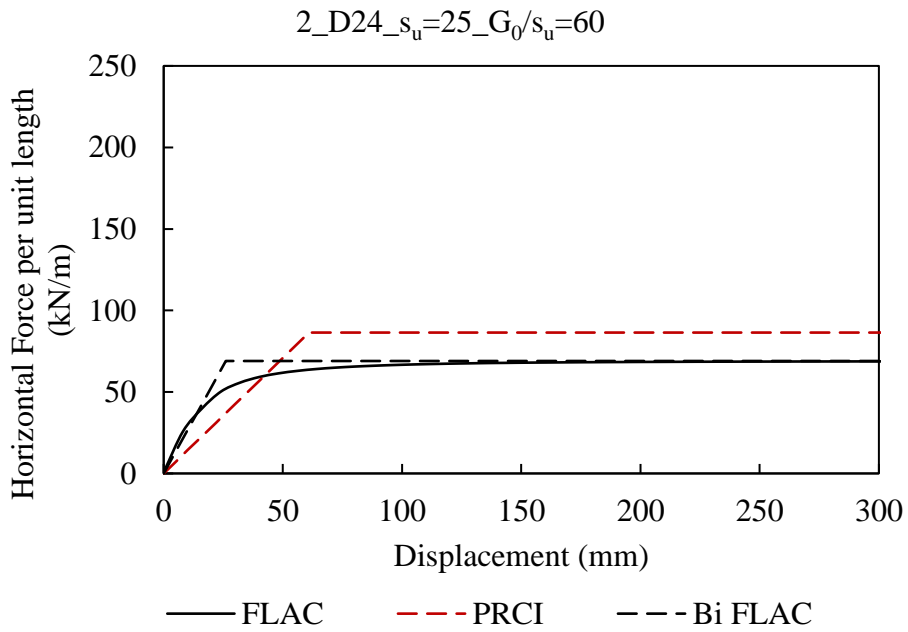
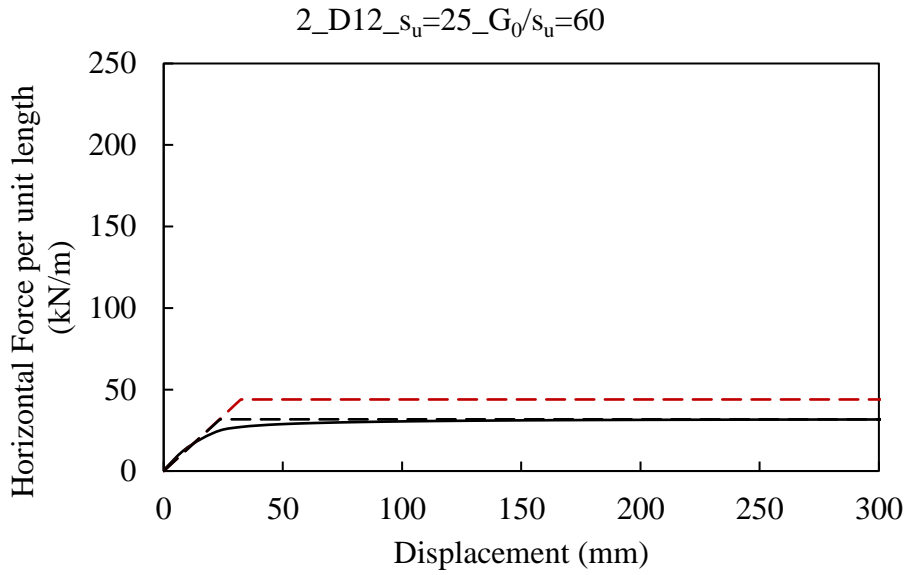


**Figure D.3 Horizontal force per unit length versus pipe displacement ( $\Delta_p/D$ ) from FLAC analyses and PRCI guidelines (2009). Analysis Case: Set A Case 2 ( $s_u = 25$  kPa,  $G_0/s_u = 60$ ,  $H/D = 2$ ): (a) NPS 12 pipe; (b) NPS 24 pipe.**

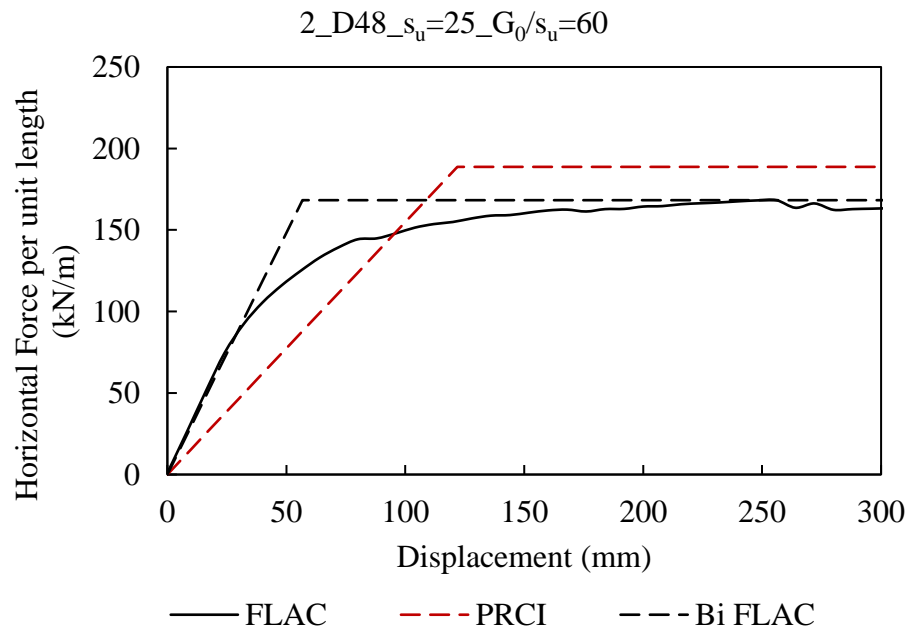
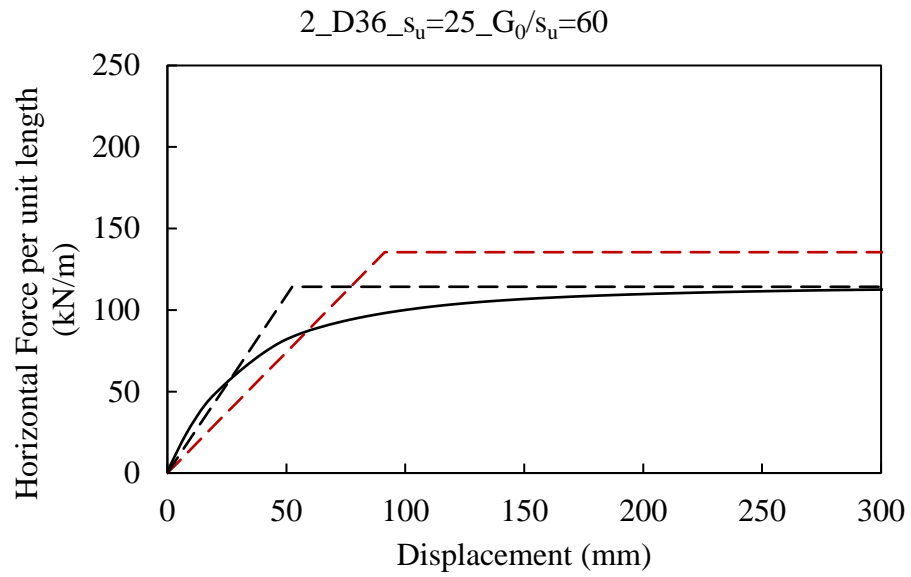


**Figure D.4 Horizontal force per unit length versus pipe displacement ( $\Delta_p/D$ ) from FLAC analyses and PRCI guidelines (2009). Analysis Case: Set A Case 2 ( $s_u = 25$  kPa,  $G_0/s_u = 60$ ,  $H/D = 2$ ): (a) NPS 36 pipe; (b) NPS 48 pipe.**

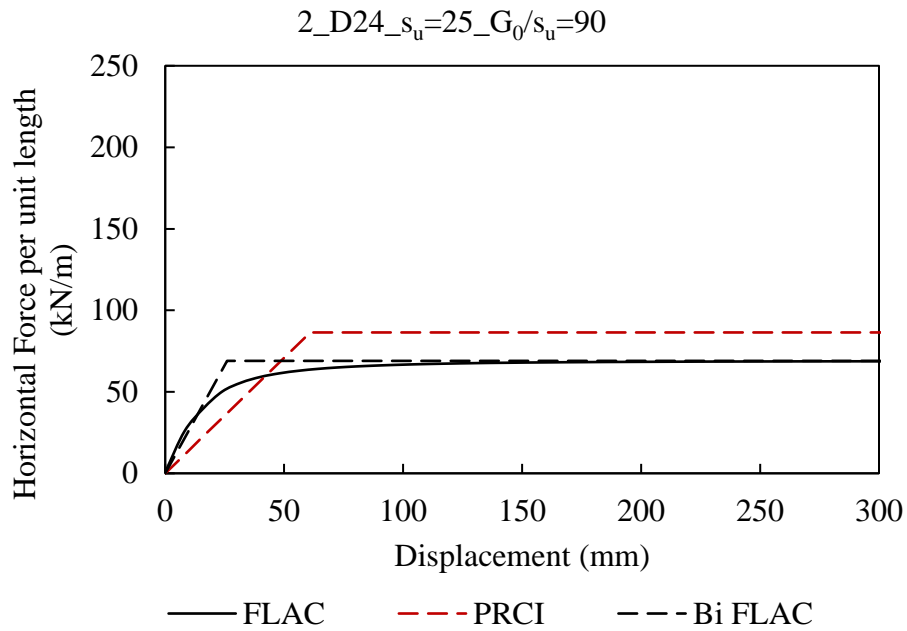
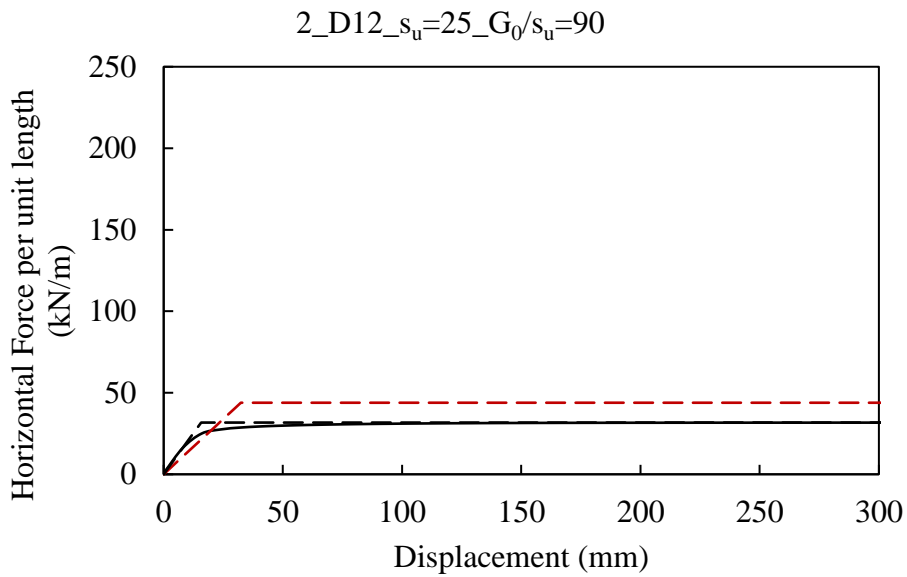


**Figure D.5 Horizontal force per unit length versus pipe displacement ( $\Delta_p/D$ ) from FLAC analyses and PRCI guidelines (2009). Analysis Case: Set A Case 3 ( $s_u = 25$  kPa,  $G_0/s_u = 90$ ,  $H/D = 2$ ): (a) NPS 12 pipe; (b) NPS 24 pipe.**

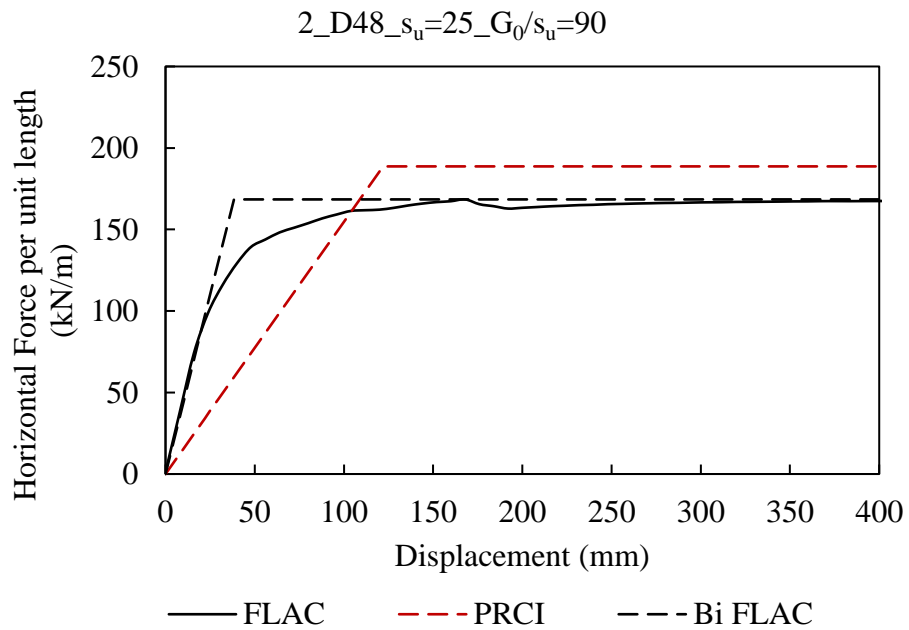
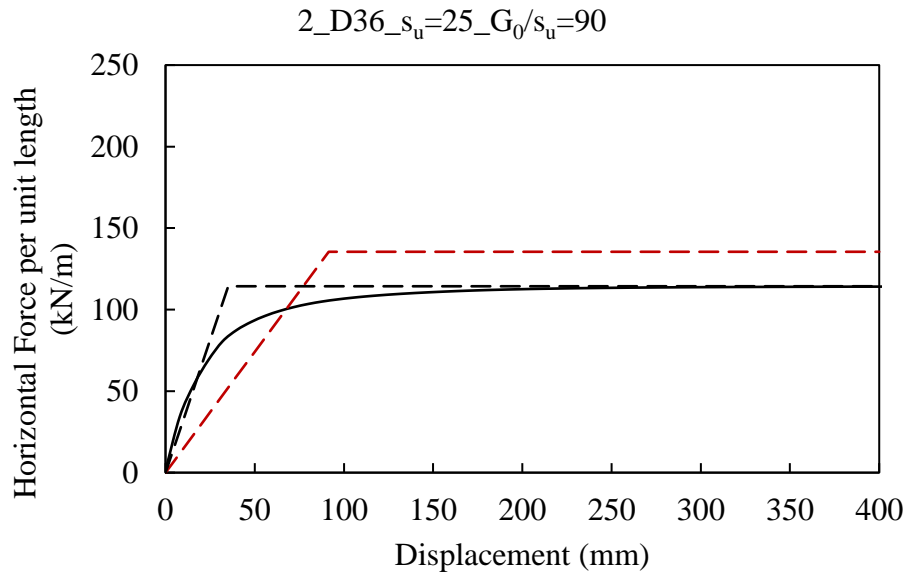


**Figure D.6 Horizontal force per unit length versus pipe displacement ( $\Delta_p/D$ ) from FLAC analyses and PRCI guidelines (2009). Analysis Case: Set A Case 3 ( $s_u = 25$  kPa,  $G_0/s_u = 90$ ,  $H/D = 2$ ): (a) NPS 36 pipe; (b) NPS 48 pipe.**

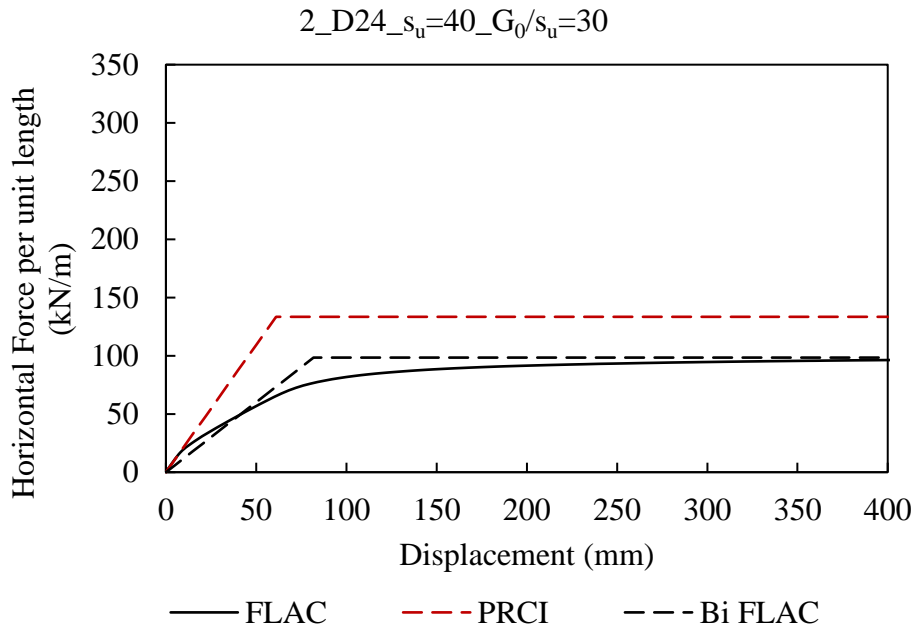
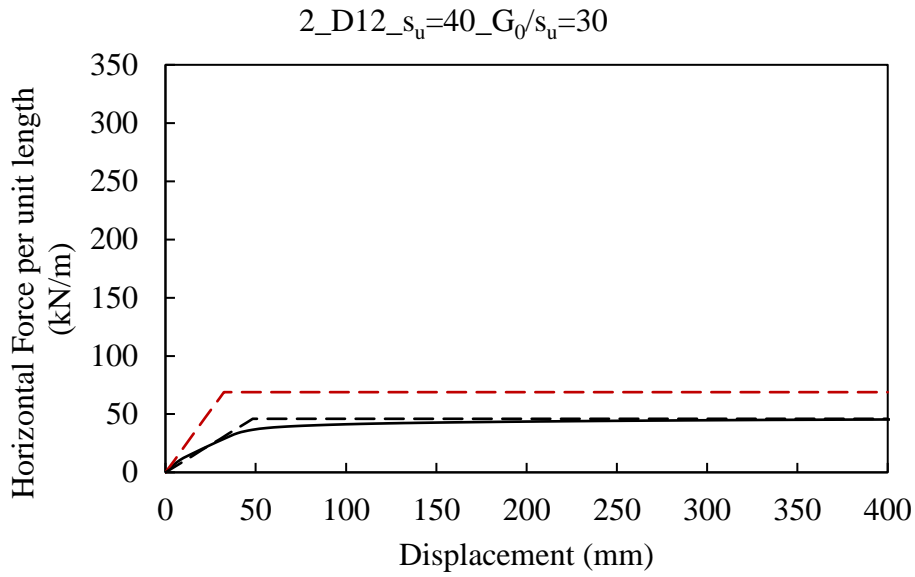


**Figure D.7 Horizontal force per unit length versus pipe displacement ( $\Delta_p/D$ ) from FLAC analyses and PRCI guidelines (2009). Analysis Case: Set B Case 1 ( $s_u = 40$  kPa,  $G_0/s_u = 30$ ,  $H/D = 2$ ): (a) NPS 12 pipe; (b) NPS 24 pipe**

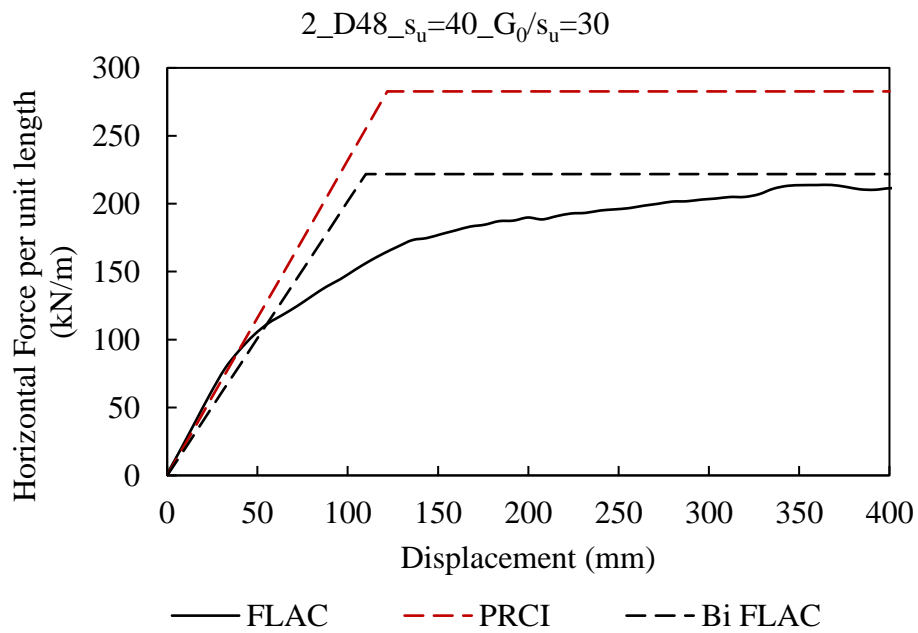
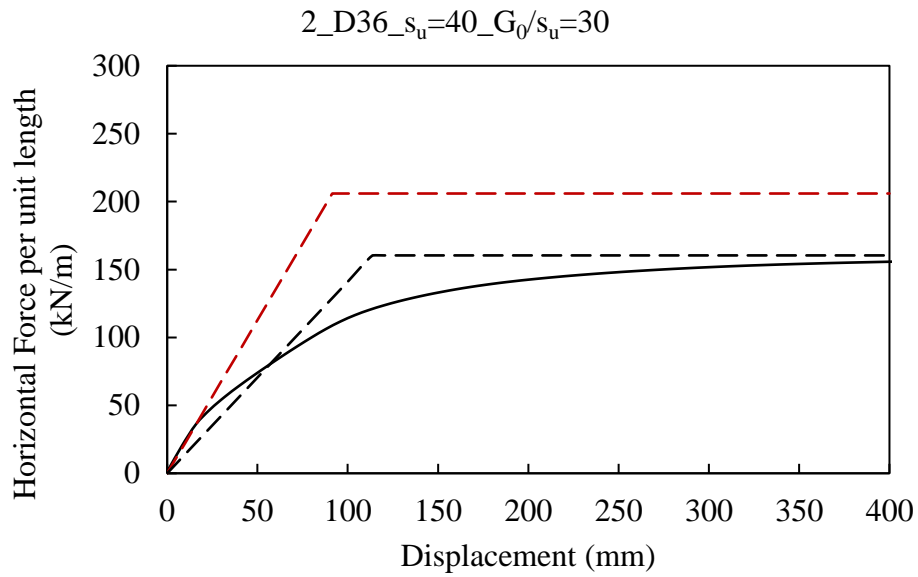


**Figure D.8 Horizontal force per unit length versus pipe displacement ( $\Delta_p/D$ ) from FLAC analyses and PRCI guidelines (2009). Analysis Case: Set B Case 1 ( $s_u = 40$  kPa,  $G_0/s_u = 30$ ,  $H/D = 2$ ): (a) NPS 36 pipe; (b) NPS 48 pipe**

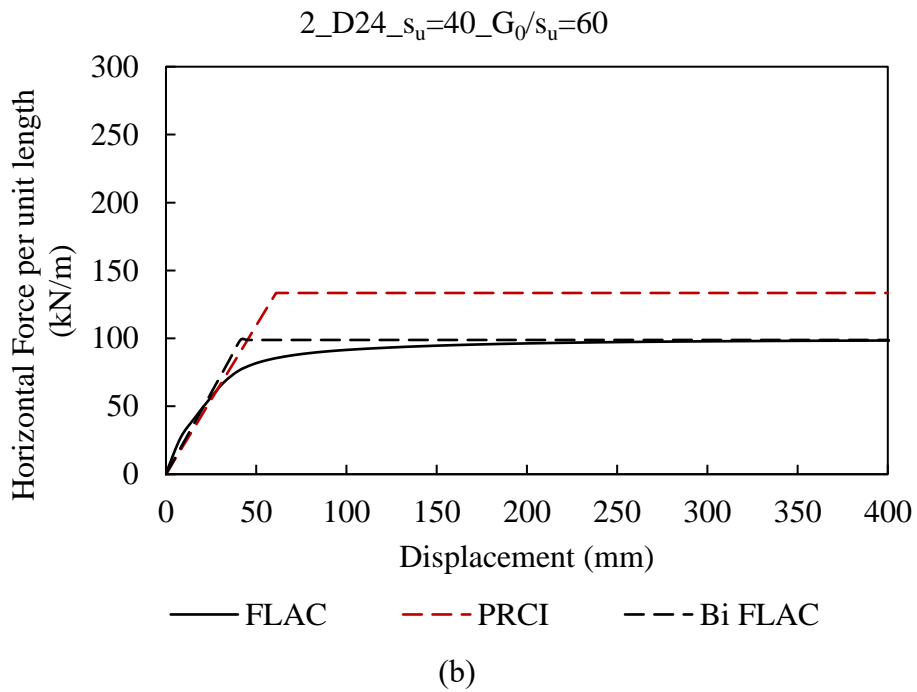
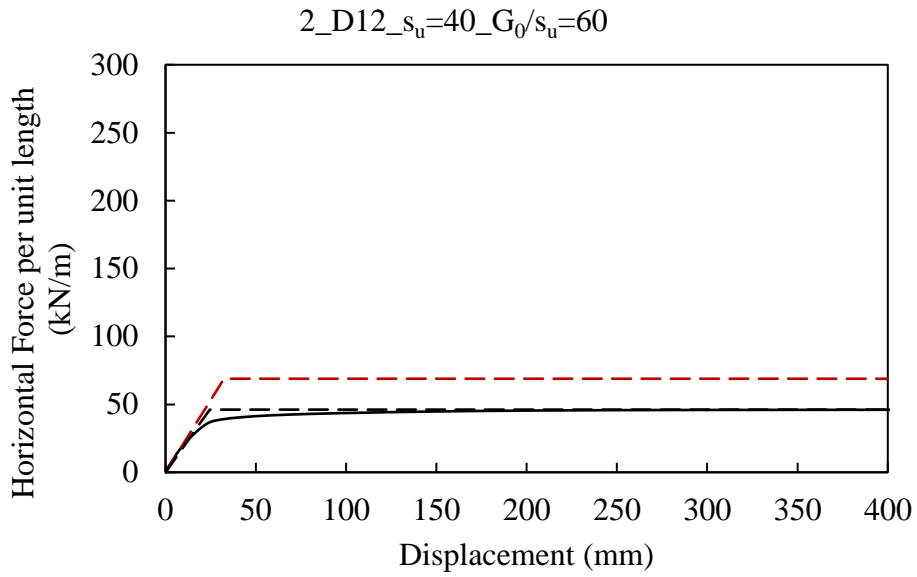


**Figure D.9 Horizontal force per unit length versus pipe displacement ( $\Delta_p/D$ ) from FLAC analyses and PRCI guidelines (2009). Analysis Case: Set B Case 2 ( $s_u = 40$  kPa,  $G_0/s_u = 60$ ,  $H/D = 2$ ): (a) NPS 12 pipe; (b) NPS 24 pipe**

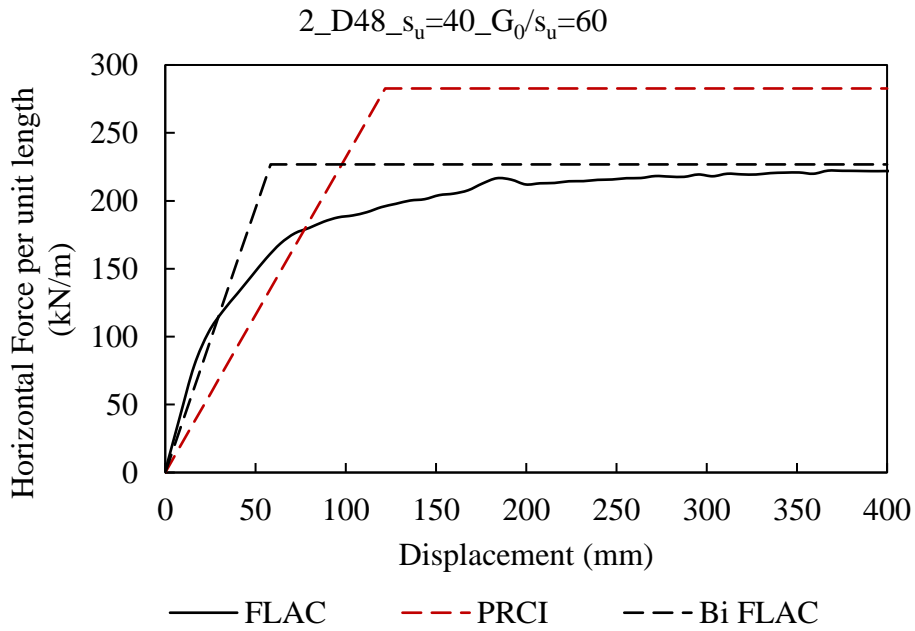
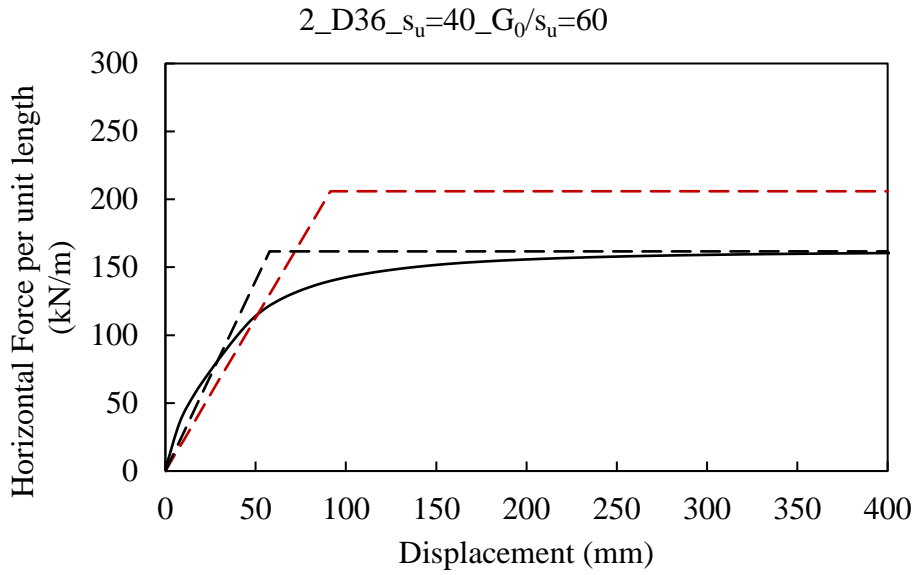


**Figure D.10 Horizontal force per unit length versus pipe displacement ( $\Delta_p/D$ ) from FLAC analyses and PRCI guidelines (2009). Analysis Case: Set B Case 2 ( $s_u = 40$  kPa,  $G_0/s_u = 60$ ,  $H/D = 2$ ): (a) NPS 36 pipe; (b) NPS 48 pipe**

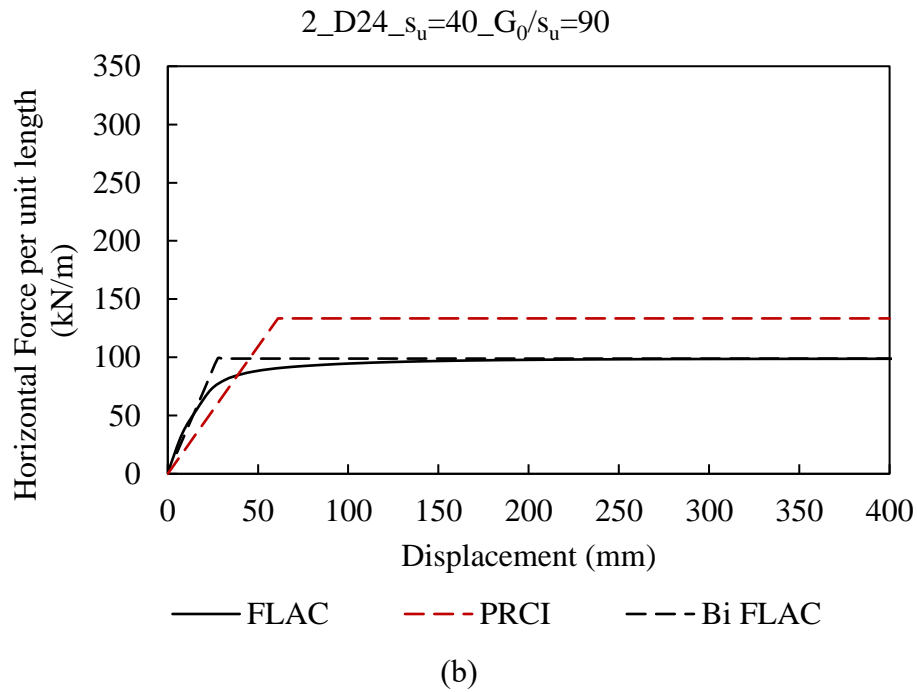
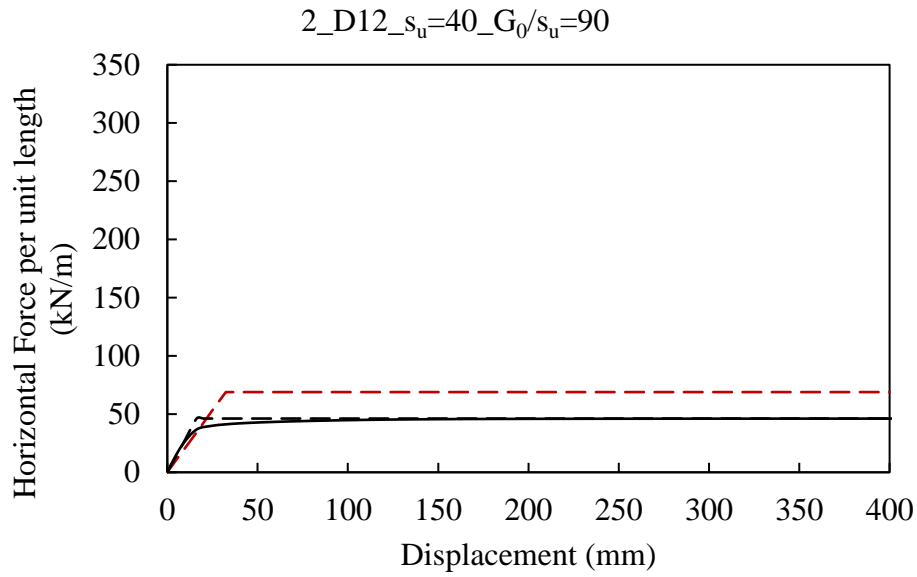


**Figure D.11 Horizontal force per unit length versus pipe displacement ( $\Delta_p/D$ ) from FLAC analyses and PRCI guidelines (2009). Analysis Case: Set B Case 3 ( $s_u = 40$  kPa,  $G_0/s_u = 90$ ,  $H/D = 2$ ): (a) NPS 12 pipe; (b) NPS 24 pipe**

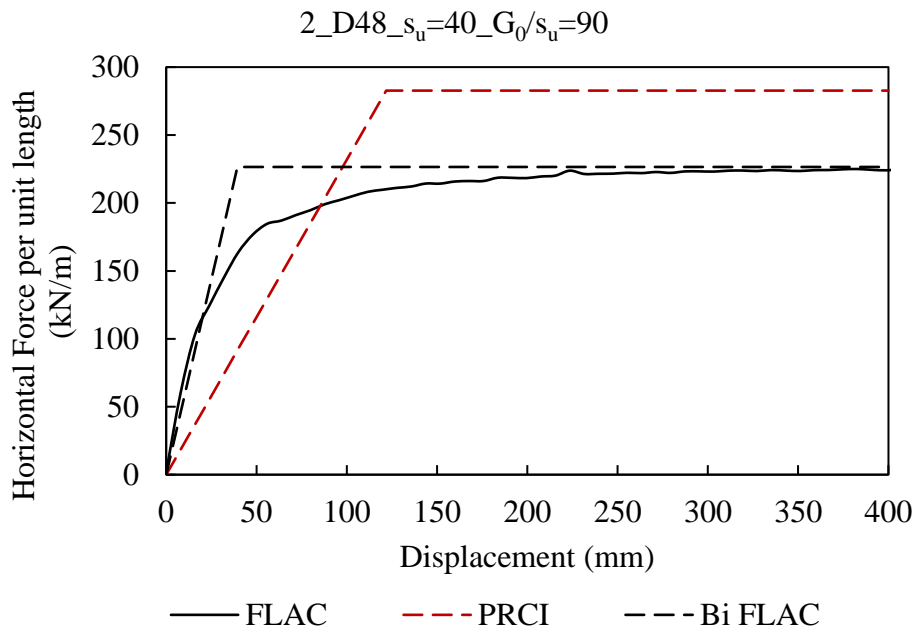
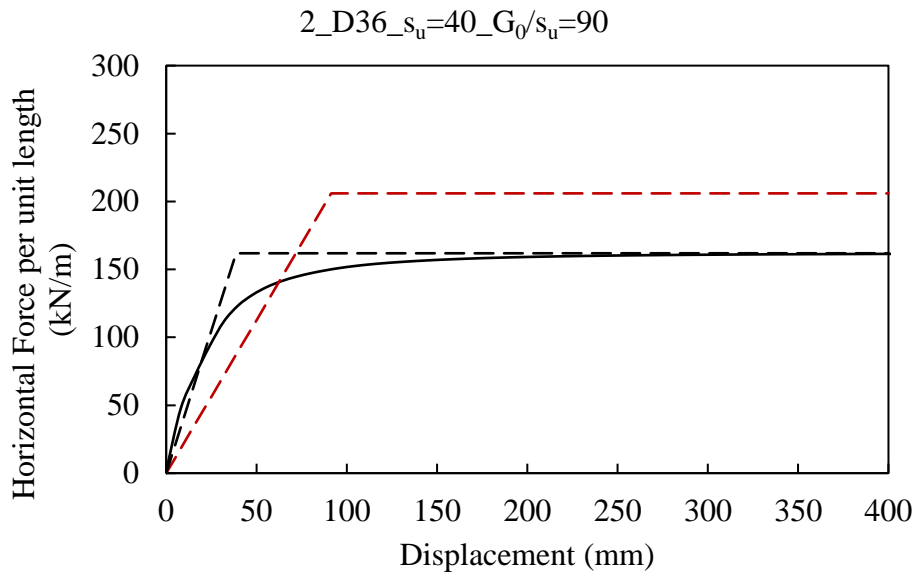


**Figure D.12 Horizontal force per unit length versus pipe displacement ( $\Delta_p/D$ ) from FLAC analyses and PRCI guidelines (2009). Analysis Case: Set B Case 3 ( $s_u = 40$  kPa,  $G_0/s_u = 90$ ,  $H/D = 2$ ): (a) NPS 36 pipe; (b) NPS 48 pipe**

**Table D.1 Summary of soil spring parameters from PRCI guidelines and FLAC modeling of lateral soil restraint**

MODEL ID	PRCI (2009)		FLAC	
	$P_u$ (kN/m)	$\Delta_p/D$	$P_u$ (kN/m)	$\Delta_p/D$
Set A Case 1	$s_u = 25 \quad G_0/s_u = 30$			
2_D12_LD_MC	43.9	0.10	40.0	0.12
2_D24_LD_MC	86.4	0.10	65.3	0.09
2_D36_LD_MC	135.5	0.10	104.2	0.08
2_D48_LD_MC	188.7	0.10	143.8	0.07
Set A Case 2	$s_u = 25 \quad G_0/s_u = 60$			
2_D12_LD_MC	43.9	0.10	33.2	0.07
2_D24_LD_MC	86.4	0.10	67.5	0.03
2_D36_LD_MC	135.5	0.10	110.6	0.05
2_D48_LD_MC	188.7	0.10	156.6	0.04
Set A Case 3	$s_u = 25 \quad G_0/s_u = 90$			
2_D12_LD_MC	43.9	0.10	33.2	0.04
2_D24_LD_MC	86.4	0.10	67.5	0.03
2_D36_LD_MC	135.5	0.10	112.7	0.03
2_D48_LD_MC	188.7	0.10	160.3	0.03
Set B Case 1	$s_u = 40 \quad G_0/s_u = 30$			
2_D12_LD_MC	68.9	0.10	47.1	0.13
2_D24_LD_MC	133.4	0.10	94.1	0.10
2_D36_LD_MC	205.9	0.10	149.5	0.09
2_D48_LD_MC	282.7	0.10	204.3	0.08
Set B Case 2	$s_u = 40 \quad G_0/s_u = 60$			
2_D12_LD_MC	68.9	0.10	48.0	0.07
2_D24_LD_MC	133.4	0.10	97.3	0.05
2_D36_LD_MC	205.9	0.10	157.9	0.05
2_D48_LD_MC	282.7	0.10	226.8	0.05
Set B Case 3	$s_u = 40 \quad G_0/s_u = 90$			
2_D12_LD_MC	68.9	0.10	48.6	0.05
2_D24_LD_MC	133.4	0.10	98.7	0.04
2_D36_LD_MC	205.9	0.10	159.8	0.03
2_D48_LD_MC	282.7	0.10	227.2	0.03

## **D.2 Comparison of P-y Curves Generated Based on the Numerical Models of the Horizontal Full-Scale Tests and PRCI Guidelines (2009)**

The bi-linear p-y curves generated based on the numerical models of the horizontal full-scale tests (a total of six cases since one case out of the total considered is a repeat test) were compared with the corresponding PRCI-based p-y curves for organic soils in this section.

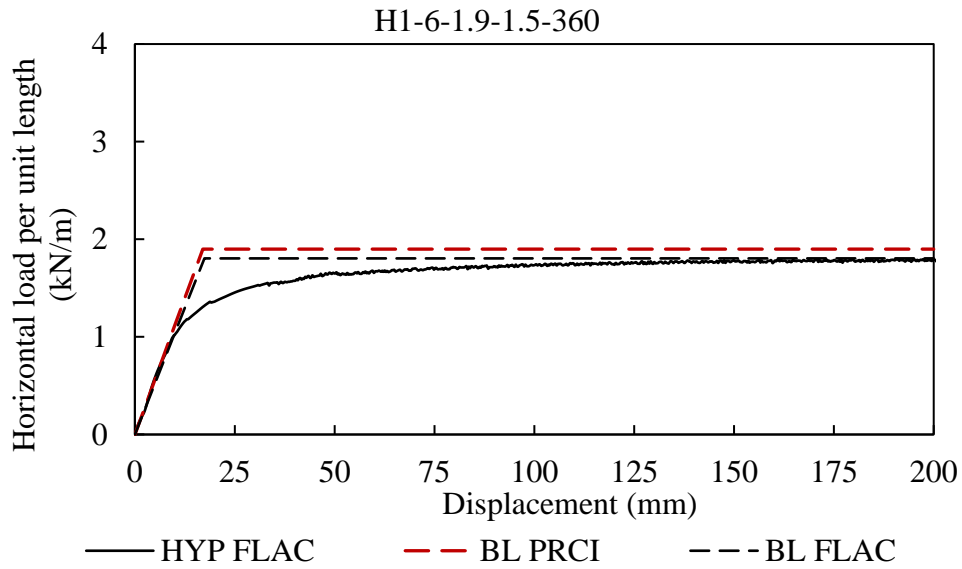


Figure D.13 Comparison of bi-linear p-y curves generated using PRCI (2009) and FLAC analyses results; Test configuration: H1-6-1.9-1.5-360

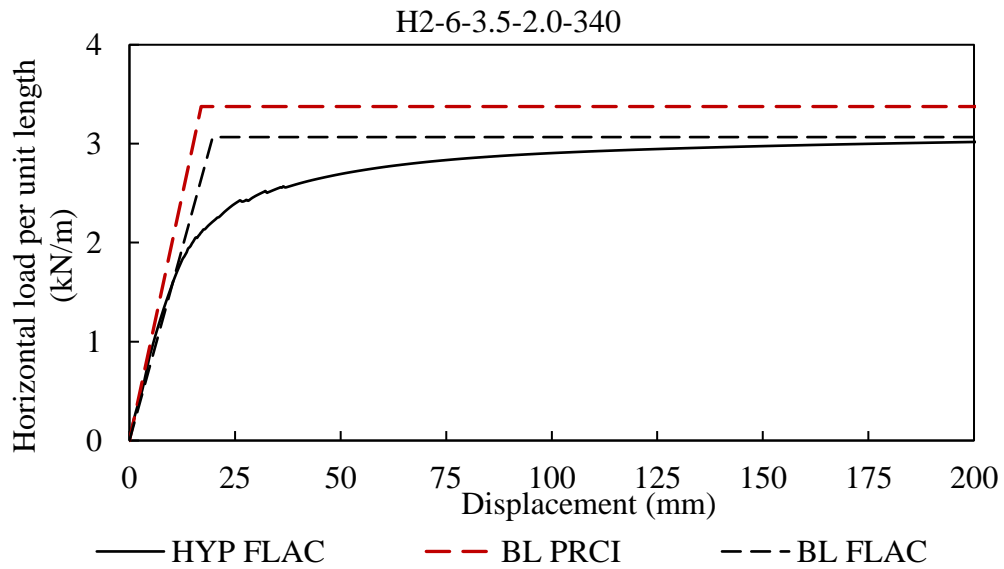


Figure D.14 Comparison of bi-linear p-y curves generated using PRCI (2009) and FLAC analyses results; Test configuration: H2-6-3.5-2.0-340

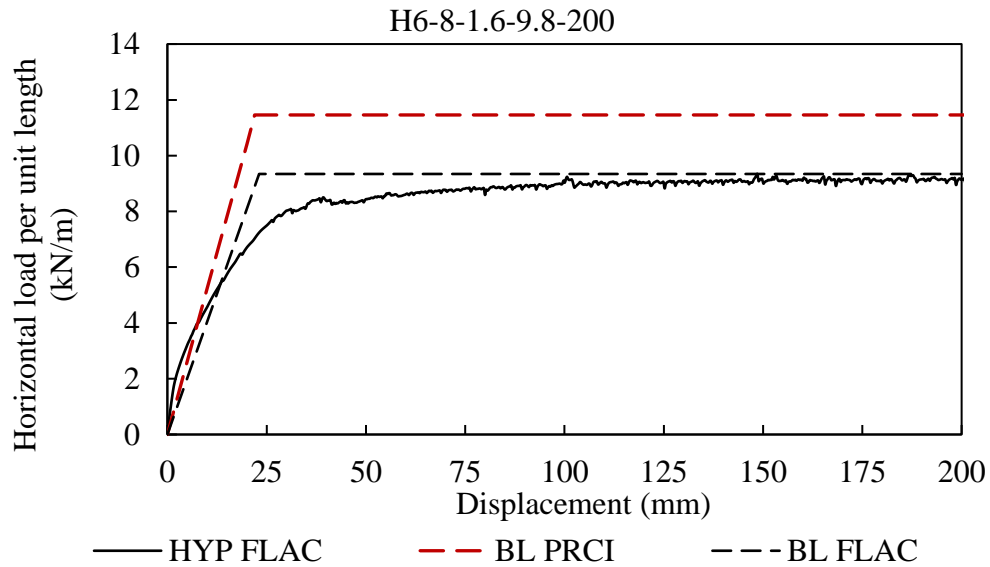


Figure D.15 Comparison of bi-linear p-y curves generated using PRCI (2009) and FLAC analyses results; Test configuration: H6-8-1.6-9.8-200

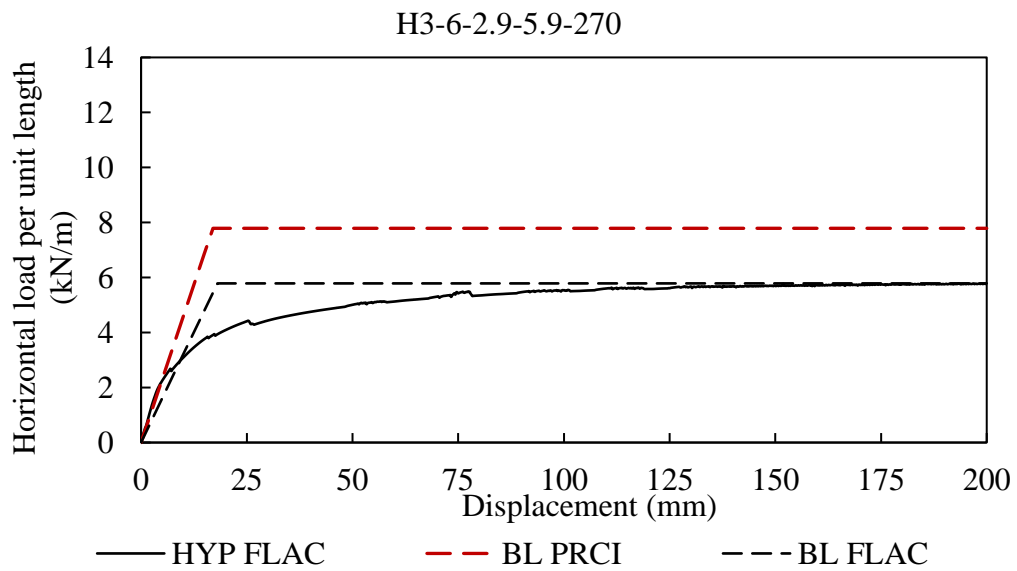


Figure D.16 Comparison of bi-linear p-y curves generated using PRCI (2009) and FLAC analyses results; Test configuration: H3-6-2.9-5.9-270

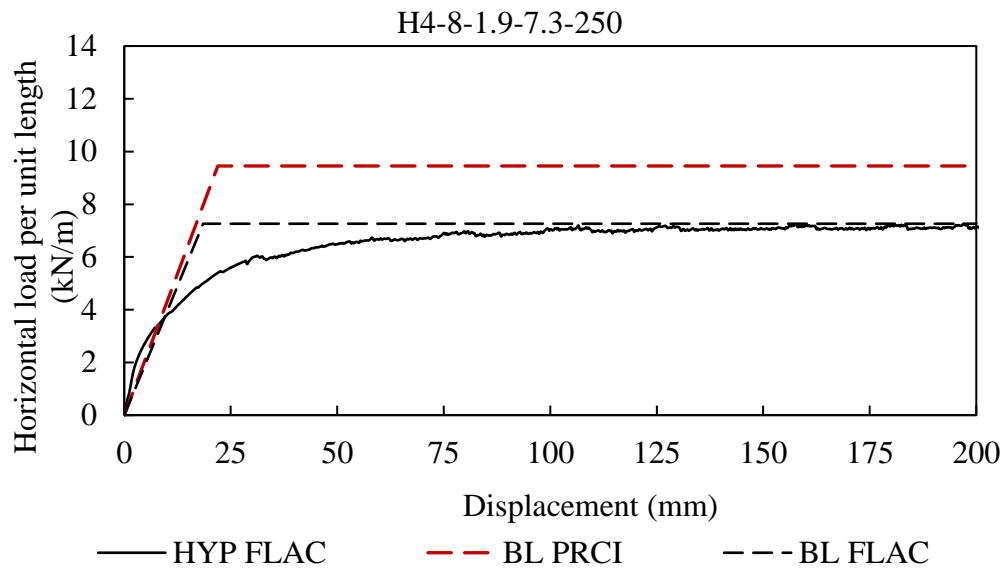


Figure D.17 Comparison of bi-linear p-y curves generated using PRCI (2009) and FLAC analyses results; Test configuration: H4-8-1.9-7.3-250

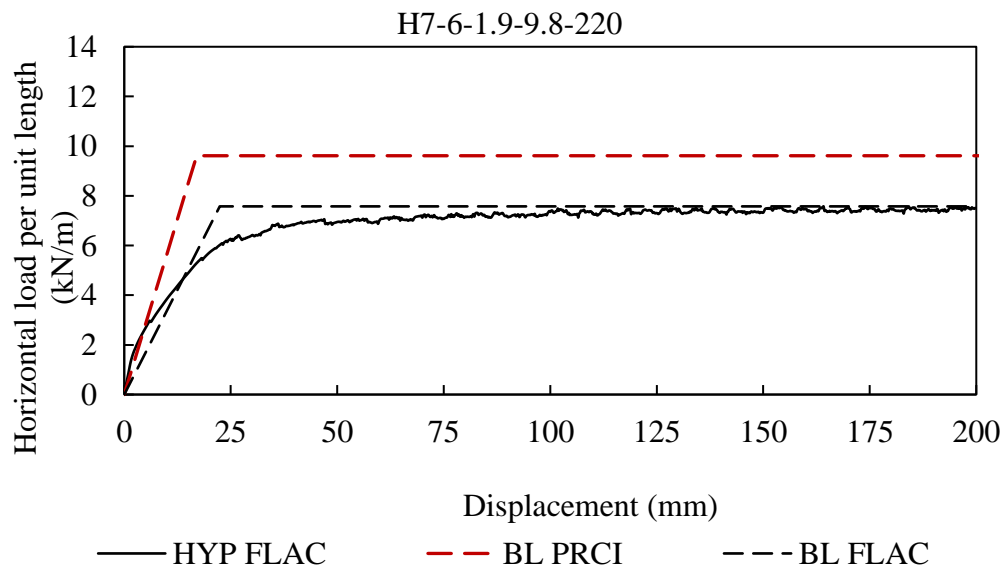


Figure D.18 Comparison of bi-linear p-y curves generated using PRCI (2009) and FLAC analyses results; Test configuration: H7-6-1.9-9.8-220

**Table D.2 Summary of soil spring parameters from PRCI guidelines and FLAC modeling of full-scale horizontal pipe displacement tests**

MODEL ID	PRCI (2009)		FLAC	
	$P_u$ (kN/m)	$\Delta_P/D$	$P_u$ (kN/m)	$\Delta_P/D$
H1-6-1.9-1.5-360	1.9	0.10	1.8	0.10
H2-6-3.5-2.0-340	2.8	0.10	3.1	0.11
H3-6-2.9-5.9-270	6.0	0.10	5.8	0.10
H4-8-1.9-7.3-250	9.2	0.10	7.3	0.08
H5-8-1.6-9.8-210	11.4	0.10	9.3	0.10
H6-8-1.6-9.8-200	11.4	0.10	9.3	0.10
H7-6-1.9-9.8-220	9.0	0.10	7.6	0.12

**D.3 Additional Analysis to Examine the Sensitivity of  $P_u$  - Comparison of P-y Curves Generated Based on the Numerical Models of the Horizontal Full-Scale Tests and PRCI Guidelines (2009)**

Additional analyses were undertaken to examine the sensitivity of the ultimate lateral soil restraint ( $P_u$ ) for the lateral full-scale tests Test Nos. H3-6-2.9-5.9-270, H4-8-1.9-7.3-250, and H6-8-1.6-9.8-200, and the results are shown below.  $s_u$  values were changed up to  $\pm 20\%$  to achieve a match with the experimental results. The bi-linear p-y curves generated based on the numerical models of the horizontal full-scale tests are compared with the corresponding load-displacement response resulted from the full-scale tests.

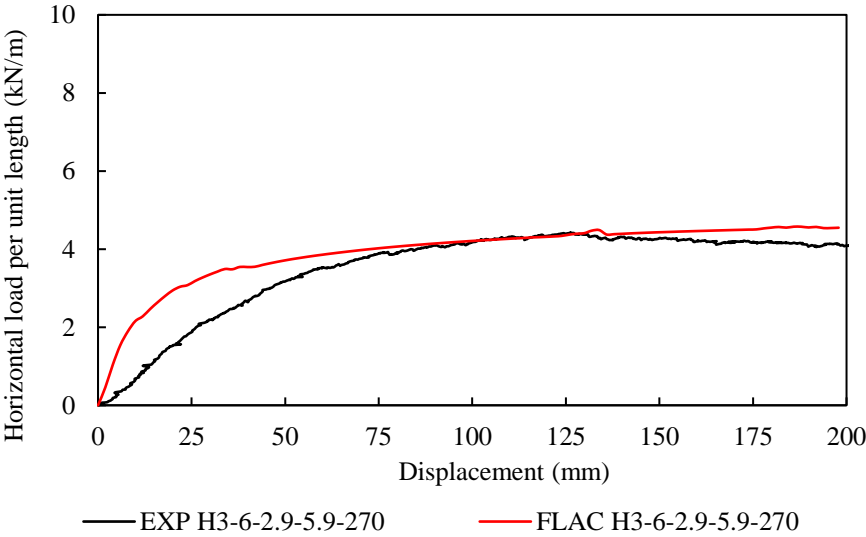


**Figure D.19 Comparison of lateral load-displacement behavior from FLAC analyses and full-scale test results – sensitivity analysis; Test configuration: H3-6-2.9-5.9-270**

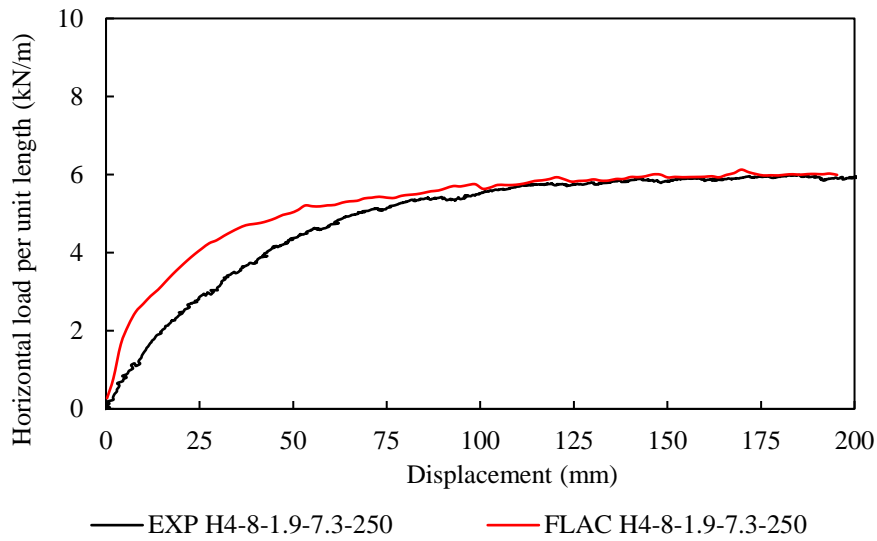


**Figure D.20 Comparison of lateral load-displacement behavior from FLAC analyses and full-scale test results – sensitivity analysis; Test configuration: H4-8-1.9-7.3-250**

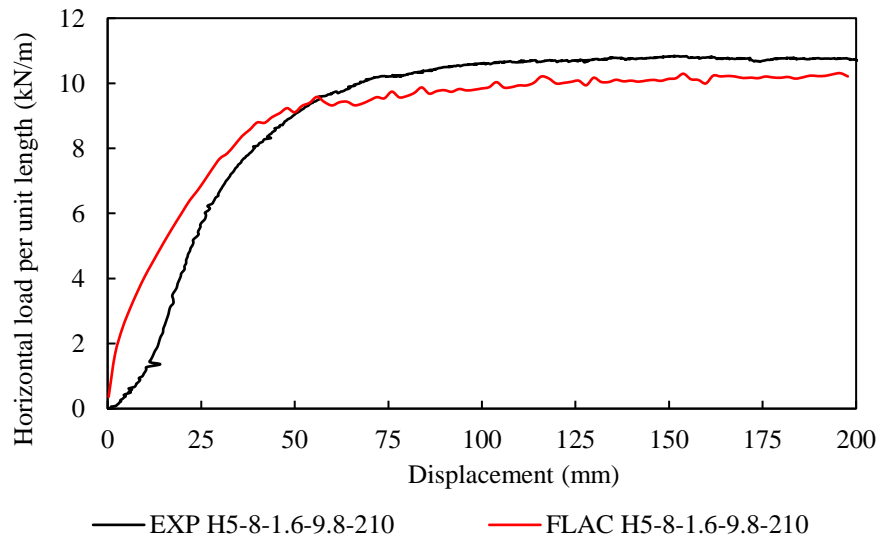


**Figure D.21 Comparison of lateral load-displacement behavior from FLAC analyses and full-scale test results – sensitivity analysis; Test configuration: H5-8-1.6-9.8-210**

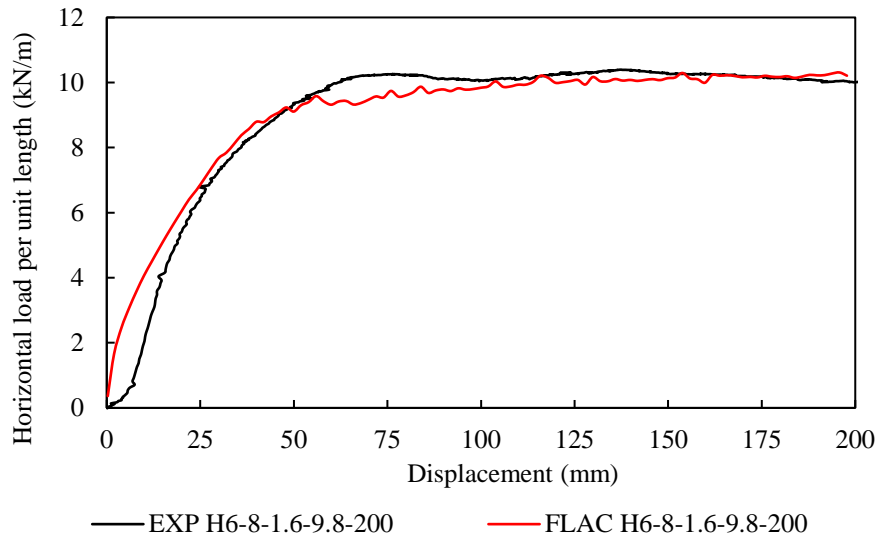


**Figure D.22 Comparison of lateral load-displacement behavior from FLAC analyses and full-scale test results – sensitivity analysis; Test configuration: H6-8-1.6-9.8-200**